7-2-2012

The geochemistry of water-filled sinkholes at Bitter Lake National Wildlife Refuge, Roswell, NM : implications for hydrochemical evolution and trophic support

Elizabeth Premo

Elizabeth A. Premo
Candidate

Earth and Planetary Sciences
Department

This thesis is approved, and it is acceptable in quality and form for publication:

Approved by the Thesis Committee:

Dr. Laura J. Crossey , Chairperson

Dr. Tobias Fischer

Dr. Clifford Dahm

THE GEOCHEMISTRY OF WATER-FILLED SINKHOLES AT BITTER LAKE NATIONAL WILDLIFE REFUGE, ROSWELL, NM: IMPLICATIONS FOR HYDROCHEMICAL EVOLUTION AND TROPHIC SUPPORT

BY

ELIZABETH A. PREMO

BACHELOR OF SCIENCE, WORCESTER POLYTECHNIC INSTITUTE, 2003

THESIS

Submitted in Partial Fulfillment of the
Requirements for the Degree of

Master of Science

Earth and Planetary Science

The University of New Mexico
Albuquerque, New Mexico

May 2012

ACKNOWLEDGEMENTS

I would like to acknowledge and thank numerous people who provided their time and expertise that aided to the completion of this research: my graduate committee – Drs. Laura Crossey (chair), Clifford Dahm, and Tobias Fisher; Michael Lee, my patient and faithful field assistant, competent in the ways of small boat handling; Mr. Jeff Sanchez, Mr. Jeff Howland and the entire Bitter Lake National Wildlife Refuge (BLNWR) staff for allowing access to my field site, organizing use of the research trailer, and supporting logistical considerations; Dr. Mehdi Ali and the staff of the University of New Mexico (UNM) Earth and Planetary Sciences (E&PS) Analytical Chemistry Lab for teaching me the skills required for analyzing major ions in water samples and supporting the running of my water suites; Dr. Viorel Atudorei and the laboratory support staff in the UNM E&PS Stable Isotopes Lab for assisting with the analysis of my entire sample suite; Dr. Mike Spilde and Mr. Ara Kooser for working with me to prepare and analyze substrate samples using the Scanning Electron Microscope (SEM); Mr. Maarten de Moor and the graduate students and staff of the UNM Volcanology (GC) Lab for assisting with operation the GC; Dr. Diana Northrop, Ms. Brandi Cron, and the laboratory staff in the UNM BioAnnex for assisting with microbiological sample preparation and processing; Mr. John Craig of the UNM BioAnnex for assisting with analysis of sample nutrient content and procurement of biological field sampling supplies; Dr. Matthew Kirk and Ms. Amy Williams for providing general support in the Diagenesis Lab; Dr. David Van Horn and Ms. Lauren Sherson for assisting with YSI sondes; Mr. Paul Tashjian of United States Fish and Wildlife for providing hydrological data and biological information; Dr. Becky Bixby in the UNM BioAnnex for providing insight into diatom identification.

THE GEOCHEMISTRY OF WATER-FILLED SINKHOLES AT BITTER LAKE NATIONAL WILDLIFE REFUGE, ROSWELL, NM: IMPLICATIONS FOR HYDROCHEMICAL EVOLUTION AND TROPHIC SUPPORT

BY

ELIZABETH A. PREMO

BACHELOR OF SCIENCE, WORCESTER POLYTECHNIC INSTITUTE, 2003

MASTER OF SCIENCE, DEPARTMENT OF EARTH & PLANETARY SCIENCES, UNM, 2012

ABSTRACT

This study provides a hydrochemical baseline survey of water-filled sinkholes at Bitter Lake Nation Wildlife Refuge (Roswell, NM). Water samples from 10 representative sinkholes taken at 1.0m increments were analyzed for major ions, stable isotopes [$\delta^{18}O$, δD], and dissolved gases. Sinkholes are surface features at a constant head boundary found at the discharge region for the Roswell Artesian Basin, recharged by upwardly flowing artesian springs. Constant head is confirmed by a lack of measured change in depth during two sampling sessions (October 2008, May 2009), low relief (<10m change across study area), and deployment of autonomous sensors (sondes).

Sinkhole waters – regardless of depth or season – fall along a common isotopic evaporation trajectory ($\delta D = 3.387*\delta^{18}O - 19.38$), and adopt a Na-Cl chemical endmember facies. Driven primarily by physical sinkhole geometry (e.g., depth and

surface area), sinkhole water follows a predictable evolutionary progression from a spring-like well-mixed ("young"), to moderately saline well-mixed ("transitional"), to saline and stratified ("old" or "evolved"), based on the relative volume of water that has entered and subsequently been evaporated from the system. The modality of water column structure may be predicted by measuring the density, TDS or conductivity at sinkhole surface, as these parameters can be used as a proxy for evolutionary "age." Simple geochemical models reveal calcium- and sulfate-bearing minerals (calcite, gypsum) precipitate early in the reaction while halite and magnesium-containing minerals precipitate late, yielding increased Cl^- and Mg^+ concentrations in fluids subjected to prolonged evaporation. More complicated models are needed to fully consider precipitation of additional mineral species and water budget.

Both PO_4 and NH_4 were present in biologically-significant concentrations in sinkholes with chemically controlled water columns, and photosynthetic bacteria were found to organize at the bottom of the photic zone. High NH_4 and CO_2 accompanying low O_2 dissolved gas values confirm the increased biological control in stratified sinkholes. Resident fish populations are affected by water chemistry which reduces reproductive success or exceed the survivable range of habitable conditions. Results of this study may be used to aid with biological resource management and to predict stratified conditions using measurable proxies.

TABLE OF CONTENTS

LIST OF FIGURES

LIST OF TABLES

CHAPTER 1: INTRODUCTION

Bitter Lake National Wildlife Refuge (the Refuge) is located in Chaves County, New Mexico (NM), near the city of Roswell (see Figure 1). The Refuge hosts 52 water-filled sinkholes, each of which varies in physical appearance, size, and resident biota Previous studies have described the geologic and hydrologic setting of the Refuge (Fielder and Nye, 1933; Summers, 1972; Land, 2006; Land and Huff, 2010; among others), identifying it as the discharge area for the dual aquifer system that forms Roswell Artesian Basin. These studies also describe the hydrochemical character of the water resulting from the dissolution of soluble Permian-aged evaporates interbedded in the San Andres limestone and the overlying Artesia Group, concluding that a common source feeds both springs and fills sinkholes. A combination of environmental and anthropogenic influences has affected water level and overflow of sinkholes since the establishment of the Refuge in 1937 (Summers, 1972; Land and Newton 2008). As groundwater flows upward through cracks and fissures in the confined carbonate aquifer, it both partially recharges the shallow unconfined alluvial aquifer, and continues to the surface as artesian springs.

While water in Refuge sinkholes has a common source, the concentration of dissolved constituents, physical characteristics and biological assemblage are not uniform among sinkholes. As previous studies characterize sinkhole water being sourced from the discharge of the principal aquifer, the observed variability concedes a complex set of conditions affecting overall water chemistry. Environmental and biological alteration of source water is the major faction, while input from waters flowing through older Permian facies or through fractures in the basement rock resulting from Laramide-aged

compressional faulting may yield (minimal) potential contributions. Although historical documents describe the changing water levels with time on the scale of decades, the short-term fluctuations in water level are due to irrigational drawdown, stream flow of the Pecos River, and day-scale fluctuation. The study area itself is a constant head boundary with low relief, and general subsurface hydrologic progression toward the Pecos River, with no observable surface overflow among sinkholes; thus, sinkholes exist as independent lake structures and variations in ecosystem structure likely due to independent conditions found within the sinkhole itself.

Previous published investigations have provided geochemical evaluation of the surface water chemistry of sinkholes. Partey et al. (2008) used measurements of [Cl-] to evaluate geochemical distribution while Land and Huff (2010) considered geochemical tracers to assess groundwater flow. The nature of karst bedrock makes hydrological studies challenging, and physical changes to local permeability can cause areas of hydrochemical dissimilarity Available hydrochemical data is currently minimal, yet prior studies have observed a wide range of solute concentrations, as along with varying salinities, pH and temperature. Factors that may alter the water chemistry include rate of evaporation, source water inflow rates, chemistry of source waters, mineral precipitation, and biological (microbial) presence. This study evaluates the sinkhole lifecycle, water column structure, and temporal variation using water chemistry analysis, stable isotopes, dissolved gases, analysis of precipitated minerals and substrates, and geochemical modeling.

Understanding the physical characteristics and hydrochemistry of these sinkholes provides the Refuge with data to aid with natural and biological resource management

practices such as selection of an appropriate habitat for restocking initiatives or identifying sensitive locations requiring additional attention for protection. For example, a number of endangered and endemic fish and invertebrate species are found in sinkholes. These species require specific habitat conditions for survival, and water quality can affect the sustainability of a population (Bednarz, 1979; Echelle, 1989). Hydrochemical analysis offers information to evaluate groundwater flow and mixing, and to better understand the chemical evolution of the water in this system that may result in alteration of aquatic habitat structure.

Several key findings were revealed over the course of this study: 1.) Surface measurements are variable among sinkholes which is most likely due to sinkhole geometry as opposed to proximity to the Pecos River; 2.) Hydrochemical evolution is bimodal with sinkhole water column being either well-mixed or stratified; 3.) Evaporation and continuous recharge are the primary processes controlling source water modification and subsequent precipitation reactions; 4.) All sinkholes have a common water source which is altered by the same climatic and environmental conditions, with stable isotopes showing evaporation; 5.) Sinkholes have a predictable lifecycle driven by continuous source water input, evaporation, precipitation reactions, chemical stratification, halite saturation and finally exhaustion; 6.) Biological presence and community is related to the stage of sinkhole lifecycle and is controlled by chemical conditions.

CHAPTER 2: BACKGROUND

LOCATION

Bitter Lake National Wildlife Refuge (BLNWR, the Refuge) is located in Chaves County, New Mexico (NM), approximately 11 miles (mi) (17.7 kilometers [km]) northeast of the city of Roswell at 33.49°N, 104.4°W at an average elevation of 3,496 feet (ft) (1,066 meters [m]) above sea level (ASL). Abutting the west banks of the Pecos River, the Refuge is approximately 80 mi (128.7 km) east of the Sacramento Mountains in an area characterized by the convergence of the desert high plains and the Chihuahuan Desert.

The Refuge encompasses 24,536 acres and is divided into three distinct non-contiguous units: the North Tract (12,160 acres, 9,620 acres of which is the Salt Creek Wilderness); the Middle Tract (approximately 11,000 acres, includes Refuge headquarters, seven playa lakes, Bitter Lake [the Refuge's namesake] and sinkholes); and the South Tract (1,400 acres of agricultural cropland) (USFWS, 2009). The Refuge was established on October 8, 1937 by Executive Order 7724 to provide refuge for and protection of migratory birds and other wildlife, and to preserve important biological resources in this, one of the most ecologically-significant wetlands in the United States desert southwest. The Refuge supports a diverse assemblage of vegetation representing Great Plains prairie grasslands, Chihuahuan Desert, and riparian and wetland vegetation. Agricultural cultivation of land in the South Tract provides grasslands wherein migratory birds may find safe haven. The Refuge is home to a diverse community: 357 bird species; 26 species of fish; 50 dragonfly species; 12 species of amphibian; 40 reptile species; and 57 reported mammal species (Tashjian, 2003). Of these species, 27 are classified as state

or federal threatened, endangered or candidate species (see Appendix A for a list of these species). Resident species include one of the largest remaining populations of the Pecos pupfish, as well as the Roswell pyrg (spring) snail, the Koster's spring snail, the Pecos assiminea and the Noel's amphipod which are relic species once associated with the Permian shallow seas formerly covering the area, and are endemic to the Refuge – with the exception of Pecos assiminea which is found in only two other known locations in west Texas and Mexico (Tashjian, 2003). The endemic Say's pond snail was last documented in the 1980s in Hunter Marsh (southern portion of Middle Tract), but is believed to be locally extinct, possibly the result of treated municipal waste water that historically entered the Refuge in this location (MacRae et al, 2001).

The most notable occupants of the Refuge are the transient birds that use the playa lakes as migratory staging areas during the winter and shorebirds' nesting sites during the summer. Legislation of the Migratory Bird Conservation Act (16 USC 715D) protects the land or waters used by migratory birds, and limits the type of activities which may occur in these areas. Additional governing legislation includes the Refuge Recreating Act (16 USC 460-1) and the Wilderness Act of 1964 (PL 88-577). A combination of the Lake St. Francis sinkhole cluster and Bitter Lake (Middle Tract) along with the Salt Creek Wilderness (North Tract) were included in the National Registry of Natural Landmarks on August 11, 1980, designated as the Bitter Lake Group (USFWS, 2009).

The region around Roswell, NM – both historically and presently – is a valuable agricultural area. Grasses and freely flowing artesian springs made the region favorable for farmers and ranchers; today the area is still largely used for agricultural purposes, with major crops being alfalfa, cotton, sorghum, pecans and chiles (Welder, 1983).

Modern day agriculture continues to utilize groundwater resources for irrigation and livestock; however, continuous use of these groundwater resources has halted the overflow of the artesian springs once observed.

The local climate is characterized semi-arid with annual precipitation sourced primarily from summer monsoon storms. According to Western Regional Climate Center (WRCC) data (1996-2008) recorded at the Roswell International Air Center (RIAC), average annual precipitation is 12.02 inches (in) (30.5 centimeters [cm]) per year (/yr) with approximately 105 days annually receiving at least 0.01 in (0.025 cm) measurable precipitation. The average daytime high temperatures recorded by WRCC (at the RIAC) ranged from 55.9 degrees Fahrenheit (^{o}F) (13.3 degrees Celsius [^{o}C]) in December to 94.8^{o}F (34.9^{o}C) in July; average daytime lows range from 25.8^{o}F (-3.4^{o}C) in December to 67.7^{o}F (19.8^{o}C) in July. On 29 July 1998, temperatures reached an extreme maximum of 111^{o}F (43.9^{o}C), and an extreme minimum of -6^{o}F (-21.1^{o}C) was recorded on 27 December 1997.

REGIONAL GEOLOGY

The geologic setting in the immediate vicinity of Roswell, NM is predominantly Permian sedimentary lithologies interbedded with evaporites and Quaternary-aged alluvium deposited by the historical migration of the Pecos River (Figure 2). These Permian facies: the San Andreas Formation and the Artesia Group (comprised of the Greyburg, Queen, Seven Rivers, Yates and Tansill Formations), represent a 30 my depositional period in the backreef Guadalupian series of the Capitan Reef structure of the Delaware Basin in southeast New Mexico and west Texas - analogous to the sabkha environment as observed near the modern-day Dead Sea. Adams and Frenzel (1950)

describe the formation of these facies in response to changing sea levels. Modern groundwater salinity and karstification of sedimentary strata is attributed to building of the reef structure, the deposition of marine and backreef sediments, sea water isolation and a semi-arid climate that promoted high evaporation rates and restricted sediment transport, yielding thick evaporite deposits across the region..

The more regional geologic setting is important for understanding the groundwater hydrology of the area (see Kelley, 1971 and Summers, 1972; also summarized in Land and Huff, 2010). The basement rocks underlying the Roswell Artesian Basin are Pre-Cambrian rhyolite with some sedimentary occurrence in southern Chavez County and metamorphic presence to the west (Kelley, 1971). Pennsylvanian-aged mudstones overlay basement rocks in some portions of the Basin. The Permian Abo formation (deposited 290-286 mya) is a dark red-brown shale that ranges in thickness from 200 to 1,400 ft (61.9 to 426.7 m), and occurs at a depth of nearly 3,000 ft (914.4 m) below ground surface near the Pecos River. The Abo grades into the overlying Yeso formation (see Figure 2). The Yeso (deposited 286-275 mya) is comprised of beds of red shales, siltstones, sandstones, limestone, and dolomite with interbedded evaporites (gypsum, anhydrite, and salt), and ranges in thickness from 1,200 to 1,800 ft (365.8 to 548.6 m) (Summers, 1972).

The San Andres formation (275-268 mya) sits on top of the Yeso as a thick-bedded grey limestone interbedded with anhydrite, gypsum, salts, and clastics, and ranges in thickness (in the subsurface) from 902 to 1706 ft (275 to 520 m) (Warren, 1989; Kelley, 1971). Differing bedding thicknesses, evaporite inclusions and clastics reveal the marine shoaling cycles that occurred during its formation. Both modern dissolution of the

limestone by meteoric and groundwater and karstic alteration of the strata developed along the unconformity between the San Andres and the overlying Artesia Group, has developed porosity making this formation an important regional aquifer.

The Permian Artesia Group (deposited 268-261 mya) overlies the San Andres formation, and provides both aquifer-bearing strata at its interface with the San Andres and aquitard strata in upper confining beds. These "red beds" have a combined thickness of over 2,000 ft (609.6 m) and are characterized by interbedded dolomite, limestone, siltstone, shale, and evaporites (gypsum-dominance at the surface, anhydrite and salts at the sub-surface), with clastic content increasing with further distance from the reef structure (Harrington, 1957; Land, 2007). In the vicinity of the Refuge, only the Seven Rivers, Grayburg and Queen members are present, with the Queen and Grayburg undivided (both deposited 268-264 mya). The lower portion of the Grayburg formation exhibits similar characteristics to the subjacent limestones of the San Andres. The predominantly sandstone, dolomite and anhydrite Grayburg formation ranges in thickness from approximately 300 to 475 ft (91.4 to 144.8 m) (Summers, 1972). The Queen formation averages 425 ft (129.5 m) thick and is comprised of fine- to very-fine grained tan and grey sandstone, dolomite and anhydrite.

The Seven Rivers formation (deposited 264-261 mya) is prominent in outcrop along the eastern banks of the Pecos River in the vicinity of the Refuge. The unit is comprised of fine- to very-fine grained red sand and mud, interbedded with gypsum and salt and may be up to 500 ft (152.4 m) thick, although it is less than 250 ft (76.2 m) thick in the proximity of the Refuge. Due to its low permeability, the Seven Rivers is a good confining layer for the artesian aquifer beneath and the shallow alluvial aquifer above it;

however, soluble evaporites in the formation are susceptible to dissolution by unsaturated groundwater and precipitation, contributing to the development of sinkholes.

Above the Seven Rivers in the vicinity of the Refuge is an assemblage of Quaternary deposits. These are dominated by fluvial sediments of the Pecos River– gravel, sand, silty-sand, and clay – unconformably on top of the Permian bedrock (Adams and Fretzel, 1950). Valley floor alluvium of the Pecos River and Rio Hondo are of Upper Pleistocene age and younger. Three alluvial terraces were deposited by the Pecos River and its tributaries during the Pleistocene: the Lakewood terrace (upper Pleistocene), Orchard Peak terrace (middle to lower Pleistocene), and Blackdome terrace (lower Pleistocene to upper Pliocene). During Pleistocene time, the climate was more pluvial, with higher precipitation and lower evaporation rates than observed present day. Approximately 4,000 to 5,000 ft (1,219 to 1,524 m) of unconsolidat ed sediments and sedimentary rock fill the Roswell Artesian Basin, form the alluvial aquifer strata, originating from a complex history of erosion and sedimentation extending from the Paleozoic through the Cenozoic (Huff, 2004). Thickness of these sediments thins with proximity to the modern Pecos River. Sinkhole deposits range from the Pleistocene to Historic and are comprised of portions of the Seven Rivers formation which have subsided, following collapse (McCraw et al, 2007).

PHYSIOGRAPHY

The landscape observed in the vicinity of the Refuge is due to a combination of Pedernal uplift and regional subsidence resulting from the dissolution of limestone bedrock and evaporites in Permian beds by unsaturated groundwater and meteoric water (Bachman, 1987). Geomorphic features in this area include the Sacramento Mountains

(approximately 70 mi [112.6 km] west of Roswell), the Rio Hondo (south of the Refuge), and the Pecos River (eastern edge of the Refuge). The steep west-facing Sacramento Mountains and the east-dipping Pecos Slope were formed during the Triassic with regional uplift associated with the Laramide Orogeny; compression ceased in the Tertiary with the onset of Basin-Range extension (Kelley, 1971; summarized in Stafford et al, 2009). The Pecos Slope extends from the crest of the Sacramento Mountains to the Pecos River, exhibiting an elevation loss of nearly 6,000 ft (1,829 m) (Land, 2003), and a relatively consistent dip of one to two degrees for Permian beds, although local dip can vary due to small-scale folding and solution subsidence (Forbes and Nance, 1997). With the exception of only a few reported instances, the majority of igneous activity is located along the western side of the Pedernal uplift (Summers, 1972).

Simultaneous with the uplift of the Sacramento Mountains, three major northeast-southwest trending wrench fault structural zones developed along the Pecos Slope: the Border Buckle, the Six-Mile Buckle and the Y-O Buckle (Land, 2007; see Figure 1). Collectively called the Pecos Buckles, these faults occur between the Sacramento Mountains and the Pecos River, and serve as prominent regional recharge areas for the artesian aquifer in the Roswell Artesian Basin (Fielder and Nye, 1933; Land, 2007), with the Y-O Buckle, south of Roswell, crossing the Pecos River, and the Border and Six-Mile Buckles crossing the Rio Hondo to the west of Roswell. The zone around each buckle is characterized by a straight narrow ridge or a series of aligned ridges and hills (Summers, 1972). The KM Fault - which does not present the same surface characteristics as the Pecos Buckles - is believed to have exhibited right-lateral motion and normal vertical displacement with last movements occurring during the Laramide (Land, 2007). Based

on current hydrologic data, no obvious change in the hydraulic gradient is associated with the Border or Six-Mile Buckles (Land, 2007), although it is believed that the faults in these structural zones may extend up from the Pre-Cambrian basement rock (Stipp, 1956; Summers 1972).

SINKHOLE FORMATION

Factors that generally contribute to sinkhole formation include faulting, deep-seated solution, and solution of carbonate and evaporitic rocks (e.g., salt, gypsum, chalk and limestone) (Merriam and Mann 1957). Unlike other sinkholes whose creation is related to sinking streams, those located at the Refuge are formed by rising fluids associated with the localized discharge of groundwater in the Roswell Artesian Basin (Land 2003, Stafford et al, 2008). Upward flowing groundwater in the vicinity of the Refuge dissolves gypsum and other evaporites occurring in the Seven Rivers formation, creating voids within the red mudstone beds. As the voids increase in size, the upper layers crumble downward, and a sinkhole is formed (Land 2003; 2006. Stafford et al 2009). The most common means of sinkhole formation associated with the Pecos River is through local dissolution near the ground surface and above the water table (Bachman, 1987). In areas where there are large depressions such as those at the Refuge and nearby Bottomless Lakes State Park, gypsum is absent in the uppermost 15 m (49.2 ft) of the Permian bedrock (Lyford 1973). Near the Pecos River, the water table is close to the surface, so as the upper strata sinks into the void created by dissolution of soluble rock, the void fills with water; such features tend to be deep with steep vertical sides (Harrington, 1957).

Sinkholes are features often associated with karst landscape like that found in the

Pecos River Valley. Karstification of the San Andres formation likely began during the late Permian when members of the Artesia Group were forming, and flowing fresh water caused dissolution of San Andres evaporates (removing 403.5 to 603.7 ft [123 to 184 m] of salt, andhydrite and gypsum); this pre-existing alteration affected the eventual course of the Pecos River and developed porosity within the limestone (Bachman, 1987; Welder, 1983).

The principle sources of minerals and soluble rock that are dissolved present day by groundwater are found west of the Pecos River; the majority of soluble constituents have already been removed from strata in close proximity to the river (Harrington, 1957). In the vicinity of Roswell, 404 to 607 ft (123 to 185 m) of evaporites have been dissolved from the upper part of the San Andres formation in the subsurface (Welder, 1983; Bachman, 1987). The dissolution of evaporites has caused subsidence as dissolved constituents are removed from the bedrock by groundwater and transported to the surface by springs or through surface seepage into the river (Harrington, 1957). In the vicinity of the Pecos River, the carbonate aquifer is under confined conditions, and has positive hydraulic head, causing groundwater to progress vertically through cracks and voids in the Seven Rivers formation. Dissolution of gypsum contributes to the formation of sinkholes at the Refuge.

HYDROLOGY

Regional hydrology has developed through a combination of the Roswell Artesian Basin, the Pecos River, and the Rio Hondo and tributaries. The Roswell Artesian Basin is a two-aquifer system comprised of an upper unconfined alluvial aquifer and an artesian confined carbonate aquifer. The Basin is bound to the west by the Sacramento and

Capitan mountain ranges (among others) and to the east by a low-elevation escarpment east of the Pecos River (Longworth and Carron, 2003). Recharge for the shallow aquifer is from upward flow of water in the artesian aquifer through faults and fractures in the Seven Rivers formation. Groundwater recharge of the alluvial aquifer occurs by direct infiltration of precipitation and surface water, while the artesian aquifer is recharged by infiltration of surface water on outcrop in areas west of the basin (Huff, 2004; Newton et al., 2009). An estimated 300,000 ac-ft/yr of recharge water to the carbonate aquifer occurs by direct filtration at outcrop in the Sacramento Mountains, precipitation and runoff from intermittent losing streams across the Pecos Slope (Barroll and Shoemaker, 2003; Land 2007).

Water-bearing zones in the artesian aquifer – although typically less than 50 ft (15 m) - range from several centimeters to nearly 100 ft (30.5 m) thick (Land 2007), and vary stratigraphically throughout the Basin. At the Basin's north extent, water level occurs in the mid-San Andres formation, and in the south near Artesian, the water table is found in the Grayburg member of the Artesian Group and upper part of the San Andres. Similarly, the water table occurs in the lower portion of the Glorietta Sandstone to the west, and the upper San Andres limestone to the east (in the vicinity of the Refuge) (Land 2007). Carbonate rocks in the San Andres of limestone and dolomite composition are dissolved by slightly acidic rainwater traveling through cracks which eventually enlarge into voids that water flows through freely. While this dissolution occurs modern day, the development of karstic porosity occurred during episodes of subareal exposure in the Permian and Pleistocene time (Fielder and Nye, 1933; Huff, 2004). The transmissivity of the aquifer ranges from 800 to 187,000 ft^2/day with a natural discharge of roughly 30,000

ac-ft/yr (~37 million m^3/yr) (Land, 2007). The observed difference among transmissivity ranges results from heterogeneous porosity across the extent of the aquifer. The majority of discharge from the artesian aquifer since the Pecos Valley began agricultural irrigation in the early 20th Century has resulted from irrigation wells; however, natural discharge into the Pecos River is also a large component, with flowing water contributing to the formation of the karst landscape and wetlands in the vicinity of the Refuge (Land, 2005).

The confined aquifer and the alluvial aquifer are separated by members of the Artesia group - primarily the Seven Rivers formation - which serve as a leaky confining layer (Havenor, 1968; Welder, 1983; Huff, 2004). The shallow alluvial aquifer partially filling the Pecos Valley is primarily Quaternary-aged sediments comprised of sand and gravel, with smaller amounts of clay and silt. The aquifer is generally less than 250 ft (76.2 m) thick and extends 10 to 15mi (16.1 to 24.1km) west of the Pecos River (Barrol and Shomaker, 2003). The unconfined aquifer is largely within valley fill alluvium deposited during the late Tertiary and Holocene on the Pecos River Floodplain as the river migrated eastward in response to the uplifting Sacramento Mountains (Welder, 1983; Land, 2003, 2007; Stafford et al 2008). The transmissivity of the alluvial aquifer averages about 13,000ft^2/day with specific yields of 0.10 to 0.20 (Huff, 2004).

Besides these two basin aquifers, ephemeral streams and regional rivers contribute to area hydrology. The Pecos River is the major river which begins its 820.2 mi (1,320 km) progression in the Sangre de Cristo Mountains in northern New Mexico, flowing from the mountains and continuing southeast across New Mexico and into Texas across the High Plains and the Edwards Plateau physiographic provinces until it converges with the Rio Grande west of Lake Amistad (Stafford et al, 2009). The majority

of the baseflow into the Pecos River in the Roswell Artesian Basin is from the regional aquifers recharged in the mountains to the west and through tributaries west of the river. From 1905-1998, the base inflow has ranged from a low of 15,000 ac-ft/yr to 120,000 ac-ft/yr, with intense irrigation yielding decreased inflow (Longwood and Carron, 2003). Prior to development in the Basin, reports indicate that numerous perennial streams originating in the Sacramento Mountains fed the Pecos River. South of the Refuge, one of the major drainages of the Basin is the Rio Hondo. Formed by the confluence of the Rio Ruidoso and the Rio Bonito, this losing river is intermittent in the vicinity of the Pecos River.

DESCRIPTION OF THE STUDY AREA

The study area encompasses 1,240 acres in the Middle Track with sites including 36 sinkholes and two springs located north of Bitter Lake (Figure 1B). Ten of the sinkholes were studied in more detail. The Pecos River runs approximately 5,000 ft (1,524 m) to the east of the study area at an elevation ranging from 3,493 to 3,507 ft (1,065 to 1,069 m). Topographically, the area characterized by low relief, and has a slight slope toward the southeast, with ground elevations ranging from a high of 3,530 ft (1,076 m) near sinkhole 01 (SH01) in the northwest portion of the study area, to a low of 3,499 ft (1,066 m) near SH26 at the south-central part on the northern shore of Bitter Lake. Discrete congregations of salt cedar are the clearest indicators of the location of a sinkhole, as the remaining landscape is blanketed by alkaline grasses often encased with salts left behind by a now dry playa lake or from leaching from the soil during precipitation events. Such grasses create a visual uniformity among the plains. Sinkholes are also marked by numbered posts emplaced by Refuge staff.

With the change in the water table due to human and agricultural use, water levels at the discharge area also receded. In an effort to maintain the flow of water from the sinkholes into the now dry playa lake which partially covered the study area, a series of drainage channels were constructed (appearing as thin lines in aerial photographs; see Figure 3). With continued water table decline, such channels were no longer necessary, and were backfilled.

The sinkholes themselves exhibit a wide range of physical characteristics, including variations in shape, diameter, depth, and water conditions. Appendix B provides a more thorough description of the morphology and hydrochemistry of the ten sinkholes selected for this study.

CHAPTER 3: METHODS

FIELD SURVEY AND DATA COLLECTION

SITE SELECTION

During the initial site survey (October 2007), 19 of the 52 water-filled sinkholes found at the Refuge were visited and evaluated based on field observations and through the survey of basic hydrochemistry (temperature, pH, conductivity, alkalinity; see Table 1). From these, 10 were chosen for detailed investigation. The selection of this representative group considered several factors observed during the initial survey:

1.) Accessibility. Depth to water level from surrounding ground varies among sinkholes, as does the structure of the sinkhole opening. The water level of some sinkholes, for example, is approximately five meters below surrounding ground, while some sinkholes have walls which are nearly vertical, providing limited access due to wall steepness, rock instability, and terrestrial plants. To obtain necessary samples, a canoe would be deployed into the sinkhole, and samples collected from the canoe deck. All necessary sampling materials would be loaded into the canoe, carried from the field vehicle, and transported to the center of the sinkhole in an attempt to sample the deepest point. As one of the aims of this research was to describe water column structure, entering the sinkhole was necessary; thus, only those sinkholes into which a canoe could be deployed were considered. Likewise, due to restrictions of vehicle travel, all supplies needed to be carried to sinkhole access points.

2.) Physical Appearance. Appendix B provides a description of physical observations for selected sinkholes. Upon initial inspection of Refuge sinkholes, several characteristics were considered: water color; density, diversity of aquatic macrophytes;

fish presence or absence; sediment color and texture; diameter; ability to see sinkhole floor; and similarity to surrounding sinkholes.

3.) Physical Parameters and Alkalinity. During the initial site visit, surface water samples were collected, as were pH, conductivity and temperature. Proximal sinkholes with differing measurements and distanced sinkholes with similar measurements were considered. Water samples were tested in the laboratory for alkalinity, and results were used as a baseline of chemical variation to identify sinks of interest. Utilizing these characteristics provided a basic discussion of dissolved constituents in the water and temperature differences described possible differences in source waters, water column depth or structure and exothermic biological processes.

The ten sinkholes (SH) selected to be included in this study were: SH01, SH11, SH16, SH17, SH19, SH21, SH22, SH32, and SH37. Their relative location is depicted in Figure 3.

INITIAL SURVEY

The initial survey included 19 sinkholes and two springs. For each sinkhole, physical observations, pH, conductivity and temperature at accessible surface locations were noted along with ease of access and depth from surrounding ground to water level. At each surface location, water samples were gathered and a field-calibrated YSI multi-probe was used to obtain field measurements. Water samples were gathered at each surface location. An untreated sample was collected in a 150mL Nalgene sample bottle triple rinsed with sample water prior to collection, and filled with zero headspace. A second sample was collected using a 60mL syringe and passed through a 0.45uL filter into a different 150mL bottle (also triple rinsed with filtered sample water). The sample

was acidified using concentrated HNO_3. The untreated sample was analyzed in the laboratory for alkalinity. Table 1 provides field parameters, observations and alkalinities for this initial survey.

WATER SAMPLE COLLECTION

An entire suite of water samples from the ten selected sinkholes was collected in each of October 2008 and May 2009 sampling sessions. These two dates were selected to represent the period of time post snowmelt input and that following irrigation demands from the summer months. The aim was to compare two times during the year and identify whether or not changes in water chemistry were significant at points following aquifer recharge and irrigation extraction. A 12-ft, fiberglass flat bottom canoe (cleaned according to Refuge specifications to protect cross-contamination between sites) was lowered into each sinkhole. Once in the water, a GeoPump, marine battery, paddle and sampling box (containing bottles, 0.45uL filters, graduated plastic beakers, nitrile gloves, HNO_3, and measuring tape with plumb bob) were placed into the canoe. The canoe was rowed to the center of the sinkhole as the measuring tape lowered to approximate depth. Beginning at the surface, water samples were collected at one-meter increments throughout the water column. In the event the bottom depth was not at an even interval, a sample was collected as close to the bottom as possible without drawing sediment to the surface. For each depth, the pump was allowed to run to cleanse the lines prior to sampling; surface samples were collected first, without the use of the pump. Once lines were cleansed (at least two minutes circulating), a 1.0L graduated beaker was triple rinsed and then filled. From this, the untreated sample was collected (with the bottle also triple rinsed by the sample as it came from the pump). The bottle was submerged into the

collected water, and capped while in the water to avoid headspace. The beaker was then emptied and re-filled for collection of the filtered and acidified sample. Here, a 60mL syringe was triple rinsed and then filled with sample. A 0.45uL filter was affixed to the end, and water was pressed through to release several drops prior to filling the sample bottle. The second bottle was triple rinsed with filtered sample prior to filling the bottle. At least 30 mL of water was filtered. In some cases (e.g., SH17, SH21, SH22), an additional filter was needed to obtain a suitable volume. Upon completion of filtration, used filters were discarded, and samples acidified to pH <1.5 using concentrated HNO_3 acid. All samples were stored in coolers filled with ice packs, and were placed in a refrigerator at the research cabin until being transported to the laboratory.

GAS SAMPLE COLLECTION

Dissolved gas samples were collected using Giggenbach bottles, evacuated prior to beginning field work to hold a pressure of <750 mTorr using a GOW-MAC gas chromatography (GC) system. Once in the field, two collection methods were employed. The first utilized a series of PVC tube segments (~2m in length) which were joined in the field to form one long pole as they were being lowered into the sinkhole. Two clamps were screwed to the first segment and held open using a small piece of wire affixed with a nylon pull-line held at the surface. When released, the two clamps would hold closed a segment of flexible tube, trapping a small volume of water at depth. Once the tube segments were affixed and lowered to the desired level, the clamps were disengaged, and a sample collected. The tubes were then pulled to the surface and a Giggenbach attached to the free end of the sample tubing. The Giggenbach neck was flushed with DI water to prevent atmospheric contamination. The free end of the Giggenbach neck was closed

using a clamped piece of flexible tubing, also filled with DI water. At this point, the bottle was inverted, the stopper opened slowly, and isolated in the tube by the two clamps was drawn into the bottle. In those instances where the vacuum did not hold, the bottle was labeled with an X to identify it as non-functional. When the sample was fully drawn into the bottle, the stopper was closed tightly and the bottle prepared for safe transportation to the laboratory. In the field, six samples: SH17, 2.5m; SH11, 3.0m; SH19, 2.5m; SH25, 1.5m; and two from SH21, 3.0m [June 2008, May 2009]) were successfully collected using this method.

The second method was used during the February 2010 field session, and employed a GeoPump set at a low speed to draw water from a known depth to the surface without degassing the sample. The Giggenbach bottle was placed in line with the outflow tube of the GeoPump, and a free piece of tubing (~1.0 m in length) was attached to the other end of the neck. The water drawn to the surface was allowed to purge the space in the neck of the Giggenbach bottle, and once all air bubbles had been removed, the stopper was opened slowly. Tubing on both sides of the Giggenbach neck were carefully observed to ensure no accidental incidence of atmospheric gasses. Both dissolved gasses and sinkhole water itself was drawn into the bottle, and the stopper screwed tightly to secure the sample. A total of 10 samples were successfully collected using this method: SH19, 1.0m; SH19 2.0m; SH17, 1.0m; SH17, 2.0m; SH37, 6.0m; SH11, 3.0m; SH11, 6.0m; SH21, 2.0m; SH21, 3.0m; and Sago Spring.

MINERALOGICAL SAMPLE COLLECTION

A mineral precipitation experiment was designed to monitor the growth rates of minerals and the presence or absence of microorganisms associated with these minerals.

Well monitoring cartridges with 0.45µm filters were tied at 1.0m intervals to a nylon line pre-measured to the water column depths of five sinkholes: SH11, SH17, SH19, SH21, and SH37. As a substrate for growth, a sterilized (heat-treated) piece of unglazed ceramic tile was placed within each well cartridge, with a second fragment secured to the exterior of the cartridge. To ensure the cartridges would remain at their intended depth, a weight was affixed to one end of the water column line while a float was tied to the other end; in this configuration, the line hung vertically in the water column. The set up was deployed into the center of each sinkhole by slowly lowering the weighted end and feeding the line slowly to avoid tangling. The float remained at the surface, allowing the line to hang vertically straight for the duration of its deployment. The first set of mineral growth cartridges were deployed from 23 November 2008 until removal on 21 February 2009 (90 days); the second set was deployed from 21 February 2009 until removal on 16-18 May 2009 (84-86 days; 16 May: SH37; 17 May: SH11, SH21, SH19; and 18 May: SH17).

Upon removal, cartridges from the first suite were removed from the main line and were individually sealed in separate sample bags; this suite was used only to calculate relative growth rate. Samples from the second suite were used for scanning electron microscope (SEM) analysis, to calculate relative growth rate, and to preserve a portion of substrate for future microbial community analysis study (see Appendix C). Each cartridge was immediately isolated by carefully placing it into a separate sample bag to minimize disturbance and prevent cross-contamination. Samples were stored in a cooler filled with ice packs until processing in the research cabin. Here, after sterilizing a pair of tweezers between each sample, both the substrate from within the cartridge and

the fragment affixed to the exterior were removed and inserted into a test tube filled with a gluteraldehyde solution to preserve microbial morphologies for SEM evaluation. Some substrate fragments were too large to fit into the test tubes. In these cases, a piece of the mineral "crust" was removed and inserted into the preservative. The remaining portion was placed into a sterile petri dish and sealed using Parafilm or labeling tape. As the exterior of the cartridge also served as substrate for mineral growth, the remaining portion was maintained in its original sample bag.

SONDE USE AND DEPLOYMENT

YSI sondes were deployed to assess water column structure and to collect several hydrochemically-important parameters at high temporal resolution. Temperature, TDS, conductivity, pH and depth were recorded during each deployment, as was DO (though fouling prevented complete DO analysis). While addressing water column structure, the sonde was programmed to take measurements at one second intervals, and was lowered slowly from the side of the canoe using a pre-measured line marked incrementally every 0.5m. Similarly, at each depth at which water samples were collected, temperature, pH, conductivity and TDS were recorded using a multi-probe. The use of a sonde allowed for these measurements to be recorded at a higher resolution along the water column.

In October 2009, a single sonde was left in place in SH17 for a period of seven days (recording measurements every 225 seconds). In February 2010, two sondes were deployed simultaneously in SH17 and SH19 (recording every 240 seconds) to determine whether changes in depth and other parameters were within comparable ranges between these two neighboring but physically unique sinkholes. In both deployments, a length of coated steel cable was drawn across the center of the sinkhole, with each end secured to

the shore using a tent spike. A tether line was used to draw the sonde across the center line to the estimated deepest point. This tether line assured a means of retrieval should the cross line fail during deployment and allowed the sonde to be emplaced without use of the canoe. Once the sonde was in place, the tether line was tied to the sinkhole number marker found at the shore. In this configuration, the sonde collected data over the designated 14-day time frame. After the collection period, the sonde was removed, was cleaned and connected with the 650 handheld computer to terminate unattended sampling and to download data. Once in the lab, data was transferred to a PC with YSI interface for analysis.

LABORATORY ANALYSIS OF COLLECTED SAMPLES

All water, gas and mineral samples were analyzed in-house at the Department of Earth and Planetary Science at the University of New Mexico (UNM), with a selected group of samples from the October 2008 suite analyzed at the UNM Biology Annex for nutrients.

MAJOR IONS

Sinkhole waters were universally very high in salinity with major ion concentrations generally above detection limits for the Perkin-Elmer ICP-OES (ICP, for cation analysis) and the Dionex DX-500 Ion Chromatograph (IC, for anion analysis); thus, all samples were diluted prior to analysis. A small volume of undiluted sample (typically </= 1.0mL) was dispensed into a clean volumetric flask and diluted with 18Ω deionized (DI) water. A piece of Parafilm was stretched over the flask opening, and the flask was inverted three times to mix after which the diluted sample was transferred into vials for processing using the IC and ICP. In some cases, multiple dilutions were needed to account for high concentration constituents (e.g., sodium and chloride).

Alkalinity was measured with the End Point Titration method with an Oakton Ion 6 Acorn Series pH/Ion/ºC Meter and standardized sulfuric acid (H_2SO_4). The majority of samples were titrated with 0.02N H_2SO_4; however, samples from SH17, SH21 and SH22 were titrated with 0.2N H_2SO_4 due to their high alkalinity.

Water chemistry was input to Phreeqc (Parkhurst, 1997) with the added capability for high ionic-strength waters. Waters were speciated, and the saturation state with respect to several minerals as well as PCO_2 was tabulated (see description below).

STABLE ISOTOPES

Stable isotopes of oxygen and hydrogen were analyzed in the UNM Stable Isotope Laboratory. Oxygen isotope ratios in waters were determined using the CO_2 equilibration technique. The water samples (1 mL each) were injected in borosilicate vials equipped with rubber septa, which were previously purged with He- CO_2 gas mixture (0.5% CO_2). After 24 hours equilibration at 25°C, the CO_2 was measured by continuous flow isotope ratio mass spectrometry using an automated CombiPal – Gas Bench system coupled to a Thermo Finnigan Delta Plus mass spectrometer. The results were corrected using the Fiji heavy isotope standard. Hydrogen isotope ratios were measured using a Delta^{plus} on-line chromium reduction system utilizing a mesh chromium HDevice reactor as described by Nelson and Dettman (2001).

DISSOLVED GASSES

A GOW MAC GC system modified to specifically analyze volcanic and hydrothermal gases was used to determine partial pressures of eight gasses: He, Ar, N_2, O_2, H_2, CO_2, CO, and CH_4 through utilization of a Thermal Conductivity Detector (TCD) and a Flame Ionization Detector (FID, for CO and CH_4). The system utilizes two sample

loops in two columns with two carrier gases both of which were calibrated prior to analysis by employing calibration gases with known concentrations or partial pressures of blended gases. Each sample was placed on the GC, and a portion of the gas was allowed to enter lines to expand by opening and then closing the Giggenbach bottle. The samples were transferred into the detectors, driven by carrier gases. Following processing, the partial pressures of gases present in the sample was calculated in mBar for each sample based on the calibration curve for each gas.

SEM ANALYSIS OF MINERAL SAMPLES

A JEOL 5800LV Scanning Electron Microscope equipped with an Oxford Analytical ultrathin-window EDS and an Oxford Isis 300 X-ray analyzer were used to analyze minerals grown through the in-situ precipitation experiment for mineral presence and composition and to identify microbial morphologies. Mineral precipitates collected in the field were preserved in 2% gluteraldehyde solution. In 1.5ml eppendorf tubes, gluteraldehyde was decanted for 12 samples (SH11, 2.0m; SH19, 0.0m; SH21: 0.0m, 1.0m, 2.0m, and 3.8m; SH37: 13.0m and 14.0m; SH17: 0.0m, 1.0m, and 2.0m). Samples were washed to replace the gluteraldehyde with alcohol by allowing samples to soak in five successive alcohol solutions, each of increasing alcohol concentration, for five minutes each; these washes were followed by three washes of 100% anhydrous alcohol. Samples were then prepared for critical point drying (CPD) by washing twice and allowing to soak for five minutes with anhydrous acetone followed by an overnight rest in a third anhydrous acetone bath. The next day, samples were moved to a plastic sieve column with a small piece of anhydrous-acetone-soaked lens paper and were placed in the CPD chamber for 25 minutes. Following drying, samples were affixed to SEM stubs

using carbon tape.

To allow for viewing with the SEM, samples were coated with gold-palladium (Au/Pd, 80/20%). Stubs with samples were inserted into the spattering unit wherein a strip of Au/Pd was subjected to an ionized gas within a vacuum chamber; atoms from the metal were removed and replaced onto the sample allowing each sample to be plated with a thin layer of Au/Pd. Once all of the 12 samples were effectively coated (some were coated twice or had a small amount of carbon paint applied to bare areas), they were viewed with the SEM. Images were assessed for dominant minerals present, mineral shape and form, and microbial presence and morphology.

CHAPTER 4: RESULTS

FIELD PARAMETERS

Field parameters (location, temperature, pH, conductivity) for all samples collected during the October 2008 and May 2009 field sessions are located in Table 2, along with Regional data from published studies (Land, 2010 [Refuge groundwater]; Newton et al., 2009 [Sacramento Mountain groundwater]; Yuan and Miyamoto, 2008 [Pecos River]), provided for comparison; results from the initial site survey are included in Table 1. Field measurements consider all depths for the 10 representative sinkholes, for a total of 55 samples per suite. A mechanical problem with the multi-probe during the October 2008 field session prevented field measurements for five (SH17, SH19, SH21, SH32 and SH37) of the 10 sinkholes. Conductivity and pH were measured in the laboratory, while an approximate temperature was calculated based on recorded May 2009 values, and the average seasonal temperature change of the other five sinkholes. Table 3 presents the range of values observed for each field session, including the abbreviated February 2009 vertical profiling and surface spatial survey. A rain event occurred the night before the October 2008 sampling of SH17, SH32 and SH37 (from 6.0m to surface).

Due to pump failure, five (of the intended 10) sinkholes were sampled in February, 2009: SH17, SH19, SH21, SH22 and SH25. Also in February, field parameters were recorded at the surface for 36 sinkholes and two springs. Table 3 displays these measurements. Figure 4 presents the spatial distribution of select hydrochemical parameters of sinkholes and springs sampled during February 2009.

Based on field parameters, water column structure generally organized bi-modally, with seven of the 10 representative sinkholes having well-mixed water columns, while three sinkholes (SH17, SH21, and SH22) demonstrating both physical and chemical partitioning. Sinkhole 22 is shallow (1.5m total depth), but it presents the same chemical character as SH17 and SH21, suggesting that if water level was deeper, it too may display obvious stratification. Figure 5 compares two sinkholes representing the opposite ends of the spectrum: SH37 is "fresh" and reflects local groundwater conditions (e.g., Sago Spring), while SH21 is saline and stratified. Regardless of sinkhole, water column structure was consistent during both the October 2008 and May 2009 field sessions; however, SH16 presented moderate variation, which may position it as a transitional configuration between the two modes. Appendix G presents vertical profiling plots for all sinkholes and sampling sessions. Among sinkholes, the following was observed for temperature, pH and conductivity:

MAJOR IONS

Major ion concentration for all of the 110 water samples from the October 2008 and May 2009 suites of samples are included in Table 2, along with published studies in the region (Land, 2010; Newton et al., 2009; Yuan and Miyamoto, 2008). Water chemistry provided details on the variation among sinkholes, both seasonal changes and water column structure differences. The dominant cation was sodium while the dominant anion was chloride. Sinkhole water chemistry is dominated by Na-Cl geochemical facies with the Ca-SO_4 facies being subdominant.

Of the 110 samples, 38 samples (34.5%) had a percent charge balance error of two or less; 58 samples (52.7%) had an error of 2-5%; and 14 samples (12.7%) had an

error of greater than 5%. For all waters, [Cl-] surpass safe drinking water limit of 250 ppm for potable water (USEPA, 2002) and are higher than water from surface springs present at the Refuge (e.g., Land [2010] reports Sago Spring having a [Cl-] of 2,050 ppm). In those sinkholes which exhibited stratification as described by physical parameters, major ions followed a similar distribution, with both SH17 and SH21 showing vertical structure of the water column (see Figure 6). Among sinkholes with well-mixed water columns, there was variation in major ion content, with SH32 and SH37 having water more closely resembling surface springs and nearby wells, while SH16 and SH11 had higher concentrations of dissolved constituents, but were not stratified. Between the two sampling sessions, concentrations remained relatively consistent, with only minor fluctuations occurring.

For waters collected from SH17, SH19, SH21, SH32 and SH37 during the October 2008 field session (30 samples), concentration of NH_4, NO_3 and PO_4 were analyzed. Results from all samples are presented in Table 5, and the vertical distribution of these parameters is presented in Figure 7. Biologically significant concentrations of these nutrients were found in stratified sinkholes (SH17, SH21).

STABLE ISOTOPES

Stable isotope results are presented in Table 2 along with published studies in the region (Land, 2010; Yuan and Miyamoto, 2008; Newton et al, 2009) for comparison. Seasonally, isotope concentration varied among all sinkholes, with heavier values, on average, occurring in the October 2008 sample suite; ranges of isotope values are presented in Table 6. Most sinkholes had consistent values throughout the water column, although SH17 and SH21 trended with depth toward heavier values, and SH19 (1.0m),

SH11 (3.0m) and SH37 (8.0m) each had a prominent spike during both seasons, implying a chemocline or region of mixing. Profiles of these values are presented in Figure 8. Seasonal variation between depth profile values within a single sinkhole were typically <1.0 ‰ for $\delta^{18}O$ and <5.0 ‰ for δD.

DISSOLVED GASES

Sixteen water samples were collected for dissolved gas analysis (CO_2, CH_4, N_2, Ar, CO, O_2, H_2, and He). These samples were collected over the course of three sampling sessions: June 2008 (one sample, SH21, 3.0m; May 2009 (five samples; SH11, 3.0m; SH17, 2.5m; SH19, 2.5m; SH21, 3.0m; and SH25, 1.5m); and February 2010 (ten samples; SH11, 3.0m, 6.0m; SH17, 1.0m, 2.0m; SH19, 1.0m, 2.0m; SH21, 2.0m, 3.0m; SH37, 6.0m; and Sago Spring). Partial pressures and dissolved gas concentrations for all 16 samples is found in Table 7. Two samples were anaylzed for helium and other noble gas isotopes, as well as ^{13}C (D. Hilton, Scripps Institution of Oceanography; L. Crossey personal communication 2012). These data are included in Table 8. The dominant dissolved gas was CO_2 with trace amounts of He occurring in SH17, SH19, SH21 and Sago Spring. The majority of the samples showed some presence of atmospheric gases as indicated by the large partial pressure of N_2 which is likely sourced from diffusion of atmospheric gases across the sinkhole surface as no gas was present in pump lines and tubing during sampling.

MINERAL PRECIPITATION

In SH11, SH17, SH19, SH21 and SH37, the two deployments of the precipitation substrates rendered mineral growth that varied both among sinkholes and with depth within individual sinkholes. Informally characterized, mineral growth was classified by

the mass of dried precipitate present on the well cartridge after removing the interior and exterior artificial substrates and hanging lines. Mass of a blank cartridge was subtracted from the total mass of the cartridge and formed minerals; approximate masses are presented in Appendix C. Among the 35 sampling locations and depths, the approximate rate of precipitation ranged from 0.0001 g/day (SH37, 4.0 m) to 0.0191 g/day (SH21, 3.8 m) for the winter deployment (23 November 2008 to 21 February 2009) while rates ranged from 0.0013 g/day (SH37, 12.0 m) to 0.2838 g/day (SH21, 2.0 m) for the spring (21 February 2009 to 16 May 2009) deployment.

SCANNING ELECTRON MICROSCOPE (SEM)

Both mineral and microbial morphologies were observed on the 12 samples prepared for and analyzed by the SEM. Mineral morphologies observed included massive amorphous fragments as well as well-formed crystals. Use of EDS on targeted minerals from SH11 (2.0m), SH17 (0.0m, 1.0m, 2.0m), SH19 (0.0m), SH21 (3.0m), and SH 37 (13.0m) indicated the dominant precipitate was gypsum, although dolomite was detected in SH19 at 0.0m.

Four of the 12 samples clearly exhibited biological morphologies, predominantly those of diatoms. In SH11 at 2.0m, an assemblage of diatoms was identified via SEM, with the most prominent species being Navicula –spp, although Brachysira was also observed. In SH17 at 2.0m, two species of Navicula were observed. One species of Navicula was observed in SH19 at 0.0m. In SH21 at 1.0m, one species of Nitzschia and a tangle of filiform fungi wrapped around massive gypsum blocks were recognized. Images of these microorganisms may be found in Appendix D. Diatoms were not limited to deep samples.

WATER QUALITY MONITORING WITH AUTONOMOUS SENSORS (SONDES)

Sondes were used in two different applications: lowering slowly to acquire a higher resolution profile of sinkhole water column than 1.0-m discrete sampling; and measuring field parameters over time to identify changes or trends. When lowered through the water columns of SH11, SH17, SH19, SH21 and SH37, measurements indicate that the water column exhibits a structure similar to that observed with discrete sampling. During the two-week deployment in February/March 2010, two sondes simultaneously measured conditions in SH17 and SH19, suspended at 1.24 m and 1.53 m depths, respectively. Over this period, recorded depths, pH, and conductivity remained essentially constant for each sinkhole. Temperature expressed a slight (0.5^{o}C) diurnal response to solar heating. Conductivity in SH17 demonstrated daily fluctuation on the same period as temperature change, with daily low temperature corresponding with that of higher conductivity (Figure 9). While dissolved oxygen was recorded, fouling of the probe (likely attributed to high salinity) prevented accurate measurement.

GEOCHEMICAL MODELLING

Physical parameters and major ion concentrations were incorporated into PHREEQC (Parkhurst, 1995) to model geochemical speciation of dissolved constituents. Saturation indices (SIs) modeled by PHREEQC for all samples are presented in Table 9; depth profiles comparing SIs for SH37 and SH21 are presented in Figure 10. All waters of the October 2008 sampling suite were saturated with calcite and gypsum, while undersaturated with halite. Samples from all depths in SH37 and SH32 at 1.5 m were undersaturated with magnesite, with the remaining 70.9% (39 samples) saturated. Of the samples in the May 2009 suite, 74.5% (41 samples) were saturated with calcite; 72.7 %

(40 samples) were saturated with gypsum; 34.5% (19 samples) were saturated with magnesite; and all samples were undersaturated with halite. Geochemist's Workbench (GWB; Bethke, 2008) was used to plot Piper diagrams, compute solution densities, and perform additional speciation calculations.

CHAPTER 5: ANALYSIS

MAJOR IONS

For all sinkhole waters, regardless of depth, the dominant hydrochemical endmember composition is Na-Cl, as can be seen in Figure 11 which depicts the hydrochemistry of regional groundwater, Sacramento Mountain springs, and the Pecos River, along with sinkhole and local spring samples from the Refuge. Water from sinkholes is chloride type, occupying the right boundary of the Piper diagram (Drever, 1997), with some sinkholes encroaching sulfate type category. Sinkholes that plot close to ~80% chloride (e.g., SH17, SH21, and SH22) are those that also exhibit stratified water column structure, highest total dissolved solids (TDS) and conductivity, and enrichment in stable isotope concentration. Meanwhile, those that plot at ~50% chloride (e.g., SH37) present lower TDS and conductivity (comparable with Refuge surface spring hydrochemistry), and have a uniform and well-mixed water column. Figure 11 displays the relative role of TDS on sinhole endmember composition. A similar relationship exists for cations, with stratified sinkholes predominantly sodium type, and well-mixed sinkholes are progressively higher in calcium. Waters contain substantial dissolved inorganic carbon (DIC), representing elevated PCO_2 conditions; however, the Piper presentation illustrates that the waters are dominated by sulfate and chloride.

Regional groundwaters (also illustrated) are interpreted to be the initial source water for the sinkholes. The hydrochemical facies of regional groundwater is Ca- HCO_3 type due to dissolution of the San Andres limestone, input of external CO_2 (Crossey et al., 2009), and modest interaction with evaporite minerals (gypsum from Permian bedrock leading to the spread of waters along the left edge of the piper diagram); those

groundwater point that exhibit greater water/rock (W/R) interaction plot closer toward the sulfate apex. Waters of similarly high proportions of calcium compared with recharge area groundwater - but with increasing proportion of sulfate and chloride - are surface springs within the Roswell Artesian Basin. These springs, while sourced from the groundwater, interact with overlying lithological units. Water from the Rio Hondo whose drainage basin and convergence with the Pecos River occurs south of the Refuge, is of $Ca\text{-}SO_4$ type hydrochemical facies (represented by open blue circles) and accords with the springs exhibiting high chloride proportions. The Pecos River, alternatively, adjoins with the sinkhole waters that are less strongly chloride type (e.g., water from SH37 and the Pecos River overlap).

The dissolution of evaporate minerals (including gypsum and halite) from Permian bedrock is a dominant influence on bulk water chemistry, although the introduction of salts from Quaternary alluvium or surficial transport of minerals present in the surrounding soil are also potentially contributive. Chloride concentrations in the Roswell Artesian Basin can range from 15 ppm (western freshwater portion of the aquifer) to 7,000 ppm (near Roswell) with chloride concentration increasing with increased depth within the aquifer (Land 2007). Between Roswell and the Pecos River, chloride concentrations may fluctuate by more than 1,500 ppm during a single irrigation cycle (Welder, 1983; Land, 2007). Salts and evaporite minerals are deposited on the surface by agricultural irrigation using groundwater from the artesian carbonate aquifer. Irrigation from the shallower alluvial aquifer utilizes water sourced from a combination of upward flow from the carbonate aquifer through the Seven Rivers formation, precipitation infiltration, and re-infiltration of irrigation water. Thus, these “younger”

minerals may trace their origin to Permian-aged evaporites, although in their current, and altered state, their contribution to overall sinkhole water chemistry is minimal. Similar to halite, low to moderate Ca-SO_4 composition contribution further reflects the dissolution of bedrock evaporites.

Samples were generally well-grouped by sinkhole, regardless of sampling suite or depth, conceding the consistency of hydrochemical signature despite measured differences in major ion concentration. Between the two sampling suites, the majority of waters exhibited slightly increased major ion concentration during May 2009. This is inconsistent with the seasonality observed in the artesian aquifer which, according to Land and Newton (2008), has [Cl-] lowest in the spring, and highest in the fall upon conclusion of the irrigation season. The sinkhole waters themselves are chemically similar to artesian aquifer water, but the seasonal inconsistency suggests that the water within the sinkholes is not a transient volume of water where it is filled by an artesian spring and subsequently drained by a secondary conduit or lateral seepage thereby continuously refilling the sinkhole with unaltered groundwater. Instead, the groundwater enters the sinkhole where it remains. Water that is removed is replaced as the sinkhole recharges consistent with local hydraulic head conditions maintaining consistent water levels. Some lateral seepage is also likely, but this progression may be hindered by impermeable strata or the subsequent clogging of flow paths by biological and authigenic mineral debris. In general, once water enters a sinkhole, it remains until it is altered by environmental and climatic factors common to all sinkholes. The aggregate data suggest that sinkholes do receive continued groundwater input at reduced levels. As the [Cl-] in sinkhole samples did not follow the same trend as that in groundwater, the implication is

that the input rate of groundwater is not high enough for chemical seasonality observed in the groundwater to be detected in sinkholes (minimum sinkhole TDS is ~10,600 mg/L; groundwater TDS values range from <500 ~6,000 mg/L).

PHREEQC

The use of PHREEQC to interpret dissolved constituents and assess the saturation of selected mineral species assists in evaluating mineral presence within a water sample. Major ions, sample temperatures, and pH are inputted into the PHREEQC model, and based on sample conditions the saturation index (SI) for various mineral species is calculated. The log PCO_2 for samples is calculated similarly, and offers insight as to the equilibrated CO_2 in the sample based on overall chemical composition (DIC) and field measurements. While the dominant endmember composition is Na-Cl, all waters are undersaturated with respect to halite. Sulfate is the next most abundant anion, and is partly controlled by precipitation of gypsum (indicated by slight supersaturation with respect to gypsum in some sinkholes). As is described below, sinkholes are observed to actively precipitate gypsum in the water column. Bicarbonate is the least dominant anion, likely also controlled partially by calcite precipitation, groundwater influx, as well as biological photosynthesis and respiration processes. PHREEQC predicts waters to be supersaturated with respect to both calcite and dolomite (though dolomite is kinetically unable to precipitate, indicated by the extremely high degrees of supersaturation observed [Drever, 1997]). Depending on the sinkhole, the saturation of both calcite and dolomite changes seasonally. Generally, the SIs for calcite were higher during the October 2008 suite, yet waters in both SH11 and SH37 varied little seasonally. Dolomite saturation was also higher among the September 2008 suite for SH01, SH16, SH17, SH19, SH21, and

SH32, while waters within SH11, SH25, and SH37 exhibited little variation. This is attributed to the seasonal differences in PCO_2 and pH. Another factor affecting dolomite supersaturation is the increasing Mg/Ca ratio as a consequence of the precipitation of both calcite and dolomite within the sinkholes.

In general, mineral saturation increased with depth for each species. Dolomite SIs showed a decrease with depth for SH37 from 7.0 m to 14.0 m as compared to the May 2009 suite, and SH22 had a much higher surface value in October 2008, with remaining water column values maintaining consistent saturation. Both gypsum and halite SIs varied little seasonally among all sinkholes. Lower values during the May 2009 session are expected as pre-irrigation high groundwater levels and snowmelt recharge bring fresh water into the system. As no discernible decline in water level was measured between the two field sessions, the source water input was sufficient to override water loss due to evaporation or hydrologic outflow. Higher saturation during the October 2008 sampling suite indicates increased mineral species saturation with a seasonal control.

The change in mineral saturation is partially in response to temperature and pH fluctuation, and to increased evaporation and irrigational water draw during the summer. During the May 2009 sampling session, temperatures were on average 3.9^{o}C warmer for all depths, while pH values remained consistent. The pH values measured for SH01, SH21, and SH32 were at least an order of magnitude higher in October 2008 for all depths. The higher temperatures in May 2009 are the result of progressive seasonal warming, although one would expect October measurements to be warmer, reflecting the summer heating cycle. While water samples were not processed during the February 2009 field session, both pH and temperature were measured in the field for five sinkholes

at all depths. Only SH17 had comparably warm temperatures at its two deepest depths, with SH19, SH21, SH22 and SH25 uniformly cooler as compared to October 2008 values. This indicates that water column cooling does occur, although not significantly enough to provoke extensive mixing; water column structure was maintained among all five of these sinkholes when compared with major suite data. Bednarz (1979) suggested that the high salinity in meromictic sinkhole lakes such as SH19 (also in this study) and SH26, may also override natural mixing tendencies.

The observed enrichment reflects the bulk water response to high evaporation rates during the summer months. The average annual pan evaporation rate (from 1950-2005) for the WRCC Bitter Lakes WL Refuge monitoring site was 88.89 in/yr (225.8 cm/yr), with the highest average monthly evaporation occurring in June (12.62 in [32.1 cm]) and the lowest in December (2.50 in [6.4 cm]). Evaporation rates are over six times greater than precipitation (rainfall) rates in the vicinity of the Refuge. As the October 2008 suite represents the post-irrigation scenario and the timeframe following long days of direct sunlight, increased salinities reflect evaporative concentration. As was observed using the SEM, minerals precipitated were largely of gypsum composition. The comparatively low SIs indices and lack of seasonal variability for gypsum among all sinkhole depths, regardless of season, suggests continued precipitation rather than episodes of dissolution.

STABLE ISOTOPES

Stable isotope values ($\delta^{18}O$ and δD) for sinkhole waters plot below the global meteoric water line (GMWL) ($\delta D=8\delta^{18}O+10$ [Craig, 1961]), but progress along a uniform and linear pattern (Figure 12). The local meteoric water line (LMWL), δD =

$8.88\delta^{18}O + 25.0$, based on Land and Huff [2010]) is also presented. The grouping of the waters and the slope of the regression through the groups suggests that all sinkhole waters are being exposed to and evaporated under a common set of environmental conditions, with some sinkholes (those with isotopic enrichment) experiencing these factors more intensely or for a longer period of time. Isotopic values were relatively uniform among all depths within a single sinkhole; however, much like what is observed physical and chemical values, water column stratification of stable isotopes exists in some sinkholes (SH17 and SH21). During both sessions, water samples from SH17 and 21exhibited higher isotope values ($\delta^{18}O$ values of 8 ‰ compared to -8 ‰ for Sago Spring, [representative of area groundwater]). When data are compared to the values presented by Land (2010), two points (Bitter Lake and Lake St. Francis) grouped well with the sinkhole trend, while the remaining points were located near the intersection of the sinkhole regression line with the LMWL. Waters samples from SH37 grouped most closely to the LMWL, and SH21 occurring furthest from the intersection.

Water data from prior studies investigating the isotopic character of the Pecos River springs and wells near the Refuge, and springs and wells in the recharge areas of the Sacramento Mountains suggest that sinkhole waters share similar characteristics with groundwater and river water, and that waters present are evaporative byproducts of the original source waters. Data from the Pecos River south of the Refuge (from Yuan and Miyamoto, 2008) follow the sinkhole regression trend (Figure 13). What this suggests is that the water present in the Pecos River is of common source as that which fills the sinkholes. However, the line falls slightly below the grouping of source water points from the groundwater and surface springs. What this means is that as the groundwater flows

into the Pecos River at its discharge near Roswell, and is further evaporated and enriched as it flows south. A slight shift of Pecos River $\delta^{18}O$ values as compared to the projection of groundwater values, and the consistency of this shift with the sinkholes regression suggests that both sinkholes and the Pecos River are experiencing the same evaporative alteration, and that the water in both is similarly sourced, possibly from a combination of groundwater inflow into both features and lateral seepage exchange from the sinkholes to the Pecos River.

Following the Pecos River south into Texas, water exhibits an increase in isotope vales, with groundwater discharge in the area of the Roswell Artesian Basin, surface transport, and evaporation altering the river water. Tritium data of Land and Huff (2010) demonstrate that most sinkholes are below detection in tritium; indicating that the sinkhole waters are older than 50 years. Carbon-14 dating results from the same study are complicated by additions of 'dead' carbon from limestone dissolution and external CO_2 sources, but are interpreted by Land and Huff to indicate groundwater ages of hundreds to thousands of years in the few sinkholes measured.

The slope of evaporation trajectories extending from the GMWL ranges from 3-5 (Sharp, 2007). As is shown in Figure 12, the slope of the regression representing sinkhole waters is 3.387; thus, the sinkhole waters are influenced by evaporation. The increase in $\delta^{18}O$ may also be attributed to the progressive equilibration of oxygen in the water with carbonate rocks (water-rock interaction; Sharp, 2007). Conversely, Hoy and Gross (1982) conclude that stable isotope values (in particular, $\delta^{18}O$) of groundwater in the Roswell Artesian Basin represent present climatic conditions and do not reflect water-rock

interaction with the carbonate bedrock. Thereby, the oxygen shift among sinkholes is mainly due to evaporative alteration of the source water.

Isotopic studies along the extent of the Pecos River describe the major source waters of the river arising from a combination of snowmelt from winter precipitation and runoff from monsoonal rainfall (Yuan and Miyamoto, 2008). In Figure 13, points from the Pecos River near the Refuge follow the same trajectory as sinkhole waters, suggesting the sinkholes have the same source water as the Pecos River, and that water within the Pecos River is subjected to evaporative alteration. Alternatively, the Pecos River is influenced by the contribution of discharge from the saline Bitter Lake wetlands. Seasonally, the isotopic data collected from the Pecos River during the winter months indicates a reduction in evaporation during this time, while the isotopic composition of the river water usually increases substantially from upstream to downstream and from cold to warm seasons due to the effects of evaporation (Yuan and Miyamoto, 2008). Among sinkholes, there is a slight post-irrigation shift toward the GMWL which is inconsistent with the seasonality observed along the Pecos River; nonetheless, the isotopic content remains similar regardless of season. The oxygen shift among river water samples is lower than that of sinkhole water, but nearly converges with the sinkhole grouping for southern river sites. Groundwater samples from Land (2010) show a slight shift as compared with the LMWL, but also align well with both the sinkhole water groupings and river water samples. The $\delta^{18}O$ of river water is on average 2‰ heavier than that of local precipitation, 4‰ heavier than that of ground water, and probably 8‰ heavier than that of the mountainous headwater; the heavier $\delta^{18}O$ in river water indicate the presence of evaporative enrichment (Yuan and Miyamoto, 2008).

The increase in $\delta^{18}O$ of groundwater in a confined carbonate aquifer as compared to its meteoric recharge waters may be attributed to water-rock interaction and dissolution of marine carbonates which have much higher $\delta^{18}O$ as compared to recharge waters (see Figure 12, from Bauer et al., 2007). During water-rock interaction processes involving carbonates, [Cl-] and δD are conservative parameters that can be used to evaluate fluid mixing (Musgrove and Banner, 1993). Figure 14 shows the relationship between these two components for sinkhole water and regional groundwater sources, chloride concentration for sinkhole samples encompass a wide range of values as compared with their δD values which occur within a relatively narrow range. The opposite is observed for springs, groundwater, and portions of the Pecos River where [Cl-] ranges are slim while δD values cover a larger range. In sinkholes like SH21 where the [Cl-] values are very high, the proportion of [Cl-] and δD confirm the role of evaporation.

WATER COLUMN STRUCTURE

The water column structure of a given sinkhole remained constant, regardless of physical measurement, chemical parameter or sampling season. See Appendix E for vertical plots presenting field and chemical parameters by sinkhole depth.

THERMAL STRATIFICATION

While subsurface connectivity may exist, sinkholes geochemically behave as independent water bodies. The majority of the sinkholes included in this study: SH01, SH11, SH16, SH19, SH25, SH32, and SH37, exhibit warm polymictic mixing characteristics due to their shallow depths, continuous circulation and lack of freezing during the winter (Wetzel, 2001). As most sinkholes are less than 4.0 m deep, water levels are generally too shallow to fully develop thermal or chemical stratification.

Figure 5 compares the change of temperature with depth for both sampling sessions for SH21 and SH37 which comprise both ends of the stratification spectrum, with SH37 being well-mixed and most closely reflecting Sago Spring-like water (as compared with other study sinkholes), and SH21 exhibiting notable stratification and highly altered water. A comparison of the depth profiles for all sinkholes may be found in Appendix E. During the October 2008 collection, waters were warm near the surface but temperatures decreased with depth for SH01, SH16, SH19, SH21, SH32 and SH37; whereas SH17, SH22, and SH25 were cooler at the surface and showed an increase in temperature with depth. Only SH11 exhibited uniformity in temperature throughout the water column. In May 2009, the distribution was slightly different, with SH19, SH21, SH22, SH25, SH32, and SH37 presenting warmer temperatures at the surface with a gradual cooling to depth, and only SH17 gradually warming with depth. Within SH01, SH11, and SH16, temperatures were more or less uniform. These three sinkholes all have a depth of or over 3.0 m, and the dissimilarity in thermal water column structure between October and May for SH01 and SH16 suggests the occurrence of seasonal mixing, with SH11 undergoing continual circulation.

Temperatures recorded during February 2009 offer clearer insight as to how sinkhole waters respond seasonally. Waters within SH21, SH22, and SH25 were cool at the surface and gradually warmed with depth; those in SH19 were warm at the surface and cooled with depth; and SH17 was cool at the surface with a warm spike at 2.0 m depth. Among these five sinkholes, thermal changes do not follow a predictable pattern when compared with other sampling months. This suggests that while sinkhole water is susceptible to seasonal thermal responses, mixing patterns are unique to an individual

sinkhole and those which present a well-mixed water column maintain that structure year-round. Interesting to note is that the temperature at depth for all but SH37 is approximately the same, with SH37 nearly 4.0^{o}C cooler, during the May 2009 field survey, while bottom temperatures in October 2008 ranged from 12.9^{o}C (SH37) to 23.9^{o}C (SH22).

CHEMICAL STRATIFICATION

Calculated density and measured conductivity, pH and [Cl-] of sinkhole waters provides a clear image of the chemical water column structure. The measured conductance of the water is directly proportional to the dissolved ions present (the higher the conductance, the greater the TDS, and density). The pH variation is a function of the photosynthesis and respiration of the biotic community as well as the alkalinity of the water. Chloride stands as the dominant anion within both sample session suites and is a conservative parameter when evaluating groundwater characteristics; none of the sinkhole water samples reached halite saturation.

Density. With the exception of SH21 and the surface sample of SH17, water density was greater during the October 2008 sampling session for all sinkholes regardless of depth. Sinkholes retained a well-mixed water column structure below a density of 1.035 g/cm^3. Unlike other parameters, SH16 exhibits notable stratification in water column structure, with a density spike at 2.0m during the October 2008 sampling session. Similarly, SH11 expressed slight increases in density at 4.0m and 7.0m during the October 2008 session. These shifts correspond with the 1.035 g/cm^3 density, suggesting that this value may be the threshold after which a sinkhole begins to adopt a stratified water column. As density relates to the mass per volume of the sinkhole water, those

waters containing high amounts of dissolved components will likewise have a higher density. Among stratified sinkholes, density increased with depth with the exception of SH17, 2.0m during the October 2008 session where the density decreased by ~0.005 g/cm^3. The observed density gradients are related to TDS increase with depth as "heavier" water sinks. Solar heating of portions of the water column closer to the surface may also contribute slightly to these gradients.

Conductivity. During the both sampling seasons, SH17, SH21 and SH22 exhibited progressively higher conductivity with increased depth. The remaining sinkholes presented minimal variation with depth, with SH16 exhibiting mild trend toward higher conductivity. For those sinkholes without a uniform water column, the distribution of conductivity follows the density gradient with the sinking of waters containing higher concentrations of dissolved constituents. In SH16, the slight shift away from uniformity may indicate the sinkhole is chemically evolving, and will in time adopt characteristics similar to SH17, SH21 and SH22. Conductivity measurements recorded during February 2009 were consistent with other sampling seasons, indicating that chemical mixing is not noticeably impacted by seasonal controls.

pH. Only SH11 maintained pH uniformity within the water column and consistency between measured values for both sampling seasons (see Figure 5). In May 2009, SH21, SH22 and SH25 had a marked increase in pH mid-water column (2.0 m, 1.0 m, and 1.0 m, respectively), as well as an overall lower pH as compared with October 2008 (which showed a gradual decrease in pH with depth). In SH17, there was not a clear progression in either season, although at a depth of 1.0 m the pH was comparatively low (7.53) in October 2008 and comparatively high (7.81) in May 2009 as related to other

points in the water column. At mid-water column in SH16, pH increased slightly in May 2009 while remaining uniform in October 2008. Both SH01 and SH19 showed a steady increase in pH with depth in May 2009, also remaining uniform in October 2008. In SH32, pH decreased with depth in October 2008 and increased with depth in May 2009. Among sinkholes, distribution of pH does not follow a consistent pattern. In SH17, SH21 and SH22 the low bottom pH could be related to presumed presence of microorganisms as anticipated by chromatic variation between sample depths may also assert a biological that could control pH.

[Cl⁻]. As is displayed in Figure 6, [Cl-] varies both seasonally and with depth. Similar to conditions observed for both conductivity and pH, most of the sinkholes exhibited relatively well-mixed water columns, with [Cl-] values remaining consistent and largely uniform within SH01, SH19 and SH25. Higher concentrations were observed in the May 2009 sampling suite for SH11 and SH37, although both sinkholes exhibited similar water column structure regardless of season. Within SH32, [Cl-] was highest at mid-water column, with lower values at depth. A similar high concentration spike was observed in SH16 at 2.0 m depth, although the analyzed value for October 2008 appears to be anomalously high as compared to other measurements, and thus may not represent the actual conditions at that depth. A complex scenario exists within SH17, SH21 and SH22. Within SH17, the May 2009 samples present a gradual increase of concentration with depth, while October 2008 samples display a spike at 1.0 m depth. In SH21, concentrations decrease slightly for both seasons at a depth of 2.0 m. Concentrations in samples from May 2009 are higher than in October 2008 for both SH21 and SH22. In

May 2009, concentrations within SH22 were uniform while October 2008 samples increased with depth.

The typically lower concentrations present within the October 2008 sampling suite suggest alteration resulting from a number of environmental factors. As the summer monsoons contribute to the recharge of the alluvial aquifer along the Pecos Slope, freshwater input may be more readily available. Conversely, with a prolonged lack of precipitation between October and May, and the continued influence of evaporation on surface water sources, the natural tendency of the fluid would be to show evaporative enrichment of dissolved constituents. The implications for chemical stratification are minimal, as most sinkholes remain well-mixed, and those with a notable gradient tend to be driven by density rather than chemical propagation.

SCANNING ELECTRON MICROSCOPE (SEM)

The SEM was used to view mineral morphologies and composition, as well as to consider the presence or absence of microorganisms (see Appendix D for SEM images). Images and EFRs show that mineral growth can either be in well-formed crystals or amorphous masses. The variation in morphologies is influenced by whether the substrate was positioned on the interior or exterior of the sampling cartridge, and the amount of biological material present on the substrate. In precipitation samples from highly depositional depths, minerals are accompanied by diatoms, bacterial films and fungi strings. This biological material appears to grow concurrently with minerals forming, thus comprising the development of pristine crystal form as observed in samples with minimal biological presence. At some depths in sinkholes with high deposition rates, large well-formed crystals are expressed but often have a sheath of biological material.

The presence of planktonic diatoms is abnormal. Diatoms were present in most of the samples, regardless of depth within the sinkholes. As diatoms are non-motile, the reason for their presence is either from upwelling in the water column, mixing causing the upward flow of diatoms and subsequent deposition on substrates, or continual slow mixing rendering transport. However, diatoms were present in stratified sinkholes suggesting different factors causing the presence of these organisms throughout the water column.

COMPARISON OF SH17 AND SH19

Throughout the study area, sinkholes exhibit unique and distinct characteristics. To better understand these variations, two sinkholes were selected for more careful consideration. Chosen due to their proximity to one another, similar size and depth, and dramatic differences in physical appearance, characteristics that potentially contribute to the heterogeneity of sinkholes throughout the Refuge were assessed. By comparing the physical observations of these sinkholes, as well as the chemical, temporal, and water column heterogeneity, it is possible to consider the external conditions that me be affecting the sinkholes, and to assist in better evaluating the sinkhole lifecycle.

Physical Appearance. Regardless of field session, water in SH17 was a hazy, turbid brown color without the floor visible, while SH19 had clear blue to turquoise water with the floor visible. Both sinkholes had submerged macrophytes, and crystalline substrate deposits along the shoreline.

Water Chemistry Chemically, the two sinkholes were different. The water column in SH17 was stratified, exhibiting four chromatically distinct water samples which also had high salinity and high isotope values within water samples. In SH19, meanwhile, all

four sample depths were clear and relatively uniform in chemistry. As physical parameters were measured during both sampling suites as well as during February 2009, a more careful evaluation of the physical parameters can shed light onto the seasonal progression of sinkhole waters. Temperatures remained consistent, despite the atmospheric seasonal changes, and SH17 did not exhibit seasonal mixing within the water column.

Dissolved Gases. For both sinkholes, dissolved gases contained high concentrations of CO_2 and evidence of atmospheric diffusion. Low concentrations of He were detected in both sinkholes. Figure 15 shows the relative proportions of N_2, Ar and He as compared with regional data points (Crossey et al. 2009). The N_2/O_2 levels in the samples are below the atmospheric ratio of these gases which is consistent with field observations and probe measurements of relatively low O_2. Elevated N_2/He ratios were observed among select samples. Two samples (Sago Spring and SH 17) were analyzed for $^3He/^4He$ isotope composition and yield R_C/R_A values of 0.17 and 0.6, respectively, indicating a mantle source for He. This could explain the source of additional external CO_2 observed in the water chemistry (Crossey et al., 2009; L. Crossey, 2011, personal communication). The dissolved gas characteristics of both sinkholes suggest similarly sourced waters which have common water-rock interaction histories.

Mineral Precipitation. Mineral growth over the course of the substrate deployment period was drastically different between the two sinkholes for the surface and 1.0m depths, while the 2.0m and bottom depths were similar in both growth rate and precipitate appearance. For SH19, mineral growth was uniform throughout the water column, and was accompanied by a think sheathing of algae over the gypsum precipitate;

this was observed for the lower two cartridges in the SH17 water column. Meanwhile, the two cartridges in SH17 closer to the surface supported extensive mineral deposition and algal growth. The dominant mineral remained gypsum, regardless of sinkhole or depth.

This deposition reflects the differing levels of mineral concentration within waters of the two sinkholes. As the dominant precipitate for both sinkholes is gypsum, the implication is that waters are supersaturated with respect to gypsum; this is confirmed through PHREEQC modeling. With the bulk water chemistry being similar, the reason for larger masses of precipitate closer to the surface is likely from evaporation concentration at the surface. The ubiquitous biological debris associated with the precipitates may imply that gypsum preferentially nucleates on biological material. Generally, the growth of gypsum was greater on the outside of the dialysis cell than on the interior substrate.

Sonde Deployment. The use of sondes in both SH19 and SH17 revealed a temporal progression of water conditions. While minimal changes to pH were observed over a two-week period, other physical changes demonstrated clearly the role of water flow and progressive mixing in the alteration of basic conditions. Temperature fluctuated in response to solar heating and nighttime cooling. As both sinkholes expressed the same fluctuations, it is reasonable to presuppose that the rate of inflow is slow enough where it does not override the solar influence. This is consistent with the water dating results of Land and Huff, 2010. The diurnal fluctuation of conductivity may also relate to the daily change in temperature as water density is affected and superficial mixing occurs. Less dense water ascends toward the surface while higher density water sinks. The higher density would result from being cool as well as having higher dissolved compound

concentration. As the range of conductivity fluctuates over a relatively small scale, it is not likely that more acute factors such as precipitation events or evaporation are affecting water chemistry at this scale.

An apparent change in depth over time was observed during the deployment which, which when corrected for atmospheric pressure changes during the measurement period, showed a maximum depth fluctuation of approximately 10.2 cm (4.0 in). Observed atmospheric pressure varied by ~20 mBar, which translates to the pressure exerted by approximately 20.3 cm (8.0 in) of water. Overall, the sonde recorded a change in water depth of approximately 30.5 cm (12.0 in). Intermittent pumping or extraction from wells in close proximity to the Refuge may yield predictable drawdown. However, as the deployments occurred during February 2010, the demand for groundwater for irrigation purposes is unlikely. It is possible that water is used for supporting livestock, or is systematically pumped to fill cisterns or tanks. During the period of observation, a precipitation event occurred that may explain depth changes during the second week. The three distinct swells can be seen to correspond with discharge levels in the Pecos River and variations in atmospheric pressure. Within a confined aquifer the size of the principle aquifer within the Roswell Artesian Basin, the potential for tidal fluctuations exist. The role of the tides in water movement was observed by Inkenbrandt et al (2005) and Marechal et al (2002) who predict water movement in response to gravitational changes associated with the lunar cycle affecting aquifer pore pressure. One component of the water level variation could be affected by tidal forces; however, a more in depth analysis of the pressure data would be required.

CHAPTER 5: DISCUSSION

Several key findings were revealed over the course of this study: 1.) Surface measurements are variable among sinkholes which is most likely due to sinkhole geometry as opposed to proximity to the Pecos River; 2.) Hydrochemical evolution is bimodal with sinkhole water column being either well-mixed or stratified; 3.) Evaporation and continuous recharge are the primary processes controlling source water modification and subsequent precipitation reactions; 4.) All sinkholes have a common water source which is altered by the same climatic and environmental conditions, with stable isotopes showing evaporation; 5.) Sinkholes have a predictable lifecycle driven by continuous source water input, evaporation, precipitation reactions, chemical stratification, halite saturation and finally exhaustion; 6.) Biological presence and community is related to the stage of sinkhole lifecycle and is controlled by chemical conditions.

The portion of the Middle Tract included in this study is a hydrologic constant head boundary, varying topographically by approximately 10 m (32.8 ft), with sinkhole water level remaining constant throughout the duration of this study. Results from the initial site visit as well as the February 2009 surface survey reveal that with the exception of superficial grouping (e.g., higher measurements of conductivity for six sinkholes near the center of the study area), there is not a dominant spatial trend. The Pecos River is approximately one kilometer from the nearest sinkhole, and this sinkhole (SH17) does not contain river-like water (as compared to river values reported by Yuan and Miyamoto, 2008), nor do sinkholes to the west reflect more saline or mature water conditions.

As was presented in Figure 12, stable isotopes in sinkhole water samples – regardless of depth - are well-grouped along an evaporation trajectory, with the linear relationship suggesting a single source water subjected to common alteration forces for all study sinkholes. Submerged springs bring saline groundwater into sinkholes and shallow pools. Groundwater salinity is derived from the dissolution of Permian-aged evaporites as groundwater progresses toward the discharge area. Sago Spring is the combination of several flowing surface springs and small pools slightly north of Bitter Lake. The discharging flow is presumed to represent the virgin groundwater in the vicinity of Middle Track sinkholes.

Water chemistry data from Sago Spring (starting composition) was input into GWB to generate a simple evaporation model (Figure 16). The model suppresses dolomite precipitation as one liter of Sago Spring water is evaporated. Early into the process, both calcite and gypsum precipitate, while magnesite precipitates after over 90% of the water is evaporated. Halite continues to be dissolved in solution until <1% of the original water volume remains. The Cl anion is a hydrochemically conservative component, and is not readily removed from the water until late into the process; thus, it may be used as a means to describe alteration of source water (i.e., fluid mixing, evaporation [Musgrove and Banner, 1993]). The concentration of fluid components that remains in solution following evaporation and subsequent precipitation is also shown in Figure 16. The accuracy of the model was tested by plotting the analyzed concentration of Cl from surface samples of three sinkholes along with associated Mg concentration; neither Ca nor SO_4 values fall on the modeled component curves. Of the three sinkholes plotted, SH37 exhibited close correlation between values of Cl and Mg as related to the

amount of water evaporated from the initial volume. The other two example points – SH16 and SH21 – while both have Cl values that plot on the model curve, present corresponding Mg values divergent from the predicted concentration. This shift indicates that the model used in this scenario does not fully account for the complexity within this system. Thus, a more complicated model is needed to describe the evaporation-precipitation reactions occurring for sinkhole waters.

The role of evaporation in this system is confirmed when the Na and Cl content of sample waters is plotted. As is show in Figure 17, the sample points for a given sinkhole, regardless of depth (in most cases) plot in a concise grouping. As a group of lower Na and Cl concentrations, SH37 plots oppositely along this line as compared with SH21 that is organized toward higher concentration values. Regardless of sinkhole, the molar plot of Na-Cl is 1:1 confirming evaporative processes are promoting the increase of these two components collinearly, and that the species is halite. As the sinkholes progress along this line, the grouping is less organized, and variability among sample depths for a given sinkhole causes a spreading data points along the line of regression. This spreading is related to the evolution of the water column structure as the sinkholes progress from a uniform, well-mixed configuration to a stratified configuration.

By considering the change of Cl with depth, the bimodal distribution of water column structure is clearly revealed, as is the reason for the grouping observed in Figure 17. In Figure 18, Cl concentrations for both sampling sessions are plotted with depth. Seasonally, concentrations do not generally exhibit dramatic fluctuation; however, May 2009 values are slightly higher for the majority of sinkhole depth measurements. The 10 sinkholes in this study occupy a relatively organized spectrum of Cl concentrations, and

demonstrate the progression from a well-mixed to stratified scenario. Sinkhole 16 is an example of a transitional body, as it shows an increased overall Cl and divergence from more uniform orientation such as that reflected by SH37. Likewise, in SH17 and SH22 whose Cl is greater than SH16, there is a remarkable range of Cl present if all depths are compared for a given sinkhole. This spreading with depth accounts for the observed lack of grouping along the Na-Cl plot for these stratified bodies. This correlation also indicates that a sinkhole like SH21 has been subjected to extensive evaporation.

The progression toward higher Cl values is also reflected in the Piper diagram in Figure 11. This diagram shows that sinkhole waters in general are of Na-Cl type endmember facies. The migration of water data points toward the Cl apex is accompanied by the progressive increase of TDS with increased Cl dominance. This suggests that sinkhole water has an overall higher concentration of dissolved constituents as it approaches the Cl endmember. For comparison, regional groundwater data is also presented. As groundwater progresses along the Pecos Slope to the discharge region at the Refuge, it is modified from its original Ca-HCO_3 type water to a fluid with greater contribution from the dissolution of evaporites – in particular, gypsum. Groundwater eventually transitions across the saline boundary near the Refuge, and discharges as water containing a combination of Ca-bearing minerals and Cl-bearing salts. Sago Spring represents this discharge chemistry, has comparably low TDS, but higher Cl than groundwater samples collected upgradient of the saline groundwater interface (see Figure 2). The Sago Spring point aligns with the trend of sinkhole data points, with SH37 representing a mildly modified version of the water, and SH21 representing a highly modified version. The trend of the water is toward complete Na-Cl dominance.

A PHREEQC model was run for sinkhole water samples to calculate the SI for halite and several other mineral species. Magnesite SI was modeled using GWB. In this system, as was modeled in the simple Sago Spring evaporation scenario, Ca-bearing minerals precipitate from solution with lesser initial concentration as compared to halite which requires the prolonged evaporation of a fluid for precipitation to occur. As this system is largely driven by evaporation, observing the progressive increase of halite in solution can be used to evaluate the extent evaporative processes have driven water chemistry. Figure 19 displays the SI of halite with depth for sinkholes during both sampling sessions. As was observed for Cl concentration with depth, the May 2009 suite was generally slightly higher, suggesting slight alteration between sampling sessions. Sinkhole 16 marks a transitional feature between sinkholes with lower overall SI values and those with higher values spanning a larger range.

Sinkholes with high halite SI values contain water that is more evolved than those with lower values. The implication of approaching halite saturation is that a larger proportion of water has been removed by evaporation as compared to those sinkholes with lower values. As mentioned previously, the water level over the duration of the study remained constant due to the groundwater constant head boundary. For a sinkhole like SH21 which is evolving toward halite saturation, water is removed by evaporation, but is recharged by inflow springs. The rapidity of subsequent hydrochemical evolution in response to this removal-recharge cycle is related to the geometry of the sinkhole. Bodies with a large surface area have greater atmospheric exposure while deeper sinkholes can more readily disperse dissolved components that remain following

evaporation. Figure 20 provides a simplified model that evaluates the mass per volume of Cl that is added to the sinkhole.

The cylinder is a geometrically analogous shape to a simplified sinkhole structure. Using the average pan evaporation rate as recorded at the Refuge (225.8 cm/yr, WRCC Bitter Lakes WL Refuge monitoring site), and using the convention correction to account for thermodynamic differences between the metallic evaporation pan and sediments in sinkhole lakes, a simple prediction of the potential increase of Cl concentration was calculated. For a sinkhole with a depth of 5.0m and surface diameter of 20m that is continuously recharged by water with Sago Spring-like chemistry, the annual increase of Cl is 694.5 mg/l. Using the same process, SH21 was modeled (3.8m depth, ~40m diameter), and had a calculated increase of 913.6 mg/l. A comparison of the actual change between October 2008 and May 2009 shows an increase that exceeds this prediction. This implies that the overall volume of SH21 may not be consistent with the simplified cylinder approach (the bottom may slope more gradually from the shore to its low point). To more thoroughly account for the discrepancy in Cl budget, a more complex model is needed that would consider surface input from precipitation and overland flow as well as lateral seepage. Because of trends in stable isotope progression, Na-Cl plots, and grouping on the Paper diagram, it is unlikely SH21 is recharged by a fluid other than Sago Spring-like water. Meanwhile, the general prediction for volume turnaround supports the continuous recharge of water following loss to evaporation, and the subsequent modification of bulk water chemistry as dissolved compounds remain in solution.

While halite precipitation was not observed among study area sinkholes, precipitation of other minerals did occur. The deployment of substrates in five sinkholes revealed variable rates of mineral growth (Appendix C). Use of the SEM determined that the dominant mineral was gypsum; however, substrates effervesced when dilute acid was applied, suggesting the presence of carbonate-bearing minerals (i.e., calcite). Figure 21 confirms that as Cl increases, the ratio of Mg/Ca also increases. This progression indicates that with continued evaporation, either the concentration of Mg is increasing, the concentration of Ca is decreasing, or that both occur simultaneously. As is suggested by the simple Sago Spring evaporation model, both gypsum and calcite precipitate early, thereby reducing the concentration of Ca in the water, and increasing the proportion of Mg/Ca. This progression is collinear with Cl until concentrations are approximately as those present in SH22 (~35ppt) where the plot occupies a wide spread of Mg/Ca ratio values. Evaporation affects Mg content predictably until sinkholes adopt a stratified water column structure, at which point the evaporation-precipitation reaction represented in Figure 21 becomes more complex, with Cl content continuing to increase without precipitation, and other ions readily removed.

The conservative nature of Cl is further portrayed in Figure 14, which plots δD values with Cl concentration. In groundwater systems, both of these parameters are conservative. What this plot shows is there is an abrupt increase in δD values over a slim Cl range for well-mixed, uniform sinkholes, while after Cl concentrations reach approximately 10ppt, the further increase of δD is minimal, with overall δD concentrations remaining +/- 10 ‰. Equilibration with the atmosphere buffers δD increase, while continuous evaporation yields progressive increase of Cl values. The

move toward higher Cl concentrations indicates the sinkhole is not simply a pool of water that is slowly evaporating, but is instead continuously refilling with source water to replenish water levels to constant head boundary depths.

This progression toward δD equilibration with atmosphere and increased Cl concentration is related to the hydrochemical maturity of the water within a sinkhole. As was shown in Figures 18 and 20, the higher the Cl, the greater the proportion of source water as compared to overall fluid volume that has passed through the sinkhole, and the progression toward the stratified modality of water column structure. These characteristics are supported by Figure 14 because as the regional groundwater enters a sinkhole, it increases both δD and Cl concentrations through an evaporation-recharge cycle. The concentration of Cl may continuously increase until halite saturation is achieved (assuming source water inflow channels flow freely), while δD equilibrates with the atmosphere. The concentration range of Cl can be used to describe the relative stage of evolution of a sinkhole, with the higher the Cl indicating a more evolved water body. The precipitation of other minerals accompanies the continued cycling of water through the sinkhole system, as does the total amount of TDS increase with increased evolution. The range of TDS for sinkholes along this evolutionary trajectory may be used to quantify "age" based on a simple surface measurement as the surface conditions provide a general reflection on the overall chemistry in the sinkhole. The general trend is that increased Cl has a corresponding increase in TDS, with surface measurements similar to the average TDS for the entire water column.

Bottom measurements for both Cl and TDS are typically greater than the water column average for either parameter. This corresponds to a gradual density gradient

expressed by both water column structure modalities, and is dependent primarily on the dissolved components content. While water temperature impacts density, the progression of calculated density values (i.e., order of arrangement of study sinkholes by density) is comparable to that expressed by Cl and TDS, as the pattern of increase reflects the orientation presented by other conservative properties (e.g., conductivity). Seasonally, all sinkholes except for SH21 had a slightly lower density among May 2009 samples as compared to October 2008. The difference is minor, and the variation is most likely due to cooler water temperatures recorded during May 2009. The density gradient is more pronounced among sinkholes with stratified modality, and this study did not find density-related seasonal water column turnover, although the majority of sinkholes remained well-mixed, with SH16 again occupying a transitional water column configuration.

The combination of stable isotope content, evaporation-precipitation reaction, progressive increase of dissolved components, and progression between water column structure modalities provides a clear process that describes the sinkhole lifecycle. This lifecycle does not define the age of the sinkhole itself, but rather the hydrochemical evolution of the water within the sinkhole. Use of sediment-based aging techniques, such as coring, would afford further discussion about the age of the sinkhole structure itself. The majority of sinkholes within the Middle Tract had developed prior to the 1937 establishment of the Refuge. At the time, the hydraulic head in the discharge area was high enough to overflow the sinkholes, allowing the intermingling of water (and non-benthic motile aquatic species). With reduction of groundwater levels, sinkholes transitioned from high volume recharge sources for area playa lakes to discrete lacustrine features. This isolation promoted the independent development of unique chemical

limnological characteristics that are continuously changing due to the evaporation-recharge cycle that drives each sinkhole.

Figure 22 outlines the sinkhole hydrochemical evolution. Source water (groundwater; Sago Spring type chemistry) enters the sinkhole, where it is subjected to low relative humidity and high local evaporation rates (WRCC Bitter Lakes WL Refuge monitoring site average pan evaporation rate of 225.8 cm/yr [1950-2005]). With the influence of evaporation removing water from the system, both salinity and stable isotope (δD and $\delta^{18}O$) content increase. As water is removed, the system is recharged to maintain hydraulic head levels. Continuous evaporation followed by subsequent recharge gradually increases the relative concentrations of dissolved constituents within the overall sinkhole water column. The initial structural modality is well-mixed water column with uniform physical and chemical parameters present, regardless of depth. Continued evaporation and recharge eventually yields mineral saturation. In this study, a simple PHREEQC and supplementary GWB model consider gypsum, calcite, magnesite and halite. Calcium-bearing minerals (calcite and gypsum) achieve saturation and precipitate from solution early in the cycle. This precipitation removes calcium from the system, while magnesium is concurrently conserved. Meanwhile, both δD and $\delta^{18}O$ concentrations continue to increase.

These general reactions continue, and the sinkholes respond by exhibiting uniform enrichment of conservative components (conductivity, Cl, Mg, δD). The rapidity of progressive enrichment is contingent on the physical geometry of the sinkhole. Broad, shallow sinkholes face higher total volume percentage overturn as opposed to deep sinkholes with lesser direct surface-atmospheric exposure. The well-mixed configuration

is maintained until Cl concentration reaches approximately 20ppt, at which point, the water column begins to exhibit a more distinct chemical gradient (TDS, density). This organization is reflected by conservative properties occupying a wider range of parameter values as compared to those sinkholes more closely reflecting Sago Spring chemistry (i.e., "younger" sinkholes). Sinkhole 16 is an example of a "transitional" body bridging the two modes as it is uniformly high in Cl, exhibits "spreading" of parameter measurements, and has occasional overlap with both well-mixed and stratified examples.

Overall stratification occurs following prolonged evaporation-recharge cycling where the proportion of dissolved components increases with continuous groundwater input. Enrichment of dissolved constituents increases the saturation of mineral species present in the water, causing increased precipitation. As with "younger" sinkholes, calcium-bearing minerals precipitate first, leaving behind magnesium. In these stratified scenarios, fluids have increased concentrations of Mg that result not from the input of a secondary Mg-rich source water, but rather from the preferential removal of other non-Mg-bearing mineral species earlier in the evaporation-precipitation reaction process. Eventually, magnesium is removed through the precipitation of magnesite; the majority of study sinkholes displayed magnesite saturation as modeled by GWB. As was shown in Figure 21, the Mg/Ca ratio increases collinearly with Cl (i.e., evaporation), but those sinkholes with stratified water columns scatter as precipitation reactions begin to occur.

Both Na and Cl content continually increase as only a minor portion of each major ion is removed through precipitation of accessory mineral species. Concentrations of these components will continue to increase, slowly approaching halite saturation. Meanwhile, further increase of δD and $\delta^{18}O$ concentrations is buffered by atmospheric

equilibration. Stable isotopes falling along the Refuge evaporation trajectory will eventually group closely to resemble a closed basin brine type congregation, while Na-Cl values will continue to follow a 1:1 molar slope.

A sinkhole will exhibit continued evaporation-recharge cycling as long as groundwater inflow channels are freely introducing new source water into the system. If unabated, it is possible for the sinkhole water to achieve saturation of and begin precipitating halite. Instead, it appears more common for recharge channels to become blocked by sediment or precipitated solids that migrate toward the low points within the sinkhole. Such blockage restricts recharge flow, causing the sinkhole to more quickly achieve halite saturation while also facing the continued depletion of remaining water, thereby yielding a dry sinkhole with precipitates coating the interior sides and walls. Peripheral plant life once sustained by sinkhole water dies and is replaced by alkaline grasses and terrestrial plants.

The main factors that affect this lifecycle progression are sinkhole geometry and connectivity to source water inflow. Reduced spring flow (drought, irrigation demands, reduction to groundwater level or hydraulic head) can accelerate the evolutionary process, and it may also affect resident biological communities. As was described by Echelle (1989), endemic fish species such as the Pecos Gambusia are threatened (and some localized populations known to have gone extinct) due to the reduction of spring flow by groundwater overdraft. While these documented incidents of population degradation are described simply as resulting from a loss of spring water flow, survivability of the Pecos Gambusia depends on water quality.

Echelle (1989) offers high TDS as an explanation for documented failure during stocking programs, while Bednarz (1979) comments on high salinity, predation, and "hardness" as limiting factors. The stocking program commented on by both authors occurred in 1973 where 19 locations were selected for transplanting, and of which, only two populations had survived when revisited in 1975. While vegetation and structural characteristics (submerged cliffs, overhangs) were similar among chosen locations, water chemistry was the most likely factor hindering the ability of introduced populations to reproduce. For example, viable populations did not exist in sinkholes with hardness >5,100 mg/l, and conductivity >28,000 μS/cm (Bednerz, 1979). As surface conductivity measurements can approximate the overall sinkhole water structure and stage in lifecycle, using the 28,000 μS/cm as a reference, 10 of the 36 sinkholes included as part of the February 2009 spatial survey would be viable transplantation options if water quality was the only consideration. Meanwhile, 10 sinkholes are predicted to exhibit water column stratification based on surface proxy where conductivity measurements over 70,000 μS/cm are likely to represent sinkholes that have transitioned from well-mixed structure.

Sinkholes in the stratified configuration pose unique biological conditions with higher nitrogen and phosphorous levels at depth while well-mixed sinkholes are homogenously low in nutrient content (Table 5; Figure 7). For both SH17 and SH21, higher ammonia concentrations at the lower two depths reflect anoxic conditions likely due to a combination of the decomposition of organic material and density controls on water column mixing. Dissolved oxygen is general negatively correlated with temperature and salinity in aquatic systems (Wetzel, 2001), and the bottom measurements of the stratified sinkholes have among the highest salinity recorded for water in this

study. While SH17 follows this trend (by exhibiting slight warming with depth), temperatures in SH21 tend to decrease by ~4^{o}C with depth which may be due to insufficient mixing or high turbidity attenuating incident solar radiation thereby reducing heating. A slight increase in temperature at 2.0m in SH21 during both sampling sessions corresponds with a band of pink water also occurring at this depth. A similar chromatic variation was observed in SH17 at 1.0m (during both sampling sessions), but without a notable temperature difference compared with the surface sample.

Photosynthetic bacteria occur in dense populations at the interface of the oxidative and reductive zones in meromictic or stagnant holomictic lakes, coloring the water pink (or green) (Takahashi and Ichimura, 1970, citing Kondrat'eva, 1965 and Pfennig, 1967). Anaerobic conditions (characterized by high ammonia content) are found in both SH17 and SH21 below the observed pink layer, with the occurrence of photosynthetic bacteria corresponding to the bottom of the photic zone. While thorough microbial analysis did not occur as part of this study, water was filtered, field treated and stored in deep freeze for future biological evaluation. The preferential organization of microorganisms at a specific depth within the sinkhole is further supported by the measured pH with depth. During the May 2009 sampling session, both SH17 and SH21 exhibited a spike in pH at depths corresponding to pink water. Likewise, log PCO_2 values for intervals below the photic zone diverge from the established -3.5 for atmosphere.

The log PCO_2 as modeled by PHREEQC is the log of the partial pressure of CO_2 in the sample as equilibrated at sample conditions (alkalinity, pH, temperature, etc.). If samples have a log PCO_2 value equal to -3.5, it means the dissolved gases in the water reflect equilibration with atmospheric CO_2 partial pressure (e.g., air saturated water;

diffusion, infiltration by atmospheric gases). If, as in the case of the majority of study sinkholes, log PCO_2 values are greater than -3.5, the partial pressure of CO_2 is greater than atmospheric. This additional CO_2 can be sourced from biological processes as well as input from deep seated fluid infiltration.

The observed change in PCO_2 with depth among nearly all sinkholes, trending toward higher values, reflects the influence of processes other than diffusion of atmospheric gases on the system. As the majority of measured pH values are greater than 6.3, bicarbonate is a major species, and changes to pH due to photosynthetic processes are observable, as are the resulting changes to log PCO_2. In stratified sinkholes, a sharp decrease in log PCO_2 is observed at the pink water level and may be attributed to the removal of CO_2 from the system by photosynthetic organisms congregated at that depth. The analyzed partial pressures of CO_2 in dissolved gas samples for select sinkholes concedes that waters containing high amounts of CO_2 are low in N_2 content. Nitrogen may be removed from the water by aquatic plants during growth and through nitrogen fixation by bacteria or algae (thereby forming NH_4). These processes coincide with lower PCO_2 values closer to the surface (photosynthesis) as well as higher PCO_2 values with increasing depth (nitrogen fixation).

Those dissolved gases with a high concentration of CO_2 indicate lithology sourced influx as well as biological effects. As shown in the gas ternary diagram in Figure 15, samples occur over a wide range of gas ratios, suggesting a complex gas scheme with multiple contributing factors. In SH17, 1.0m (pink water), He is present, and is accompanied by low N_2 and high CO_2 content. This demonstrates a biologically-controlled sample site with accessory lithology-derived input. Presumably, N_2 has been

removed by planktonic algae or macrophytes, CO_2 may arise from respiration processes or from inflowing groundwater subject to slow diffusion as controlled by high water density, and He enters the sinkhole from recharge water. This sample was also analyzed for $^{3}He/^{4}He$ content (0.601) and $\delta^{13}C$ (-11.5 ‰), which together suggest the input of deeply seated source water, and are unlikely derived from biological processes (Crossey et al., 2009). The plotted orientation of several samples within the zone as defined by Giggenbach (1993) that represent crust or mantle derived fluids: the samples also group near other spring/groundwater-derived volatiles in the region. Six points contain very small amounts of He, although they occupy a range of N_2/Ar values that include air and air saturated water. The grouping of points near the Ar apex consists of samples that are proportionally high Ar content, but contain CO_2 as the dominant gas when other gas species in the mix are considered. Thus, dissolved gases offer a glimpse into the complex combination of hydrological and biological influences that support the continuing process of sinkhole hydrochemical evolution.

CHAPTER 6: CONCLUSION

Through the course of this study, an evaluation of the hydrochemistry of water-filled sinkholes at Bitter Lake National Wildlife Refuge occurred, and determined that sinkholes exhibit bimodal water column structure (well-mixed or stratified) that is organized in response to the density of the water within the sinkholes (with a water density of ~1.035 g/cm^3 forming the modal transition threshold). The change in density is driven by an increase in TDS following prolonged evaporation that yields increased Cl (and Mg) concentrations as calcium- and sulfate-bearing minerals (calcite, gypsum) precipitate from solution following saturation. Even with continuous precipitation, all species exist in high concentrations as water increases. Source water is chemically similar to shallow springs found at the Refuge (Sago Spring), and emerges at the discharge area of the Roswell Artesian Basin already containing high salinity due to dissolution of Permian-aged evaporites in the subsurface. This water is also high in CO_2 content and may contain traces of He, suggesting emergent water is a combination of groundwater (dominant) and deeply sourced fluids (minor). Once in the sinkholes, evaporation drives chemical evolution, with the physical geometry of an individual sinkhole contributing the greatest control on the rate of lifecycle progression.

The geochemical and isotopic composition of the suite of sinkholes examined in this study exhibit a remarkably complete sequence of progressive chemical and isotopic evolution that allowed for characterization of sinkhole lifecycle. Among the 10 focal sinkholes, a range of physical and chemical parameters were explored, with results organized in a meaningful pattern. By itself, a sinkhole is an independent lake structure whose water chemistry is subject to change, driven by a source water input, evaporation,

and chemical evolution (enrichment, precipitation). The pattern of modification is traceable to conservative properties that can be quantified and used as proxies to define the placement of a sinkhole along its evolutionary path.

The continuous (albeit relatively slow) evolution affects the biological ecosystems that have developed in and around an individual sinkhole. Food availability, predation, reproductive success, and sustainable ranges of water quality conditions (i.e., salinity, alkalinity, temperature) determine whether a population can survive in a given habitat. With already isolated (and in some cases endemic) communities sustained by a specific sinkhole's conditions, alteration of the water chemistry as part of the sinkhole lifecycle progression can extinct a resident population. Endemism is threatened by the reduction of source water input and natural climatic impacts from prolonged drought.

Seasonal alteration of water level and composition is minimal, with such fluctuations due to changes in water demands (plants, agricultural, anthropogenic, etc.) and recharge from snowmelt or infiltration of precipitation. By vertically profiling sinkhole water columns, aspects of the underlying hydrological character of the region were exposed. Elevated CO_2 values, relatively heavy carbon isotope values, helium concentration, and helium isotopic data suggest connectivity with deeper fluids. Additionally, both PO_4 and NH_4 were present in biologically-significant concentrations in sinkholes with chemically controlled water column structures. While future research is needed to better quantify the role of biological influence on hydrochemical evolution (e.g., microbial presence/respiration, macrophyte use of dissolved nutrients), water chemistry does in part affect ecological diversity observed among sinkholes.

Refuge sinkholes play an important biological role by sustaining resident and transient species, but they also provide useful hydrochemical information that considers the complex relationship between groundwater flow and regional climatic controls on natural water systems. This study found that evaporation and continuous groundwater discharge are major factors driving ecological sustainability as aquatic resources like the sinkholes are continuously altered. It also found that great diversity has developed at the Refuge in response to water chemistry, and sinkholes are a delicate and valuable resource with great potential for future research initiatives.

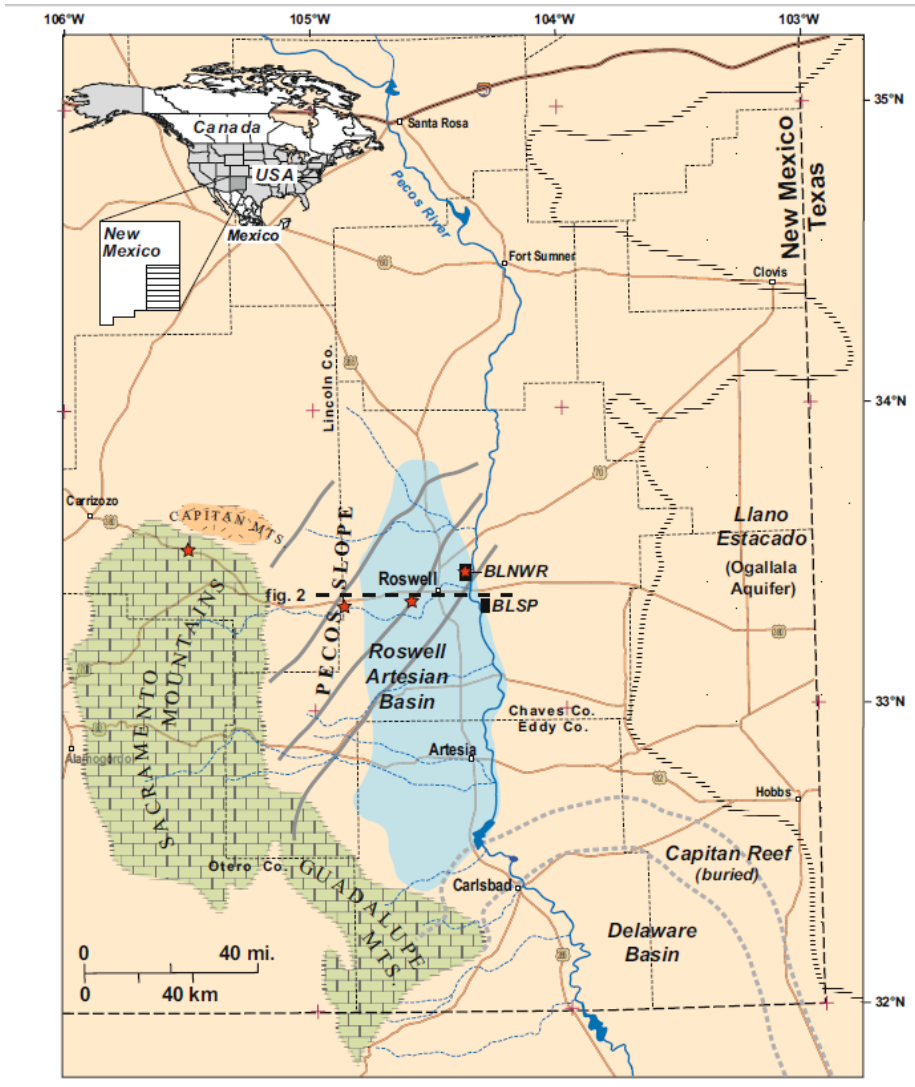

Figure 1: Regional Map. Regional map of southeastern New Mexico, showing the location of Bitter Lakes National Wildlife Refuge (BLNWR) and Bottomless Lakes State Park (BLSP). Red stars indicate the locations of precipitation sampling stations. The Pecos 'Buckles' are shown by gray lines extending NE–SW across the Pecos Slope (L-R: Serrano, Border, Six-Mile, and T-O Buckle). Brown lines represent roadways. Note: The dashed line in the map center identifies the location of cross-section in the next figure. *From Land and Huff (2010).*

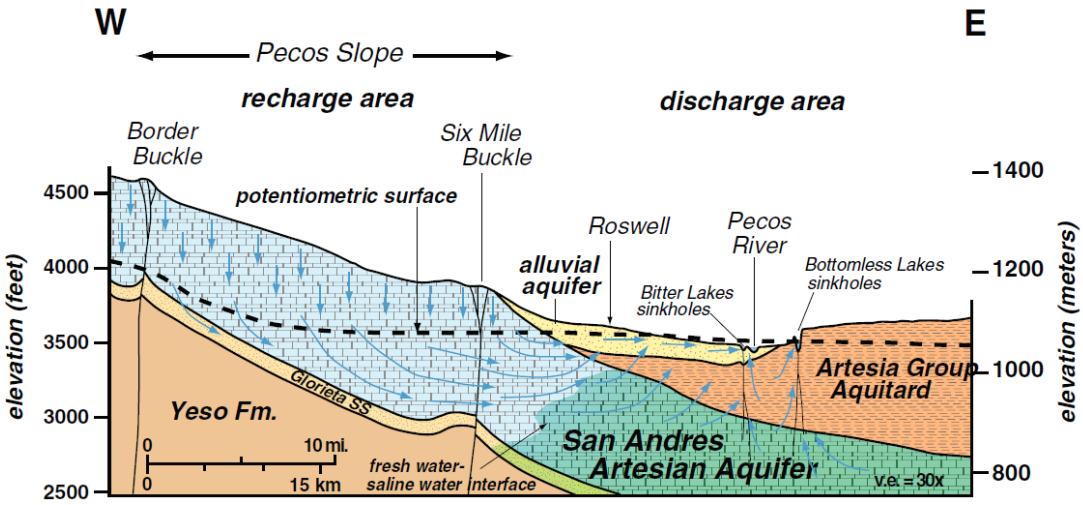

Figure 2: Hydrostratigraphic Cross-Section. West–east hydrostratigraphic cross-section of the Roswell Artesian Basin, showing generalized direction of groundwater flow paths through the artesian aquifer system. Elevation is relative to sea level. Vertical exaggeration (v.e.) = 30×. The location of the section is shown in Figure 1 by the dashed line. Groundwater along the Pecos Slope (recharge area) acquires solutes as it flows toward the Pecos River. Discharge of springs at the Refuge contain saline water flowing from the San Andres, through the Artesia Group, and passing through a thinning portion of the alluvial aquifer. *From Land and Huff, 2010.*

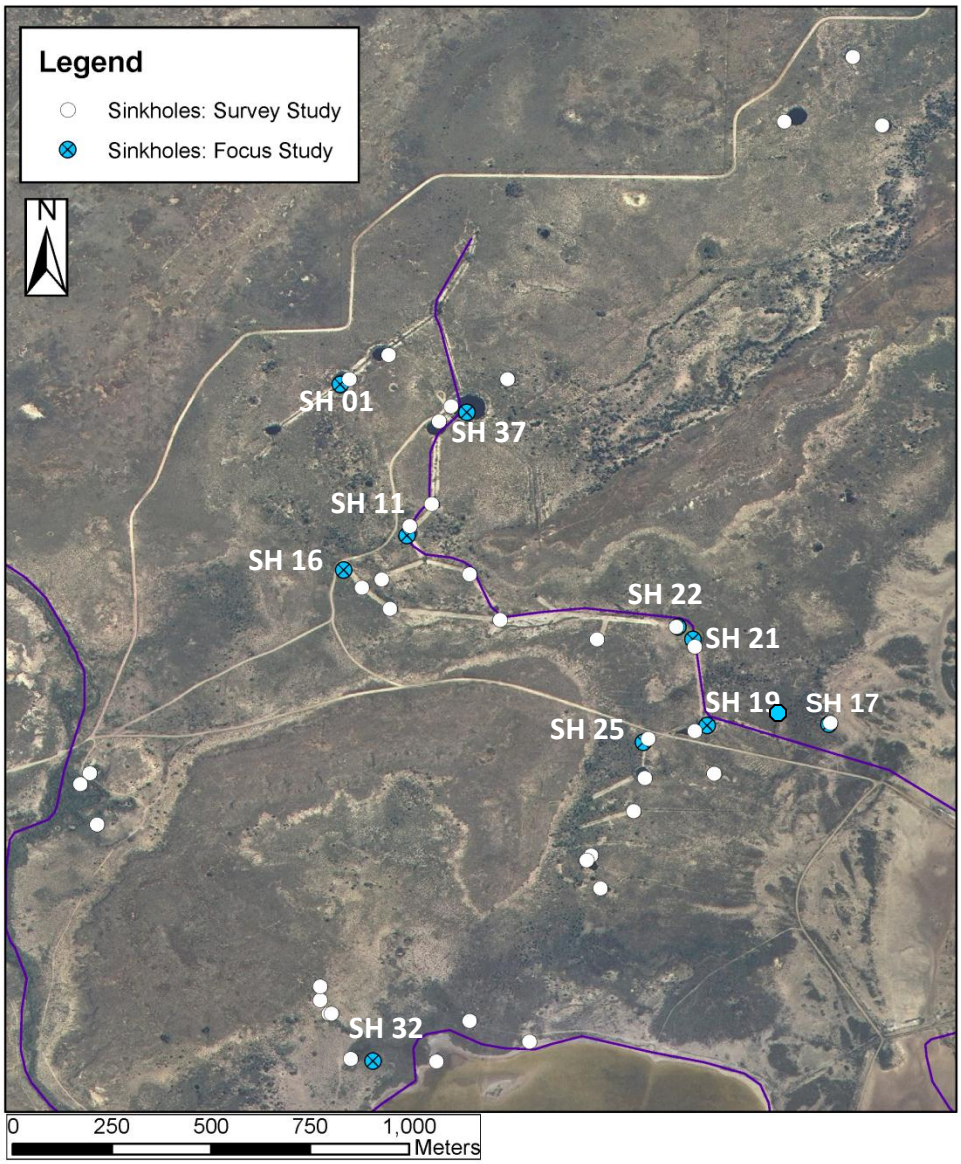

Figure 3. Locations of Study Sinkholes. Map of the study area with sinkhole locations and ID number. White points refer to all sinkholes visited as part of this study. Blue points identify locations of the 10 representative sinkholes that are the primary focus of this study. All study sinkholes are located in the Middle Tract portion of the Refuge. The Pecos River is to the east (off location map), and Bitter Lake is to the south (slightly east of sinkhole [SH] 32).

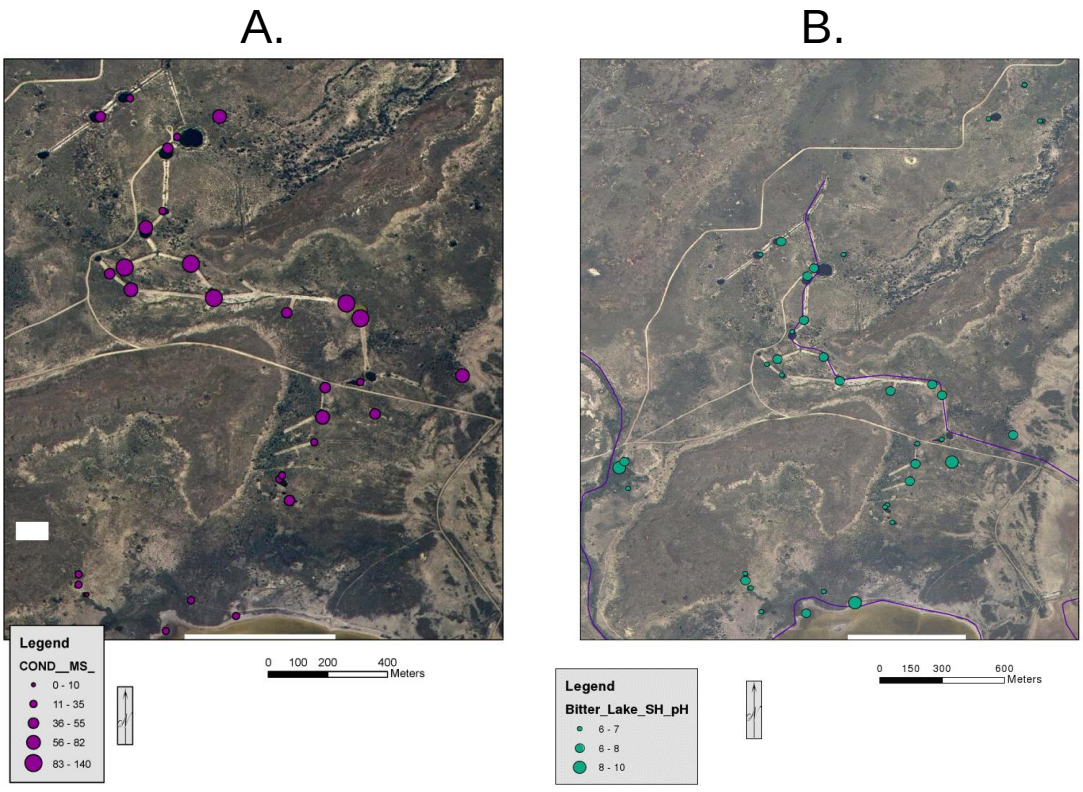

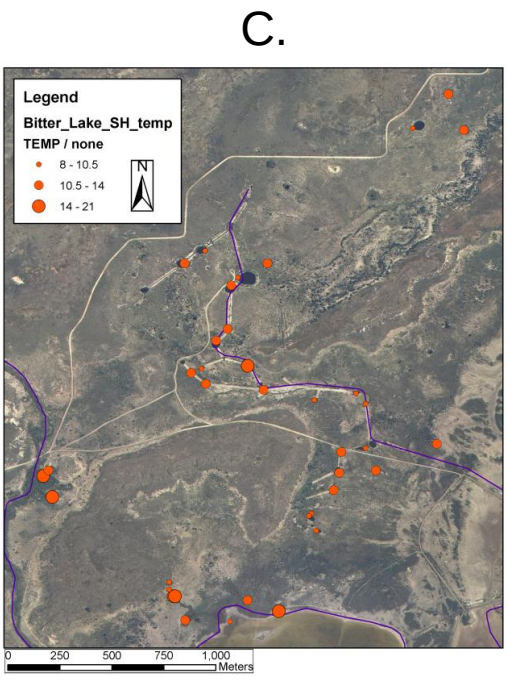

Figure 4. Spatial Distribution of Surface Parameters. These maps display the spatial distribution of hydrochemical field parameters from February 2009 survey session. (A) The distribution of conductivity shows a slight decrease with proximity to Bitter Lake (south) and to the north of the Middle Tract group. A band of comparatively high conductivity arises across the central sinkhole grouping with highest values recorded for SH21. (B) The distribution of pH shows high values for sinkholes close to Bitter Lake and at select locations in the peripheral of the central grouping. The majority of the sinkholes were of neutral pH. (C) The temperature distribution displays warm surface water slightly north of Bitter Lake and to the west.

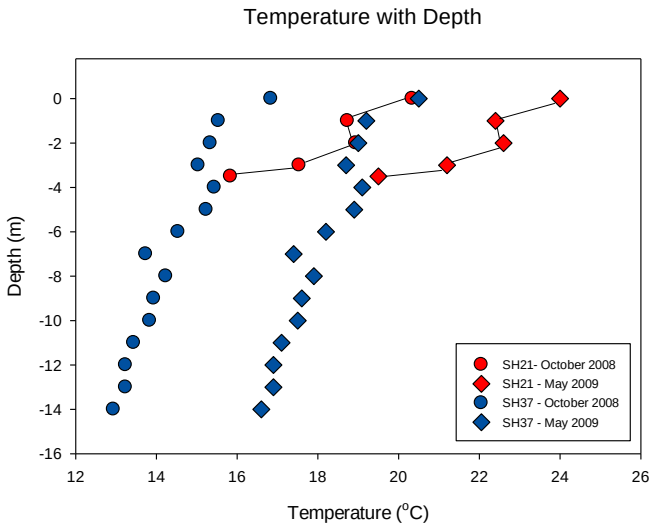

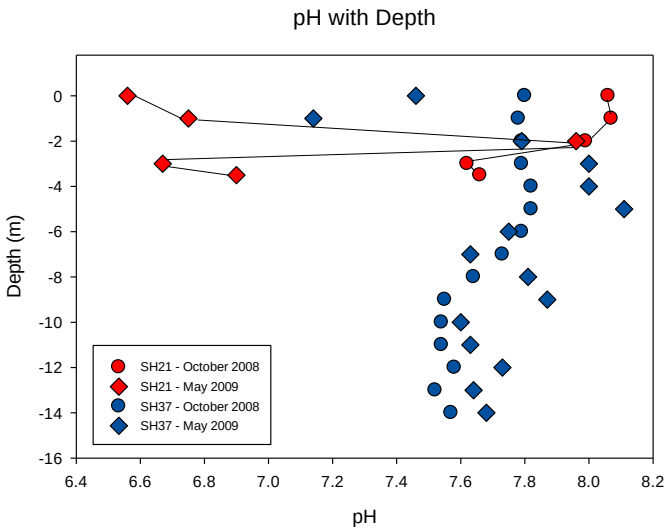

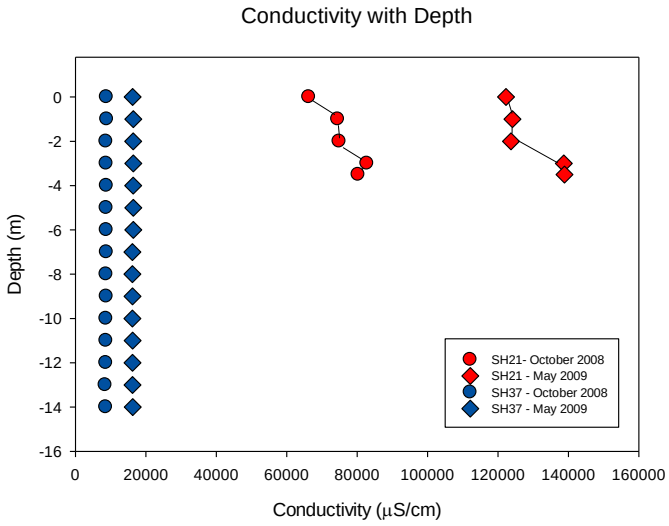

Figure 5. Field Parameters with Depth. These three plots show the change in temperature, pH and conductivity with depth for SH37 (well-mixed) and SH21 (stratified). These two sinkholes are used for comparison as they occupy opposite ends of the range of sinkhole conditions observed as part of this study. Measured parameters exhibit a slight seasonal divergence while revealing bimodal water column structures.

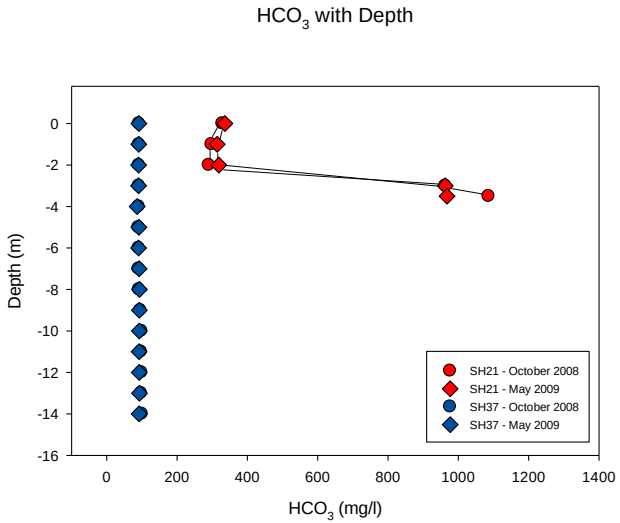

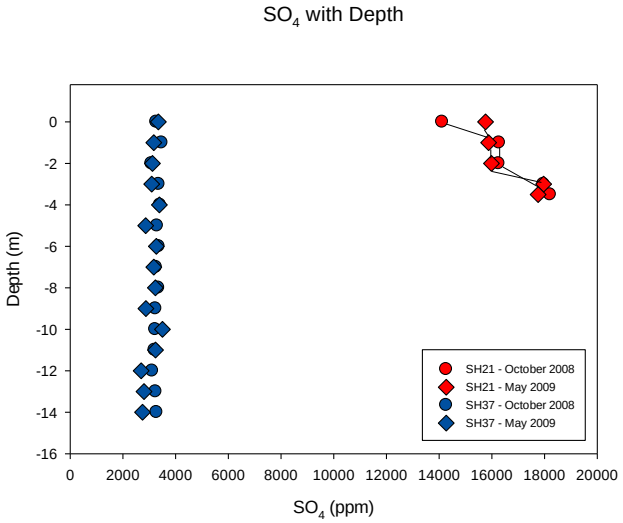

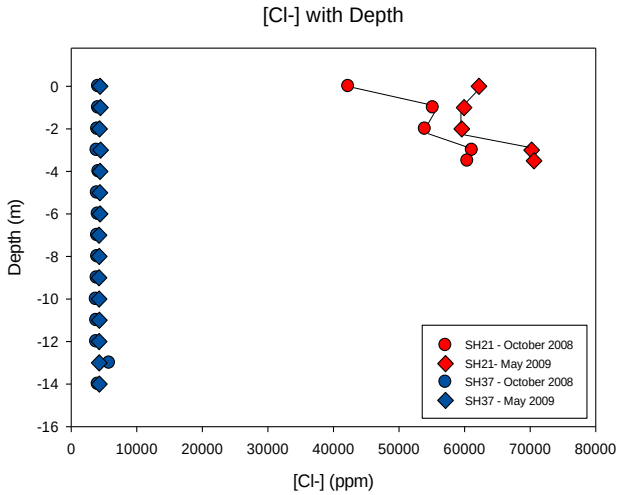

Figure 6. Major Ions with Depth. Figures 6a (Anions) and 6b (Cations, next page) compare major ion concentration by depth for SH21 and SH37. For anions, the water column of SH21 exhibits stratification, while SH 37 is well-mixed. Seasonal variation is minimal. This is similarly observed for cations; however, Ca concentrations are comparable between the two sinkholes. Regardless of component, higher concentrations are accompanied by a structured water column, while SH37, falling in the lower ranges for ionic concentration, is relatively uniform throughout the entire water column.

Figure 6a: Anions

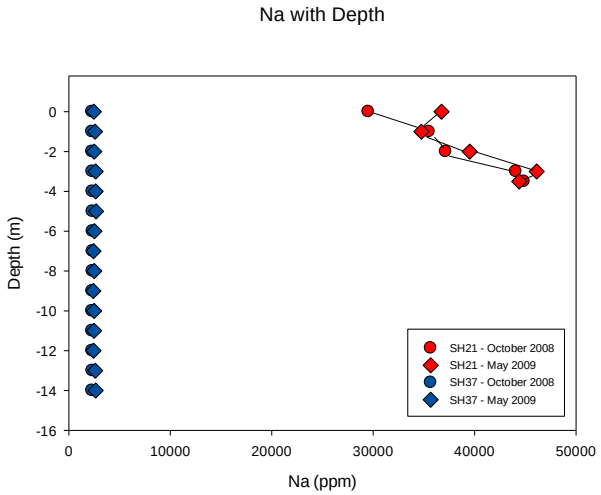

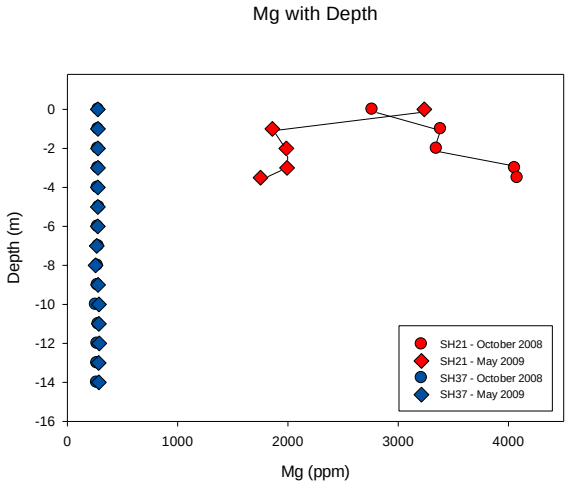

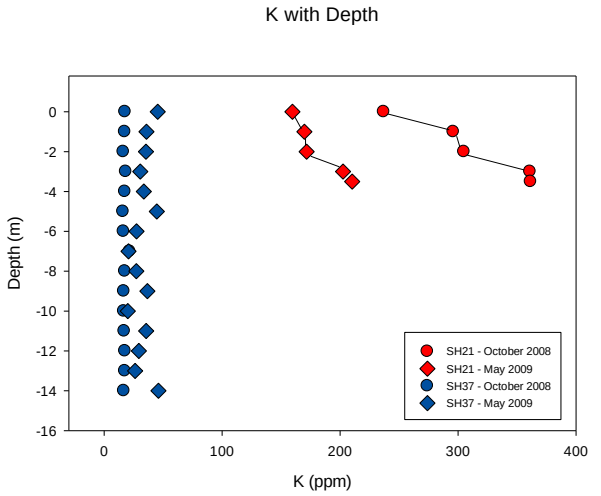

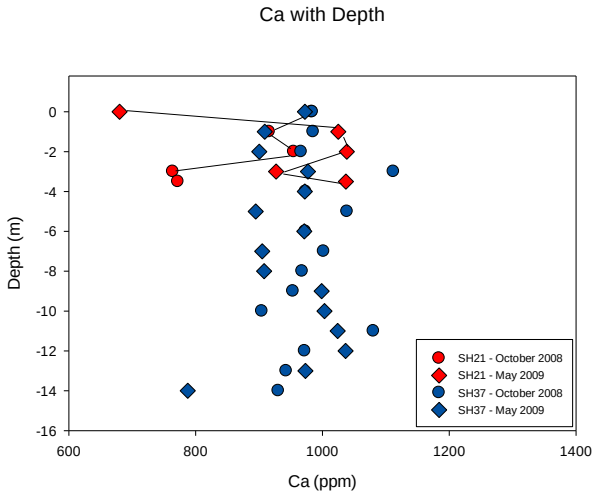

Figure 6b. Cations (figure 6. cont.)

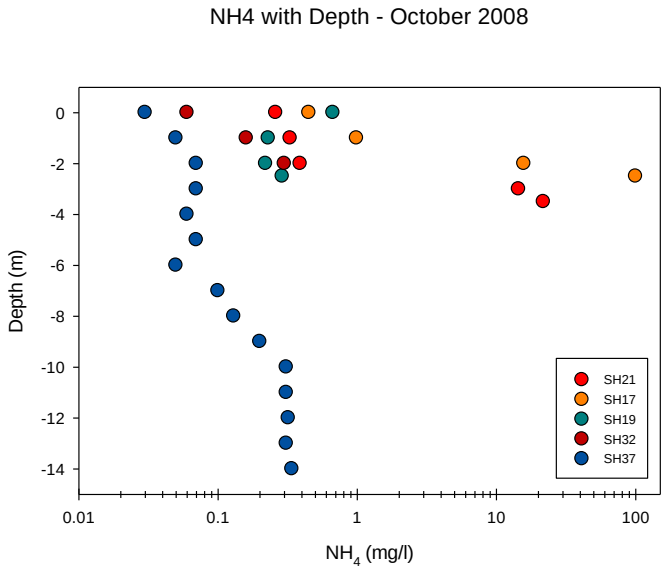

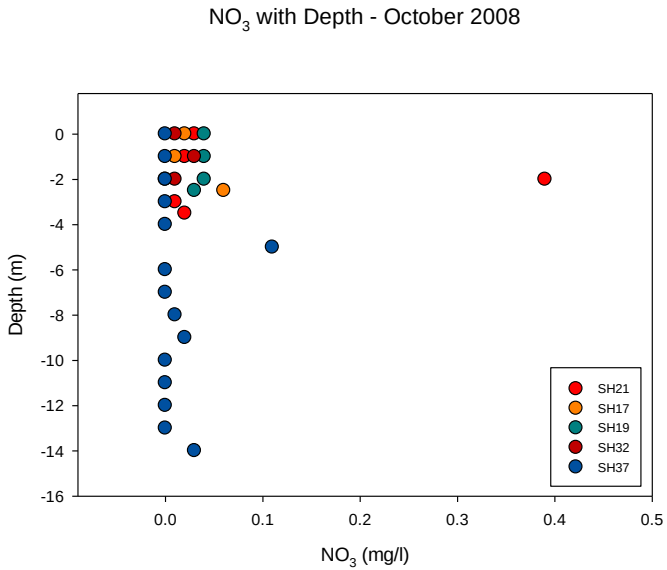

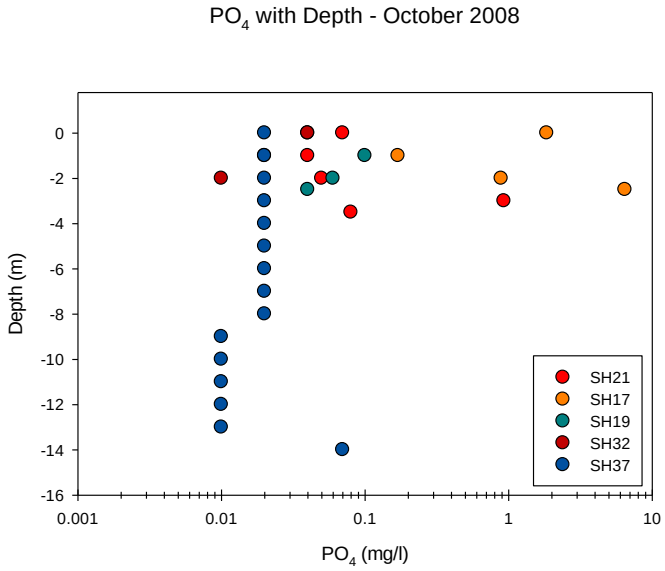

Figure 7. Nutrients with Depth. Five sinkholes from the October 2008 sampling session were analyzed for nutrients. Each of the five trended toward increased NH4 with depth, while stratified sinkholes contained biologically significant concentrations with depth. SH17 also trended toward higher PO4 with depth, although decreased sharply at 1.0m before rebounding to greater concentrations. SH17 also exhibited an increase of NO3 with depth. This nutrient data suggests that biological processed (decomposition, respiration) are contributing to overall water chemistry.

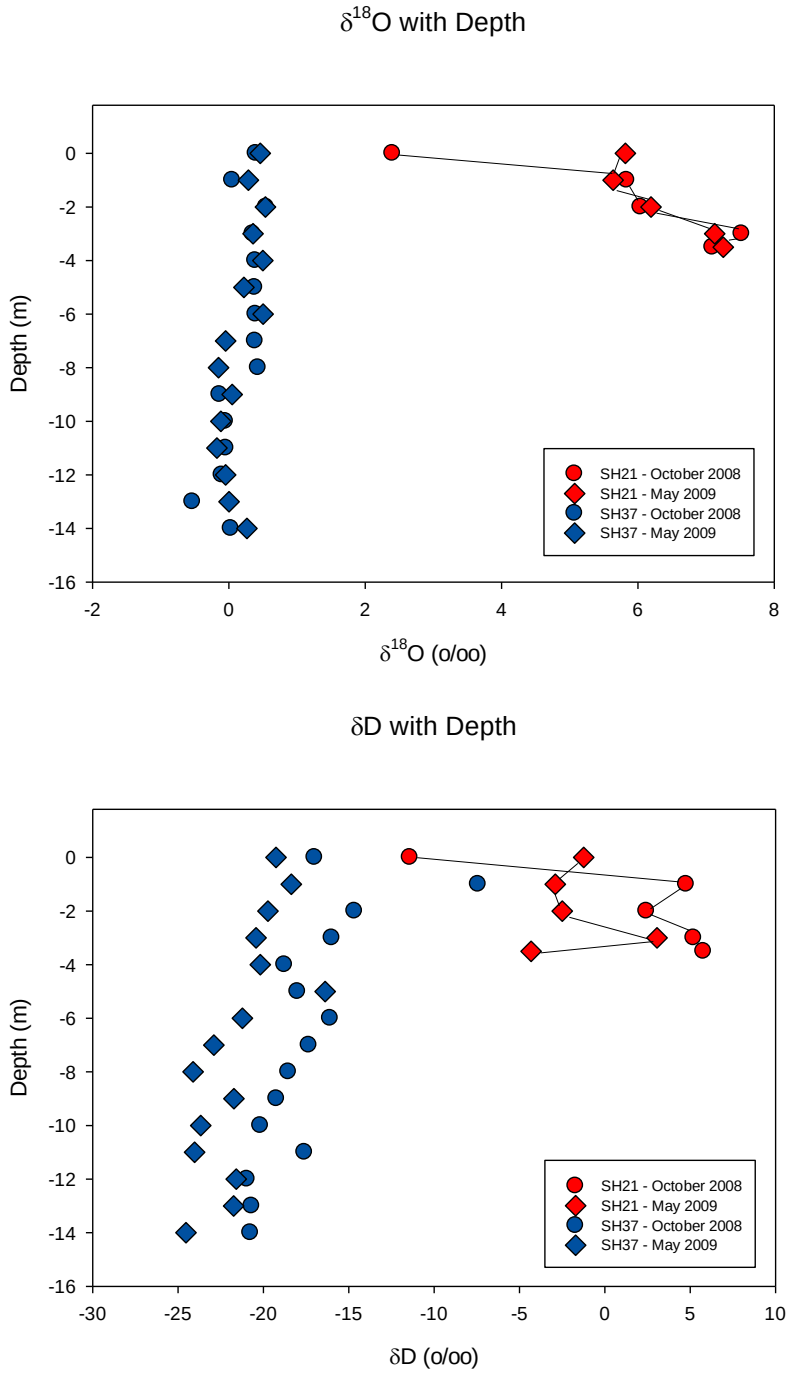

Figure 8: Stable Isotopes with Depth. Both d18O and dD were analyzed for each sample. While fluctuation along the water column does occur, it is generally within established error ranges, with a notable exception being the increase from surface to depth for SH21.for both isotope values. Higher isotope values are found among SH21 as compared with SH37..

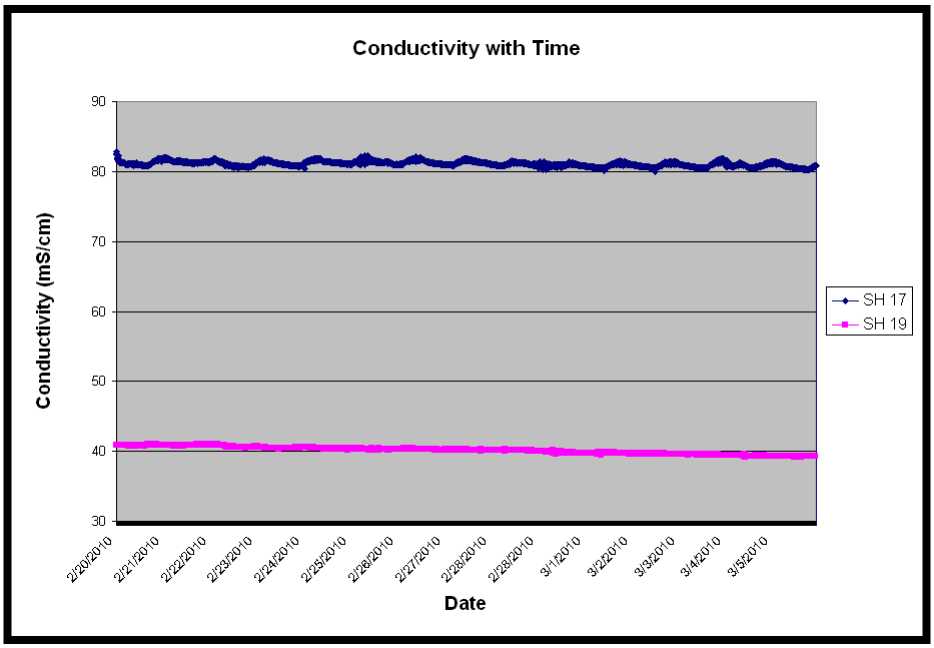

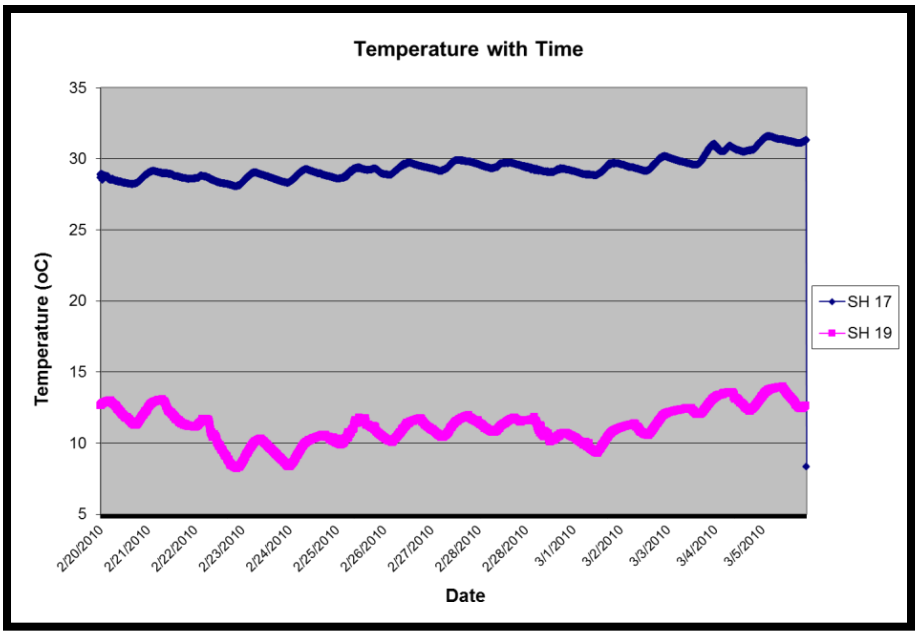

Figure 9: Two-Week Sonde Deployment. Sondes were deployed over a two-week time frame in Feb/Mar 2010 within SH17 and SH19. Conductivity varied minimally for SH19 while SH17 exhibited slight variation consistent with daily temperature fluctuation. Temperature was recorded with time. SH17 had consistently higher temperatures that changed little except for daily solar heating. SH19 had a larger fluctuation throughout the deployment although the signature preserved daily changes as well.

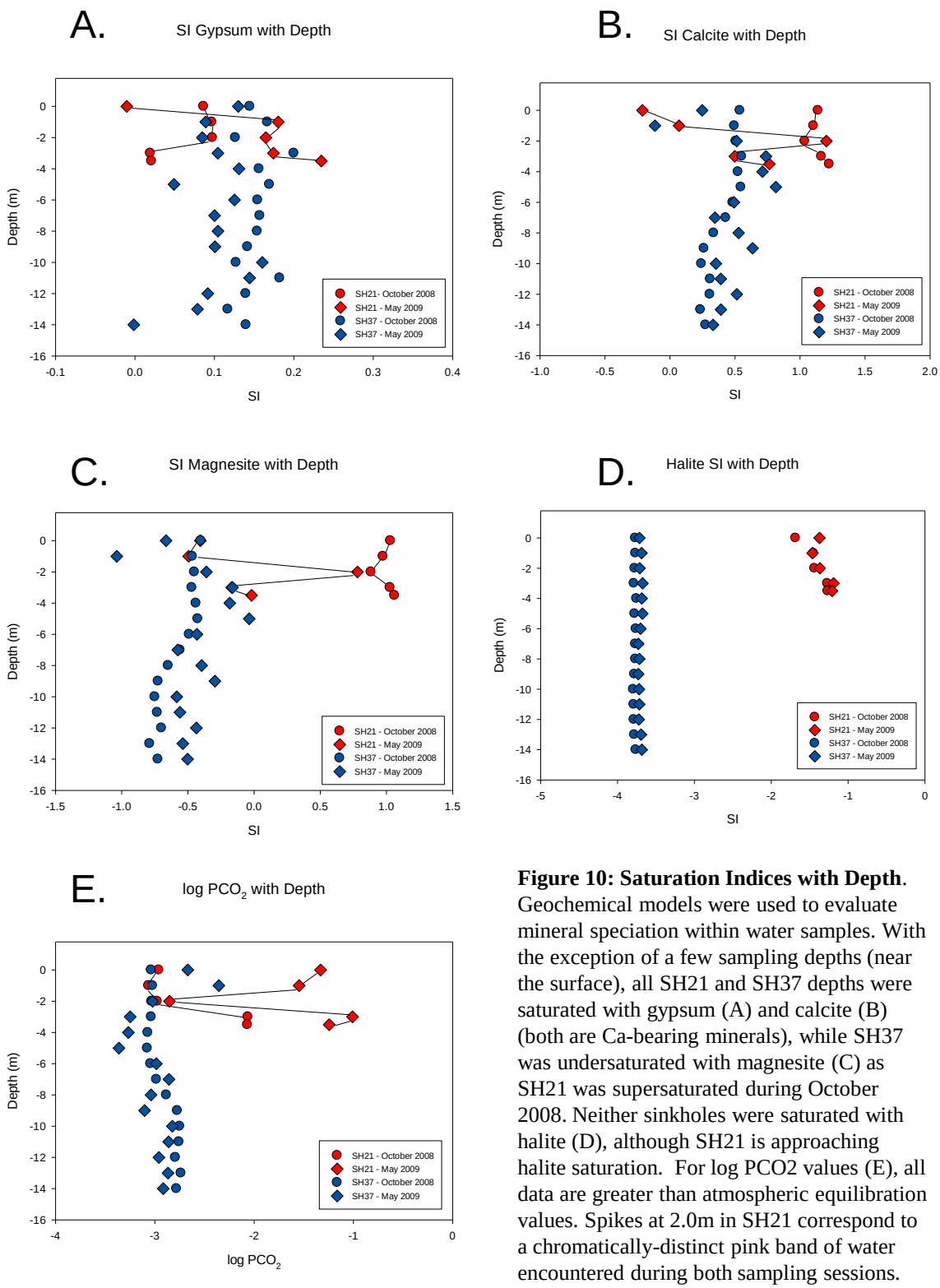

Figure 10: Saturation Indices with Depth. Geochemical models were used to evaluate mineral speciation within water samples. With the exception of a few sampling depths (near the surface), all SH21 and SH37 depths were saturated with gypsum (A) and calcite (B) (both are Ca-bearing minerals), while SH37 was undersaturated with magnesite (C) as SH21 was supersaturated during October 2008. Neither sinkholes were saturated with halite (D), although SH21 is approaching halite saturation. For log PCO2 values (E), all data are greater than atmospheric equilibration values. Spikes at 2.0m in SH21 correspond to a chromatically-distinct pink band of water encountered during both sampling sessions.

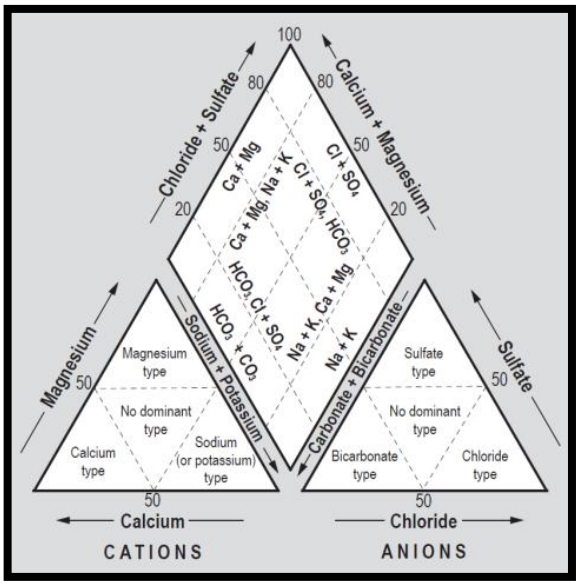

Figure 11: Piper Diagram. Sinkhole water samples plot with Na-Cl type endmember facies (Drever, 1997). Regional groundwater is initially Ca-HCO_3 type, acquiring evaporites as it progresses along the Pecos Slope. In the vicinity of the Refuge, groundwater is saline and surface spring water (Sago Spring, orange circle) contains salts upon discharge. The proportion of Cl increases concurrently with TDS among sinkholes demonstrating the progressive water column evolution from spring-like, well-mixed to mature, stratified. Purple circles indicate sinkhole water congregation at Na and Cl apices.

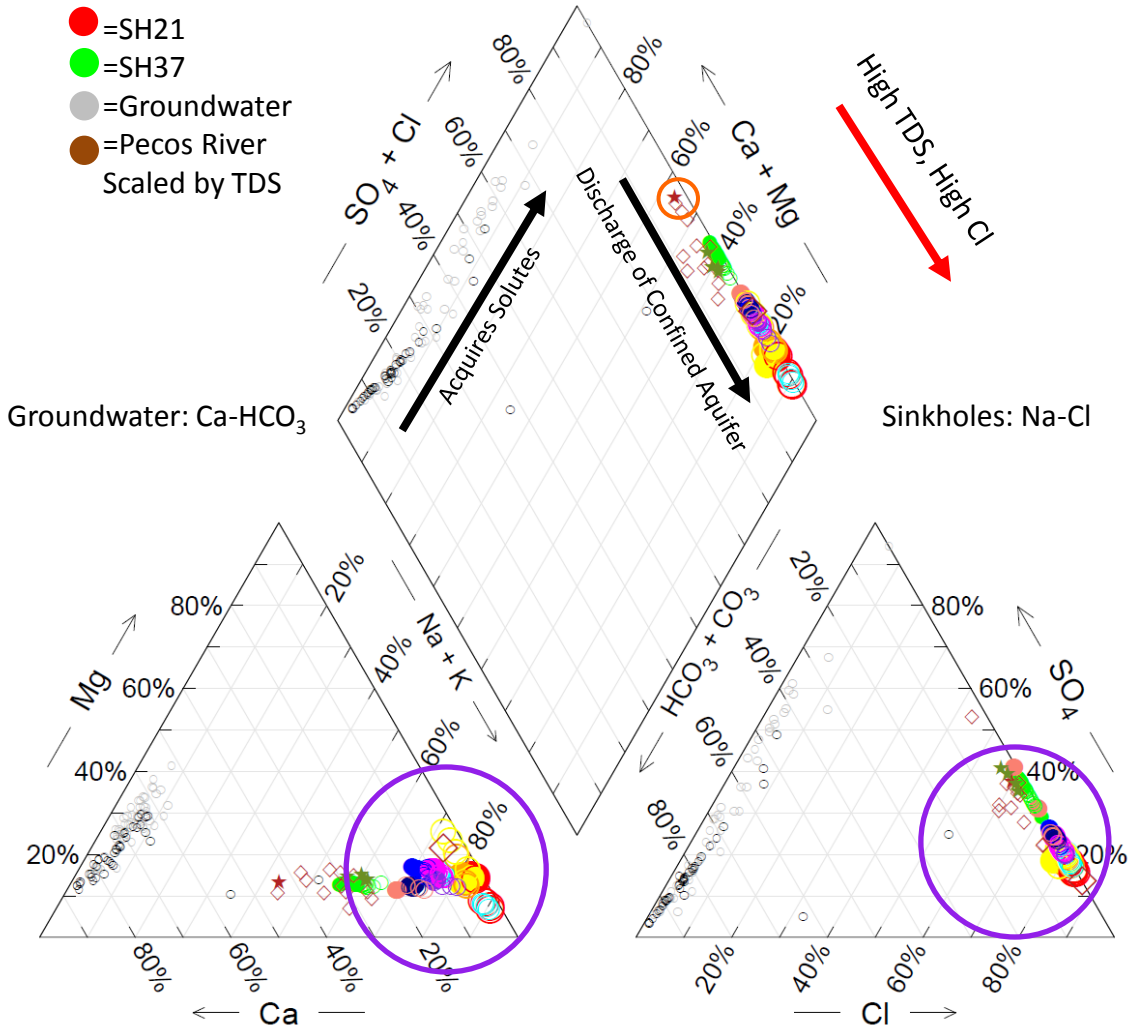

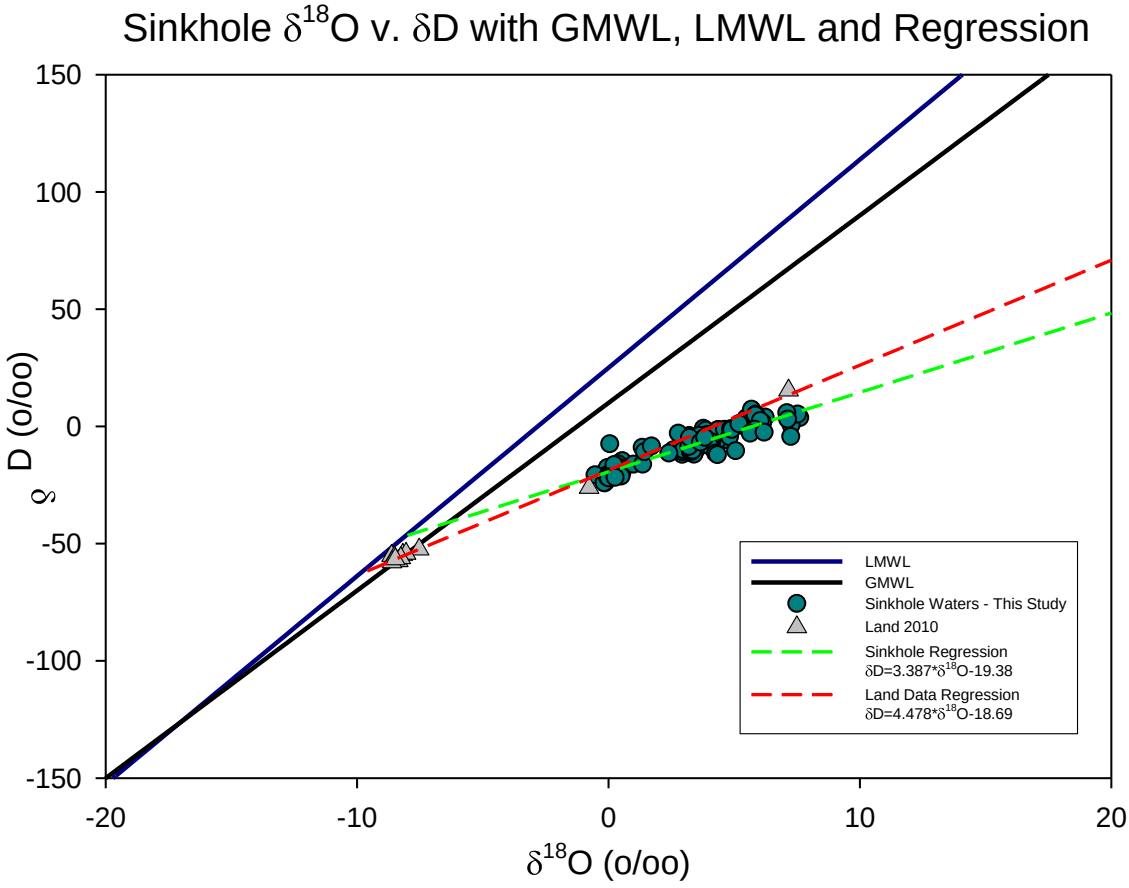

Figure 12: Sinkhole $\delta^{18}O$ v. δD with GMWL, LMWL and Regression . The plot of dD with d18O reveals an evaporation trajectory that describes the group of sinkhole samples. Data from Land (2010) plot similarly, but are defined by a slightly different regression. Both LMWL and GMWL are provided as reference. The grouping of sinkhole waters suggests alteration by a common set of factors, with evaporation from the open surface (per Baur et al., 1997) dominant in this system.

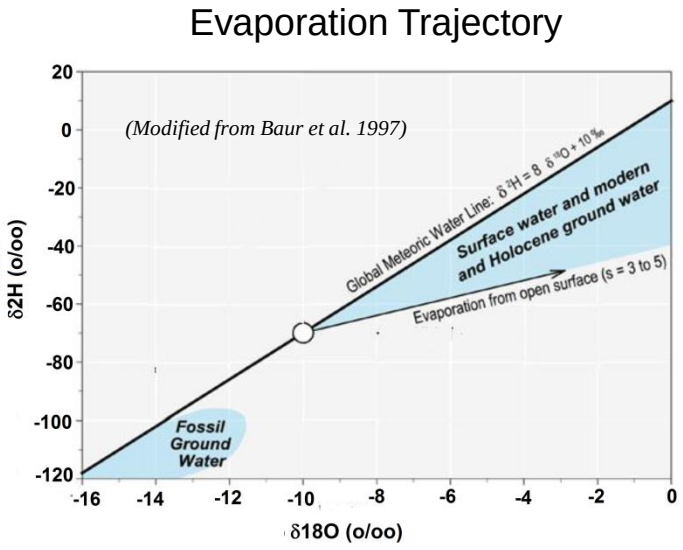

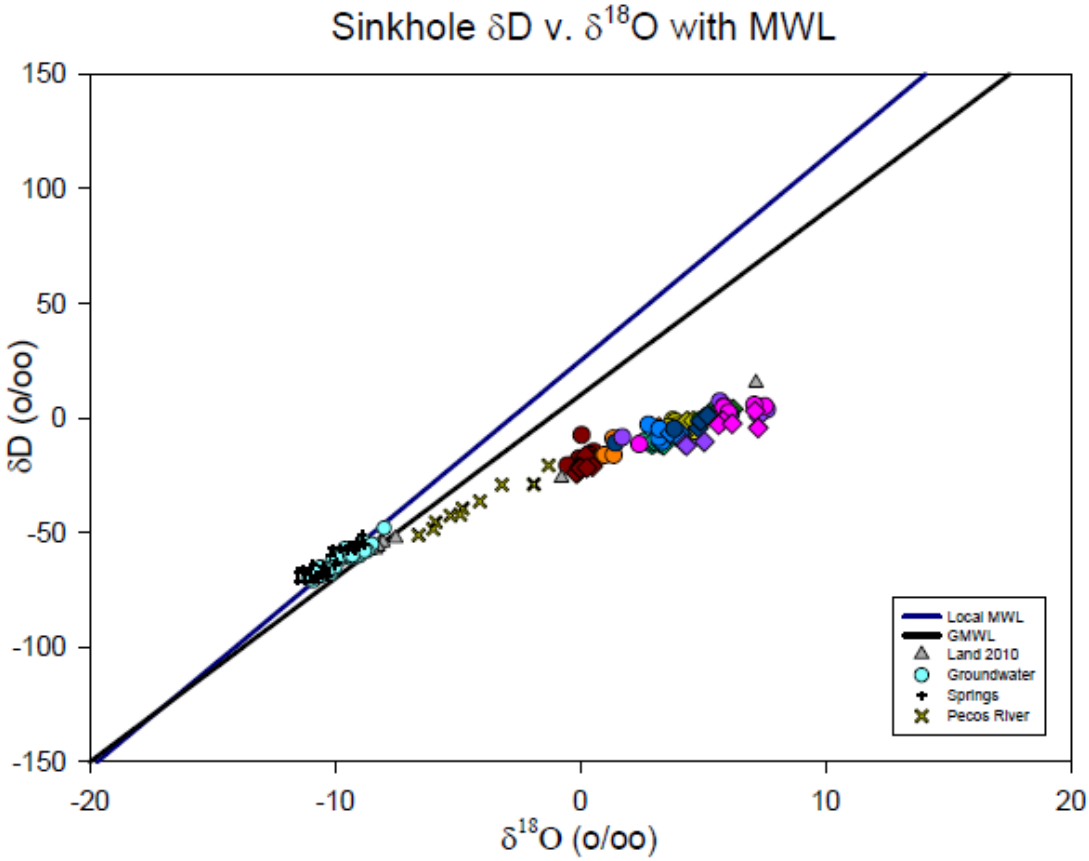

Figure 13: $\delta^{18}O$ v. δD with MWL and Pecos River. This plot depicts the progression of sinkhole waters, drawing comparison with Pecos River water, and regional groundwater and springs. Pecos River points are from Yuan and Miyamoto (2008); springs and groundwater are from Newton et al. (2009), and Land (2010) provides groundwater samples from the Refuge. The Pecos River values follow the sinkhole trend, while groundwater (whether collected from the Pecos Slope or closer to the Refuge) is consistent with meteoric water. In the vicinity of the Refuge, the Pecos River receives input from aquifer discharge which mixes with precipitation input from the headwaters, direct input, or overland flow.

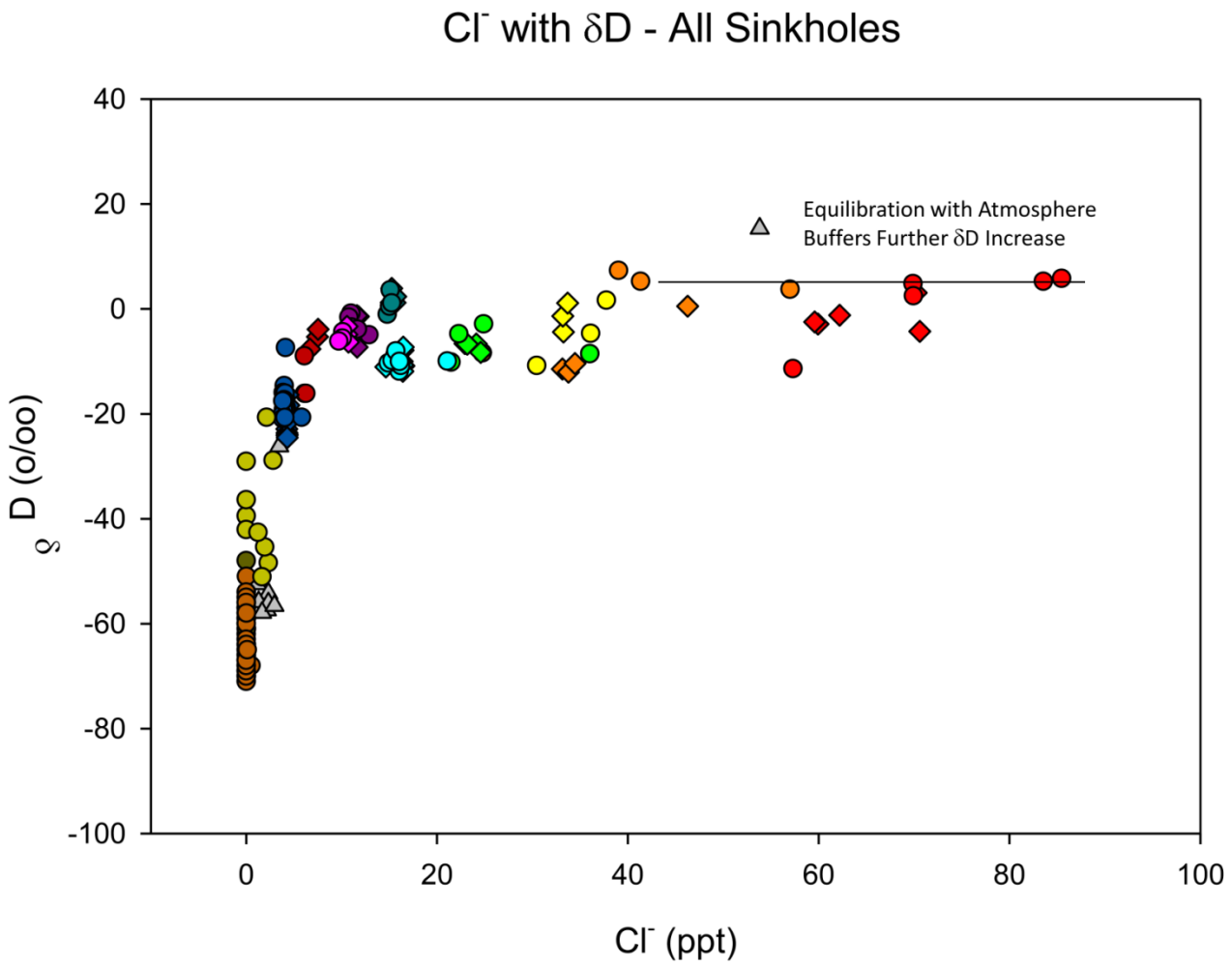

Figure 14: [Cl-] with δD – All Sinkholes. Both Cl and δD values increase as they progress from spring-like to stratified. A threshold for δD is reached upon equilibration with the atmosphere, buffering further increase; meanwhile, Cl continues to increase suggesting evaporation is a factor in this relationship.

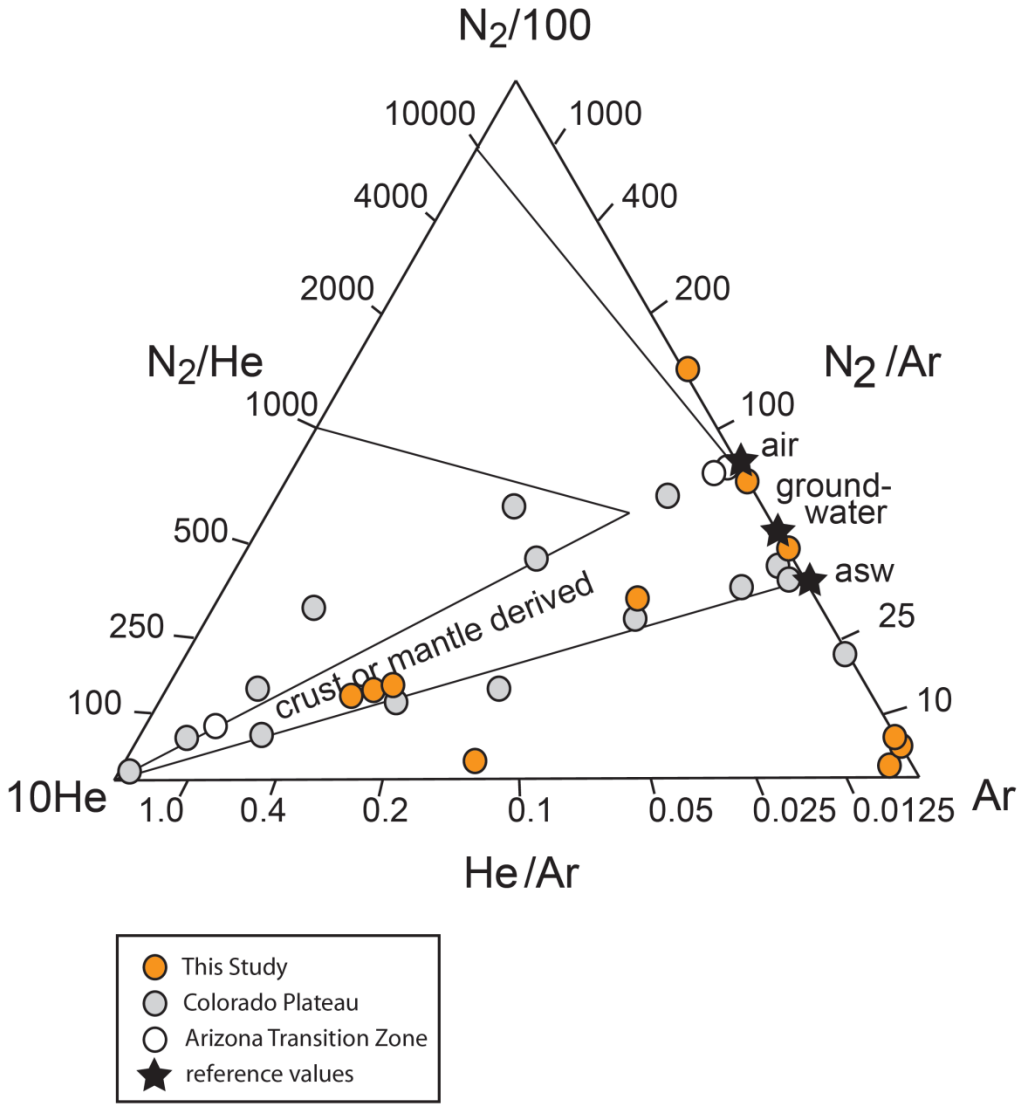

Figure 15: Dissolved Gas Ternary Diagram. Gas compositions (orange) are from Bitter Lake sinkholes sampled as part of this study. Samples collected during February 2010 have been corrected to a N2:Ar ratio of air saturated water (ASW) because of oxygen interference yielding incorrectly high Ar values. Several of these samples occupy the ternary zone defining waters derived from crust or mantle sources, as were discribed by Giggenbach et al. (1993); fields for crustal and mantle-derived gases, air, and air-saturated water are also from that study. Also shown are springs from the Colorado Plateau and Arizona Transition Zone (Crossey et al., 2006). Sinkhole waters present a wide range of N_2/He values.

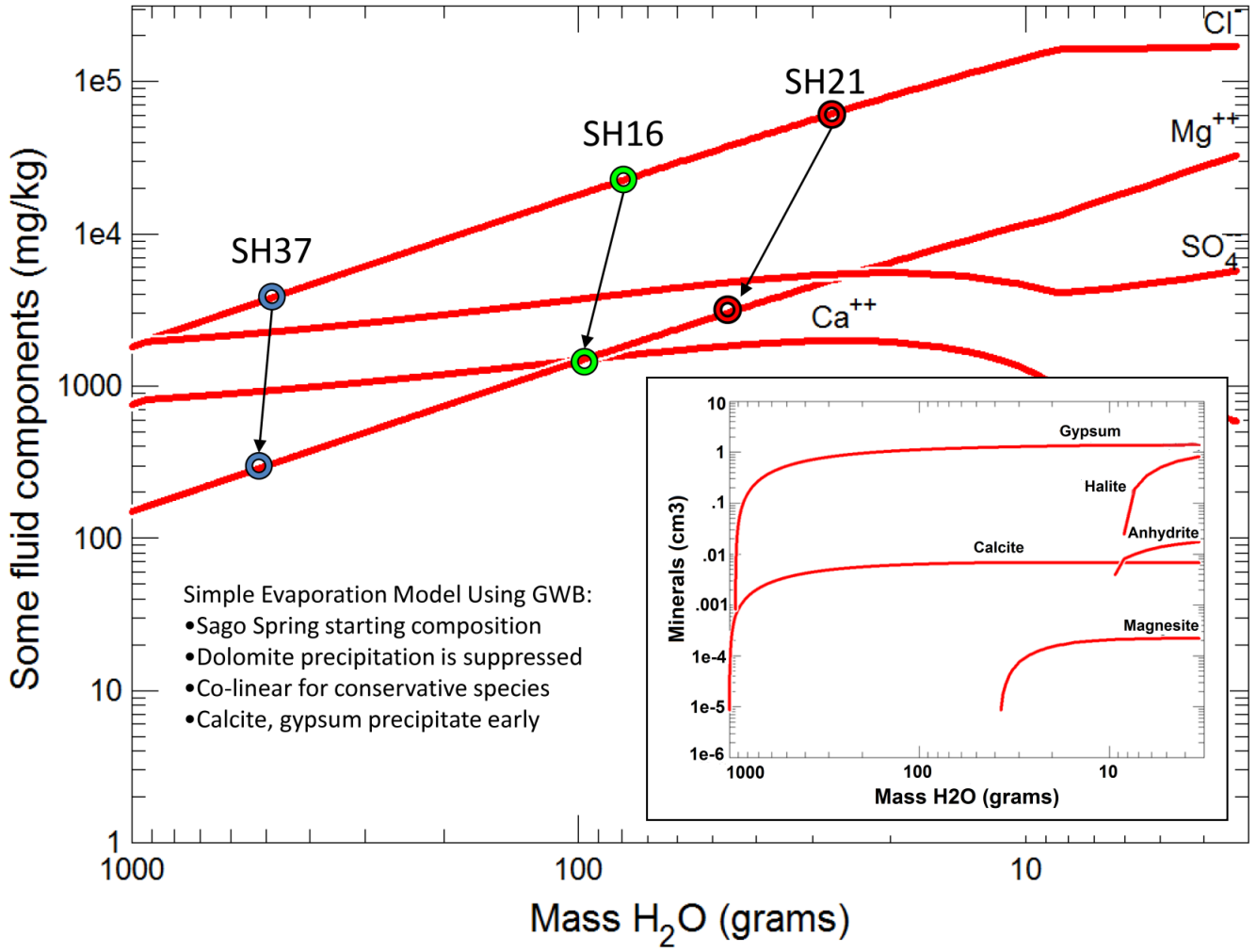

Figure 16: Simple Evaporation of Sago Spring Water. Dolomite was suppressed as 1.0L of Sago Spring water was evaporated. Inlaid image shows minerals species precipitation curves for the reaction, while the main image models the content of major ions that remain in solution. Colored circles relate the actual analyzed concentration for Cl and Mg in three sinkholes. As the points do not align, the implication is a more complex model is needed to define the evaporation-precipitation reactions in this system

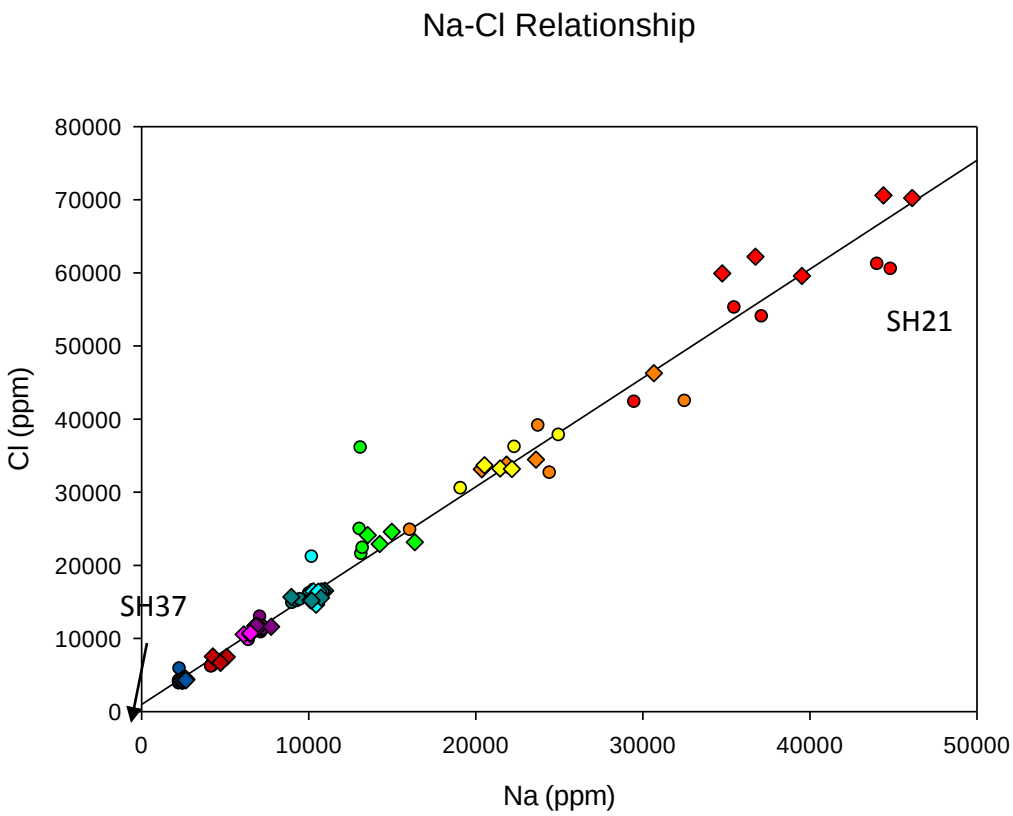

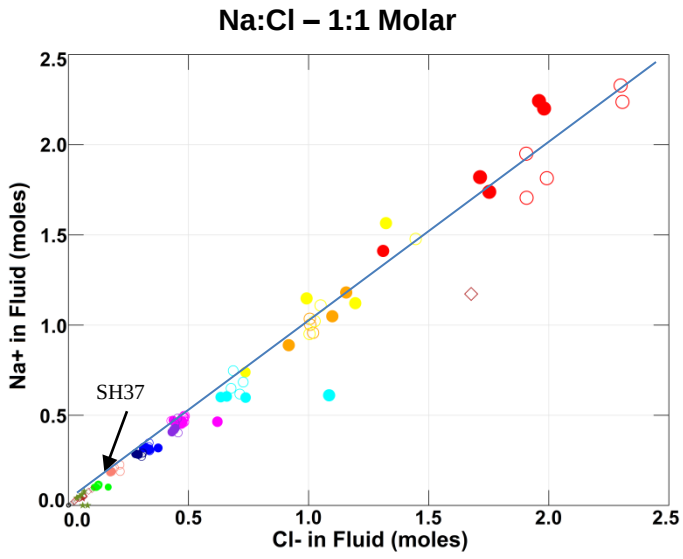

Figure 17: Na-Cl, Concentration and Molar. The content of Na and Cl among samples increase co-linearly suggesting the continued evolution of a common source water containing. The molar content of both ions follows a 1:1 line suggesting the dissolution of halite is the dominant contribution to Na-Cl content in sinkhole fluid.

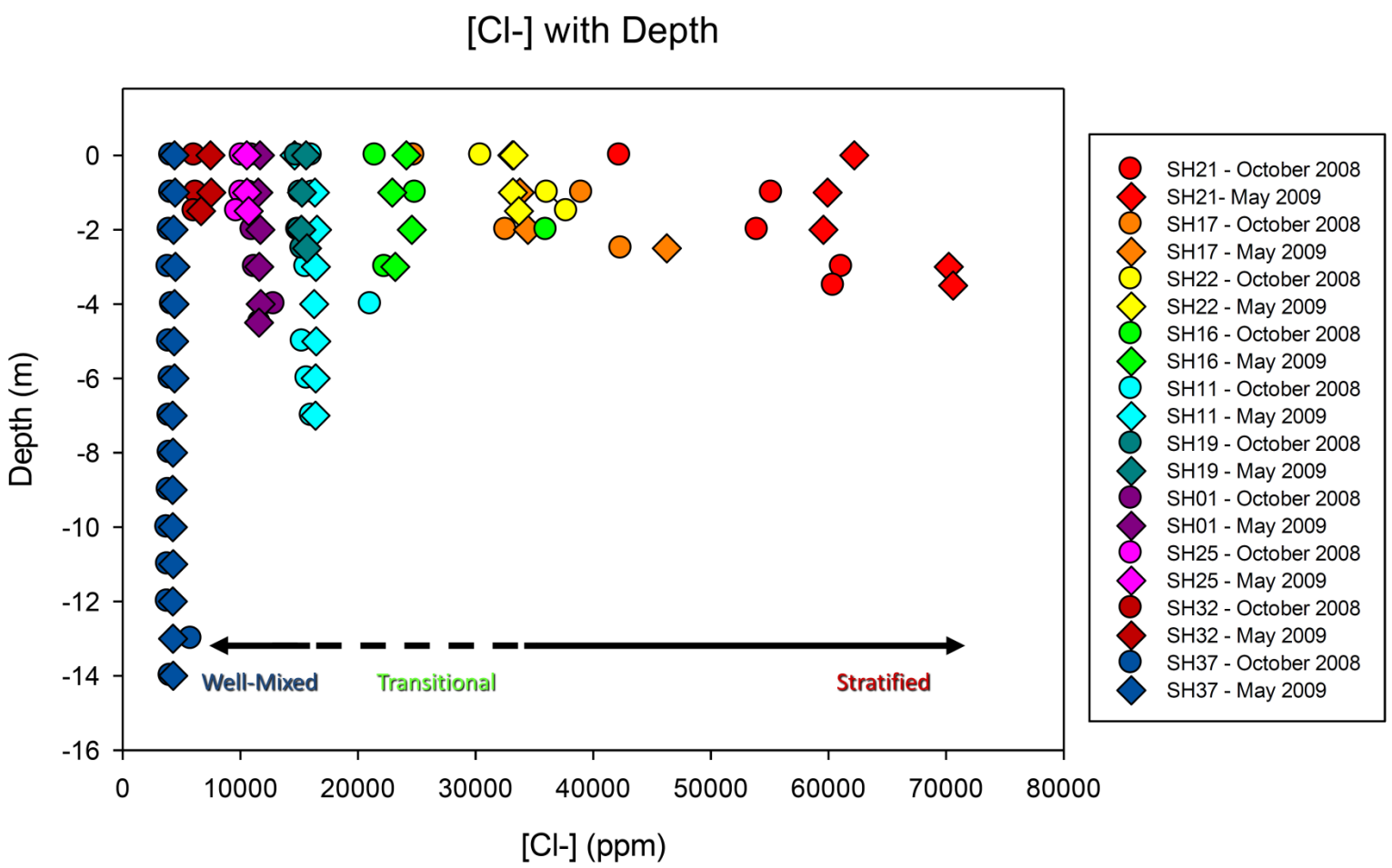

Figure 18: [Cl-] with Depth – All Sinkholes. Sinkholes organize along a gradient based on Cl content in water. Well-mixed sinkholes tend to have lower Cl concentrations, while as Cl increases, sinkholes adopt more structure and complexity in their water columns. Cl is considered a conservative property in this system because it does not readily precipitate, and water response to continuous accumulation is used to describe sinkhole lifecycle.

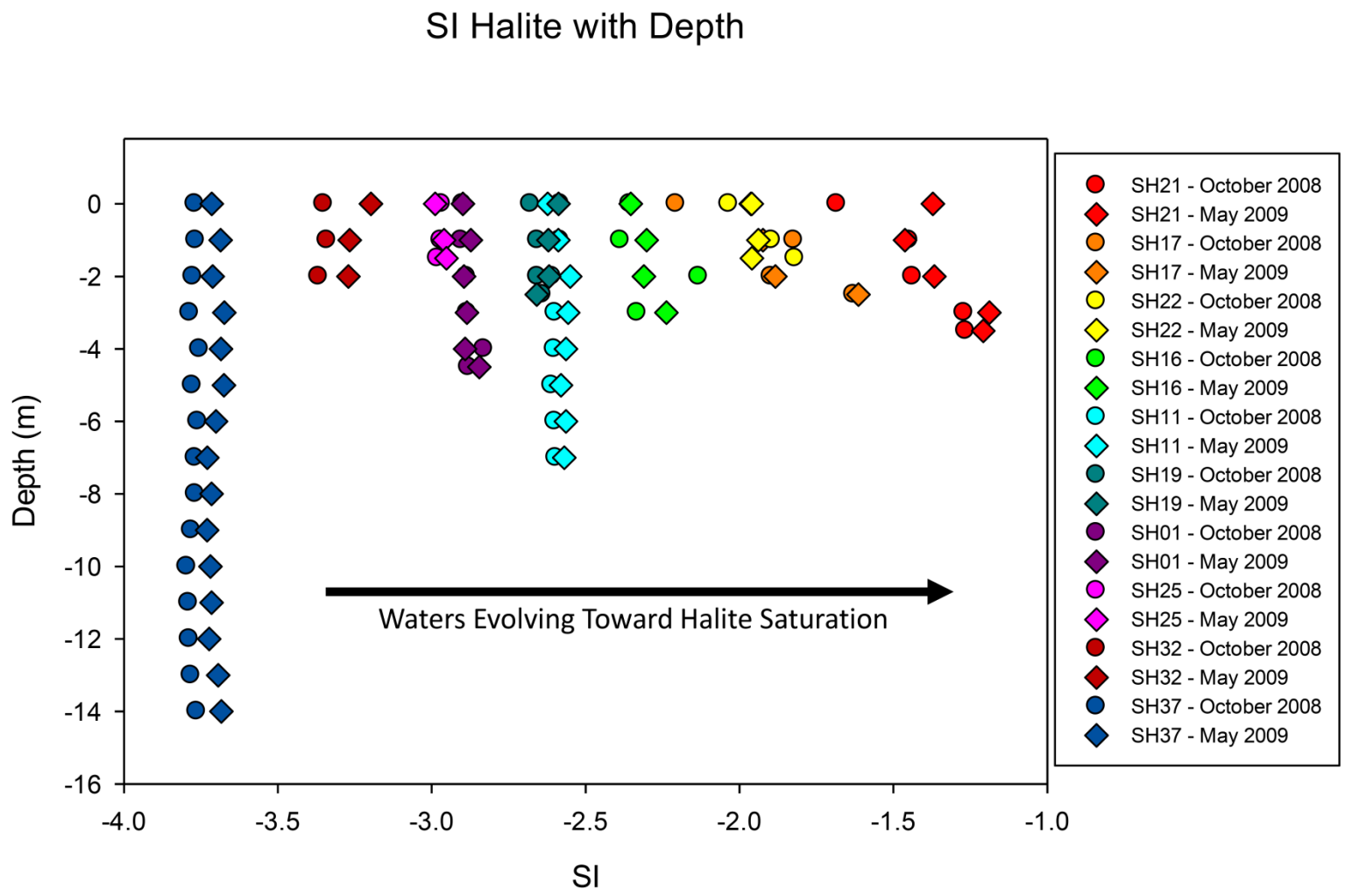

Figure 19: SI Halite with Depth – All Sinkholes. As water is evaporated, Na-Cl is left behind. Evan as galite does not readily precipitate, sinkhole water remains undersaturated. Sinkholes with stratified water columns are approaching saturation.

Approximation of Volume Loss Due to Evaporation

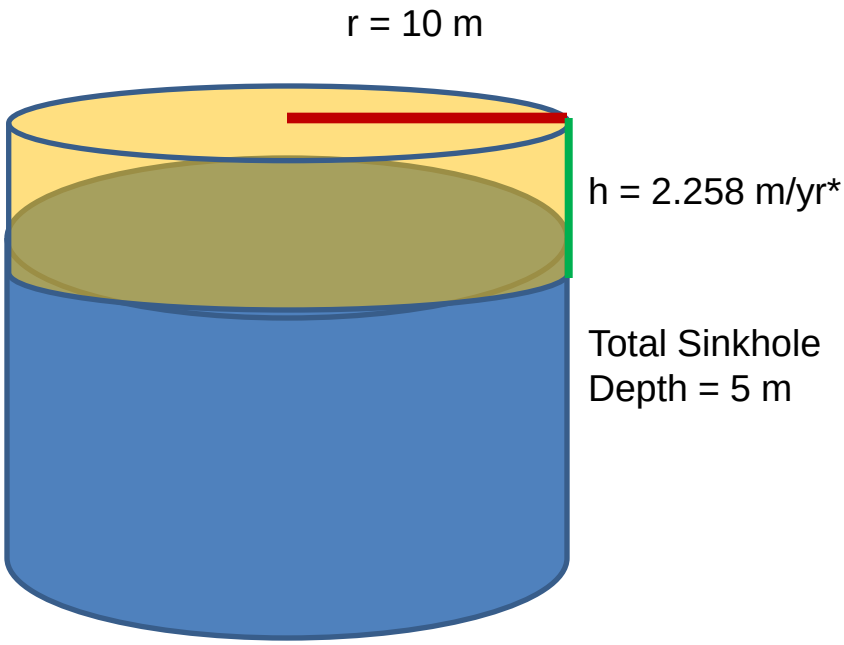

Figure 20: Approximation of Volume Loss Due to Evaporation. The cylinder represents a simple sinkhole geometry. The average pan evaporation rate is 2.258 m/yr, represented by "h" in the diagram above. For a sinkhole with a surface diameter of 10 m, the annual loss of water due to evaporation is $V = pr^2h = p10^2*2.258 = 709.4\ m^3/yr$. In this simple cylinder, the overall volume is approximately 1,571 m^3. Thus, ~45% of the total sinkhole volume is evaporated and subsequently recharged by source water inflow. Removal of this water leaves behind dissolved components. The predicted concentration of Cl in source water (e.g., Sago Spring-like input) is 2,050 mg/l; the total number of liters of water lost over a year-long period is 709,400 l/yr. The annual input of "new" Cl in a sinkhole this size is 1,454 kg/yr. Standard textbook methods suggest multiplying pan evaporation rates by 0.75 to account for thermodynamic differences between the metal pan and non-metal lake sediments. Assuming this correction, the loss may be recalculated to 532.1 m^3/yr, with the annual "new" Cl input modified to 1,091 kg/yr. Using this corrected value, the annual input of "new" Cl would be 694.5 mg/l. Using this approach, SH21 – 3.8 m depth, with a diameter of 40 m – would have a "new" Cl increase of 913.6 mg/l. Actual values had a greater increase from October 2008 to May 2009 than suggested by this calculated approach.

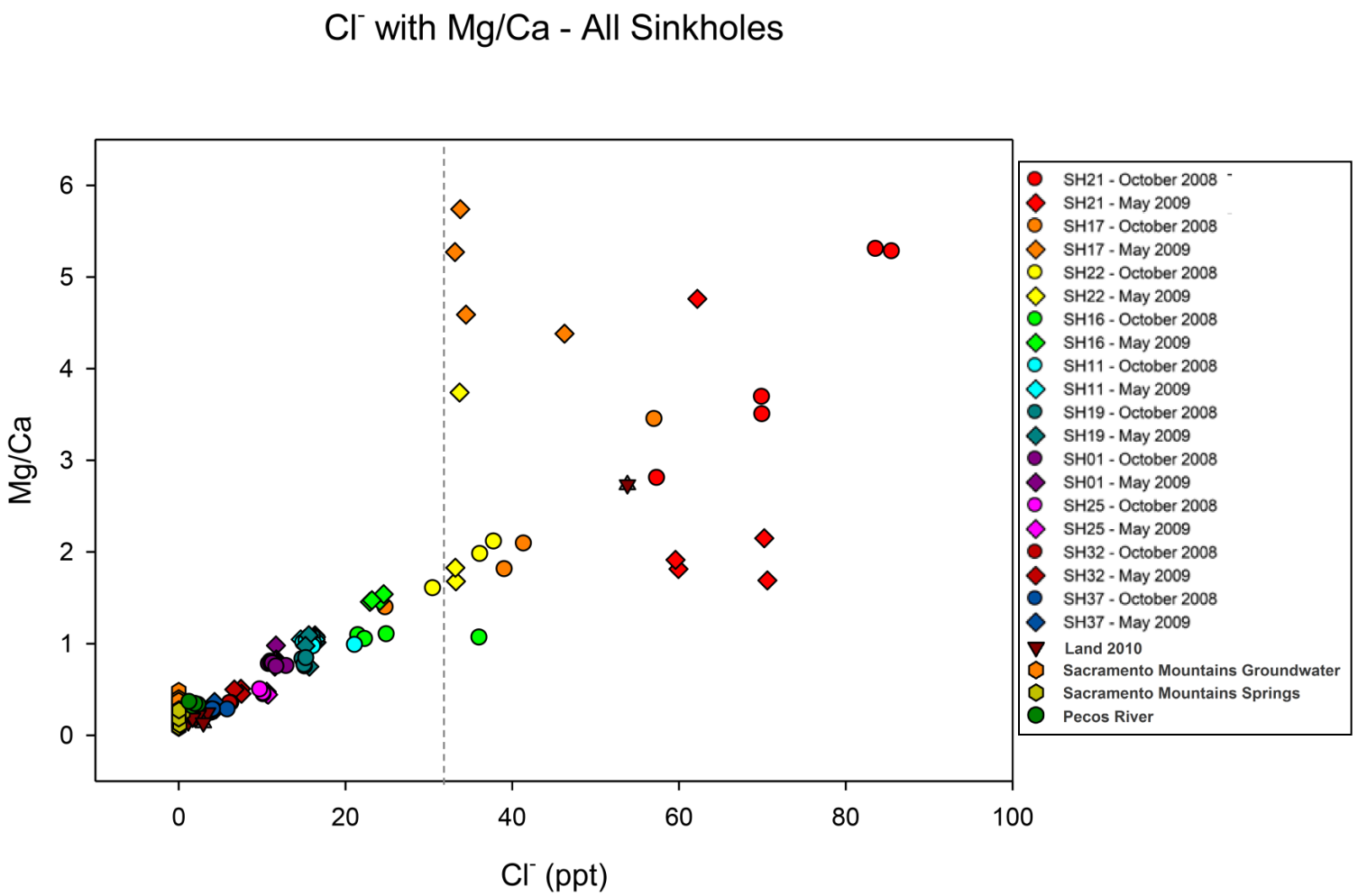

Figure 21: Cl with Mg/Ca. The linear relationship between Cl and the ratio of Mg:Ca shows that with increasing Cl, the relative amount of Mg also increases. All SH17 (May 2009) samples plot well above the linear grouping, with the high point being sample at 1.0m. Precipitation of calcite and gypsum removes Ca from the system, increasing the proportion of Mg. The linear relationship implies concurrent change in both Cl and Mg/Ca which is likely due to evaporation and subsequent precipitation of mineral species.

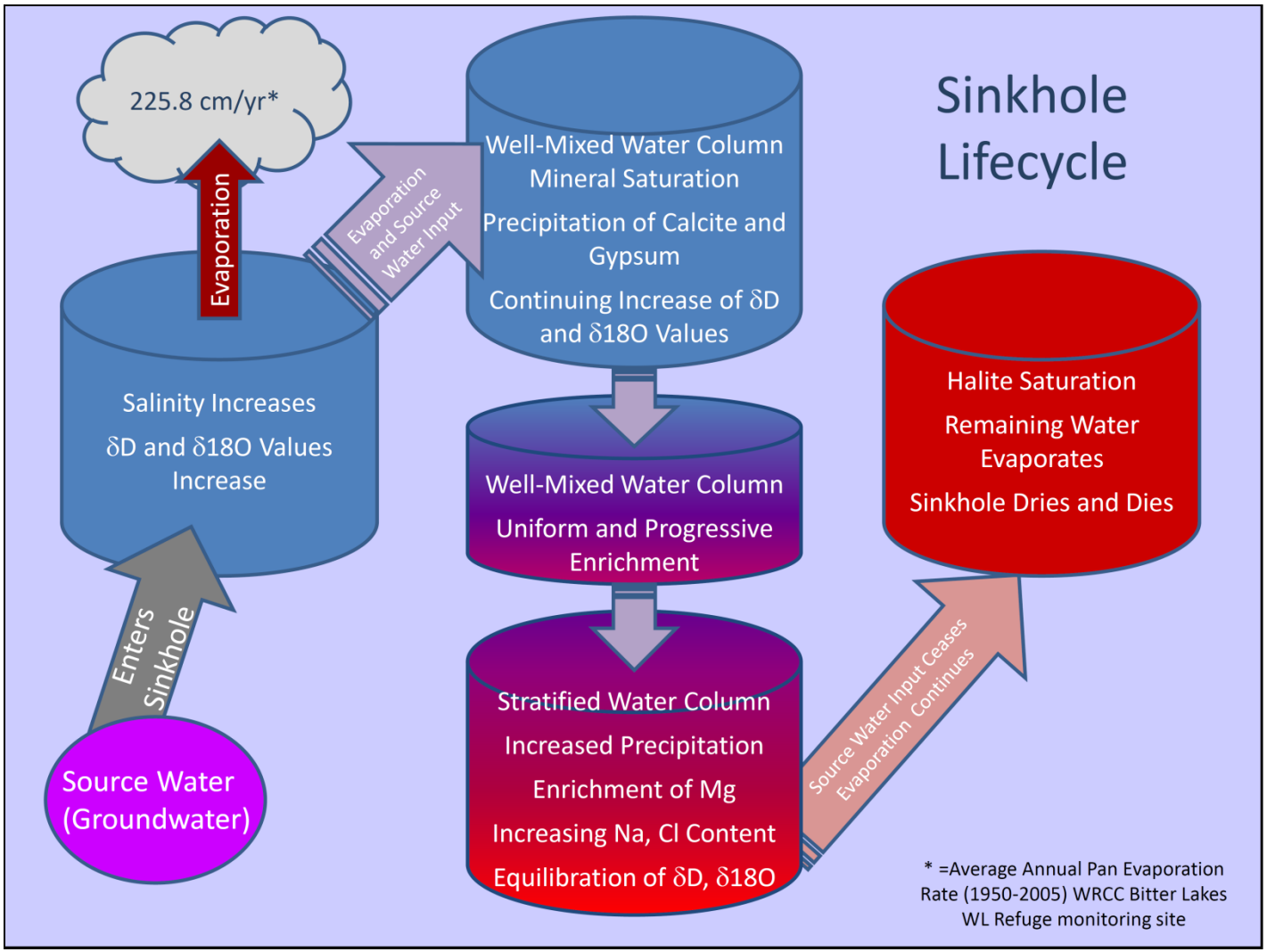

Figure 22: Sinkhole Lifecycle

Table 1. Initial Site Survey Parameters

Sinkhole	Depth (m)	Sample ID	Date	Temperature (oC)	pH	Conductivity (mS/cm)	Alkalinity (mg/L HCO3)
17	surface	SH17-071020-B	20-Oct-07	19.3	8.28	66.8	198.61
2	surface	SH02-071020-B	20-Oct-07	18.6	8.03	25.4	93.36
22	surface	SH22-071020-B	20-Oct-07	18.8	7.51	65.5	230.03
24	surface	SH24-071020-B	20-Oct-07	20.2	7.86	46.2	151.02
21	surface	SH21-071020-B	20-Oct-07	19.2	8.07	106.6	263.90
8	surface	SH08-071020-B	20-Oct-07	14.6	8.19	53.7	168.10
4	surface	SH04-071020-B	20-Oct-07	15.2	8.23	34.2	133.63
9	surface	SH09-071020-B	20-Oct-07	18.5	8.07	36.5	125.70
6	surface	SH06-071020-B	20-Oct-07	18.2	8.35	58.1	155.59
7	surface	SH07-071021-B	20-Oct-07	19	8.13	12.03	83.29
3	surface	SH03-071021-B	20-Oct-07	17.7	8.27	27.3	95.49
25	surface	SH25-071020-B	20-Oct-07	17.4	8.97	26.8	57.05
37	surface	SH37-071021-B	20-Oct-07	19.6	8.07	15.43	90.92
26	surface	SH26-071020-B	20-Oct-07	18.1	7.32	50.7	151.32
15	surface	SH15-071021-B	20-Oct-07	15	7.91	42.8	129.66
31	surface	SH31-071021-B	20-Oct-07	14.3	8.09	9.4	133.93
38	surface	SH38-071021-B	20-Oct-07	16.5	7.14	8.58	166.58
19	surface	SH19-071020-B	20-Oct-07	18.4	7.86	41.1	93.97
1	surface	SH01-071021-B	20-Oct-07	19	8.07	33.8	107.70

Table 2. Water Chemistry

Sample_ID	Spring_name	Temp_degC	pH	Cond_uS	Ca_ppm	Mg_ppm	Na_ppm	K_ppm	HCO3 mg/L	Cl_ppm	SO4_ppm	% balance	delD	del18O
210-9	Sinkhole 21	20.34	8.06	66,300	983	2,763	29,520	237.0	329.2	42,272	14,117	2.45	-11.41	2.40
211-9	Sinkhole 21	18.74	8.07	74,500	916	3,384	35,510	296.0	298.4	55,173	16,277	-0.63	4.77	5.84
212-9	Sinkhole 21	18.94	7.99	74,900	955	3,347	37,150	305.0	290.4	53,954	16,254	2.15	2.44	6.04
213-9	Sinkhole 21	17.54	7.62	82,800	764	4,056	44,060	361.0	963.5	61,135	17,961	4.16	5.21	7.52
2138-9	Sinkhole 21	15.84	7.66	80,300	772	4,079	44,870	361.5	1,086.1	60,446	18,210	5.26	5.78	7.09
220-9	Sinkhole 22	13.80	8.09	88,500	1,124	1,805	19,130	118.4	350.8	30,453	10,663	-2.21	-10.80	1.43
221-9	Sinkhole 22	22.00	7.99	96,000	1,065	2,110	22,350	142.0	230.6	36,100	11,546	-2.43	-4.71	3.83
2215-9	Sinkhole 22	23.90	6.46	113,600	1,172	2,480	25,000	182.5	1,338.1	37,751	11,560	1.01	1.61	6.13
170-9	Sinkhole 17	16.24	8.15	39,300	976	1,366	16,100	73.0	257.5	24,758	8,357	-0.76	-8.40	1.71
171-9	Sinkhole 17	16.44	7.53	54,500	1,141	2,070	23,770	159.2	294.1	39,032	11,940	-3.40	7.28	5.69
172-9	Sinkhole 17	17.74	7.71	56,700	1,032	2,162	24,460	168.7	714.5	32,583	12,216	4.53	5.21	5.86
1725-9	Sinkhole 17	17.84	7.94	68,300	861	2,973	32,540	242.6	3,258.3	42,383	13,659	5.43	3.71	7.61
370-9	Sinkhole 37	16.84	7.80	8,820	984	279	2,290	17.7	91.8	4,097	3,271	-3.66	-17.00	0.40
371-9	Sinkhole 37	15.54	7.78	8,920	986	278	2,288	17.5	92.1	4,109	3,470	-4.89	-7.42	0.05
372-9	Sinkhole 37	15.34	7.79	8,700	967	276	2,289	16.3	91.5	3,979	3,087	-2.04	-14.66	0.55
373-9	Sinkhole 37	15.04	7.79	8,740	1,112	277	2,305	18.3	91.5	3,881	3,359	-0.54	-15.99	0.35
374-9	Sinkhole 37	15.44	7.82	8,800	974	274	2,319	17.5	90.9	4,170	3,410	-4.88	-18.77	0.39
375-9	Sinkhole 37	15.24	7.82	8,750	1,039	285	2,322	16.0	90.3	3,926	3,298	-1.18	-18.00	0.38
376-9	Sinkhole 37	14.54	7.79	8,790	973	274	2,333	16.4	90.9	4,059	3,358	-3.60	-16.08	0.39
377-9	Sinkhole 37	13.74	7.73	8,800	1,002	280	2,331	21.5	91.0	3,959	3,253	-1.68	-17.33	0.39
378-9	Sinkhole 37	14.24	7.64	8,730	968	272	2,328	17.5	91.8	3,984	3,347	-3.14	-18.53	0.43
379-9	Sinkhole 37	13.94	7.55	8,790	954	273	2,300	16.6	95.8	3,895	3,239	-2.41	-19.23	-0.14
3710-9	Sinkhole 37	13.84	7.54	8,680	905	256	2,286	16.7	98.7	3,774	3,230	-2.72	-20.17	-0.05
3711-9	Sinkhole 37	13.44	7.54	8,690	1,081	279	2,285	17.0	97.6	3,832	3,207	0.07	-17.59	-0.04
3712-9	Sinkhole 37	13.24	7.58	8,650	972	270	2,297	17.6	98.8	3,811	3,115	-0.85	-20.96	-0.10
3713-9	Sinkhole 37	13.24	7.52	8,460	943	268	2,309	17.6	97.9	5,798	3,243	-15.57	-20.69	-0.53
3714-9	Sinkhole 37	12.94	7.57	8,610	931	266	2,290	16.7	100.1	4,058	3,279	-4.56	-20.75	0.03
160-9	Sinkhole 16	18.40	8.21	67,900	1,310	1,436	13,180	77.7	162.3	21,477	7,344	-0.17	-10.20	3.35
161-9	Sinkhole 16	16.70	8.18	68,700	1,233	1,362	13,080	70.3	160.2	24,884	7,619	-7.39	-2.91	2.78
162-9	Sinkhole 16	15.90	8.21	68,500	1,276	1,365	13,140	70.9	158.0	36,013	12,263	-25.92	-8.59	3.20
163-9	Sinkhole 16	15.60	8.23	68,600	1,292	1,360	13,260	71.0	164.1	22,291	7,303	-1.86	-4.76	3.22
010-9	Sinkhole 01	18.50	7.92	41,400	1,108	893	7,135	48.1	116.2	10,981	5,093	2.65	-0.85	3.77
011-9	Sinkhole 01	17.80	7.86	41,500	1,135	886	7,185	50.6	114.0	10,764	5,235	3.37	-1.62	3.87
012-9	Sinkhole 01	16.60	7.89	41,800	1,136	895	7,256	49.3	113.8	11,015	5,151	3.16	-3.50	3.94

Sample_ID	Spring_name	Temp_degC	pH	Cond_uS	Ca_ppm	Mg_ppm	Na_ppm	K_ppm	HCO3mg/L	Cl_ppm	SO4_ppm	% balance	delD	del18O
013-9	Sinkhole 01	17.20	7.87	41,700	1,138	895	7,137	49.2	114.1	11,227	4,499	3.51	-4.66	3.70
014-9	Sinkhole 01	17.50	7.92	41,500	1,183	898	7,127	50.1	113.7	12,879	5,007	-2.75	-4.96	4.02
0145-9	Sinkhole 01	17.50	7.91	41,600	1,197	902	6,947	50.2	115.9	11,669	4,572	1.30	-3.88	3.62
110-9	Sinkhole 11	17.60	7.81	54,300	1,123	1,207	10,360	66.0	144.0	16,033	6,192	2.03	-11.91	2.93
111-9	Sinkhole 11	18.80	7.99	54,500	1,183	1,185	10,300	66.3	142.8	16,189	6,125	1.66	-10.80	2.93
112-9	Sinkhole 11	17.70	8.00	54,500	1,169	1,184	10,490	69.2	144.2	14,901	6,223	5.28	-10.32	3.07
113-9	Sinkhole 11	18.20	8.01	54,800	1,254	1,194	10,270	67.8	142.8	15,589	6,255	3.13	-8.83	3.56
114-9	Sinkhole 11	17.50	8.03	54,800	1,200	1,187	10,220	73.9	146.7	21,083	7,648	-11.20	-9.98	3.06
115-9	Sinkhole 11	18.20	8.03	54,700	1,141	1,177	10,210	69.1	145.2	15,296	6,216	3.13	-9.84	3.22
116-9	Sinkhole 11	18.40	8.03	54,300	1,099	1,185	10,220	68.8	142.2	15,694	6,333	1.86	-8.08	3.12
117-9	Sinkhole 11	17.30	8.06	55,100	1,218	1,185	10,060	68.1	149.9	16,053	6,980	-0.25	-10.05	2.58
190-9	Sinkhole 19	19.94	8.13	28,300	1,066	889	9,059	71.2	87.6	14,784	6,098	-2.17	-1.04	4.86
191-9	Sinkhole 19	19.04	8.15	28,000	1,183	893	9,318	71.3	86.6	15,096	6,045	-1.23	3.59	5.48
192-9	Sinkhole 19	18.24	8.06	28,300	1,188	917	9,345	71.6	89.1	15,021	6,123	-0.87	0.47	5.29
1925-9	Sinkhole 19	17.74	8.02	28,200	1,088	920	9,522	81.1	88.5	15,249	6,051	-1.02	1.11	5.20
250-9	Sinkhole 25	13.60	9.13	38,200	1,309	590	6,356	36.2	50.4	10,109	4,303	2.05	-4.44	4.01
251-9	Sinkhole 25	13.60	9.11	38,300	1,275	594	6,350	40.1	48.0	10,065	4,275	2.11	-5.64	4.66
2515-9	Sinkhole 25	14.50	9.16	38,100	1,184	595	6,444	37.0	51.6	9,706	4,364	3.16	-6.20	3.35
320-9	Sinkhole 32	17.84	8.84	11,730	1,053	375	4,253	25.8	53.8	6,108	3,791	3.25	-16.15	1.00
321-9	Sinkhole 32	16.84	8.71	11,830	1,062	376	4,245	24.3	54.0	6,254	3,847	2.24	-16.16	1.36
3215-9	Sinkhole 32	16.04	7.62	11,840	1,059	374	4,193	159.2	64.7	6,089	5,788	-4.13	-8.96	1.34
210-5	Sinkhole 21	24.00	6.56	122,300	680	3,237	36,740	159.6	336.0	62,200	15,760	-4.65	-1.234	5.8175
211-5	Sinkhole 21	22.40	6.75	124,100	1,025	1,859	34,752	169.7	314.0	59,925	15,876	-8.17	-2.898	5.6371
212-5	Sinkhole 21	22.60	7.96	123,700	1,039	1,986	39,520	171.6	319.0	59,571	15,986	-2.01	-2.492	6.1935
213-5	Sinkhole 21	21.20	6.67	138,700	927	1,993	46,120	202.5	962.8	70,225	17,967	-3.25	3.059	7.1265
2138-5	Sinkhole 21	19.50	6.90	138,900	1,037	1,752	44,400	210.2	967.7	70,602	17,758	-5.42	-4.313	7.2525
220-5	Sinkhole 22	27.00	6.99	82,900	1,019	1,711	21,460	87.9	148.5	33,246	10,890	-1.73	-4.428	4.8155
221-5	Sinkhole 22	21.30	8.11	85,000	1,021	1,865	22,160	79.7	142.5	33,169	10,600	0.50	-1.363	4.8995
2215-5	Sinkhole 22	20.90	7.68	85,000	728	2,722	20,520	84.4	170.8	33,681	9,607	0.09	1.1	5.1915
170-5	Sinkhole 17	19.90	6.48	78,000	730	3,848	20,360	65.8	186.0	33,131	10,989	3.08	-11.44	4.2615
171-5	Sinkhole 17	20.10	7.81	78,200	640	3,673	21,840	69.0	183.0	33,760	10,567	4.50	-12.071	4.3315
172-5	Sinkhole 17	21.40	7.29	83,300	732	3,359	23,600	78.1	194.0	34,457	11,890	4.63	-10.406	5.0555
1725-5	Sinkhole 17	21.50	6.23	105,400	754	3,303	30,660	114.6	2,982.5	46,266	13,484	0.35	0.513	7.2665
370-5	Sinkhole 37	20.50	7.46	16,250	972	276	2,470	45.4	91.5	4,414	3,346	-4.22	-19.2575	0.4601
371-5	Sinkhole 37	19.20	7.14	16,440	909	277	2,589	35.8	91.2	4,463	3,175	-3.14	-18.363	0.2879
372-5	Sinkhole 37	19.00	7.79	16,390	900	278	2,504	35.4	90.5	4,329	3,123	-3.01	-19.729	0.5361
373-5	Sinkhole 37	18.70	8.00	16,420	977	278	2,646	30.6	90.5	4,484	3,095	-1.29	-20.429	0.3545
374-5	Sinkhole 37	19.10	8.00	16,410	972	276	2,641	33.6	86.5	4,409	3,388	-2.44	-20.182	0.4985
375-5	Sinkhole 37	18.90	8.11	16,430	895	276	2,686	44.6	91.6	4,382	2,867	0.15	-16.378	0.2205

Sample_ID	Spring_name	Temp_degC	pH	Cond_uS	Ca_ppm	Mg_ppm	Na_ppm	K_ppm	HCO3mg/L	Cl_ppm	SO4_ppm	% balance	delD	del18O
376-5	Sinkhole 37	18.20	7.75	16,430	971	276	2,529	27.4	90.6	4,402	3,268	-3.14	-21.227	0.5037
377-5	Sinkhole 37	17.40	7.63	16,160	905	267	2,431	20.6	92.0	4,246	3,173	-3.87	-22.898	-0.0462
378-5	Sinkhole 37	17.90	7.81	16,180	908	256	2,505	27.2	93.0	4,275	3,233	-3.66	-24.118	-0.1501
379-5	Sinkhole 37	17.60	7.87	16,200	999	279	2,420	36.6	92.8	4,248	2,873	-0.61	-21.726	0.0485
3710-5	Sinkhole 37	17.50	7.60	16,170	1,003	287	2,498	20.0	92.8	4,272	3,503	-3.21	-23.669	-0.1167
3711-5	Sinkhole 37	17.10	7.63	16,240	1,024	286	2,486	35.6	92.0	4,297	3,239	-1.74	-24.031	-0.1757
3712-5	Sinkhole 37	16.90	7.73	16,200	1,037	289	2,435	29.4	92.5	4,264	2,693	1.21	-21.592	-0.0464
3713-5	Sinkhole 37	16.90	7.64	16,210	973	284	2,604	26.2	93.0	4,278	2,803	1.45	-21.74	0.0025
3714-5	Sinkhole 37	16.60	7.68	16,280	788	286	2,642	46.0	92.0	4,297	2,748	-0.29	-24.534	0.2640
160-5	Sinkhole 16	21.00	7.44	60,900	449	657	13,536	64.5	156.8	24,118	7,359	-11.26	-6.693	4.1065
161-5	Sinkhole 16	21.50	8.06	61,100	460	669	14,254	54.5	157.0	22,917	6,707	-6.00	-6.602	4.0635
162-5	Sinkhole 16	21.00	8.09	62,000	425	653	14,978	69.5	156.0	24,582	6,887	-7.09	-8.299	4.0205
163-5	Sinkhole 16	21.00	7.67	62,000	443	652	16,354	106.5	157.0	23,170	6,889	-0.62	-6.747	3.6575
010-5	Sinkhole 01	21.50	6.18	35,700	858	840	6,805	81.0	115.2	11,669	4,952	-2.87	-5.727	4.3548
011-5	Sinkhole 01	21.70	6.34	36,100	1,070	801	7,295	82.0	114.0	11,523	4,431	2.28	-1.39	4.3672
012-5	Sinkhole 01	21.70	6.41	36,200	974	806	6,815	62.5	114.0	11,705	4,471	-1.45	-3.704	4.1305
013-5	Sinkhole 01	21.50	6.40	36,300	996	807	7,026	53.5	114.2	11,612	4,471	0.07	-7.31275	4.0875
014-5	Sinkhole 01	21.70	7.46	36,200	1,034	808	6,861	59.5	118.0	11,744	4,628	-1.36	-1.473	4.3465
0145-5	Sinkhole 01	22.20	7.44	36,200	1,062	802	7,753	51.5	115.3	11,598	4,471	4.02	-1.289	4.6155
110-5	Sinkhole 11	20.50	7.93	46,500	1,089	1,138	10,440	133.6	151.3	14,620	5,812	6.10	-11.065	3.2525
111-5	Sinkhole 11	20.70	7.99	46,700	1,022	1,113	10,132	103.2	141.6	16,349	5,793	0.15	-10.006	2.9835
112-5	Sinkhole 11	21.00	8.02	46,600	1,090	1,104	10,984	139.2	150.1	16,525	5,853	2.97	-10.87	3.2648
113-5	Sinkhole 11	20.50	8.06	46,700	1,077	1,089	10,854	105.6	149.5	16,425	5,836	2.56	-7.915	3.8865
114-5	Sinkhole 11	20.70	8.03	46,700	1,052	1,087	10,770	128.8	148.5	16,287	5,682	2.81	-11.174	3.4262
115-5	Sinkhole 11	20.80	8.08	46,700	1,011	1,082	10,288	84.0	148.9	16,450	5,963	-0.12	-7.288	3.2805
116-5	Sinkhole 11	21.20	8.05	46,700	1,059	1,073	10,752	64.8	148.3	16,415	6,230	1.27	-11.888	3.3988
117-5	Sinkhole 11	20.80	8.03	46,800	969	1,012	10,584	44.0	150.1	16,400	5,832	0.56	-10.703	3.2945
190-5	Sinkhole 19	23.60	7.26	45,200	783	855	10,744	158.4	80.5	15,587	5,271	2.66	1.19	6.0001
191-5	Sinkhole 19	22.70	7.28	45,400	1,099	854	10,118	137.6	84.3	15,245	5,224	2.58	3.917	6.2315
192-5	Sinkhole 19	21.90	7.20	45,500	870	848	10,174	147.2	80.5	15,195	5,165	2.01	1.213	6.0555
1925-5	Sinkhole 19	21.40	8.25	45,500	1,129	845	8,962	174.4	80.5	15,670	5,303	-3.13	2.345	5.8595
250-5	Sinkhole 25	24.00	8.10	32,500	1,233	558	6,117	65.5	48.2	10,546	4,522	-2.25	-4.903	4.3645
251-5	Sinkhole 25	23.10	8.99	32,500	1,188	564	6,507	67.5	47.0	10,568	4,497	-0.26	-3.342	4.2105
2515-5	Sinkhole 25	22.40	8.72	32,900	1,284	570	6,518	65.5	49.0	10,707	4,421	0.16	-6.336	4.0955
320-5	Sinkhole 32	21.50	6.91	25,300	826	418	5,090	67.5	115.9	7,462	3,276	3.13	-5.332	3.3925
321-5	Sinkhole 32	20.50	7.12	25,600	905	411	4,261	60.3	116.5	7,524	3,333	-3.22	-3.908	3.2095
3215-5	Sinkhole 32	19.70	7.40	25,800	825	411	4,727	42.9	118.4	6,661	3,069	5.23	-7.645	3.9905

Table 3: Range of Major Ion Results

		MINIMUM			MAXIMUM		
	Major Ion	Sinkhole	Depth (m)	ppm	Sinkhole	Depth (m)	ppm
October 2008	Ca	21	3.0	764.0	16	0.0	1,310.0
	Mg	37	10.0	256.0	21	3.8	4,079.0
	Na	37	10.0	254.0	21	3.8	44,870.0
	K	37	5.0	15.9	21	3.8	361.5
	HCO_3	25	1.0	47.9	17	2.5	3,258.3
	Cl	37	10.0	3,774.4	21	3.0	61,135.3
	SO_4	37	2.0	3,087.1	21	3.8	18,210.3
May 2009	Ca	16	2.0	424.5	25	1.5	1,284.0
	Mg	37	8.0	256.2	17	0.0	3,848.0
	Na	37	9.0	2,420.0	21	3.0	46,120.0
	K	37	10.0	20.0	19	2.5	174.4
	HCO_3	25	1.0	46.98	17	2.5	2,982.5
	Cl	37	7.0	4,245.5	21	3.8	70,602.3
	SO_4	22	1.0	1,600.04	21	3.0	17,966.8

	Nutrient	Sinkhole	Depth (m)	mg/l	Sinkhole	Depth (m)	mg/l
October 2008	NH_4	37	0.0	0.03	17	2.5	>100
	NO_3	37 & 17*		0.00	21	2.0	0.39
	PO_4	37 & 32**		0.01	17	2.5	6.5

Table 4. Surface Measurements for Spatial Analysis (February 2009)

Sinkhole Number	Elevation	LAT	LONG	Northing	Easting	pH	Temp	DO (mg/L)	Cond (mS/cm)	Cond (ppt)
SH17	1066	33o29'4.6"	104o24'28.4"	124428	3844690	8.29	11.9	11.66	76.3	
SH19	1065	33o29'0.45"	104o24'37.9"	124180	3844717	8.6	11.5	14.22	51.3	25.7
SH20	1063	33o29'3.9"	104o24'39.5"	124137	3844700	6.76	10	9.76	15	7.55
SH26	1059	33o29'0.1"	104o24'43.6"	124023	3844593	8.31	11.2	12.03	59.1	29.6
SH30	1067	33o28'57.4"	104o24'44.5"	123990	3844511	7.56	11.3	13.12	29.6	14.8
SH27N	1066	33o28'53.8"	104o24'48.0"	123889	3844407	6.82	9.5	9.72	19.51	9.73
SH27S	1066	33o28'53.4"	104o24'48.3"	123882	3844396	6.71	9.6	7.82	33	16.5
SH29	1064	33o28'51.1"	104o24'47.2"	123902	3844323	6.77	10.3	13.73	39.5	19.7
SH21	1069	33o29'10.8"	104o24'39.5"	124159	3844914	7.87	8.3	9.73	140	69.9
SH22	1063	33o29'12.4"	104o24'41.0"	124122	3844967	8.29	8.2	13.38	86.8	43.3
SH24	1063	33o29'11.4"	104o24'47.5"	123951	3844952	7.71	10.2	12.67	54.6	27.1
SH25	1067	33o29'3.3"	104o24'43.3"	124038	3844690	7	11.5	11.46	36.1	18.1
SH32	1063	33o28'37.0"	104o25'0.61"	123372	3843930	8.04	10.4	9.5	27.1	13.5
SH31	1062	33o28'37.2"	104o25'7.6"	123333	3843941	7.38	12	10.54	10.04	5.03
Sago Spring 1	1061	33o28'40.9"	104o25'9.4"	123304	3844061	6.73	16.9	3.72	9.32	4.65
Sago Spring 2	1063	33o28'40.9"	104o25'9.2"	123302	3844060	7.31	16.7	4.1	9.34	4.67
SH42S	1066	33o28'42.0"	104o25'10.1"	123283	3844097	8.35	10.1	10.96	24	12
SH42N	1064	33o28'43.1"	104o25'10.1"	123285	3844128	7.47	9.8	6	13.65	6.83
SH38	1067	33o28'56.3"	104o25'28.3"	122849	3844580	7.34	14.9	6.21	8.86	4.42
SH34	1066	33o29'00.5"	104o25'289.2"	122840	3844712	7.91	11.6	12.87	28.1	14.1
SH33	1070	33o28'59.6"	104o25'29.7"	122823	3844687	9.66	15.9	23.13	25.6	12.8
SH07	1067	33o29'53.6"	104o24'32.2"	124468	3846223	7.35	9.8	23.49	13.07	6.56
SH05	1069	33o29'53.3"	104o24'24.5"	124669	3846196	6.2	11.2	12.32	76.9	38.4
SH06	1069	33o29'58.9"	104o24'26.6"	124629	3846372	7.19	11.1	13.73	71.1	35.5
SH11	1062	33o29'20.6"	104o25'02.8"	123850	3845273	6.28	11	17.7	55.8	27.9
SH10	1069	33o29'22.4"	104o25'1.0"	123631	3845323	7.67	10.6	15.97	31.4	15.7
SH52	1066	33o29'16.3"	104o25'05.1"	123508	3845145	7.83	9.4	16.51	86.9	43.3

Table 4, Continued

Sinkhole Number	Elevation	LAT	LONG	Northing	Easting	pH	Temp	DO (mg/L)	Cond (mS/cm)	Cond (ppt)
SH43	1065	33o29'15.6"	104o25'6.7"	123466	3845128	6.82	12.9	6.86	48.1	24
SH14	1066	33o29'13.9"	104o25'04.4"	123521	3845070	7.08	11.4	16.04	78.4	39.2
SH13	1066	33o29'16.7"	104o24'57.9"	123696	3845142	8.2	14.9	19.71	107.7	54
SH44	1068	33o29'13.0"	104o24'55.4"	123752	3845020	7.55	12.8	22.27	108.1	54
SH09	1072	33o29'29.2"	104o25'00.4"	123669	3845533	8.08	12.6	17.3	46.2	23.1
SH37	1068	33o29'30.4"	104o24'59.4"	123694	3845568	7.89	10.4	17.67	16.99	8.49
SH08	1069	33o29'32.6"	104o24'54.8"	123823	3845625	7.25	12	19.87	77.3	38.8
SH03	1068	33o29'34.6"	104o25'04.5"	123577	3845712	7.64	10.07	18.9	34.3	17.1
SH01	1075	33o29'32.6"	104o25'07.7"	123487	3845657	7.44	10.8	20.76	42.4	21.2
SH39	1065	33o28'38.6"	104o24'53.0"	123717	3843949	9.4	15.3	22.24	30.6	15.3
SH40	1067	33o28'40.3"	104o24'57.9"	123594	3844014	7.44	11.4	20.27	28.6	14.3

Table 5. Nutrient Content Analysis

Sample ID	Sinkhole	Depth (m)	NH4-N R^2=0.9999 +/- 0.01 mg/L	NO3-N R^2=0.9999 +/- 0.01 mg/L	PO4-P R^2=0.9999 +/- 0.01 mg/L
1700	17	0.0	0.45	0.02	1.85
1701	17	1.0	0.99	0.01	0.17
1702	17	2.0	15.76	0.00	0.89
1725	17	2.5	>100	0.06	6.47
1900	19	0.0	0.67	0.04	0.04
1901	19	1.0	0.23	0.04	0.10
1902	19	2.0	0.22	0.04	0.06
19275	19	2.75	0.29	0.03	0.04
2100	21	0.0	0.26	0.03	0.07
2101	21	1.0	0.33	0.02	0.04
2102	21	2.0	0.39	0.39	0.05
2103	21	3.0	14.43	0.01	0.93
2138	21	3.8	21.76	0.02	0.08
3200	32	0.0	0.06	0.01	0.04
3201	32	1.0	0.16	0.03	0.02
3202	32	1.5	0.30	0.01	0.01
3700	37	0.0	0.03	0.00	0.02
3701	37	1.0	0.05	0.00	0.02
3702	37	2.0	0.07	0.00	0.02
3703	37	3.0	0.07	0.00	0.02
3704	37	4.0	0.06	0.00	0.02
3705	37	5.0	0.07	0.11	0.02
3706	37	6.0	0.05	0.00	0.02
3707	37	7.0	0.10	0.00	0.02
3708	37	8.0	0.13	0.01	0.02
3709	37	9.0	0.20	0.02	0.01
3710	37	10.0	0.31	0.00	0.01
3711	37	11.0	0.31	0.00	0.01
3712	37	12.0	0.32	0.00	0.01
3713	37	13.0	0.31	0.00	0.01
3714	37	14.0	0.34	0.03	0.07

Samples are from the October 2008 sampling suite.

Table 6: Range of Stable Isotope Values.

		MINIMUM			MAXIMUM		
	Isotope	Sinkhole	Depth (m)	‰	Sinkhole	Depth (m)	‰
October 2008	δD	37	12.0	-20.956	17	1.0	7.282
	$\delta^{18}O$	37	13.0	-0.533	17	2.5	7.610
May 2009	δD	37	14.0	-24.530	19	1.0	3.917
	$\delta^{18}O$	37	11.0	-0.176	17	2.5	7.267

Table 7. Gas Analysis Results

Sinkhole	Depth	Date	File Name	CO2 % of total	CH4 % of total	CO % of total	Ar % of total	N2 % of total	He % of total	H2 % of total	O2 % of total
11	3.0	Feb10	S113210F	60.492	0.149	NR	0.694	34.717	NR	0.233	3.714
11	6.0	Feb10	S116210F	53.297	0.615	NR	0.742	37.104	NR	0.493	7.748
21	2.0	Feb10	S212210F	22.438	0.153	0.440	1.406	70.285	NR	0.122	5.155
21	3.0	Feb10	S213210F	1.672	0.134	0.077	1.743	87.175	0.075	0.096	9.027
19	1.0	Feb10	S191210F	1.808	0.349	0.531	1.670	83.500	0.396	0.545	11.200
19	2.0	Feb10	S192210F	4.472	0.580	4.990	1.613	80.634	0.441	NR	7.270
17	1.0	Feb10	S171210F	72.095	0.272	1.147	3.453	22.165	0.428	0.247	0.193
17	2.0	Feb10	S172210F	41.091	0.094	0.371	1.108	55.381	NR	0.064	1.891
37	6.0	Feb10	S376210bF	0.984	0.321	NR	1.764	88.196	NR	0.047	8.688
Sago Spring	0.0	Feb10	SAGO210F	69.331	0.119	0.188	0.554	27.687	0.117	0.123	1.881
17	2.5	May09	S172559F	99.960	NR	NR	0.001	0.039	NR	0.000	0.001
11	3.0	May09	S11359F	89.798	6.345	NR	1.049	2.094	0.003	0.001	0.710
19	2.5	May09	S192559F	71.109	10.681	9.023	0.986	6.634	0.000	0.001	1.566
21	3.0	May09	S21359F	97.897	NR	NR	0.264	1.487	NR	0.001	0.351
25	1.5	May09	S251559F	98.932	NR	NR	0.133	0.760	NR	0.001	0.174
21	3.8	Jun08	S21368F	99.696	NR	0.257	0.000	0.047	NR	0.000	0.000

Note: Values of Ar for the February 2010 sampling dates were corrected to reflect N2:Ar ratio (50:1) of air saturated water (ASW) due to high O2 dissolved gas results causing interference, and rendering high Ar values.

Table 8. Gas Analysis – He3/He4

Sample #	Sinkhole	Depth (m)	^4He mcc/kg	Ne mcc/kg	N_2 cc/kg	Ar cc/kg	Total CO_2 (cc/kg)	Methane (cc/kg)	$(^3He/^4He)$ $(^3He/^4He)_{AIR}$	(He/Ne) (He/Ne)sol	$(^3He/^4He)_{COR}$ $(^3He/^4He)_{AIR}$	$CO_2/^3He$ (x 10^{-9})	d ^{13}C ($^o/_{oo}$)
LC10-NM-BLSH 17	17	2.0	20	80	5.71	0.15	88.5	n.d.	0.991	1.02	0.601	1845349	-11.5
LC10-NM-BL Sago Sp	Sago Spring	0.0	497	299	11.26	0.28	38.8	0.09	0.290	6.93	0.170	386	-9.3

Results from L.J. Crossey (2012), personal communication

Samples collected during February 2010 sampling session.

Table 9. Geochemical Modeling - Saturation Indices

Sample	Sinkhole	Depth (m)	SI Calcite	SI Dolomite	SI Gypsum	SI Halite	PCO2
210-9	21	0	1.1385	3.2473	0.0864	-1.6836	-2.9598
211-9	21	1	1.104	3.2976	0.0968	-1.4492	-3.0628
212-9	21	2	1.0369	3.1411	0.0975	-1.4378	-2.976
213-9	21	3	1.1646	3.5662	0.0193	-1.2709	-2.0619
2138-9	21	3.8	1.2243	3.6593	0.0208	-1.2658	-2.0666
220-9	22	0	1.1862	2.9886	0.1488	-2.0346	-2.9344
221-9	22	1	1.0072	2.8421	0.1159	-1.8955	-2.9848
2215-9	22	1.5	0.3971	1.6612	0.1354	-1.8197	-0.6092
170-9	17	0	1.0852	2.7518	0.0518	-2.2064	-3.1032
171-9	17	1	0.6735	2.0677	0.1554	-1.8234	-2.402
172-9	17	2	1.1369	3.0639	0.0946	-1.8974	-2.2088
1725-9	17	2.5	1.9531	4.9109	0.0053	-1.6292	-1.8446
370-9	37	0	0.5375	0.9438	0.1445	-3.769	-3.0367
371-9	37	1	0.4949	0.8377	0.1667	-3.7667	-3.0227
372-9	37	2	0.506	0.8589	0.1264	-3.7762	-3.0327
373-9	37	3	0.5514	0.8874	0.2001	-3.7861	-3.0353
374-9	37	4	0.5231	0.8912	0.1563	-3.7541	-3.0698
375-9	37	5	0.5452	0.9199	0.1694	-3.7778	-3.0756
376-9	37	6	0.4823	0.7952	0.1545	-3.7602	-3.0426
377-9	37	7	0.429	0.671	0.1572	-3.7684	-2.9838
378-9	37	8	0.3365	0.4977	0.1539	-3.768	-2.8834
379-9	37	9	0.2613	0.3492	0.1417	-3.7808	-2.7732
3710-9	37	10	0.2415	0.3032	0.1273	-3.7956	-2.7491
3711-9	37	11	0.3088	0.3902	0.1822	-3.7897	-2.7561
3712-9	37	12	0.3062	0.4133	0.1395	-3.7877	-2.7934
3713-9	37	13	0.2343	0.2785	0.1169	-3.7817	-2.7361
3714-9	37	14	0.2736	0.3571	0.1398	-3.7631	-2.7811
160-9	16	0	1.097	2.6942	0.154	-2.3563	-3.3604
161-9	16	1	1.0227	2.5198	0.0924	-2.3869	-3.3313
162-9	16	2	1.1254	2.7393	0.3524	-2.1325	-3.3895
163-9	16	3	1.0879	2.6191	0.154	-2.3326	-3.3863
010-9	1	0	0.6847	1.7224	0.1054	-2.8993	-3.1233
011-9	1	1	0.6184	1.5664	0.1247	-2.904	-3.0694
012-9	1	2	0.6322	1.5803	0.1193	-2.8872	-3.1082
013-9	1	3	0.6374	1.5958	0.0754	-2.8846	-3.0829
014-9	1	4	0.7081	1.7306	0.1214	-2.8303	-3.1369

Sample	Sinkhole	Depth (m)	SI Calcite	SI Dolomite	SI Gypsum	SI Halite	PCO2
0145-9	1	4.5	0.7126	1.7329	0.1009	-2.8808	-3.1168
110-9	11	0	0.6341	1.7403	0.0922	-2.5826	-2.9426
111-9	11	1	0.836	2.1302	0.1087	-2.583	-3.1358
112-9	11	2	0.8144	2.0754	0.109	-2.6088	-3.1489
113-9	11	3	0.8646	2.157	0.1392	-2.5995	-3.1609
114-9	11	4	0.8697	2.1728	0.1119	-2.6015	-3.1737
115-9	11	5	0.8475	2.1571	0.1031	-2.6102	-3.1758
116-9	11	6	0.8261	2.1375	0.0936	-2.5997	-3.1843
117-9	11	7	0.9034	2.2349	0.1691	-2.5967	-3.1991
190-9	19	0	0.7354	1.8657	0.1052	-2.6793	-3.4817
191-9	19	1	0.7794	1.8982	0.1383	-2.6564	-3.516
192-9	19	2	0.7002	1.7384	0.1435	-2.656	-3.4085
1925-9	19	2.5	0.6158	1.6021	0.1033	-2.6405	-3.3716
250-9	25	0	1.2376	2.4995	0.1612	-2.968	-5.0349
251-9	25	1	1.2023	2.443	0.1496	-2.97	-5.0191
2515-9	25	1.5	1.2367	2.5595	0.1267	-2.9815	-5.0549
320-9	32	0	1.1371	2.2584	0.1231	-3.3514	-4.5126
321-9	32	1	1.0456	2.0585	0.1324	-3.3406	-4.3395
3215-9	32	1.5	0.119	0.2036	0.2539	-3.3676	-3.0325
210-5	21	0	-0.2118	0.8447	-0.0103	-1.3716	-1.3298
211-5	21	1	0.0692	0.9641	0.1805	-1.4624	-1.5461
212-5	21	2	1.2029	3.2609	0.1648	-1.3668	-2.852
213-5	21	3	0.4981	1.8985	0.1743	-1.1883	-1.0083
2138-5	21	3.8	0.7641	2.3058	0.2346	-1.2077	-1.2436
220-5	22	0	-0.0713	0.6631	0.0942	-1.9605	-2.0623
221-5	22	1	0.8596	2.4986	0.0718	-1.9387	-3.3291
2215-5	22	1.5	0.4204	1.9232	-0.1117	-1.9597	-2.7804
170-5	17	0	-0.7365	-0.253	-0.0971	-1.9636	-1.5225
171-5	17	1	0.4666	2.1926	-0.1738	-1.9235	-2.9234
172-5	17	2	0.083	1.3481	-0.082	-1.8835	-2.3253
1725-5	17	2.5	0.3405	1.8355	-0.0167	-1.6136	-0.0661
370-5	37	0	0.2475	0.4169	0.1301	-3.7148	-2.6673
371-5	37	1	-0.1162	-0.299	0.0891	-3.6861	-2.3546
372-5	37	2	0.5131	0.9626	0.0848	-3.7118	-3.0217
373-5	37	3	0.7379	1.3715	0.1044	-3.6738	-3.2485
374-5	37	4	0.7116	1.326	0.131	-3.6846	-3.2664
375-5	37	5	0.8143	1.5606	0.0491	-3.6752	-3.361
376-5	37	6	0.4916	0.8727	0.1253	-3.7006	-2.9848

Sample	Sinkhole	Depth (m)	SI Calcite	SI Dolomite	SI Gypsum	SI Halite	PCO2
377-5	37	7	0.346	0.5856	0.1002	-3.729	-2.8576
378-5	37	8	0.5278	0.9374	0.1045	-3.7151	-3.038
379-5	37	9	0.635	1.14	0.1006	-3.7296	-3.1026
3710-5	37	10	0.3535	0.5907	0.1604	-3.7188	-2.8238
3711-5	37	11	0.3904	0.6459	0.1443	-3.7156	-2.8608
3712-5	37	12	0.5142	0.885	0.0917	-3.7229	-2.9591
3713-5	37	13	0.3916	0.6609	0.0787	-3.6938	-2.8671
3714-5	37	14	0.331	0.63	-0.0015	-3.6835	-2.9151
160-5	16	0	-0.0199	0.6195	-0.2837	-2.3531	-2.502
161-5	16	1	0.5849	1.8351	-0.2753	-2.3019	-3.156
162-5	16	2	0.5452	1.771	-0.3225	-2.311	-3.1961
163-5	16	3	0.1712	1.0062	-0.3127	-2.2375	-2.7514
010-5	1	0	-1.0742	-1.67	0.0042	-2.8986	-1.3292
011-5	1	1	-0.8191	-1.2771	0.0439	-2.8729	-1.4917
012-5	1	2	-0.7809	-1.1563	0.02	-2.8952	-1.56
013-5	1	3	-0.7887	-1.1838	0.0248	-2.8853	-1.5524
014-5	1	4	0.2929	0.9672	0.0527	-2.8917	-2.6088
0145-5	1	4.5	0.2655	0.9022	0.0339	-2.8456	-2.6011
110-5	11	0	0.7825	2.0613	0.0582	-2.6231	-3.0359
111-5	11	1	0.8043	2.1279	0.0374	-2.5886	-3.1263
112-5	11	2	0.8744	2.2402	0.0518	-2.5501	-3.1382
113-5	11	3	0.8972	2.2786	0.0501	-2.5569	-3.1872
114-5	11	4	0.8653	2.2262	0.033	-2.5637	-3.1519
115-5	11	5	0.8984	2.3106	0.0422	-2.5802	-3.2055
116-5	11	6	0.8845	2.2648	0.0678	-2.5638	-3.1745
117-5	11	7	0.8398	2.1822	0.0181	-2.5691	-3.1445
190-5	19	0	-0.2093	0.136	-0.0966	-2.5878	-2.5799
191-5	19	1	-0.0289	0.3375	0.0451	-2.6209	-2.5844
192-5	19	2	-0.2373	0.0095	-0.0493	-2.6186	-2.5254
1925-5	19	2.5	0.8607	2.0862	0.081	-2.6589	-3.6511
250-5	25	0	0.6136	1.4001	0.1453	-2.9885	-3.6632
251-5	25	1	1.1734	2.5299	0.1212	-2.9599	-4.8544
2515-5	25	1.5	1.0763	2.2973	0.1436	-2.9523	-4.4427
320-5	32	0	-0.3091	-0.4357	-0.0534	-3.1975	-2.0334
321-5	32	1	-0.0501	0.0234	0.0101	-3.2667	-2.2404
3215-5	32	1.5	0.1663	0.4827	-0.0566	-3.2705	-2.5289

APPENDICES

APPENDIX A: SENSITIVE, THREATENED AND ENDANGERED SPECIES AT BITTER LAKE NATIONAL WILDLIFE REFUGE

Listed Federal and State Species Found at the Refuge

Common Name	Scientific Name	Occurrence	Status
Arkansas River Shiner	*Notropis girardi*	Resident	NMT
Arid Land Ribbon Snake	*Thamnophis proximus*	Resident	NMT
Bigscale Logperch	*Percina macrolepia*	Resident	NMT
Greenthroat Darter	*Etheostoma lepidum*	Resident	NMT
Koster's Tryonia	*Tryonia kosteri*	Resident	CA/NME
Least Shrew	*Cryptotis parva*	Resident	NMT
Mexican Tetra	*Astyanax mexicanus*	Resident	NMT
Noel's Amphipod	*Gammarus desperatus*	Resident	NME
Pecos Assiminea Snail	*Assiminea pecos*	Resident	CA/NME
Pecos Bluntnose Shiner	*Notropis simus Pecosensis*	Resident	T/NMT
Pecos Gambusia	*Gambusia nobilis*	Resident	End/NME
Pecos Pupfish	*Cyprinodon pecosensis*	Resident	CA
Pecos River Muskrat	*Ondatra zabethicus ripensis*	Resident	SoC
Pecos Sunflower	*Helianthus paradoxus*	Resident	T
Roswell Pyrg Snail	*Pyrgulopsis roswellensis*	Resident	CA/NME
Western River Cooter	*Pseudemys gorzugi*	Resident	NMT
Wright's Marsh Thistle	*Cirsium wrightii*	Resident	SoC
Wrinkled Marsh Snail	*Stagnicola caperata*	Resident	NME
American Bald Eagle	*Haliaeetus leucocephalus*	Migrant	End/NMT
American Peregrine Falcon	*Falco peregrinus anatum*	Migrant	NMT
Baird's Sparrow	*Ammodramus bairdi*	Migrant	NMT
Bell's Vireo	*Vireo bellii*	Migrant	NMT
Brown Pelican	*Pelicanus occidentalis*	Migrant	End/NME
Lesser Prairie Chicken	*Tympanuchus pellidicinctus*	Migrant	CA
Mountain Plover	*Charadrius montanus*	Migrant	CA
Neotropic Cormorant	*Phalacrocorax olivaceus*	Migrant	NMT
Southwest Willow Flycatcher	*Empidonax traillii*	Migrant	End/NME
Interior Lest Tern	*Sterna antillarum athalassos*	Breeding	End/NME
Black-footed Ferret	*Mustela nigripes*	Hypothetical	End
Swift Fox	Vulpes velox velox	Hypothetical	CA

From MacRae, Lusk and Radke, 2001.

End = Federally Endangered; T = Federally Threatened; CA = Federal Candidate Species; NME = New Mexico Endangered; NMT = New Mexico Threatened; PE = Proposed Listing as Federally Endangered.

APPENDIX B: DESCRIPTION OF STUDY SINKHOLES

LOCATION OF SINKHOLES

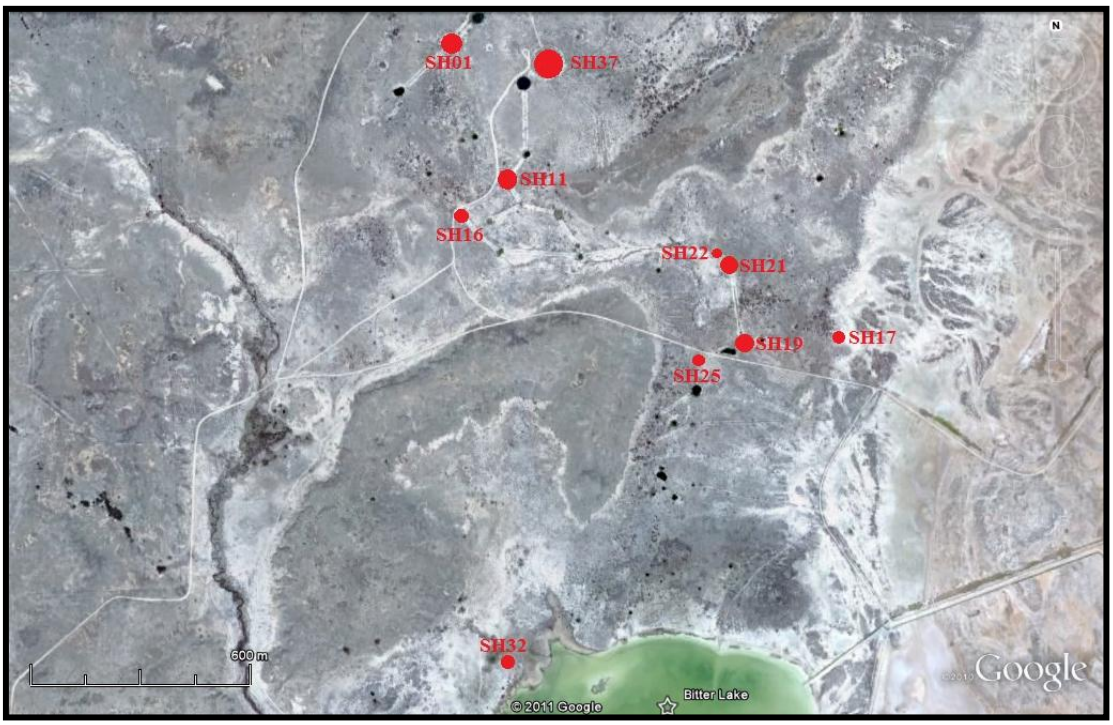

DIRECTIONS: *From Albuquerque/Santa Fe, take 285 South to Roswell, NM. At the first set of lights in Roswell (Pine Lodge Road, Wal-Mart on the right, observe USFWS Refuge sign) take a left, and drive east for approximately seven miles. Pass through the Refuge entrance gate (a key code is needed if entering after hours). The visitor center will be on the right and Refuge Headquarters on the left. Follow the main road north. There is a locked gate; seek permission from Refuge staff for access. Follow the road toward the left (note research trailers on the left). The road turns right/northeast sharply and becomes an embankment among playa flats. Bitter Lake will be on the left/west. Veer left where the road T's. Several sinkholes will be visible on either side of the road. Continue west. Where the road diverges, continue right to Lake St. Francis, or left to access Bitter Lake and Sago Spring.*

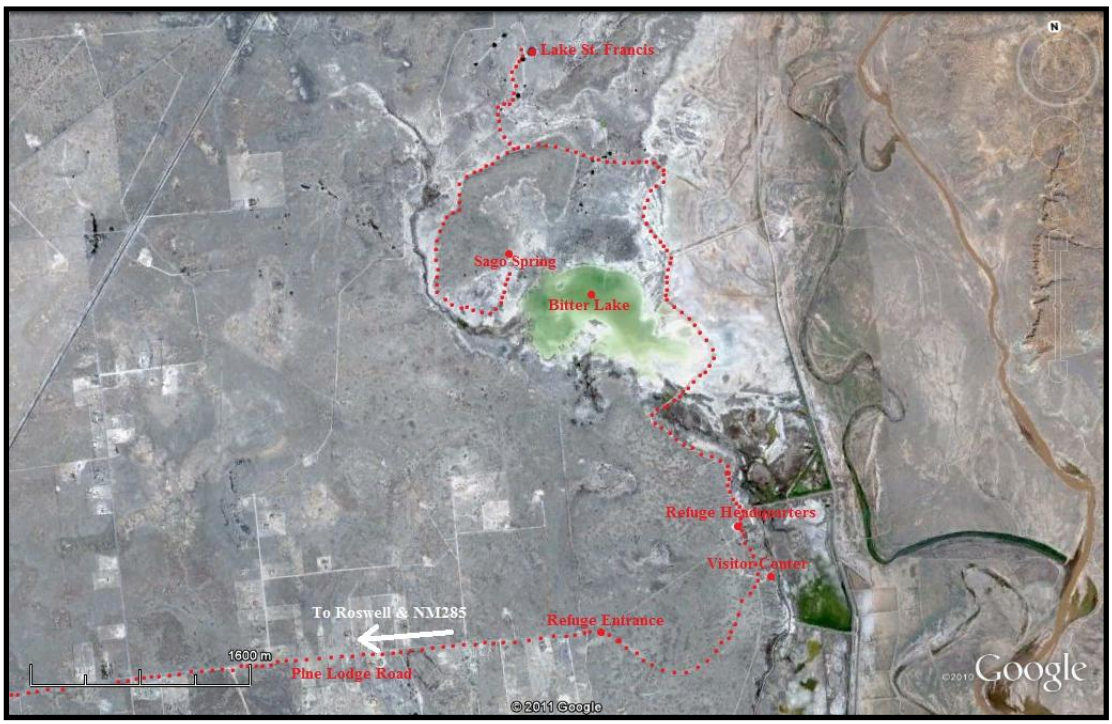

SINKHOLE 01 (SH01)

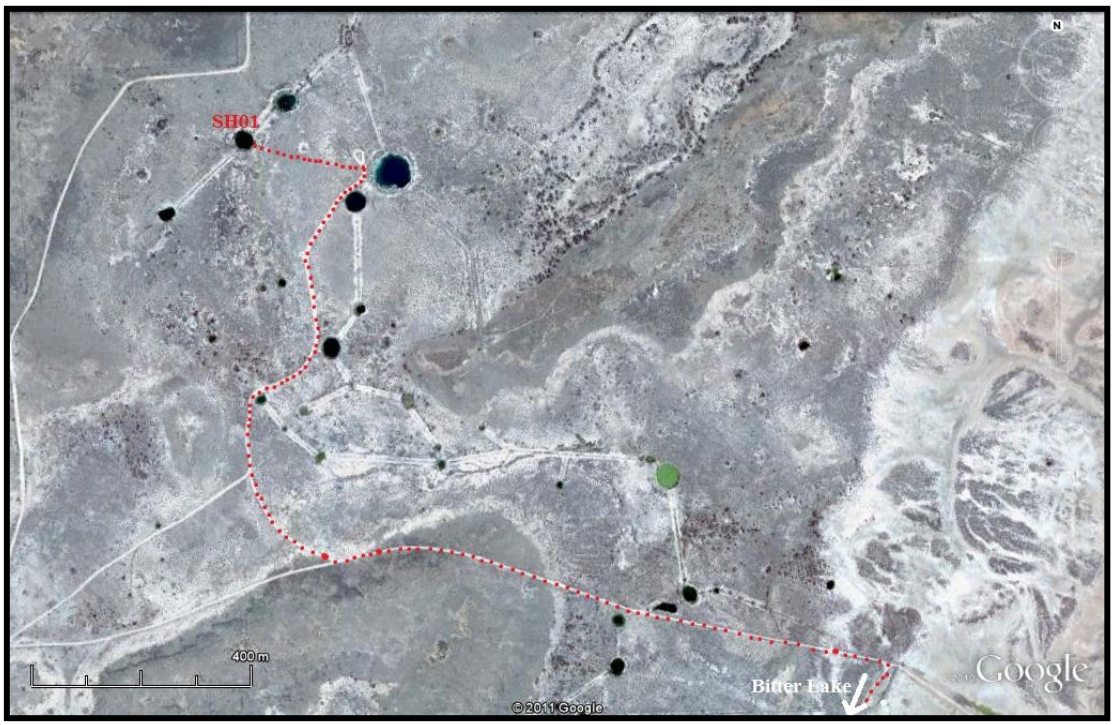

Depth	4.5 meters
Diameter	35.72 meters
Simple Volume	~4,509.5 m^3
Stratification	Uniform Water Column. pH= ~8.0 throughout (fall); ~6-7, lower at top (spring). conductivity= ~41mS/cm throughout (fall); ~36mS/cm throughout (spring). Temperature= ~17^oC throughout (fall); ~21^oC throughout (spring).
Accessibility	From the road which terminates in a cul-de-sac at SH37 (Lake St. Francis), proceed ~300m northwest. SH01 is the center sinkhole in a line of three large sinkholes. Water level is approximately four meters below the surrounding ground level. A well-used natural ramp is located on the southeast edge of the sinkhole. Some of the surrounding landscape is unstable and care should be taken not to tread on sinkhole deposits not supported from beneath; large cracks exposing these voids indicate these areas.
Description	SH01 is a large sinkhole with clear water of low turbidity with a small fish population. Submerged macrophytes are white and feathery, and a few bushes and trees grow from the side of the sinkhole.
Data Collected	Water samples for major ions and stable isotopes. Physical field parameters.

SINKHOLE 11 (SH11)

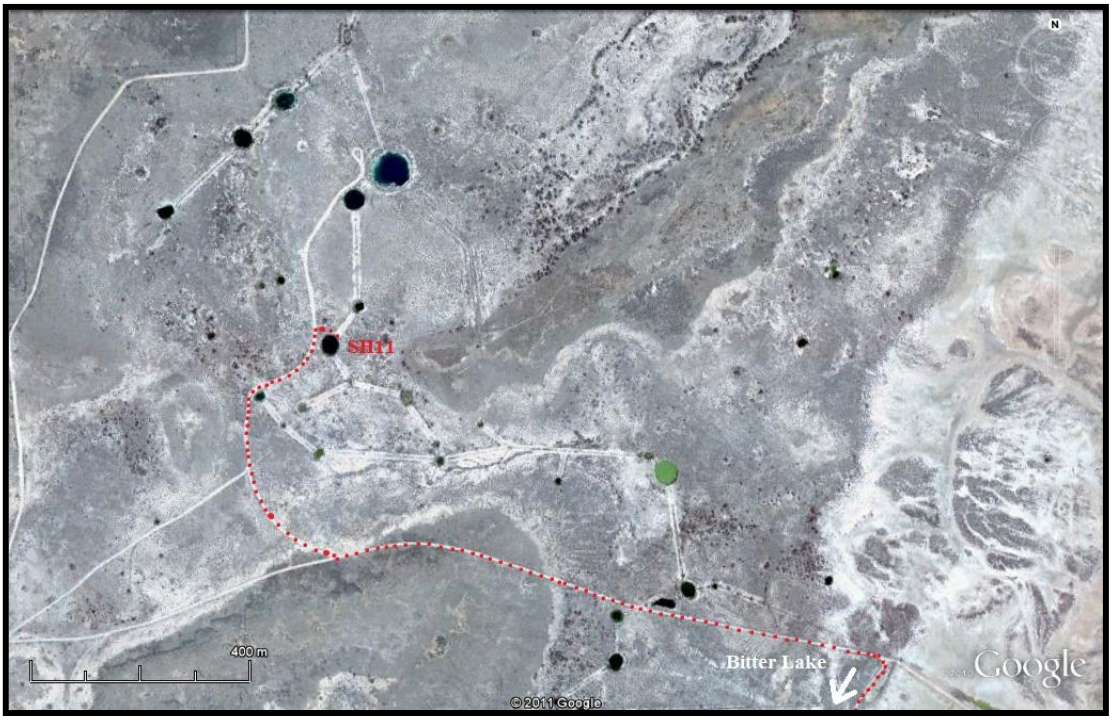

Depth	7.4 meters
Diameter	32.40 meters
Simple Volume	~6,101.1 m^3
Stratification	Uniform Water Column. pH= ~8.0 throughout (fall and spring). Conductivity= ~54mS/cm throughout (fall); ~46mS/cm throughout (spring). Temperature= ~18^oC throughout (fall); ~20^oC throughout (spring).
Accessibility	SH11 is clearly visible on the east side of the road leading to SH37 (Lake St. Francis). Parking on the road to the west of the sinkhole, walk ~30m to the north edge. Water level is approximately three meters below the surrounding ground level. Access is difficult, but a point of previous entry is obvious, and corresponds with a filled in drainage channel. Two people are needed – one at the water level and the other at ground level - if entering with a canoe or sampling equipment as the access point is steep with minimal shore.
Description	SH11 is a large sinkhole with green to brown-green colored water. Insect eggs are commonly observed on the water surface, and algae floats in the water.
Data Collected	Water samples for major ions and stable isotopes. Physical field parameters. Mineral precipitation experiment. Dissolved gases. Vertical SONDE deployment.

SINKHOLE 16 (SH16)

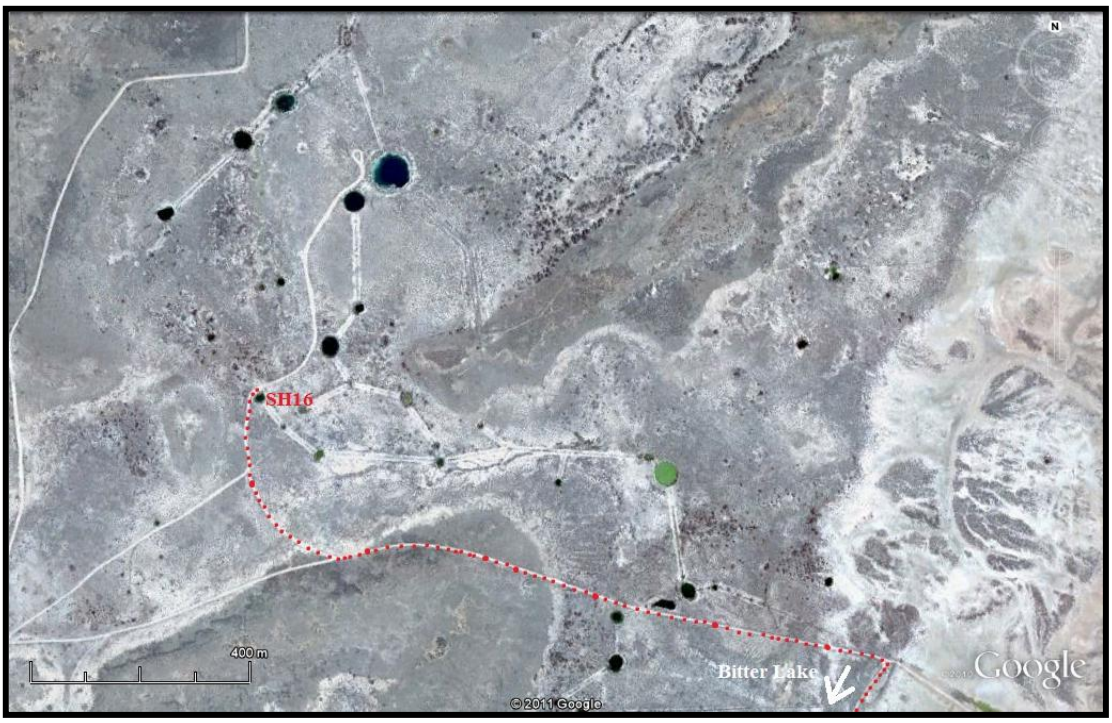

Depth	3.1 meters
Diameter	18.44 meters
Simple Volume	~827.9 m^3
Stratification	Uniform Water Column. pH= ~8.2 throughout (fall); ranges from 7.4-8.1 (spring). Conductivity= ~68mS/cm throughout (fall); ~62mS/cm throughout (spring). Temperature= 18°C at the surface cooling to ~16°C near the bottom (fall); ~21°C throughout (spring).
Accessibility	SH16 is a small sinkhole clearly visible on the east side of the road leading to SH37 (Lake St. Francis), and is south of SH11. Parking on the road to the west of the sinkhole, walk ~10m. Water level is <1.0m the surrounding ground level. Access is possible from any side of the sinkhole, but utilizing previously used access point to the northwest reduces impact.
Description	SH16 is a medium to small sinkhole with brown, tea-colored water.
Data Collected	Water samples for major ions and stable isotopes. Physical field parameters.

SINKHOLE 17 (SH17)

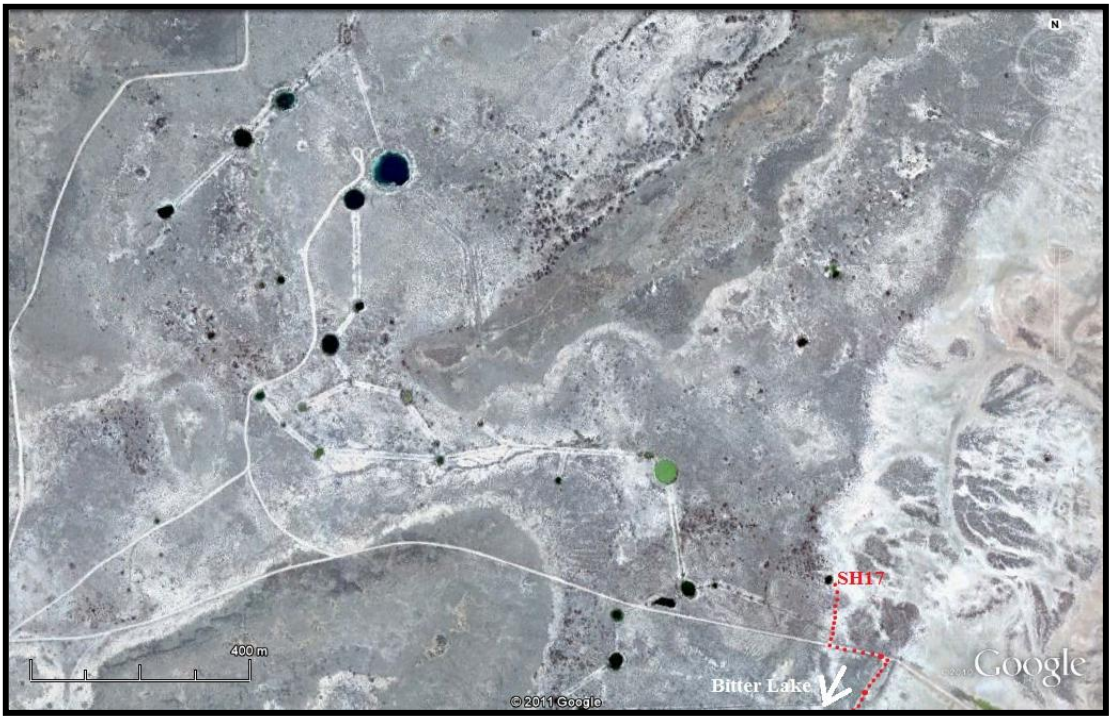

Depth	2.5 meters
Diameter	16.93 meters
Simple Volume	~562.8 m^3
Stratification	Stratified Water Column. Conductivity and temperature increase with depth. pH varies with depth, with highest measurement mid-water column. Water is clear to light yellow at the surface; bright yellow at meter one; pink at meter two; and dark yellow to yellow-brown at the bottom.
Accessibility	SH17 is a small sinkhole which is not clearly visible from the road. The presence of salt cedar in an otherwise alkaline grass plane is the most obvious marker. When following the main road north from the Refuge headquarters, the road curves east. Approximately 250m from the curve is a patch of cleared soil on the north side of the road which is an appropriate parking location. From this clear spot, SH17 is approximately 200m north-northwest, crossing over a partially filled in drainage channel after which is a large area cleared of grass. Water level is <1.0m to 1.0m above the surrounding ground level. Access the sinkhole on an obvious beach along the southeast side of the sinkhole. The sediment is saturated sulfate-rich mud, and caution must be taken to remain as far away as possible from the water-shore interface.
Description	SH17 is a small, shallow sinkhole with brown to tea-coloration at the surface, but variable water color with depth. Frequently inhabited with aquatic invertebrates, fish and insects, this sinkhole is a biological hotspot. Grasses and tree branches submerged have developed a thick gypsum crust. This sinkhole is particularly pungent.
Data Collected	Water samples for major ions and stable isotopes. Physical field parameters. Mineral precipitation experiment. Dissolved gases. Long-term SONDE deployment.

SINKHOLE 19 (SH19)

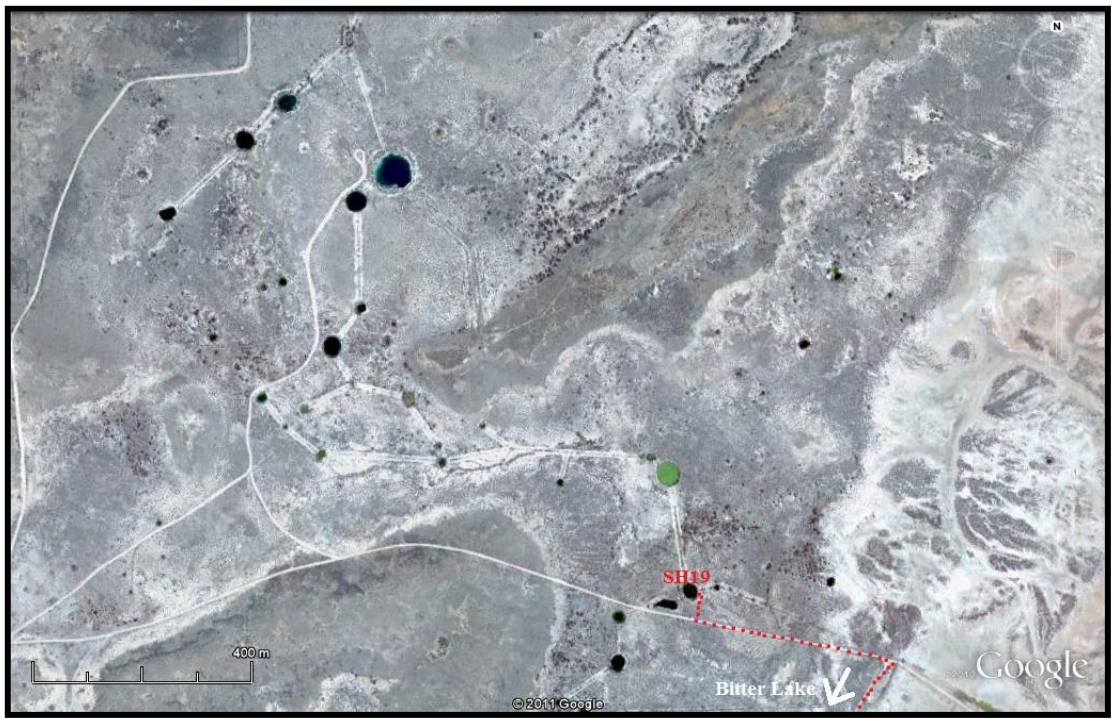

Depth	2.5 meters
Diameter	34.04 meters
Simple Volume	~2,275.1 m^3
Stratification	Uniform Water Column. Temperature, conductivity and pH exhibit little variation.
Accessibility	SH19 is a medium sinkhole which is clearly visible from the road and is easily found by viewing nearby SH20 directly north of the road, and progressing slightly northeast. There is an area cleared of grass slightly southeast of the sinkhole suitable for parking, and accessing SH19 is most easily achieved by entering where a filled in diversion channel creates a ramp and natural shore on the east-northeast side of the sinkhole. Water level is ~2.0m below the surrounding ground level. Be aware of snakes and hornets.
Description	SH19 is a wide, shallow sinkhole with blue to blue-green water. The bottom is visible from the surface as are the submerged macrophytes which cover a large percent of the sinkhole subsurface. Surrounding substrate is crystalline, white to grey and pink in color.
Data Collected	Water samples for major ions and stable isotopes. Physical field parameters. Mineral precipitation experiment. Dissolved gases. Vertical SONDE deployment. Long-term SONDE deployment.

SINKHOLE 21 (SH21)

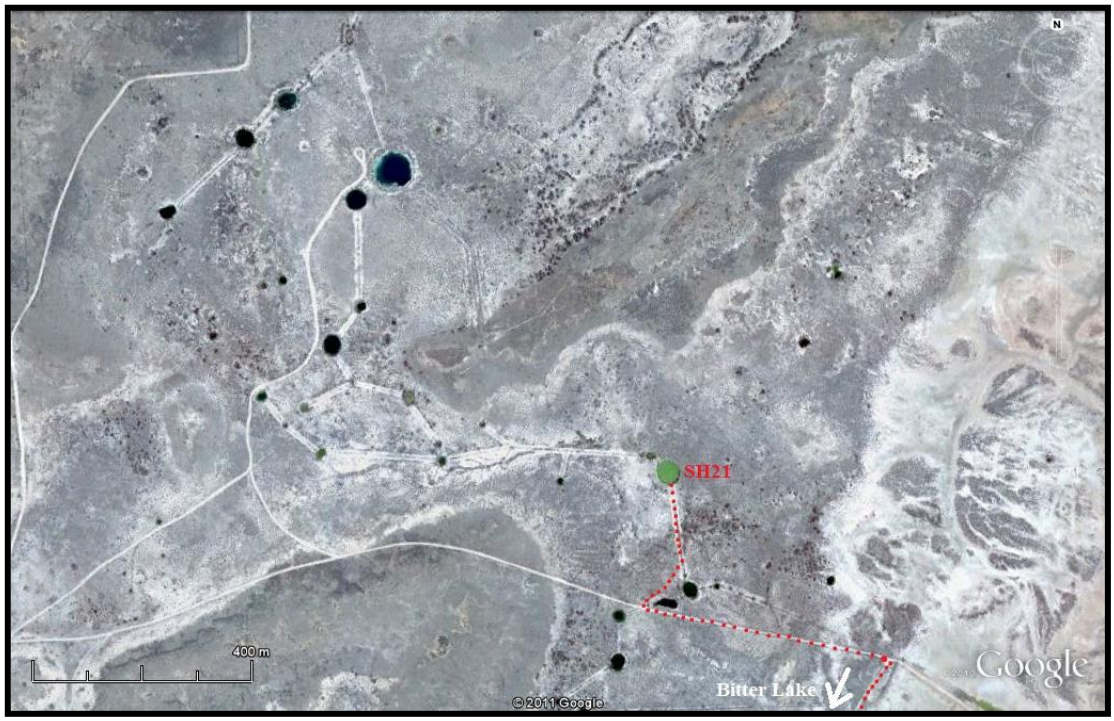

Depth	3.8 meters
Diameter	40.93 meters
Simple Volume	~4,999.8 m^3
Stratification	Stratified Water Column. Conductivity increase with depth. pH varies with depth, with highest measurement mid-water column. Temperature differences change seasonally. Water is brown to yellow at the surface; bright yellow at meter one; pink at meters two and three; and dark yellow to yellow-brown at the bottom.
Accessibility	SH21 is a medium to large sinkhole which is not clearly visible from the road. The presence of salt cedar in an otherwise alkaline grass plane is the most obvious marker and is the cleared filled-in drainage channel extending from SH20 and creating the access point into SH21. Along the main road there is a cleared space slightly west of the closest sinkhole – SH20. Driving directly to SH21 is not permitted, and equipment must be carried ~200m from the road to the sinkhole. Water level is <2.0 m below the surrounding ground level. Access the sinkhole on an obvious ramp at the south side of the sinkhole which has numerous bushes and woody plants growing along the side.
Description	SH21 is a medium-large, moderately deep sinkhole with brown to tea-coloration at the surface, but variable water color with depth. Frequently inhabited with aquatic invertebrates, fish and insects, this sinkhole is a biological hotspot. Grasses and tree branches submerged have developed a thick gypsum crust. The sediment is saturated sulfate-rich mud; this sinkhole is particularly pungent. Conditions at SH21 are particular extreme; salinity and conductivity are the highest recorded among sinkholes.
Data Collected	Water samples for major ions and stable isotopes. Physical field parameters. Mineral precipitation experiment. Dissolved gases. Vertical SONDE deployment.

SINKHOLE 22 (SH22)

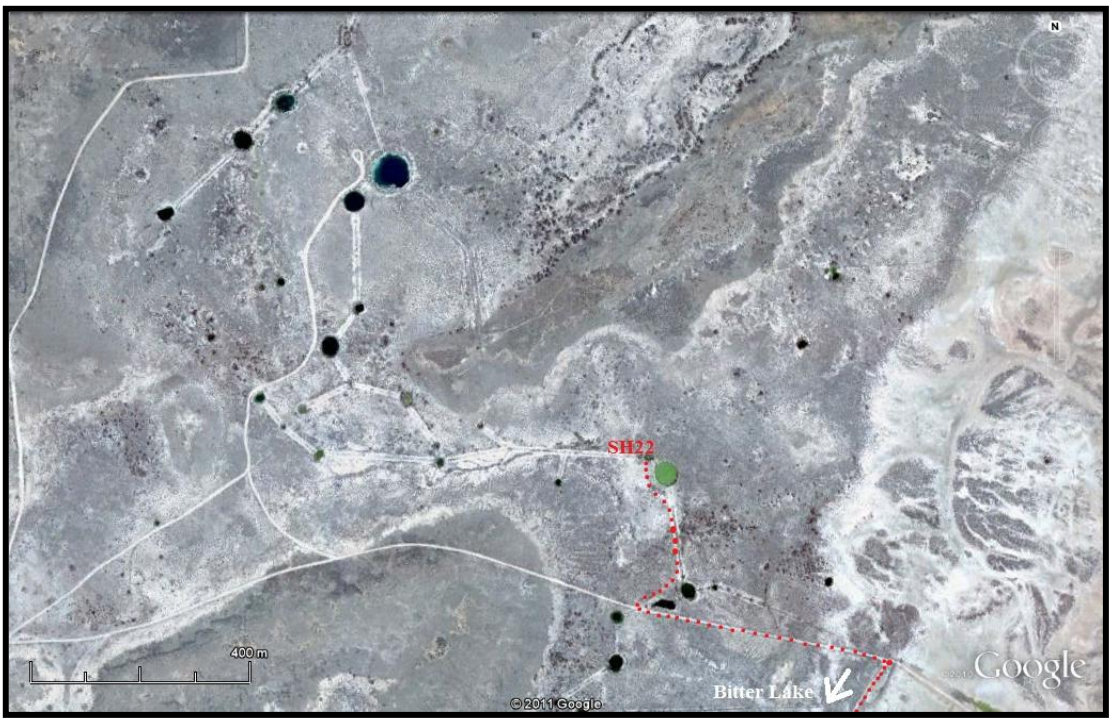

Depth	1.5 meters
Diameter	10.65 meters
Simple Volume	~133.6 m^3
Stratification	Mildly Stratified Water Column. Conductivity remains relatively constant, while temperature and pH vary with depth. Water is yellow to tea-colored at the surface; bright yellow at meter one; and dark yellow to yellow-brown at the bottom.
Accessibility	SH22 is a very small sinkhole which is not clearly visible from the road. Located northeast of SH21, it is easiest found by traveling from the road and going to SH21, then walking around is perimeter to the west. Access the sinkhole on the south side through a clearing among salt cedars. Water level is 1.5m below the surrounding ground level. The drop-of is steep, but not very long. A tiny staging area has hard-packed footing, and equipment may be lowered from the above ground level. The canoe barely fits into the sinkhole.
Description	SH22 is a very small, shallow sinkhole with brown to tea-coloration at the surface. SH22 maintains the highest fish density of all other sinkholes. The exterior of the sinkhole has a thick presence of salt cedar and other trees and bushes. Grasses and tree branches submerged have developed a thick gypsum crust. This sinkhole is particularly pungent.
Data Collected	Water samples for major ions and stable isotopes. Physical field parameters.

SINKHOLE 25 (SH25)

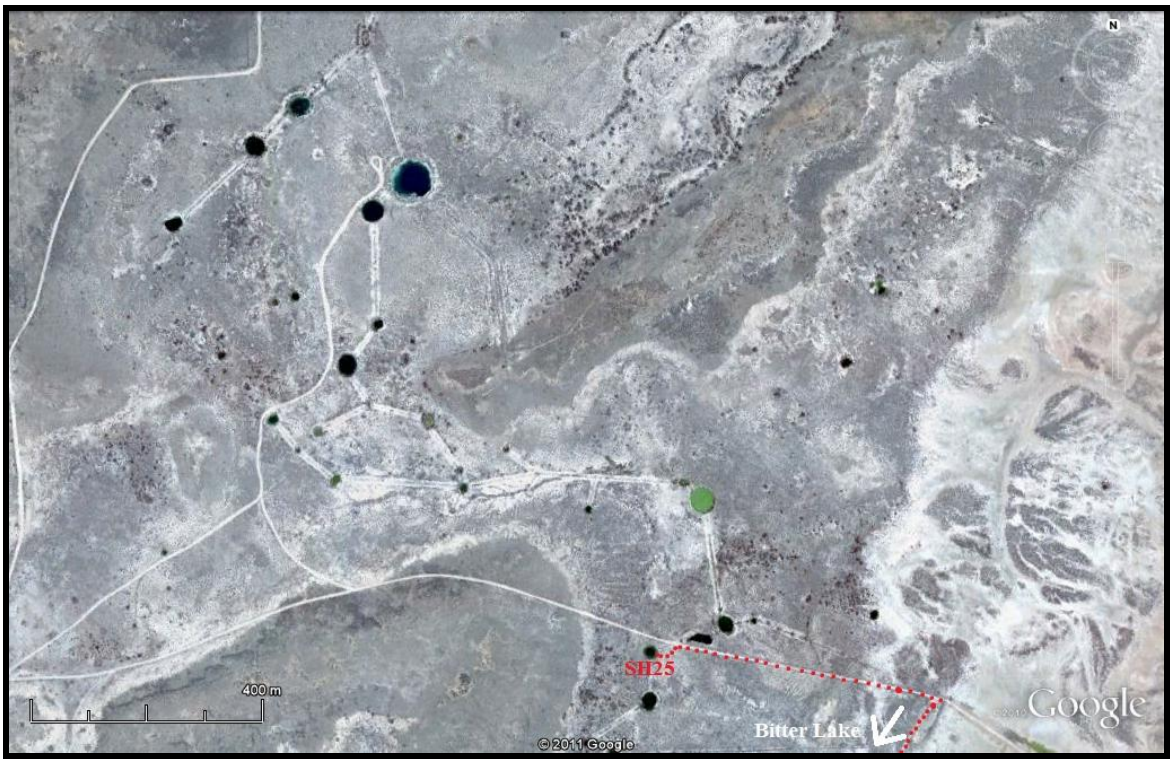

Depth	1.85 meters
Diameter	22.91 meters
Simple Volume	~762.6 m^3
Stratification	Uniform Water Column.
Accessibility	SH25 is a medium-small sinkhole clearly visible from the road. If traveling on the main road, it is on the south side, nearly directly across the street from SH20. Parking either at the clearing west of SH20, or along the road in front of SH25, the sinkhole is most easily accessed by using the shallow sloping ramp on the southeast side. Water level is <1.0m below the surrounding ground level. Alkaline grasses and aquatic plants pose the greatest (albeit minimal) access hindrance to SH25.
Description	SH25 is a medium-small, shallow sinkhole with brown to tea-coloration at the surface, but otherwise very clear water. Many different types of dragonflies may be observed during the warm months. Water is relatively fresh, and houses a blanket of submerged macrophytes that blanket the bottom of the sinkhole.
Data Collected	Water samples for major ions and stable isotopes. Physical field parameters.

SINKHOLE 32 (SH32)

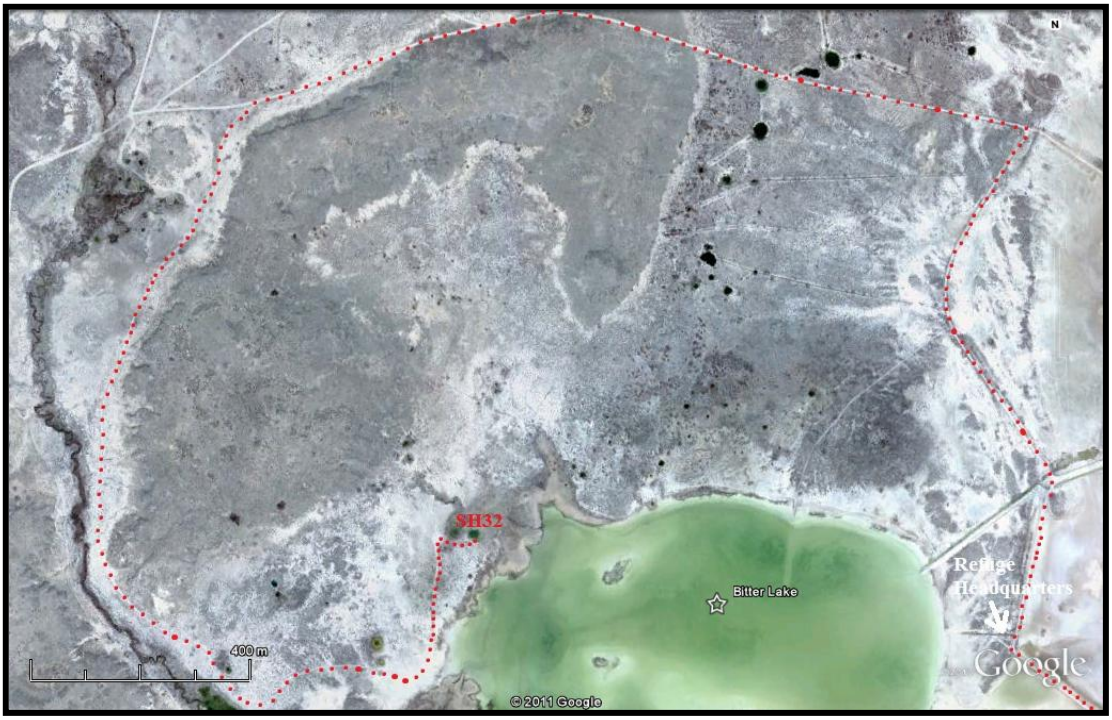

Depth	2.3 meters
Diameter	21.94 meters
Simple Volume	~869.5 m^3
Stratification	Uniform Water Column.
Accessibility	SH32 is a small sinkhole is visible from the road, but is located farther south than other sinkholes. Follow the main road north from the Refuge headquarters. Pass SH25 and SH20. Where the road forks, keep left. The road curves toward the south and toward Bitter Lake. A series of spring-fed wetlands will be on the right/west-southwest. The road curves left, to the north and ends in a large clearing. Bitter Lake is to the southeast. SH32 is approximately 30m east of the clearing. The area around SH32 is quite grassy, and care should be taken to avoid stepping in water concealed with grass. Access the sinkhole on the southwest edge where is shallow shore is visible. Water level is approximately equal to surrounding ground level and Bitter Lake.
Description	SH32 is a small, shallow sinkhole with clear water and thick aquatic plant growth. Located ~100m from both Bitter Lake and Sago Spring, the water is "fresher" than other sinkholes. Land-based grasses conceal the sinkhole from view from the road during the summer and fall. Submerged macrophytes extend from the sinkhole bottom to nearly the water's surface.
Data Collected	Water samples for major ions and stable isotopes. Physical field parameters.

SINKHOLE 37 (SH37), LAKE ST. FRANCIS

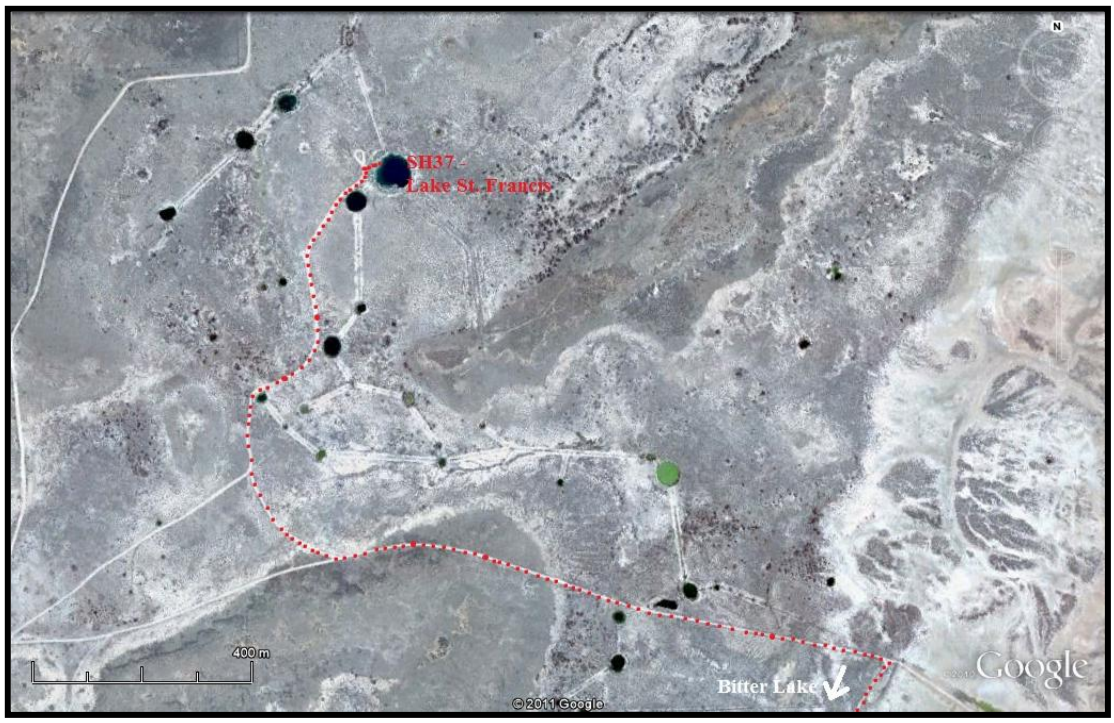

Depth	14.15 meters
Diameter	71.17 meters
Simple Volume	56,291.1 m^3
Stratification	Uniform Water Column.
Accessibility	SH37 is a large sinkhole which is clearly visible from the road. Follow the main road north from the Refuge headquarters, and continue west when the road curves. Pass SH20 and SH25. At the fork, veer right/north, passing several sinkholes on the right. The road terminates with a cul-de-sac. SH37 is on the right/east. Access the sinkhole on the obvious beach on the west edge. Although covered with grasses and brush, the path to the water is relatively well-traveled.
Description	SH37- also named Lake St. Francis - is a large, deep sinkhole with clear blue to green-blue water. The sinkhole hosts a large fish population which may be readily observed from shore. It is also home to a marine algae not found elsewhere in terrestrial natural water systems. The "freshest" sinkhole, SH37 has less aquatic vegetation than others, and is ~2.5m below surrounding ground level.
Data Collected	Water samples for major ions and stable isotopes. Physical field parameters. Mineral precipitation experiment. Dissolved gases. Vertical SONDE deployment.

APPENDIX C: MINERAL PRECIPITATION EVALUATION

Approximate Masses and Mineral Growth Rates – First Deployment

Sinkhole	Depth (m)	Total Mass (g)	Cartridge	Cartridge Mass + Bag	Mass of Precipitate	Growth Rate (g/day)
11	0.0	12.770	g	12.558	0.212	0.0071
	1.0	13.530	g	12.558	0.972	0.0324
	2.0	13.120	g	12.558	0.562	0.0187
	3.0	13.700	g	12.558	1.142	0.0381
	4.0	12.891	g	12.558	0.333	0.0111
	5.0	9.250	w	8.919	0.331	0.0110
	6.0	9.230	w	8.919	0.311	0.0104
	7.0	9.370	w	8.919	0.451	0.0150
17	0.0	8.980	w	8.919	0.061	0.0020
	1.0	8.880	w	8.919	-0.039	-0.0013
	2.0	9.540	w	8.919	0.621	0.0207
	2.5	8.540	w	8.919	-0.379	-0.0126
19	0.0	9.010	w	8.919	0.091	0.0030
	1.0	8.970	w	8.919	0.051	0.0017
	2.0	9.250	w	8.919	0.331	0.0110
	2.5	9.050	w	8.919	0.131	0.0044
21	0.0	9.430	w	8.919	0.511	0.0170
	1.0	9.330	w	8.919	0.411	0.0137
	2.0	10.240	w	8.919	1.321	0.0440
	3.0	10.160	w	8.919	1.241	0.0414
	3.8	10.640	w	8.919	1.721	0.0574
37	0.0	9.040	w	8.919	0.121	0.0040
	1.0	12.980	g	12.558	0.422	0.0141
	2.0	12.970	g	12.558	0.412	0.0137
	3.0	12.820	w	8.919	3.901	0.1300
	4.0	12.570	g	12.558	0.012	0.0004
	5.0	9.020	w	8.919	0.101	0.0034
	6.0	8.990	w	8.919	0.071	0.0024
	7.0	9.010	w	8.919	0.091	0.0030
	8.0	8.950	w	8.919	0.031	0.0010
	9.0	12.913	g	12.558	0.355	0.0118
	10.0	9.000	w	8.919	0.081	0.0027
	11.0	12.690	g	12.558	0.132	0.0044
	12.0	12.770	g	12.558	0.212	0.0071
	13.0	12.780	g	12.558	0.222	0.0074
	14.0	12.890	g	12.558	0.332	0.0111

Ceramic substrates affixed to the interior and exterior of the cartridges were removed on-site. A small amount of precipitate from each substrate was removed and stored in a 30mL vial with a small amount of SLB added until just covering the precipitate (for microbial analysis); the two substrates were placed in a 50mL sample vial with 10mL gluteraldehyde wherein substrate-grown precipitate was stored for later preparation and SEM analysis. Images of these substrates are presented in the following pages. The cartridge and cartridge-grown precipitate were placed in a separate bag for each location. In the laboratory, these were removed from the bags and allowed to air dry. Once dried, the mass of each was measured and compared with a blank cartridge to approximate the total mass of precipitate present. Precipitation rates were calculated by dividing total growth mass by the number of days left hanging in the sinkhole.

Approximate Masses and Mineral Growth Rates – Second Deployment

Depth (m)	Total Mass (g)	Cartridge	Cartridge Mass + Bag	Mass of Precipitate	Growth Rate (g/day)
0.0	9.290	W	8.919	0.371	0.0071
1.0	9.530	W	8.919	0.611	0.0117
2.0	9.460	W	8.919	0.541	0.0104
3.0	9.360	W	8.919	0.441	0.0085
4.0	9.420	W	8.919	0.501	0.0096
5.0	9.410	W	8.919	0.491	0.0094
6.0	9.450	W	8.919	0.531	0.0102
7.0	9.959	W	8.919	1.040	0.0200
0.0					0.0000
1.0					0.0000
2.0					0.0000
2.5					0.0000
0.0	9.350	W	8.919	0.431	0.0083
1.0	9.490	W	8.919	0.571	0.0110
2.0	9.470	W	8.919	0.551	0.0106
2.5	9.640	W	8.919	0.721	0.0139
0.0	26.410	W	8.919	17.491	0.3364
1.0	30.340	W	8.919	21.421	0.4119
2.0	32.760	W	8.919	23.841	0.4585
3.0	11.370	W	8.919	2.451	0.0471
3.8	11.590	W	8.919	2.671	0.0514
0.0					0.0000
1.0					0.0000
2.0					0.0000
3.0					0.0000
4.0					0.0000
5.0	9.180	W	8.919	0.261	0.0050
6.0	9.150	W	8.919	0.231	0.0044
7.0	9.161	W	8.919	0.242	0.0046
8.0	9.120	W	8.919	0.201	0.0039
9.0	9.270	W	8.919	0.351	0.0067
10.0	9.160	W	8.919	0.241	0.0046
11.0	9.240	W	8.919	0.321	0.0062
12.0	9.030	W	8.919	0.111	0.0021
13.0	9.141	W	8.919	0.222	0.0043
14.0	9.160	W	8.919	0.241	0.0046

SINKHOLE 11 (SH11)

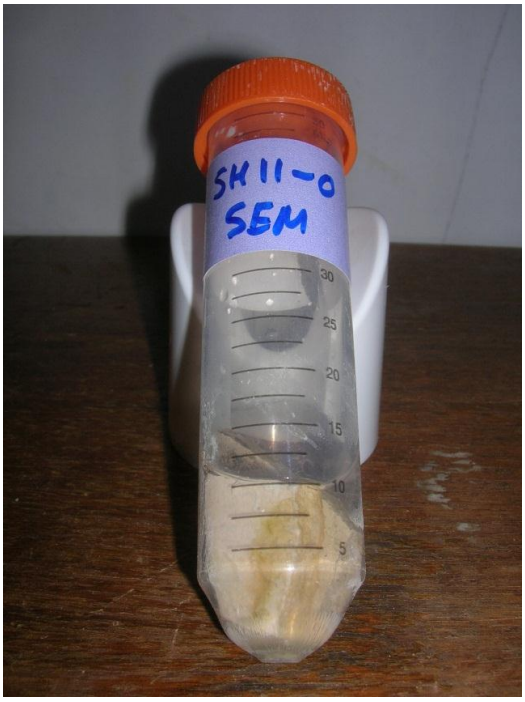

SH11 – Depth 0.0m – Exterior and Interior

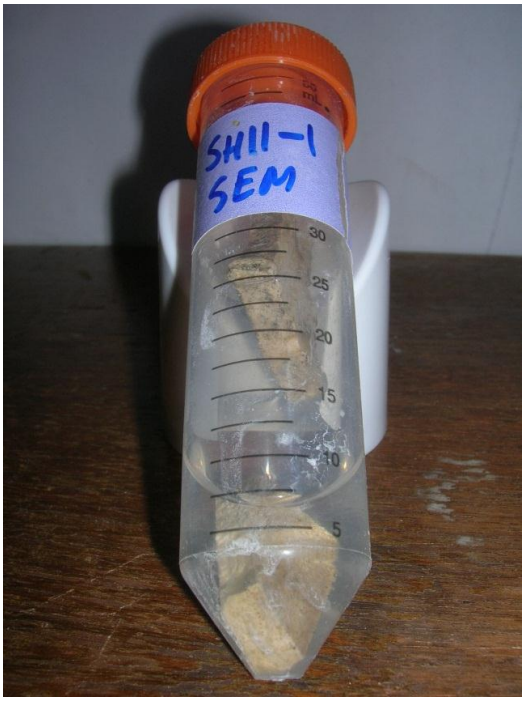

SH11 – Depth 1.0m – Exterior and Interior

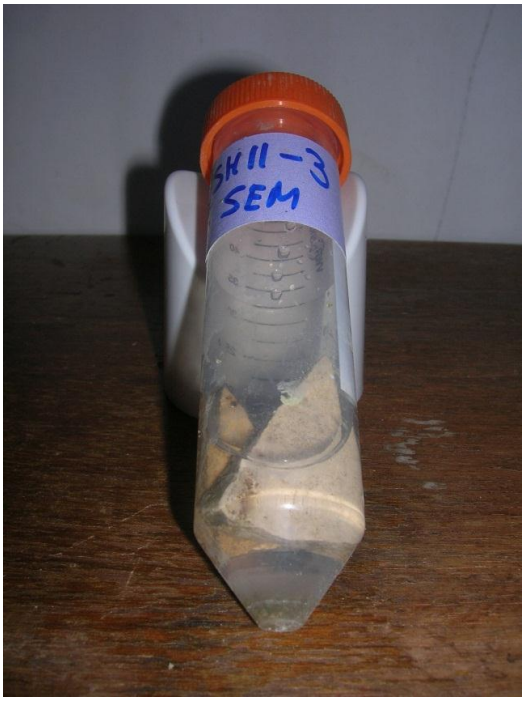

SH11 – Depth 2.0m – Exterior and Interior

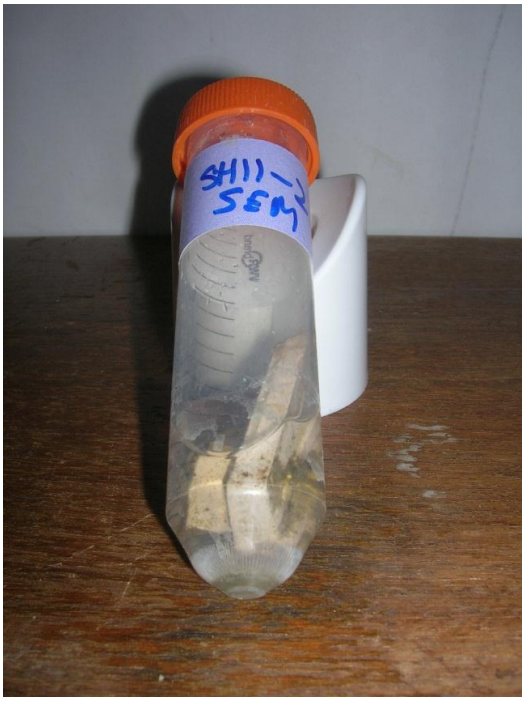

SH11 – Depth 3.0m – Exterior and Interior

SH11 – Depth 4.0m – Exterior and Interior

SH11 – Depth 5.0m – Exterior and Interior

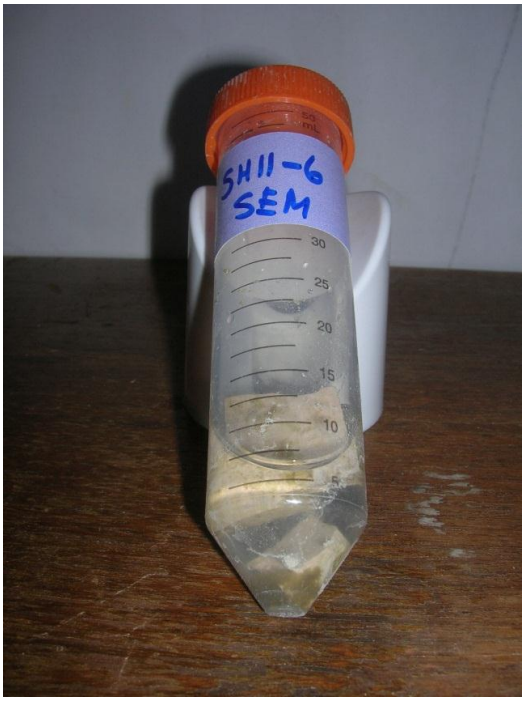

SH11 – Depth 6.0m – Exterior and Interior

SH11 – Depth 7.0m – Exterior and Interior

SINKHOLE 17 (SH17)

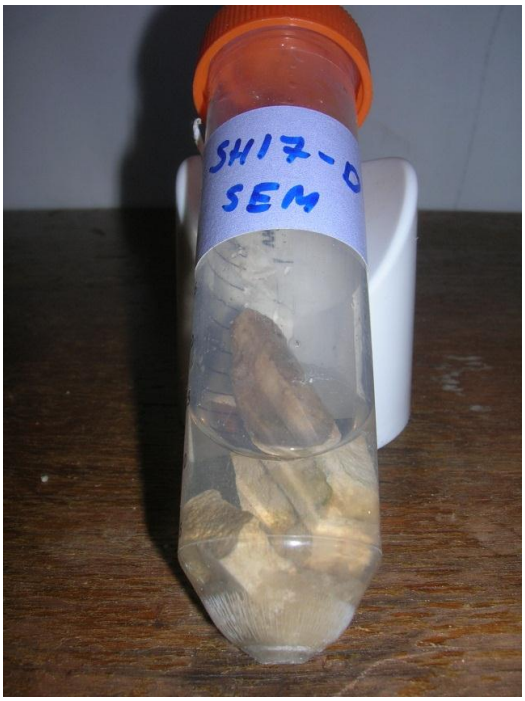

SH17 – Depth 0.0m – Exterior and Interior

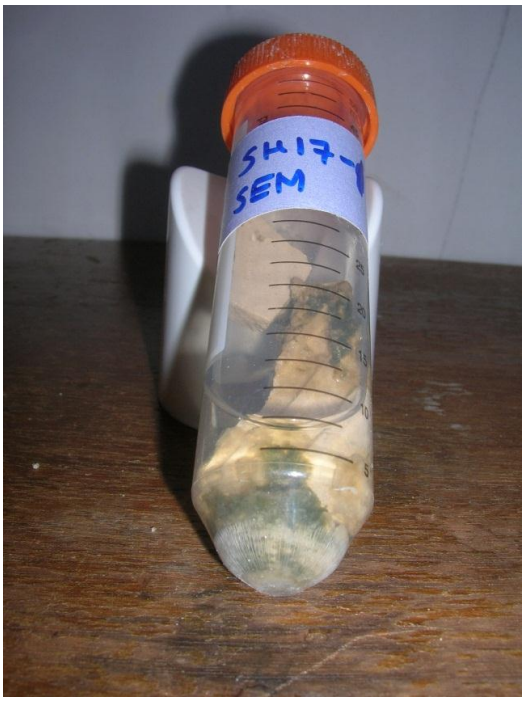

SH17 – Depth 1.0m – Exterior and Interior

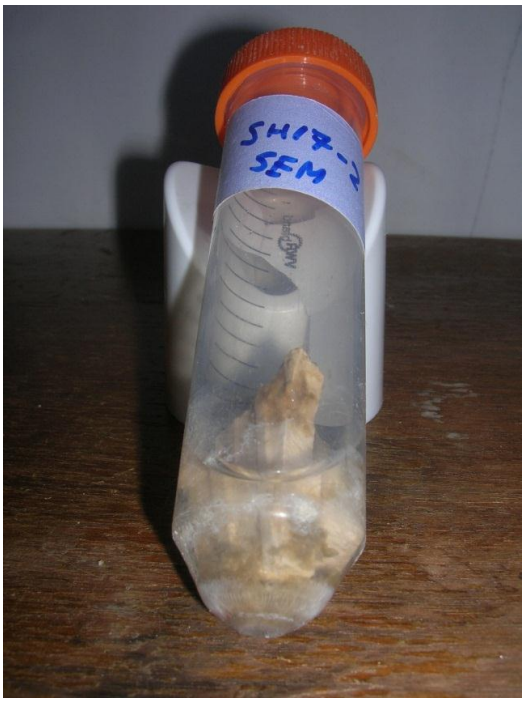

SH17 – Depth 2.0m – Exterior and Interior

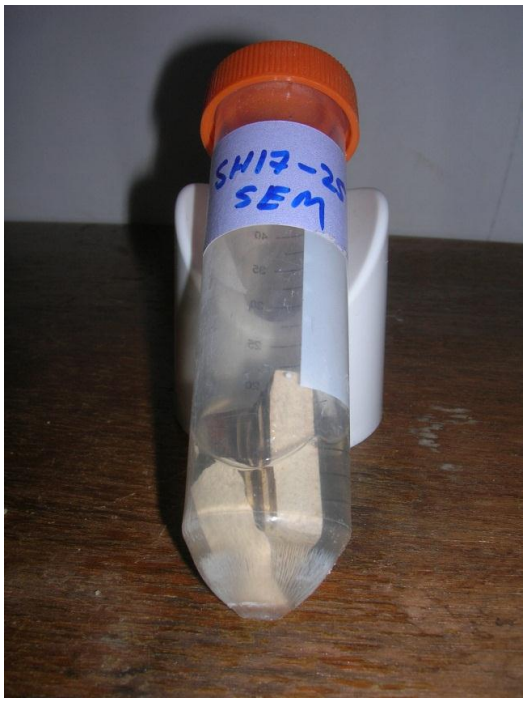

SH17 – Depth 2.5m – Exterior and Interior

SINKHOLE 19 (SH19)

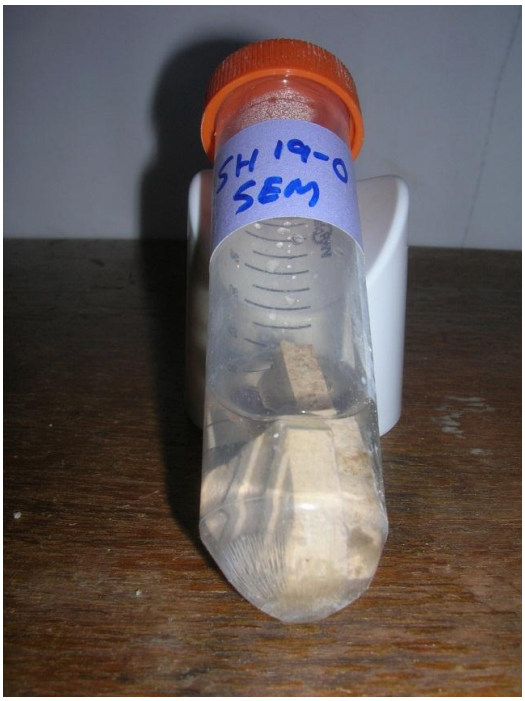

SH19 – Depth 0.0m – Exterior and Interior

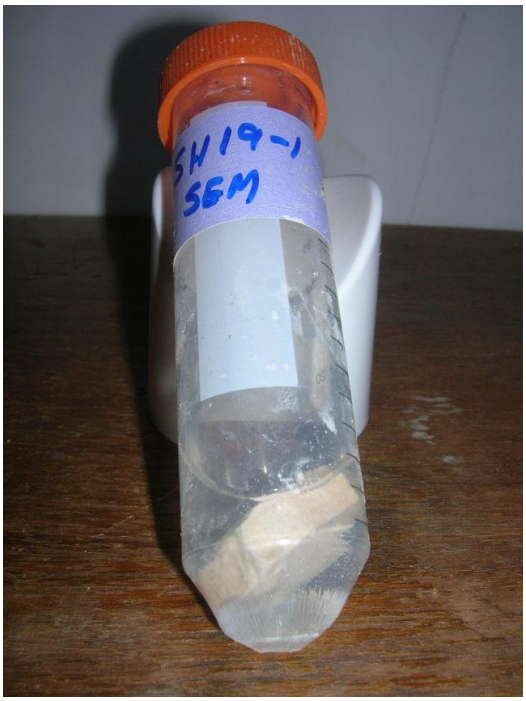

SH19 – Depth 1.0m – Exterior and Interior

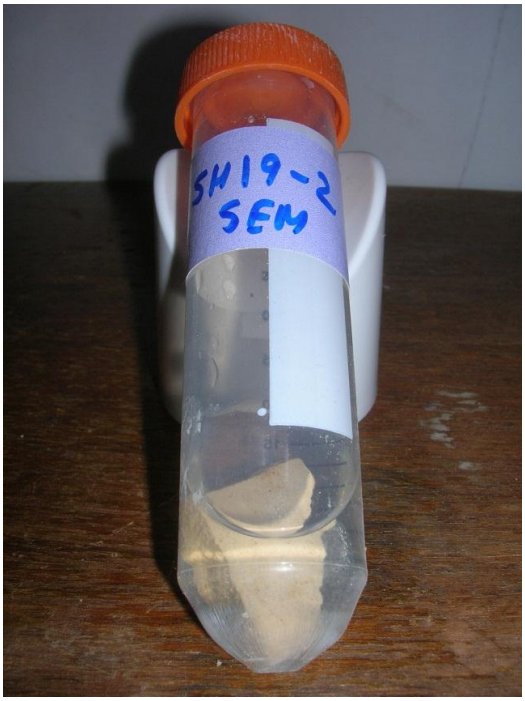

SH11 – Depth 2.0m – Exterior and Interior

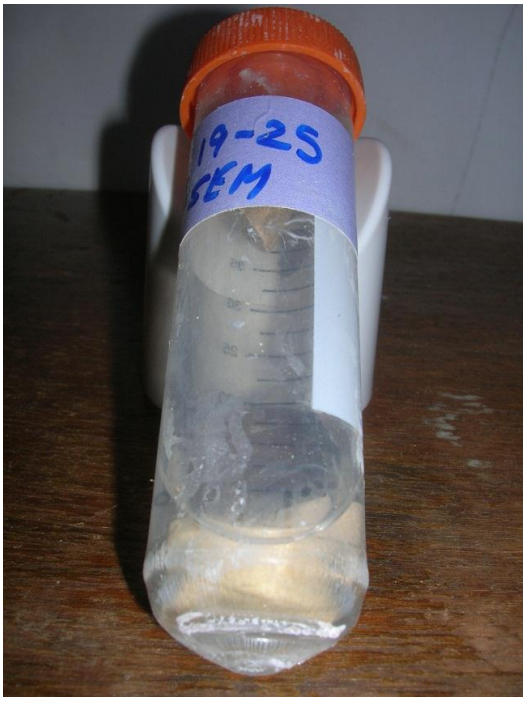

SH11 – Depth 2.5m – Exterior and Interior

SINKHOLE 21 (SH21)

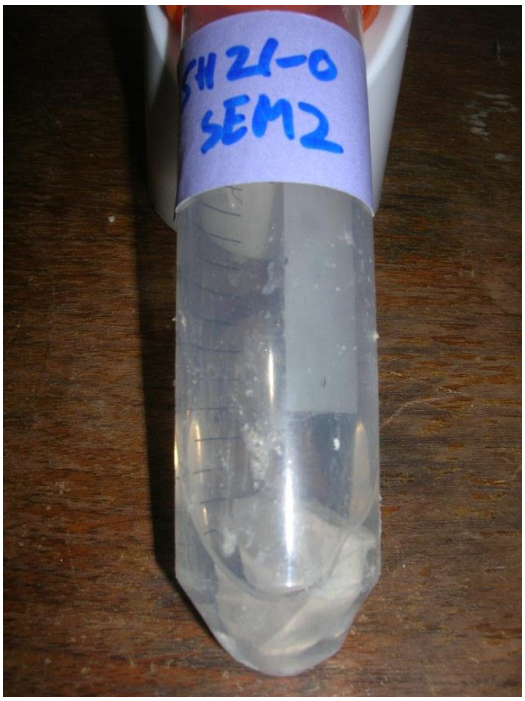

SH21 – Depth 0.0m –Interior

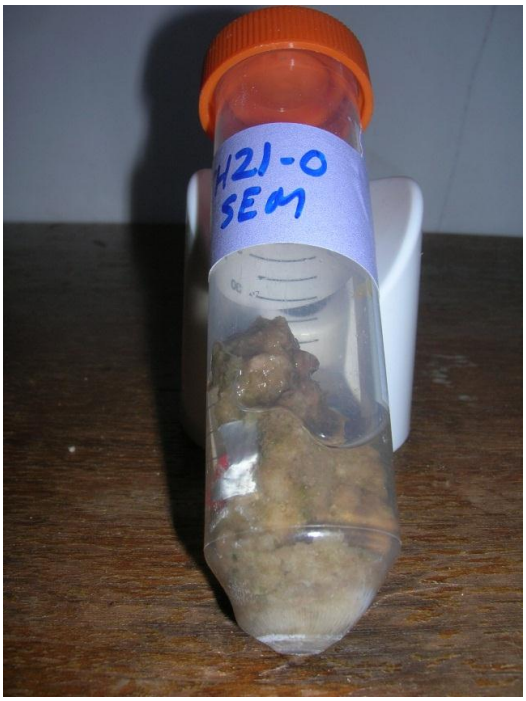

SH21 – Depth 0.0m – Exterior

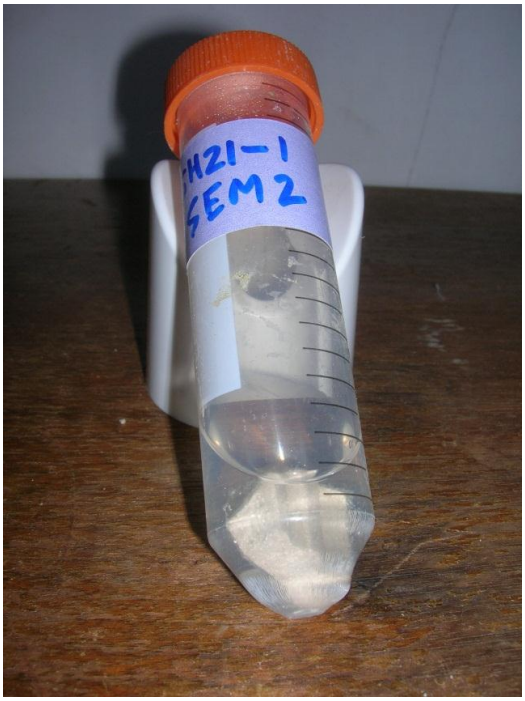

SH21 – Depth 1.0m – Interior

SH21 – Depth 1.0m – Exterior

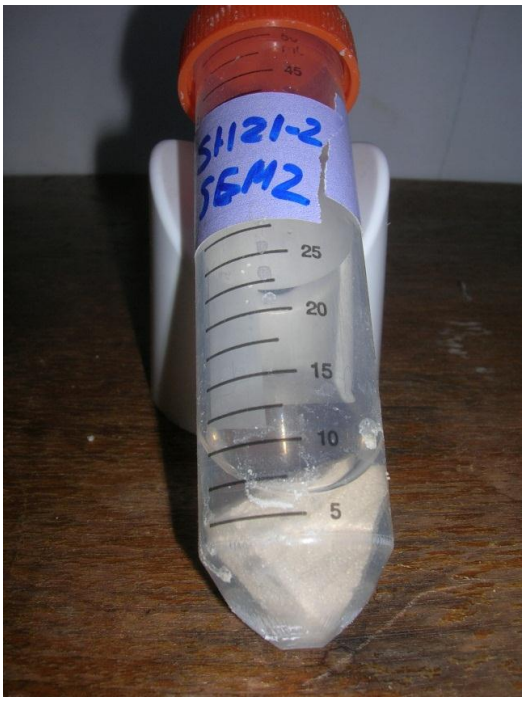

SH21 – Depth 2.0m – Interior

SH21 – Depth 2.0m – Exterior

SH21 – Depth 3.0m – Exterior and Interior

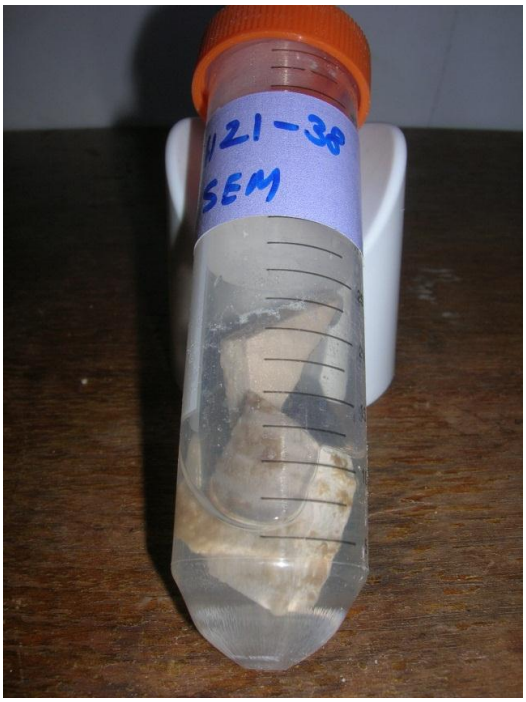

SH21 – Depth 3.8m – Exterior and Interior

SINKHOLE 37 (SH37)

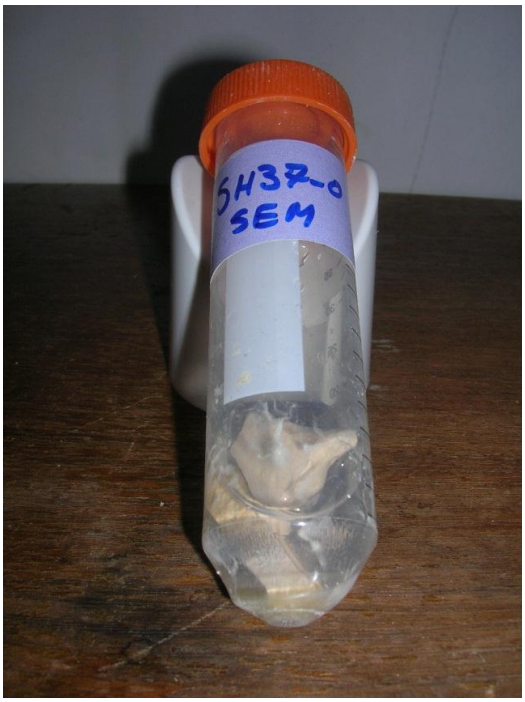

SH37 – Depth 0.0m – Exterior and Interior

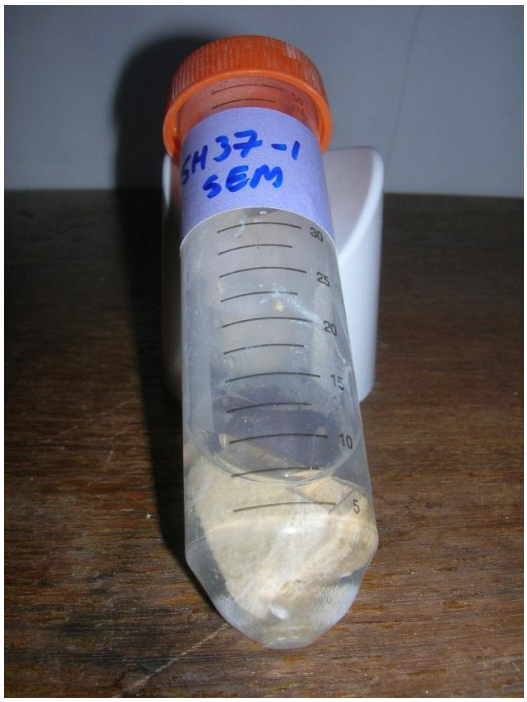

SH37 – Depth 1.0m – Exterior and Interior

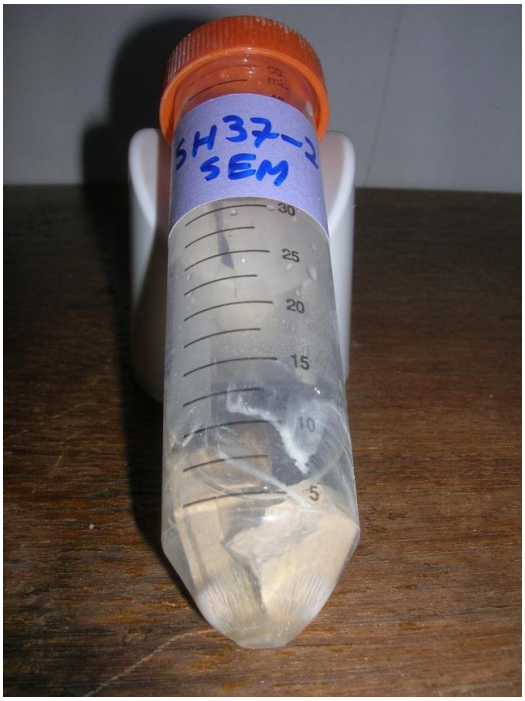

SH37 – Depth 2.0m – Exterior and Interior

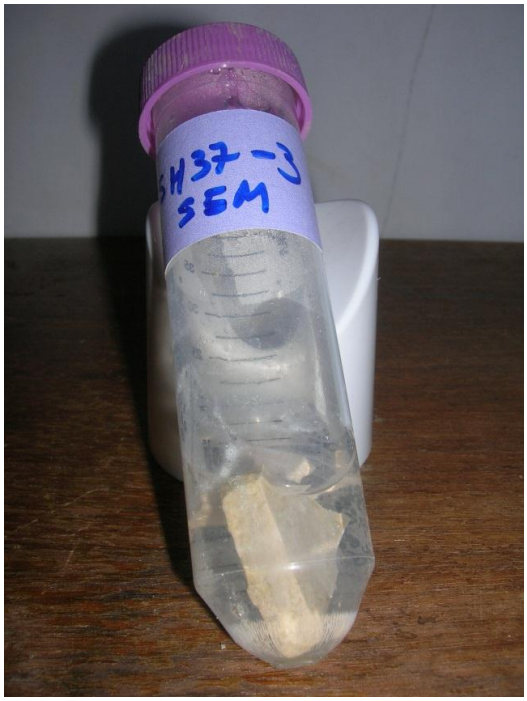

SH37 – Depth 3.0m – Exterior and Interior

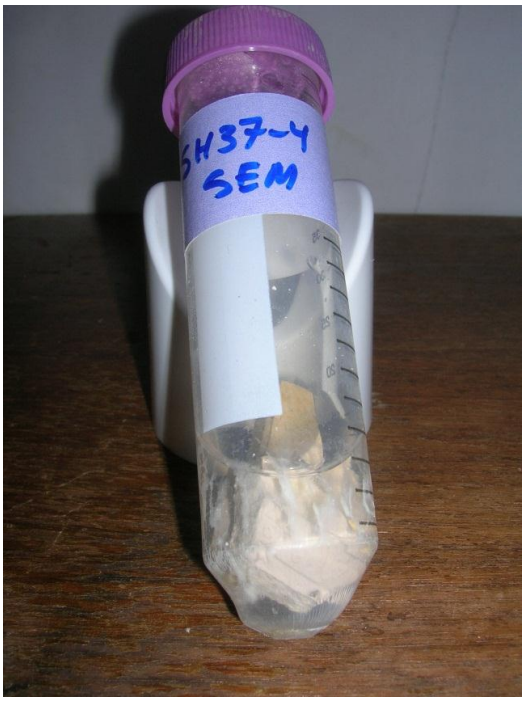

SH37 – Depth 4.0m – Exterior and Interior

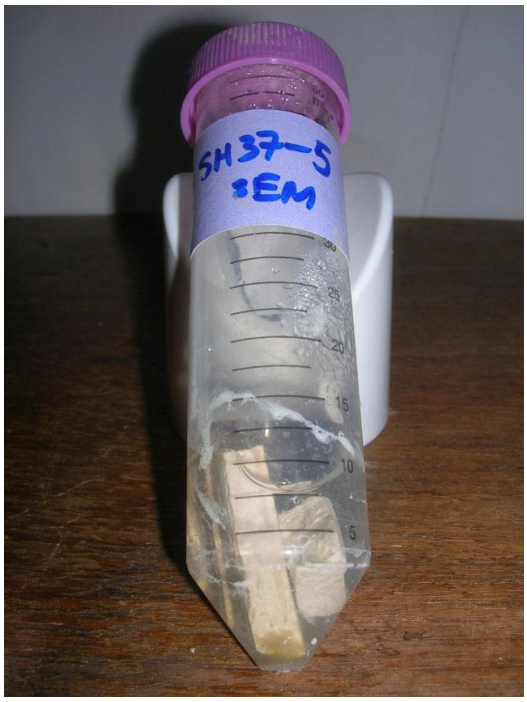

SH37 – Depth 5.0m – Exterior and Interior

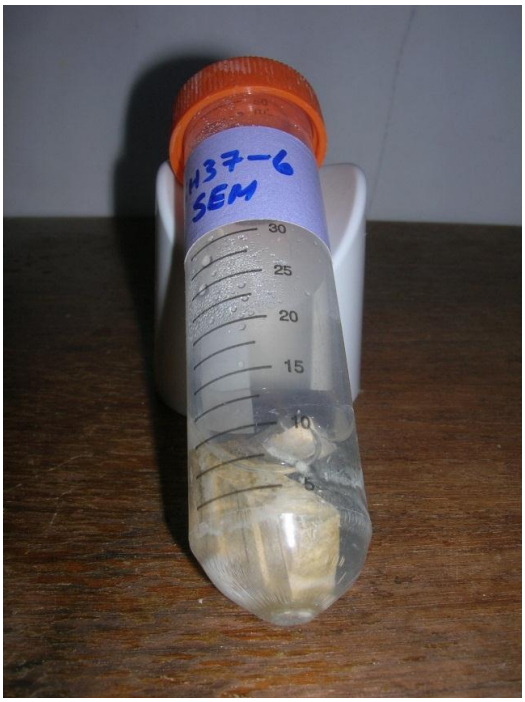

SH37 – Depth 6.0m – Exterior and Interior

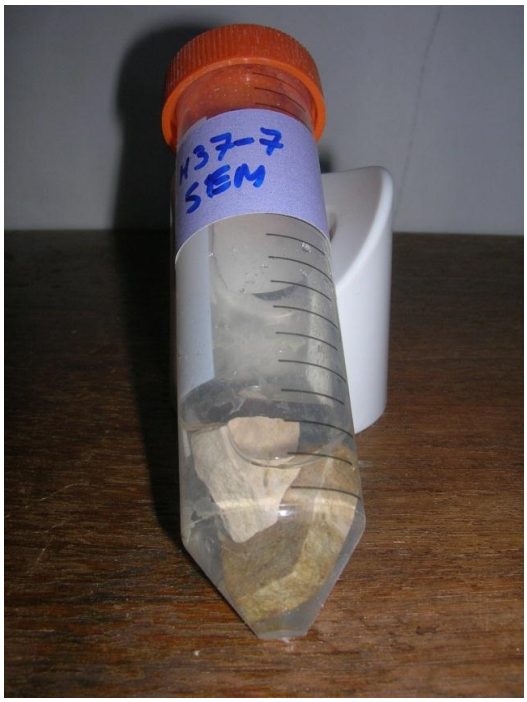

SH37 – Depth 7.0m – Exterior and Interior

SH37 – Depth 8.0m – Exterior and Interior

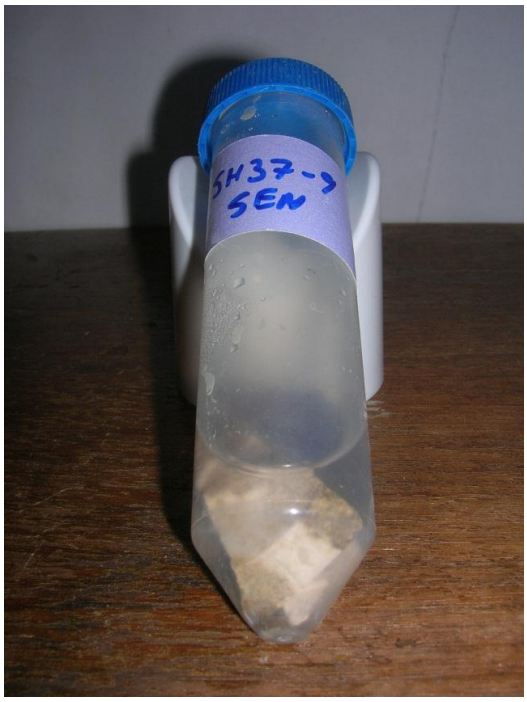

SH37 – Depth 9.0m – Exterior and Interior

SH37 – Depth 10.0m – Exterior and Interior

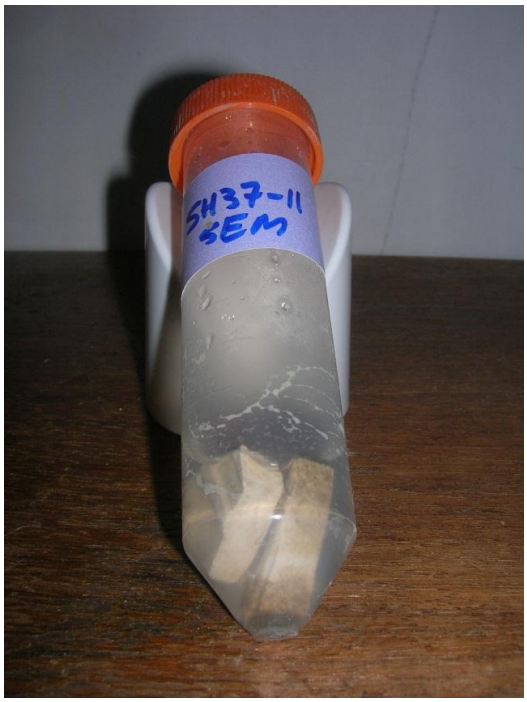

SH37 – Depth 11.0m – Exterior and Interior

SH37 – Depth 12.0m – Exterior and Interior

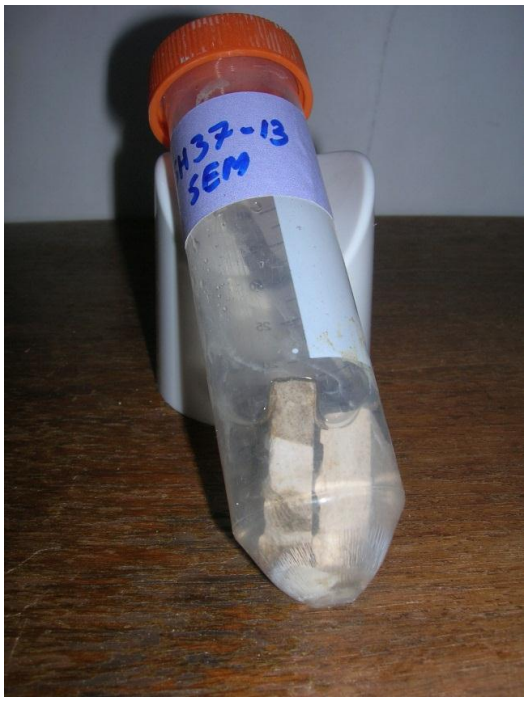

SH37 – Depth 13.0m – Exterior and Interior

SH37 – Depth 14.0m – Interior

SH37 – Depth 14.0m – Exterior

APPENDIX D: SCANNING ELECTRON MICROSCOPE

SEM IMAGES

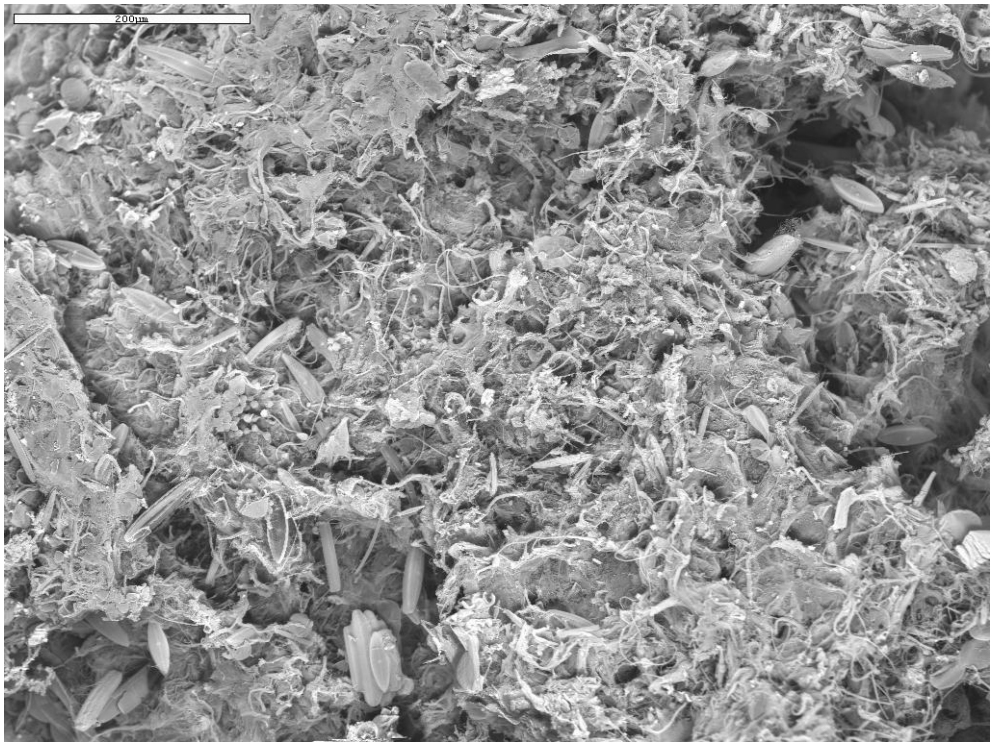

SH19, 0.0m (BL2-1)

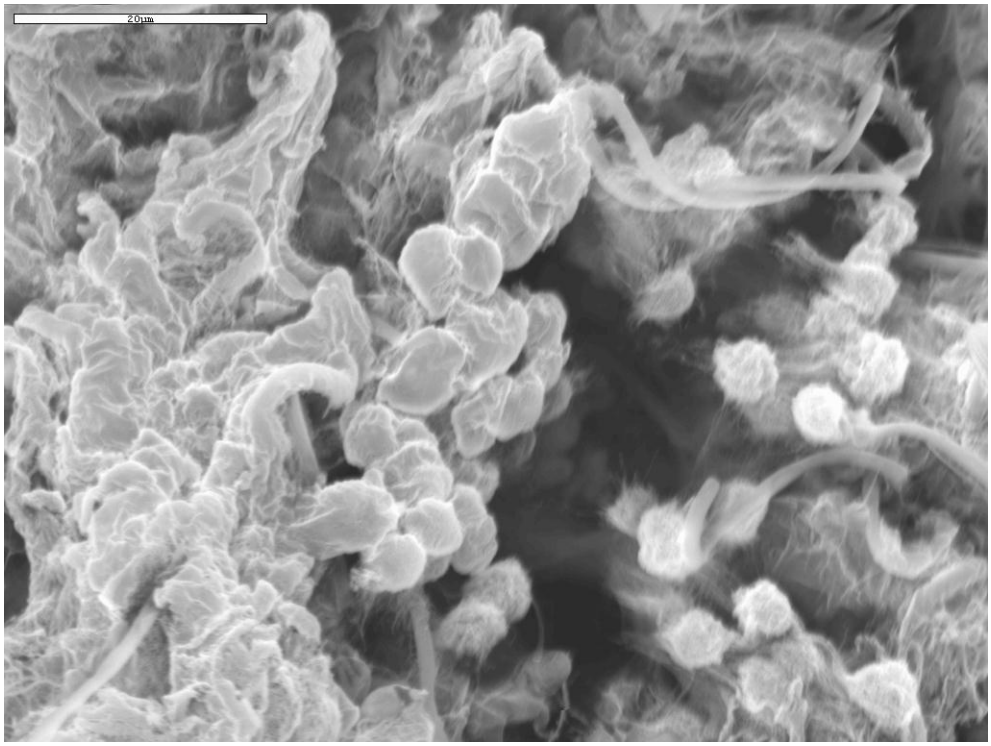

SH19, 0.0m (BL2-4)

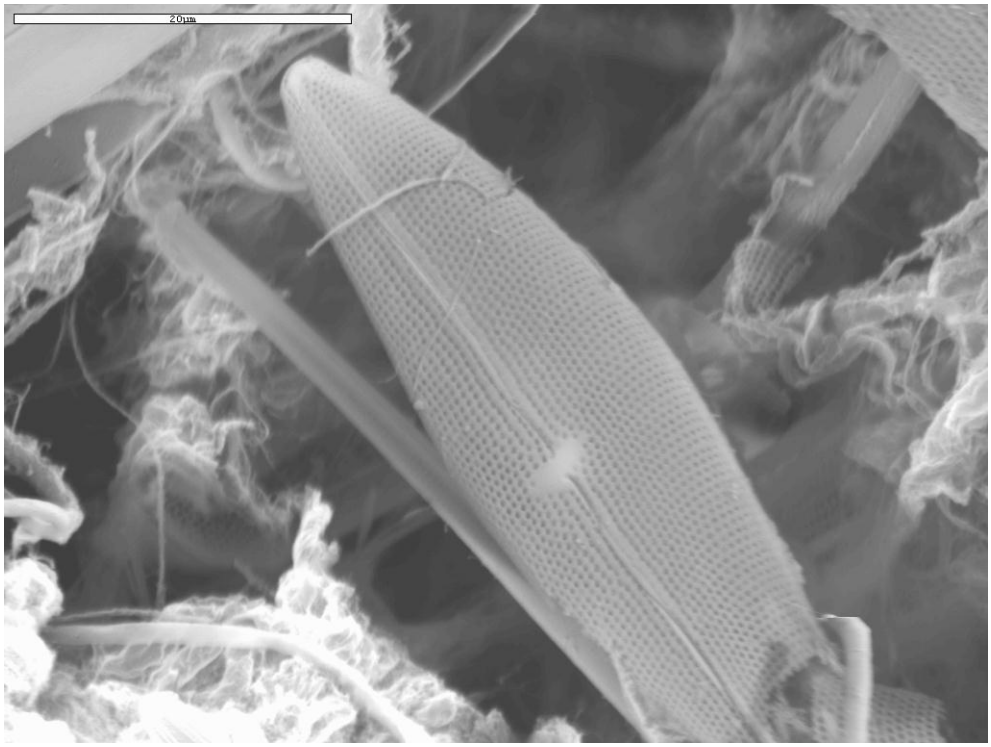

SH19, 0.0m (BL2-5)

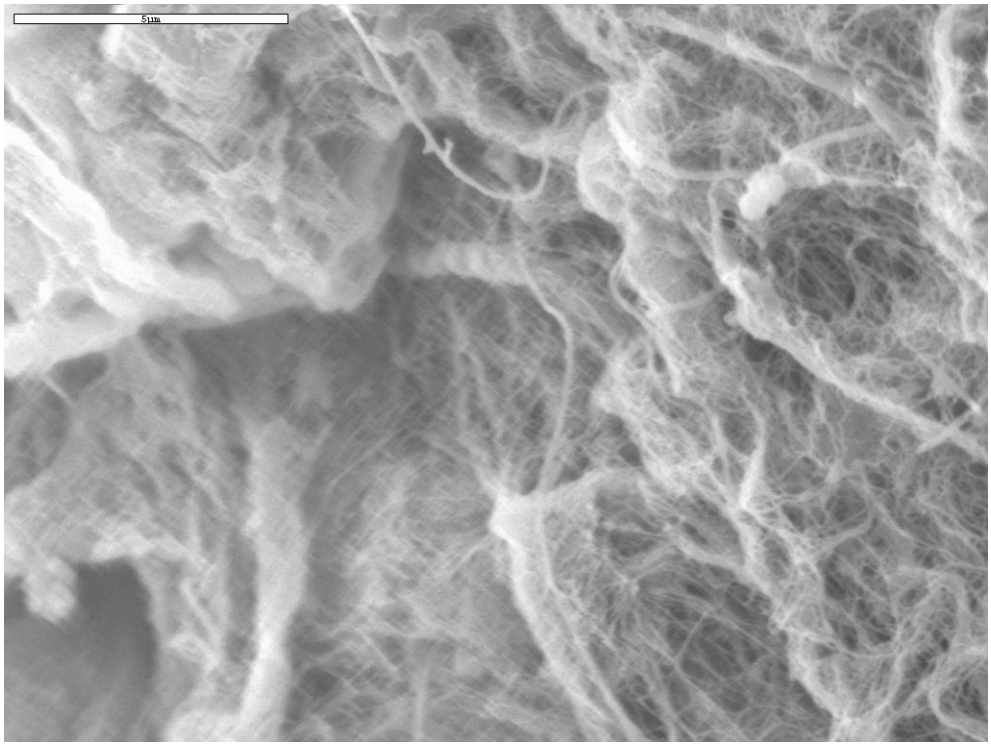

SH19, 0.0m (BL2-6)

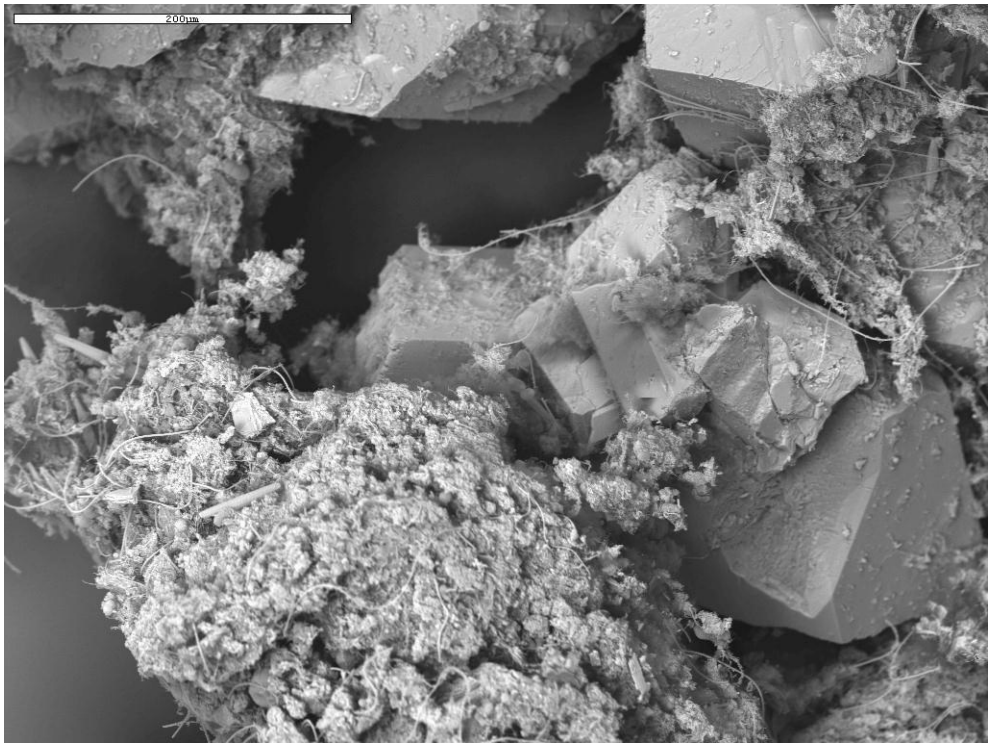

SH21, 1.0m (BL3-1)

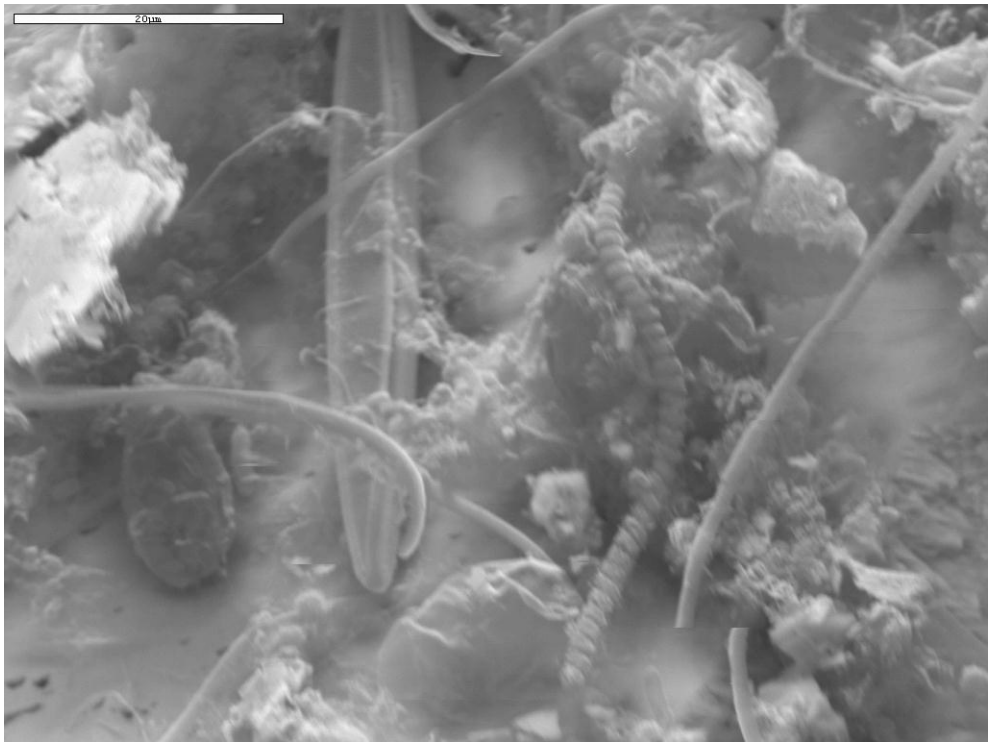

SH21, 1.0m (BL3-2)

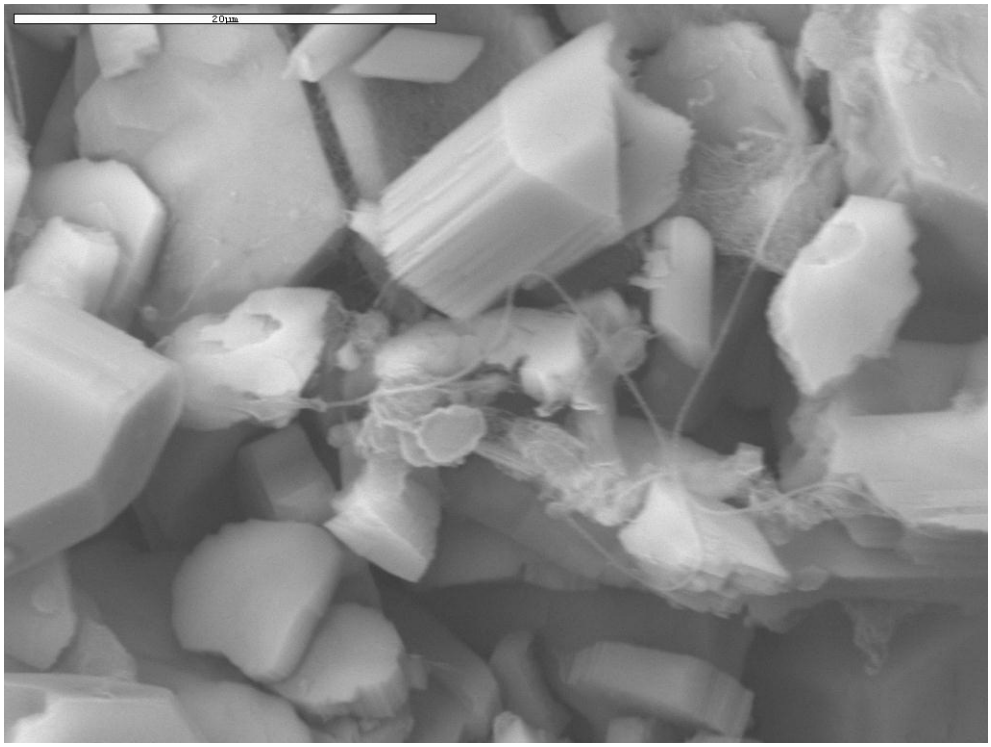

SH37, 14.0m (BLS7-1)

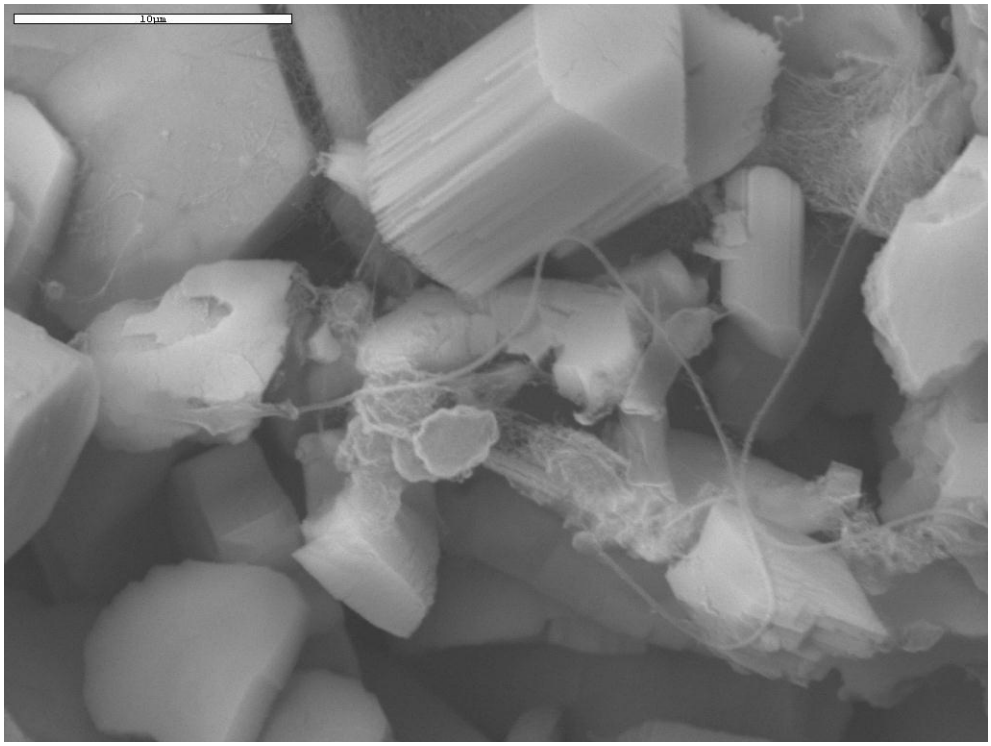

SH37, 14.0m (BLS7-2)

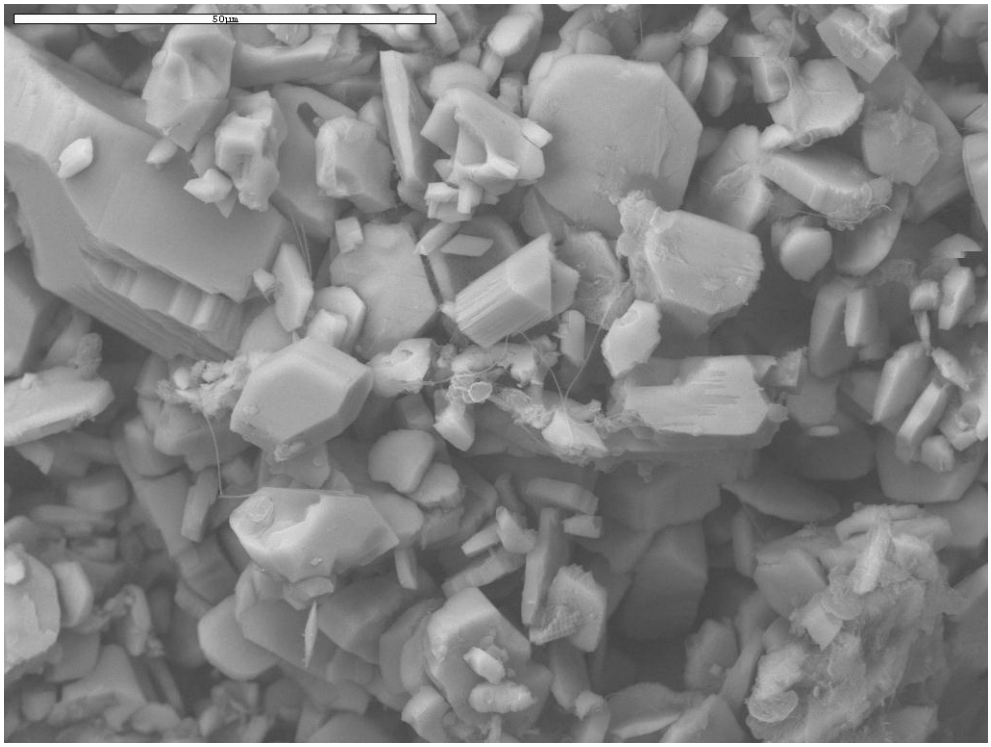

SH37, 14.0m (BLS7-3)

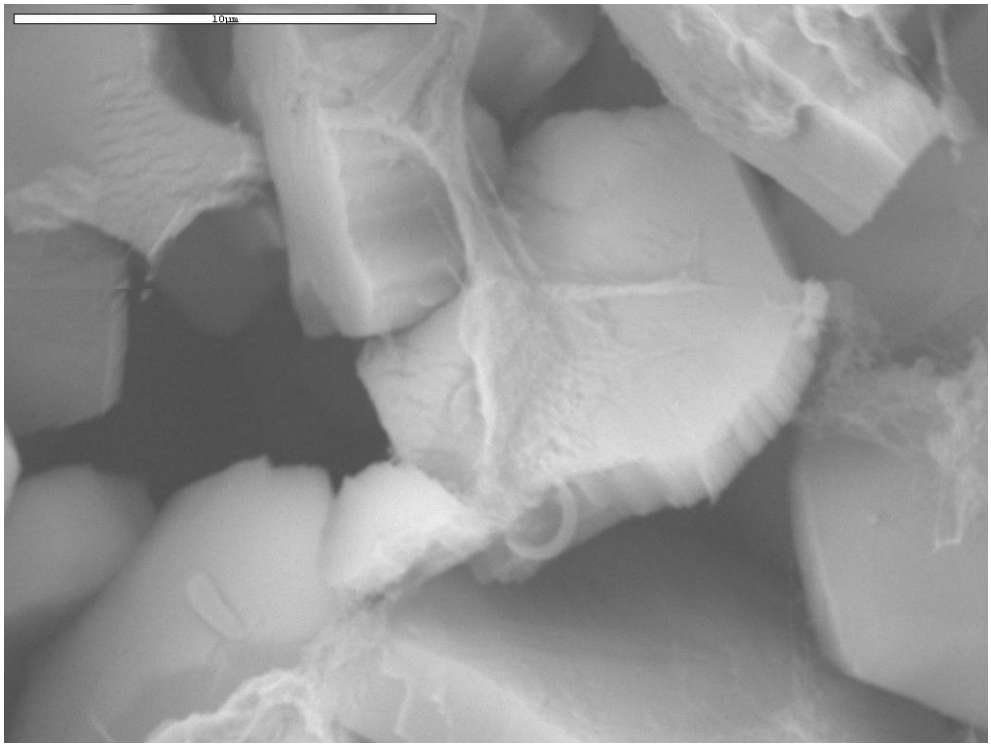

SH37, 14.0m (BLS7-4)

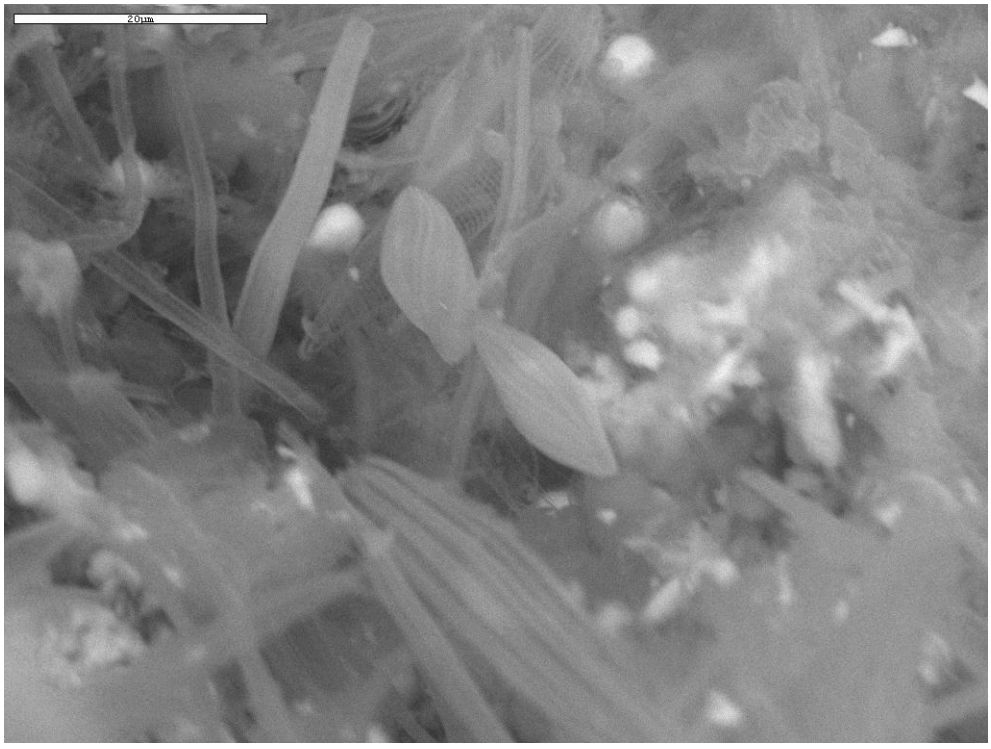

SH11, 2.0m (BLS1-1)

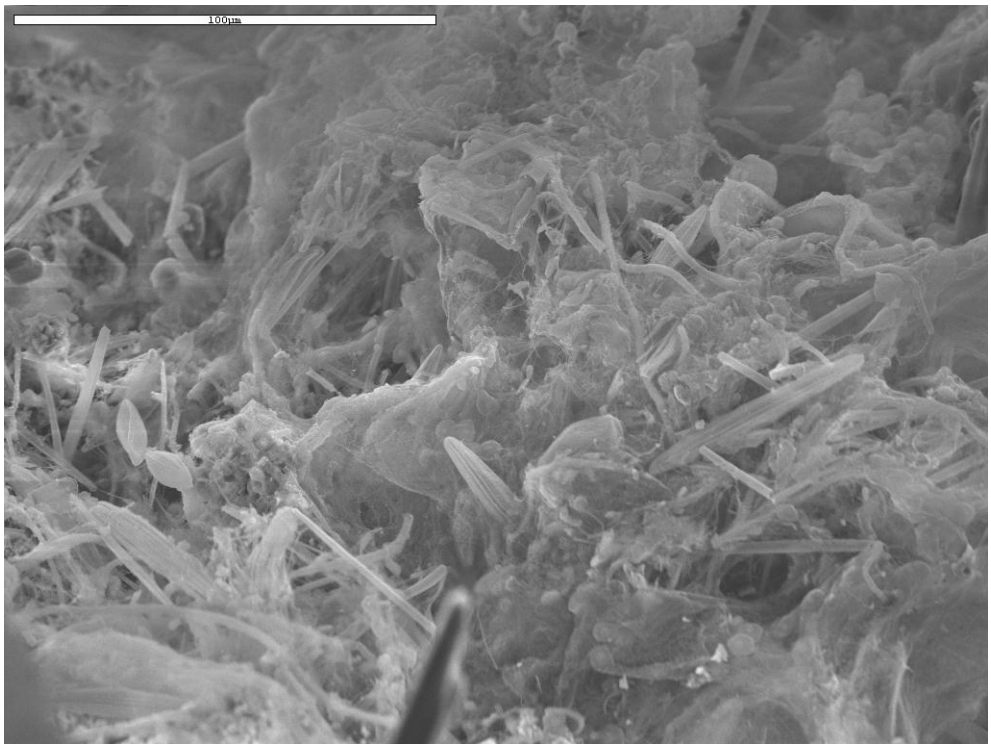

SH11, 2.0m (BLS1-2)

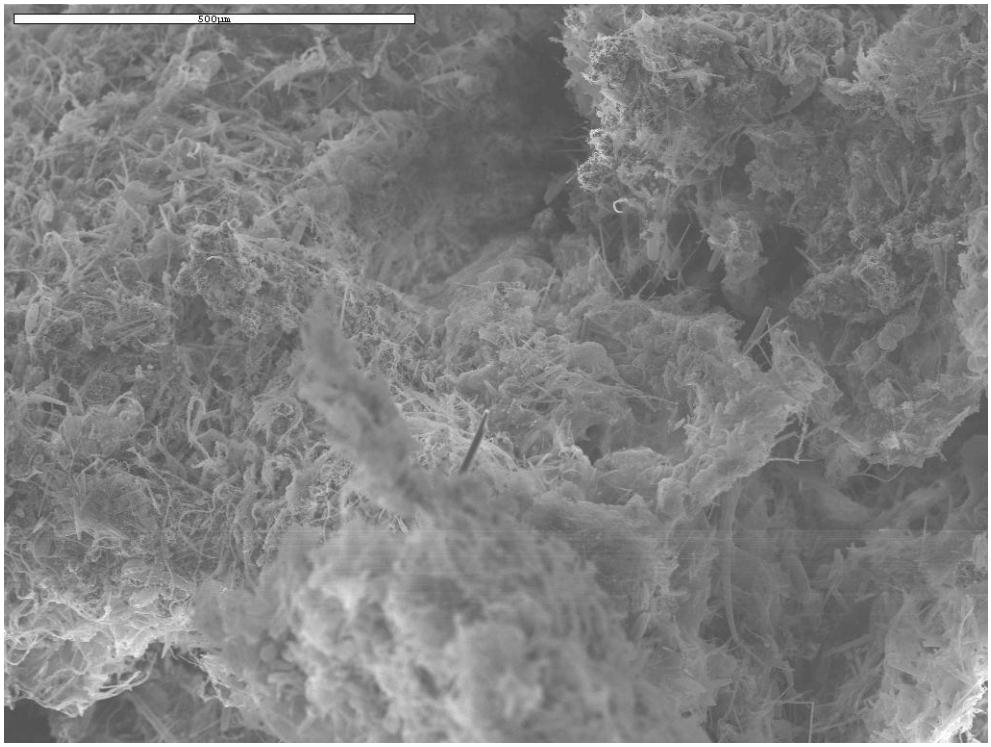

SH11, 2.0m (BLS1-3)

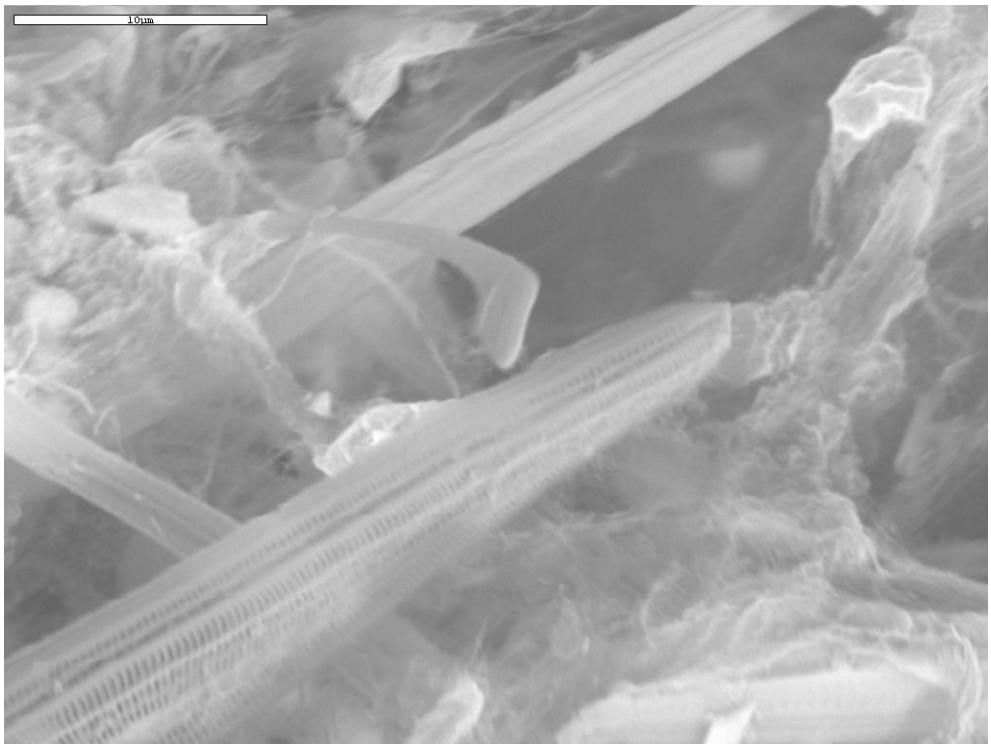

SH11, 2.0m (BLS1-4)

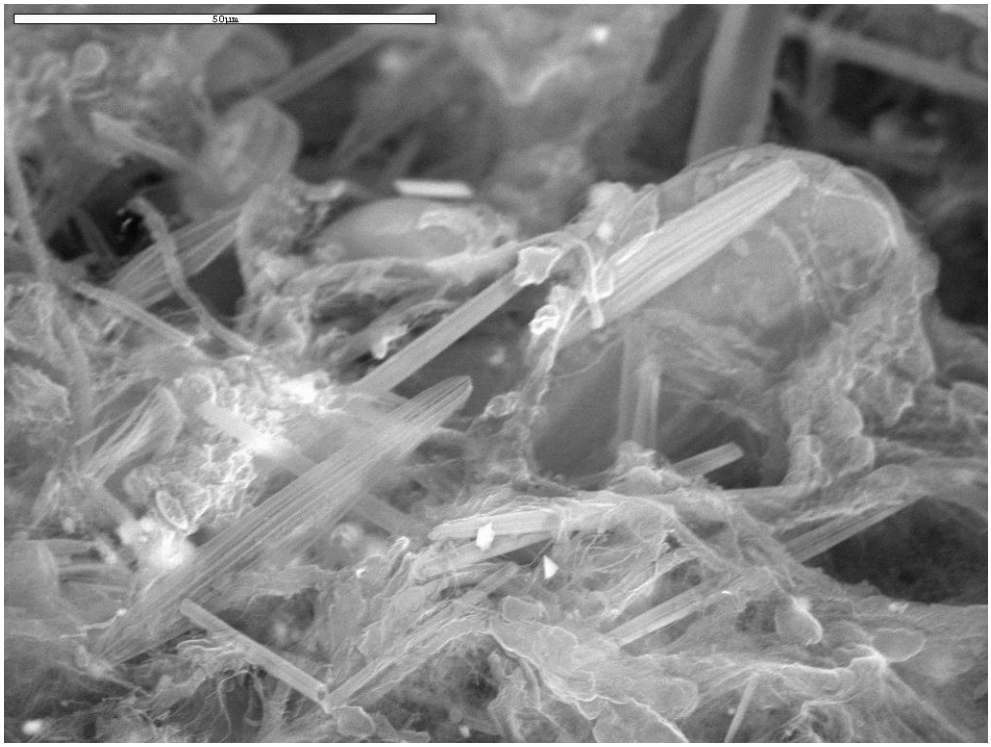

SH11, 2.0m (BLS1-5)

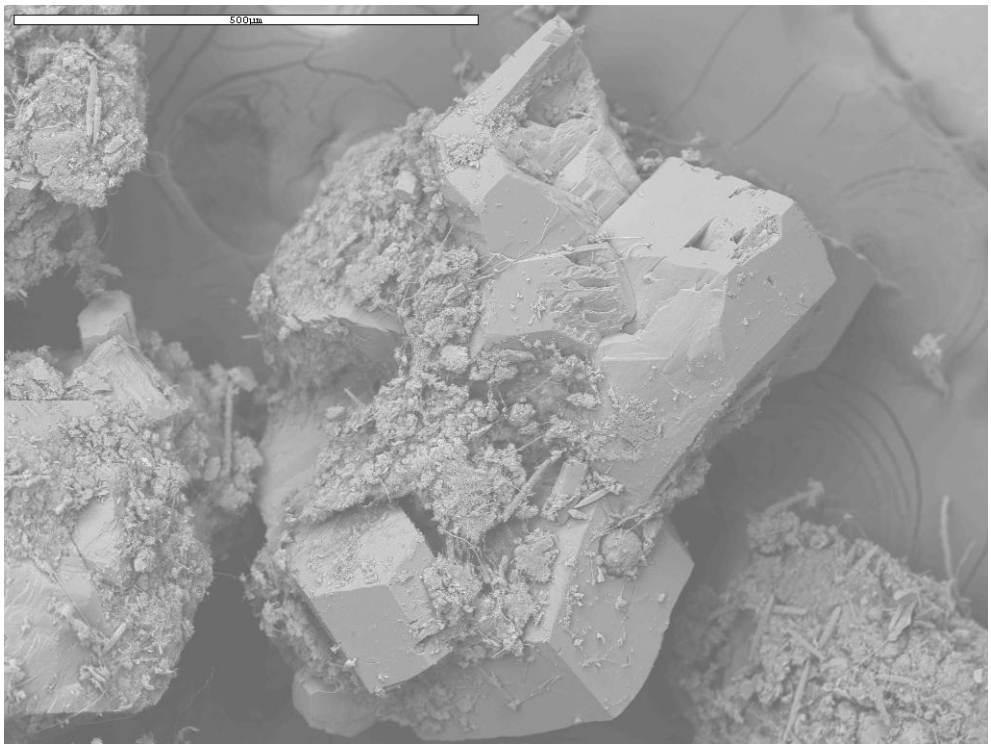

SH37, 13.0m (BL12-1)

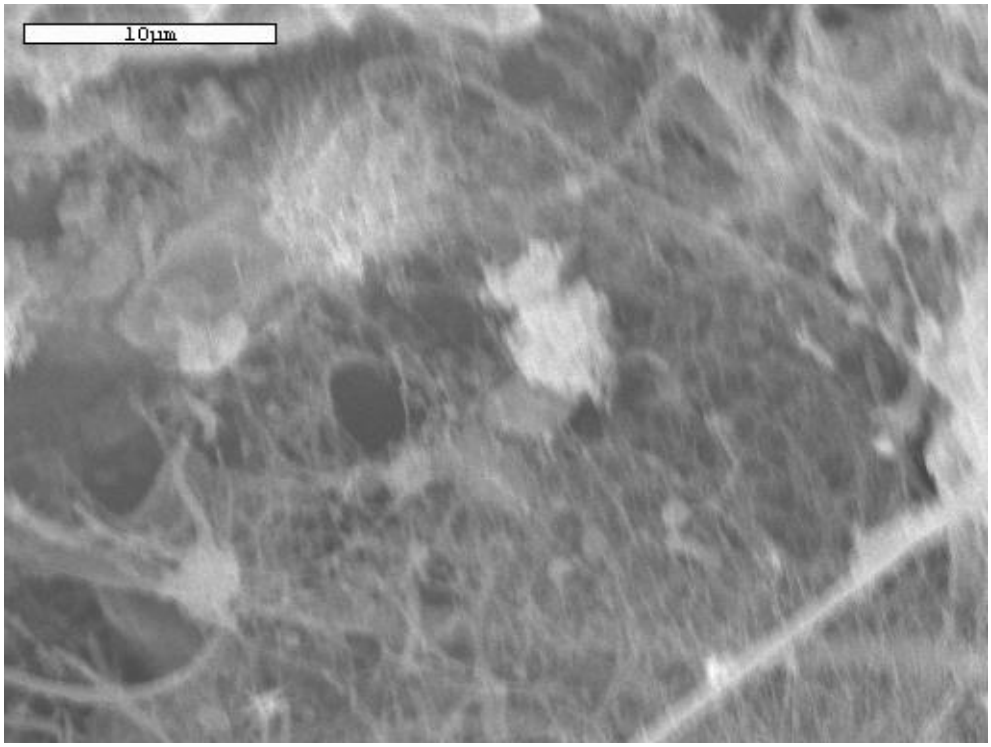

SH37, 13.0m (BL12-2)

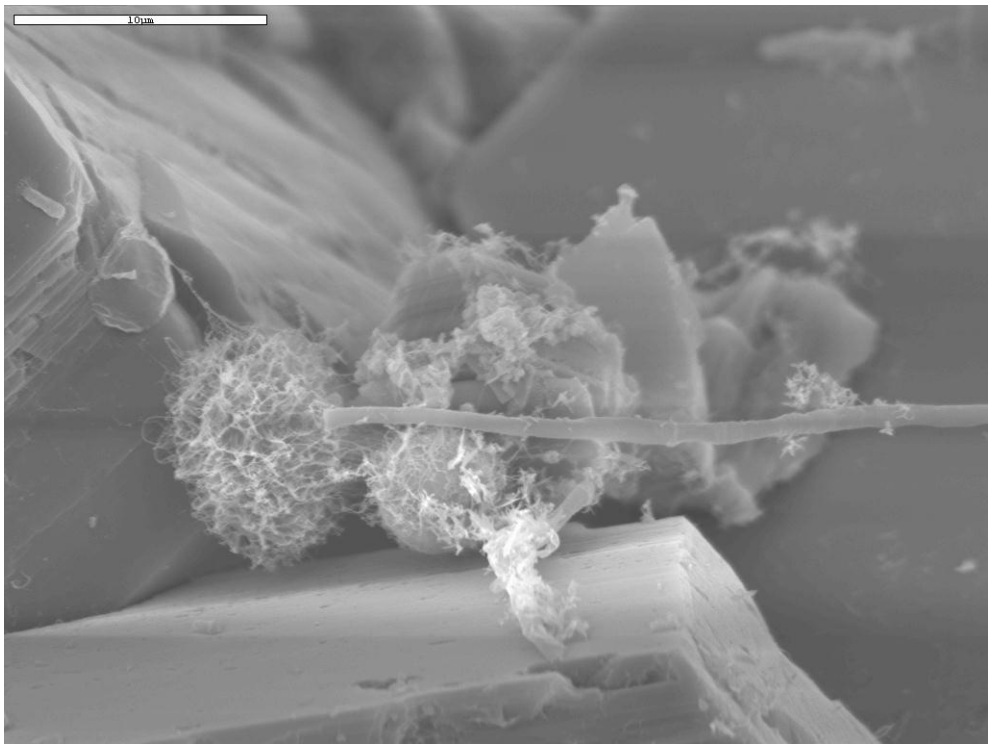

SH37, 13.0m (BL12-3)

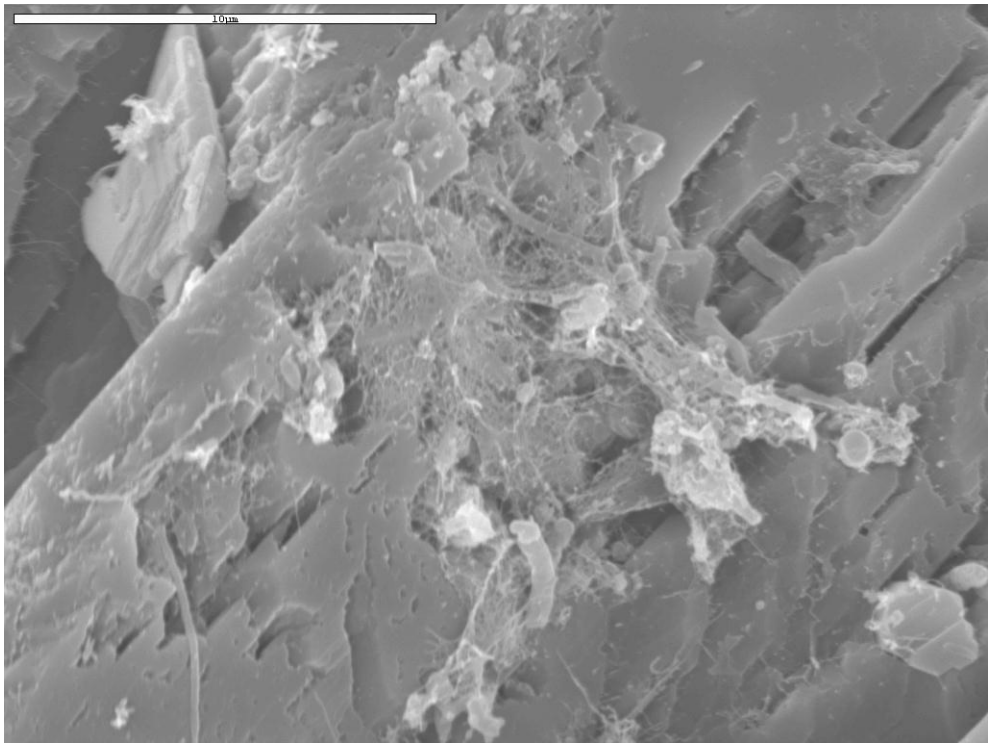

SH37, 13.0m (BL12-5)

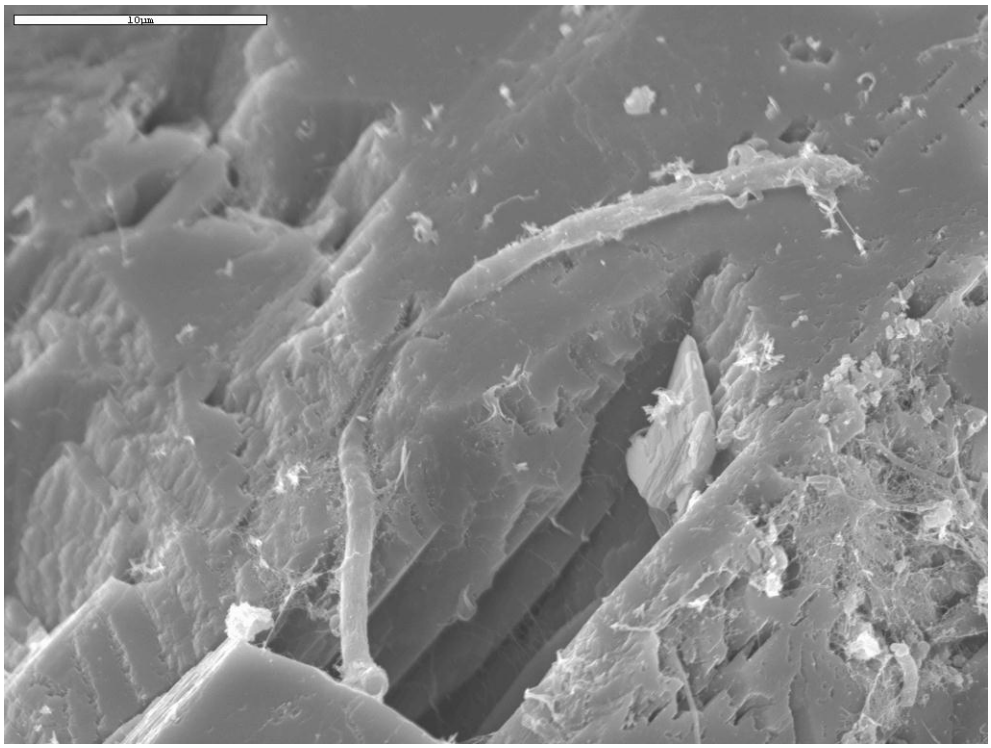

SH37, 13.0m (BL12-6)

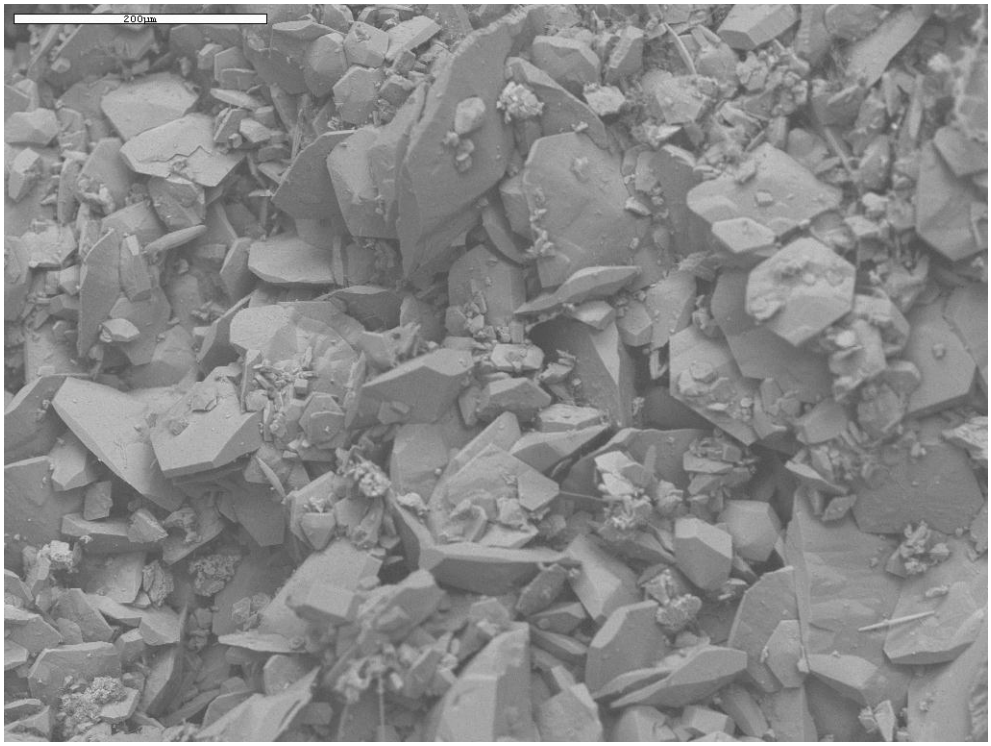

SH17, 2.0m (BL10-1)

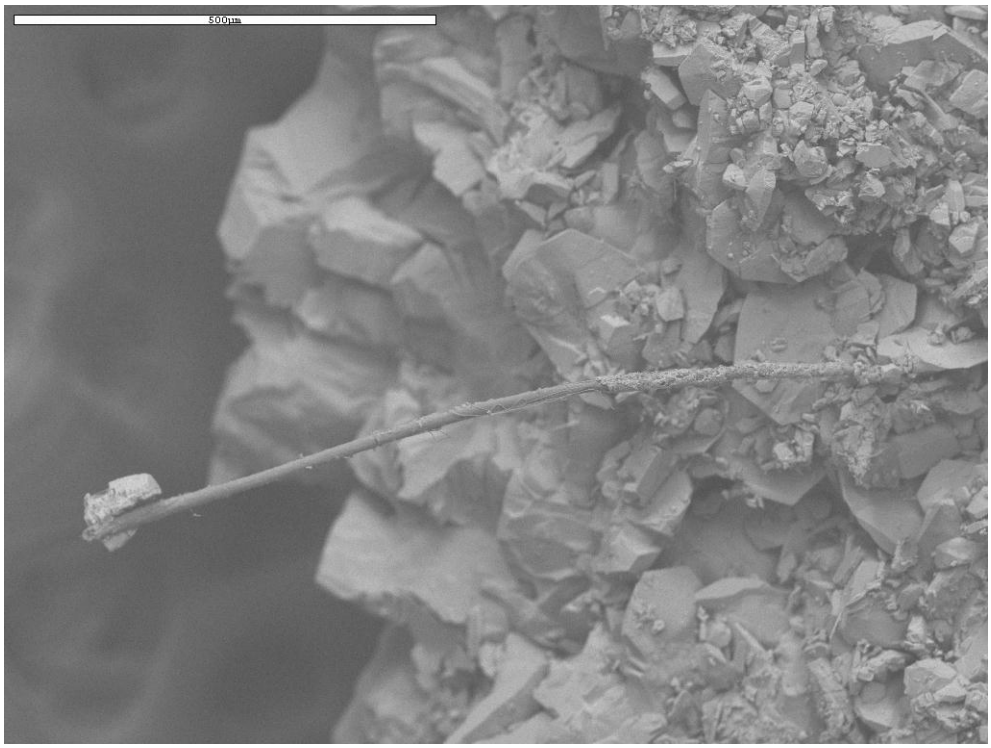

SH17, 2.0m (BL10-3)

SH17, 2.0m (BL10-4)

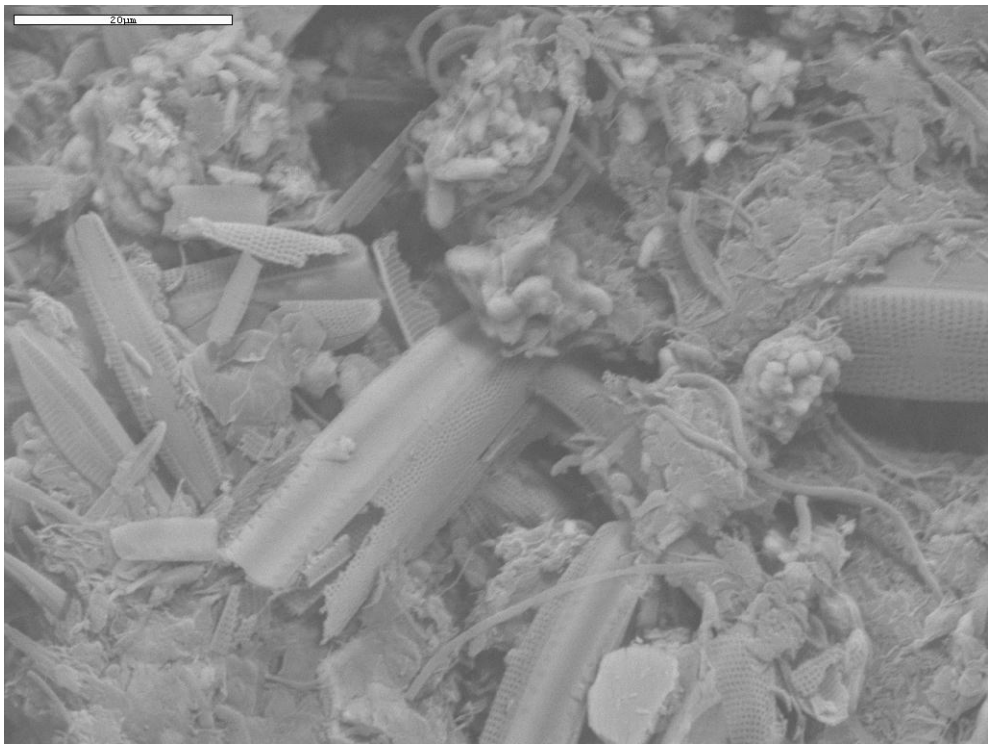

SH17, 2.0m (BL10-5)

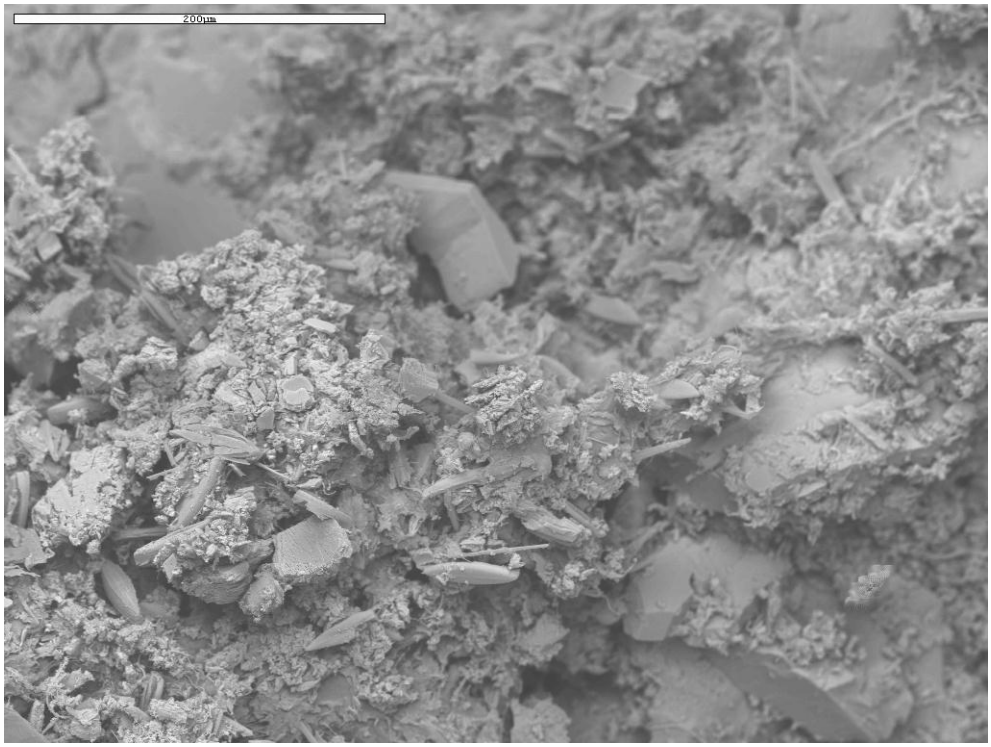

SH17, 0.0m (BL9-1)

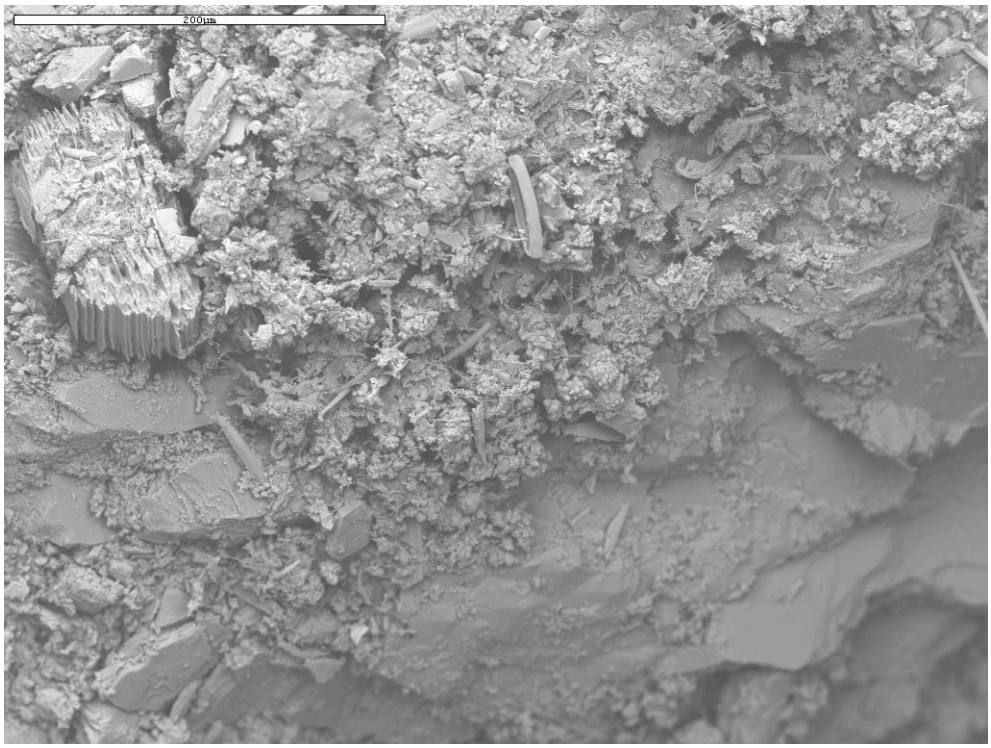

SH17, 0.0m (BL9-2)

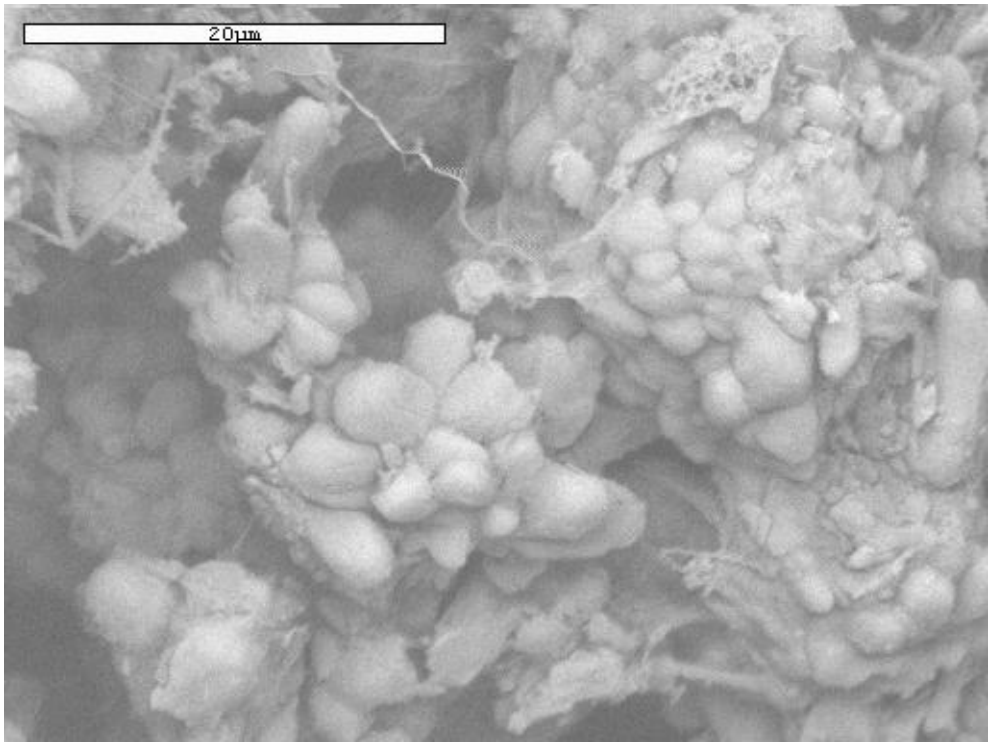

SH17, 0.0m (BL9-4)

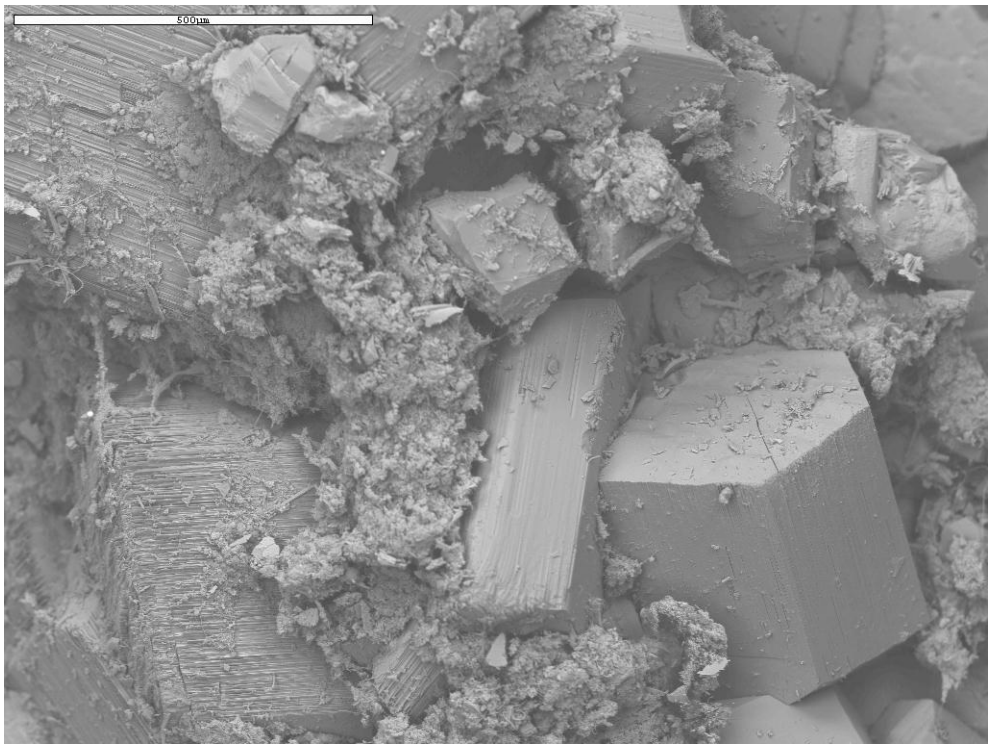

SH21, 3.0m (BL5-1)

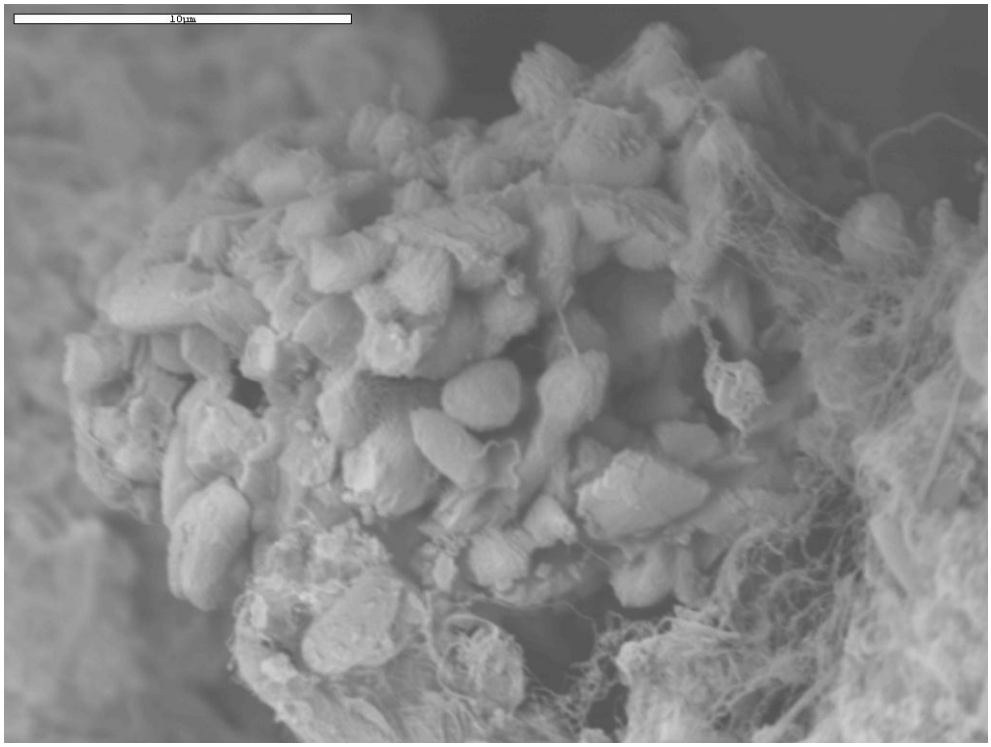

SH21, 3.0m (BL5-4)

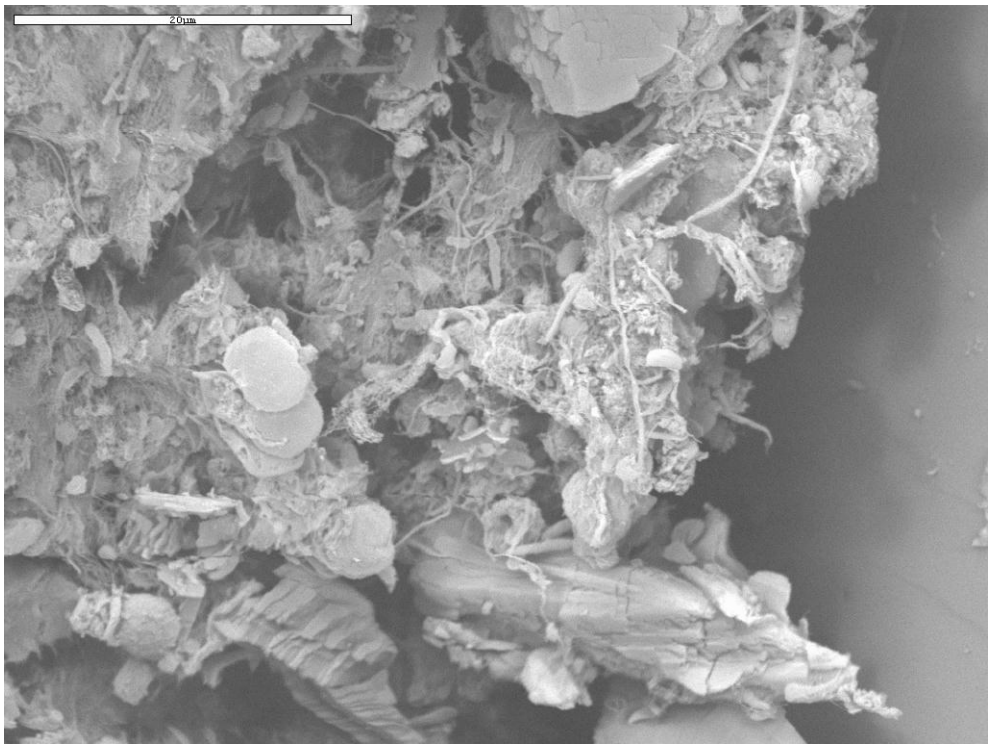

SH21, 3.0m (BL5-7)

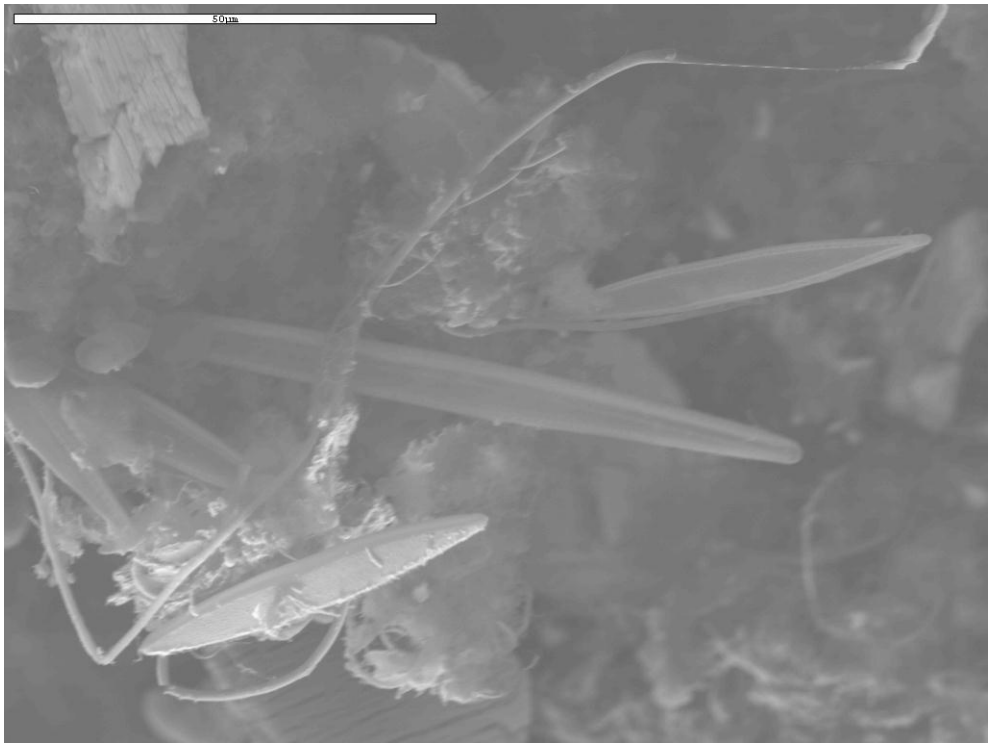

SH21, 1.0m (BL3-6)

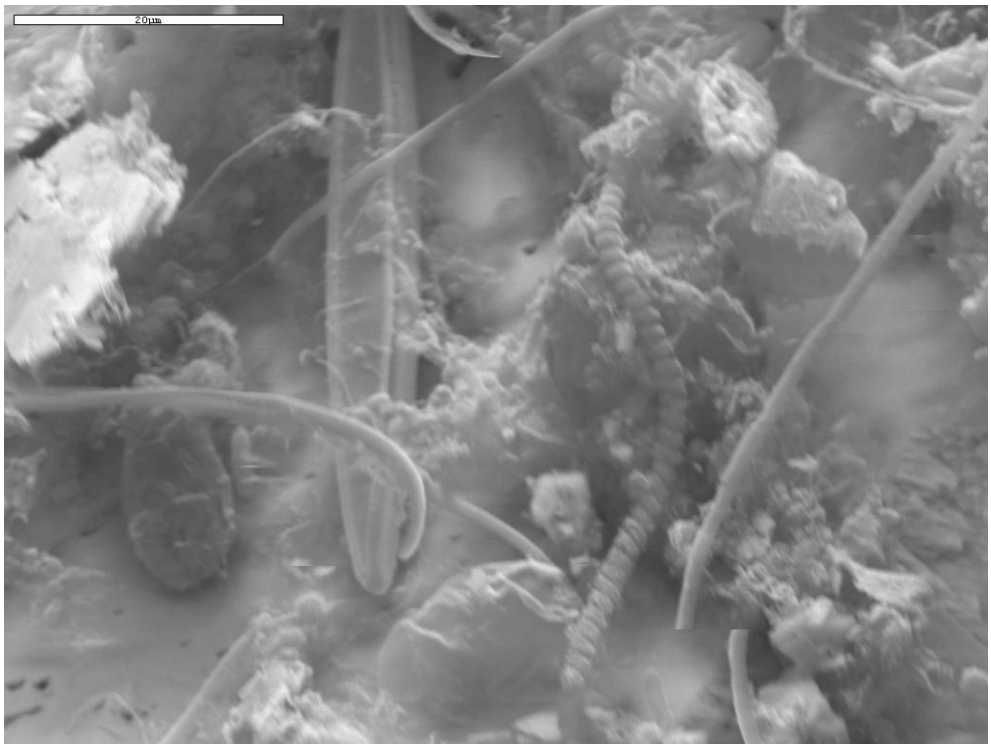

SH21, 1.0m (BL3-2)

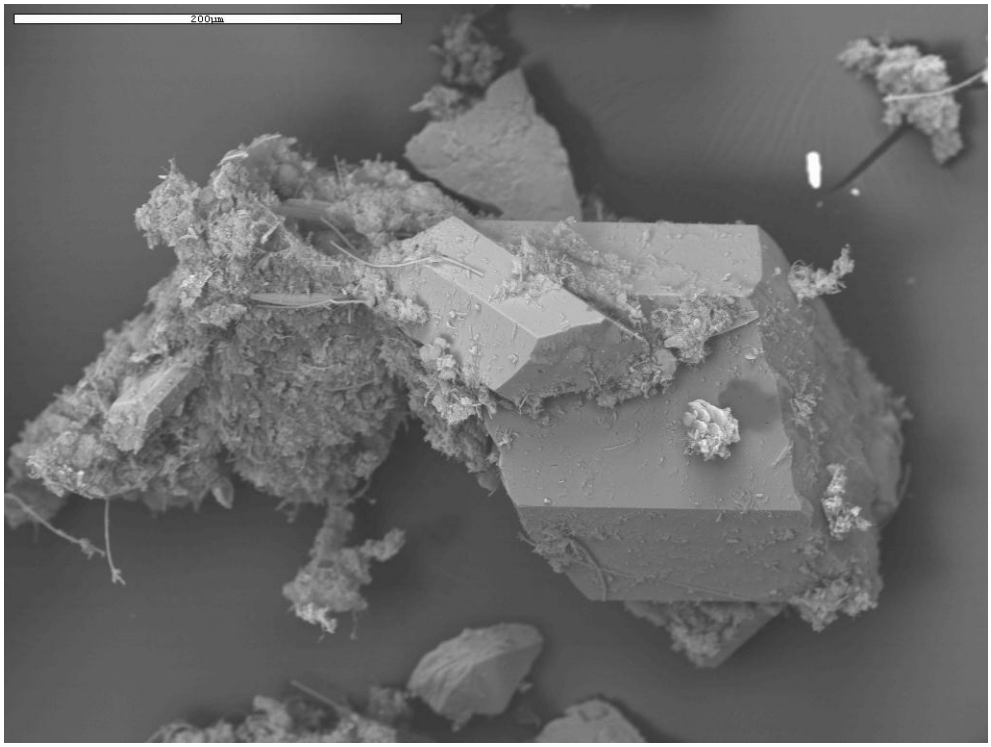

SH21, 1.0m (BL3-3)

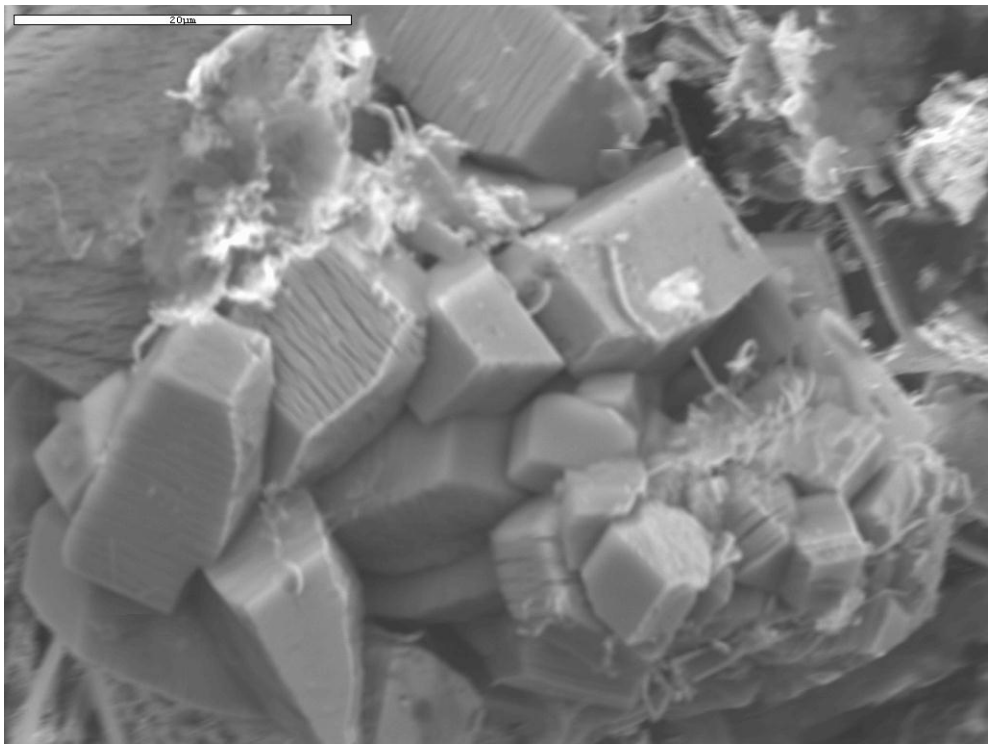

SH21, 1.0m (BL3-4)

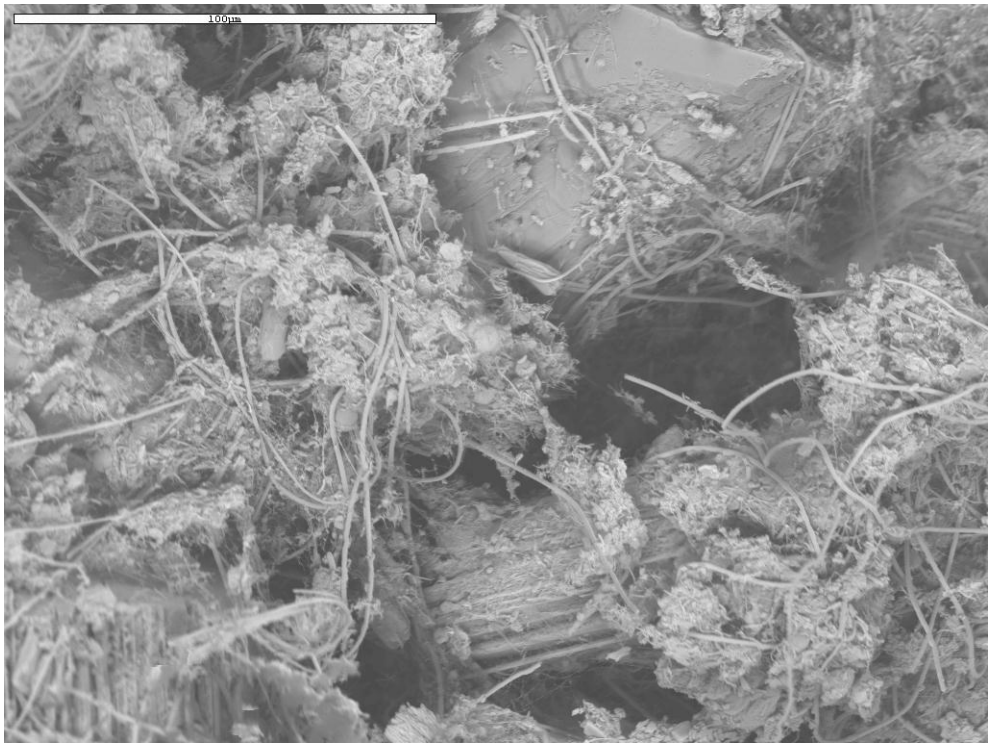

SH21, 1.0m (BL3-5)

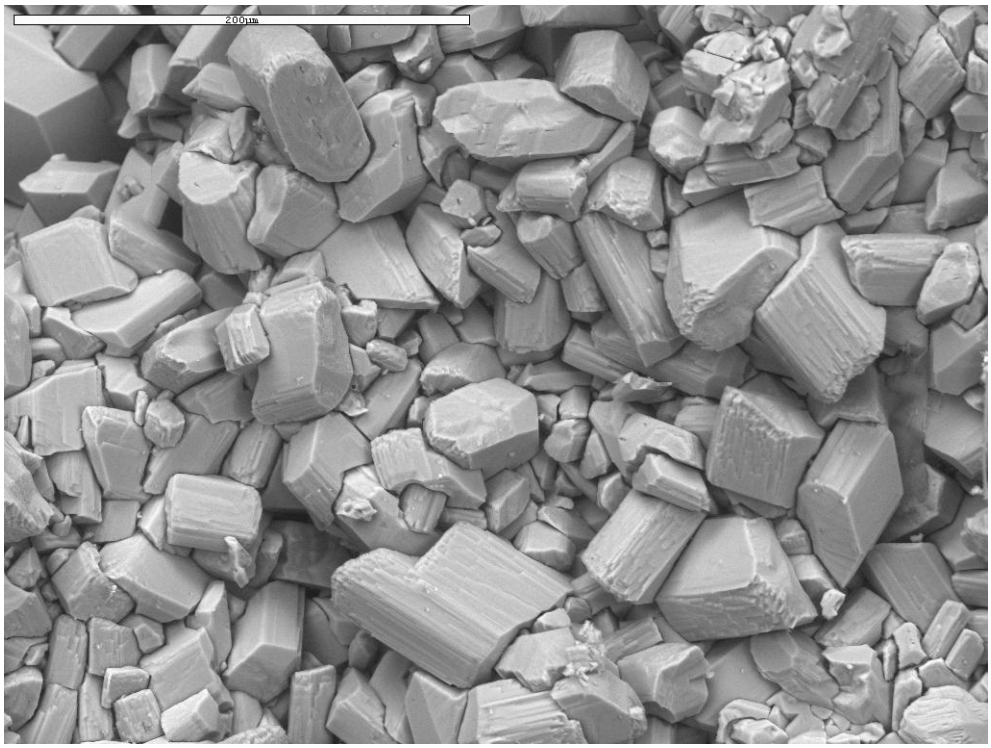

SH17, 1.0m (BLS11-1)

EDS SPECTRUM

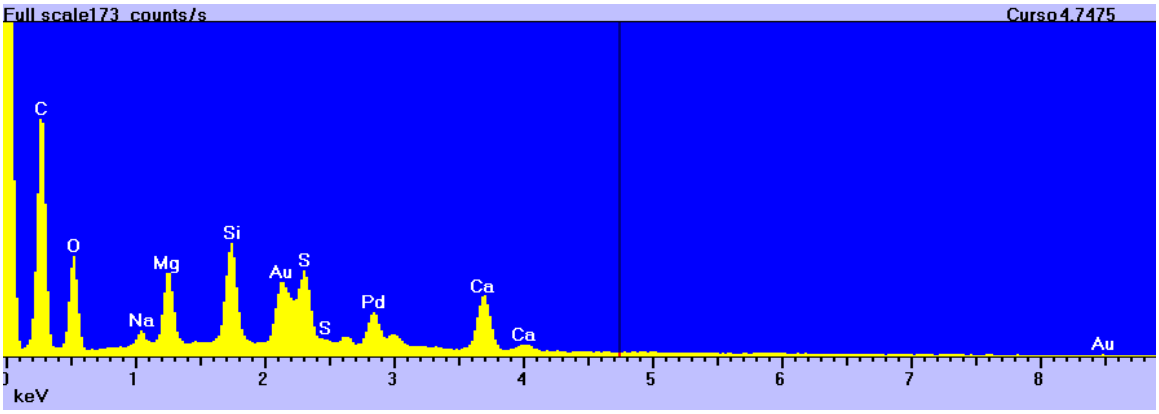

SH19, 0.0m (BL2-2)

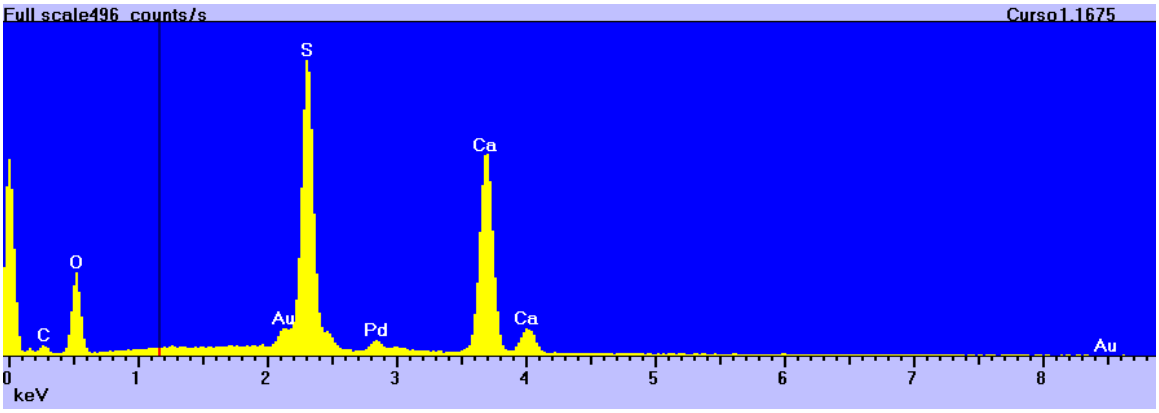

SH19, 0.0m (BL2-3)

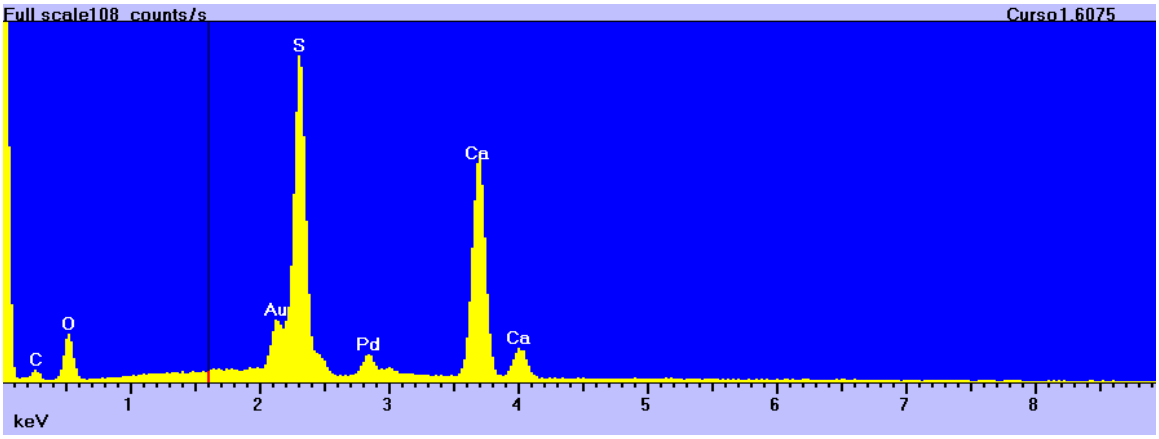

SH21, 3.0m (BL5-2)

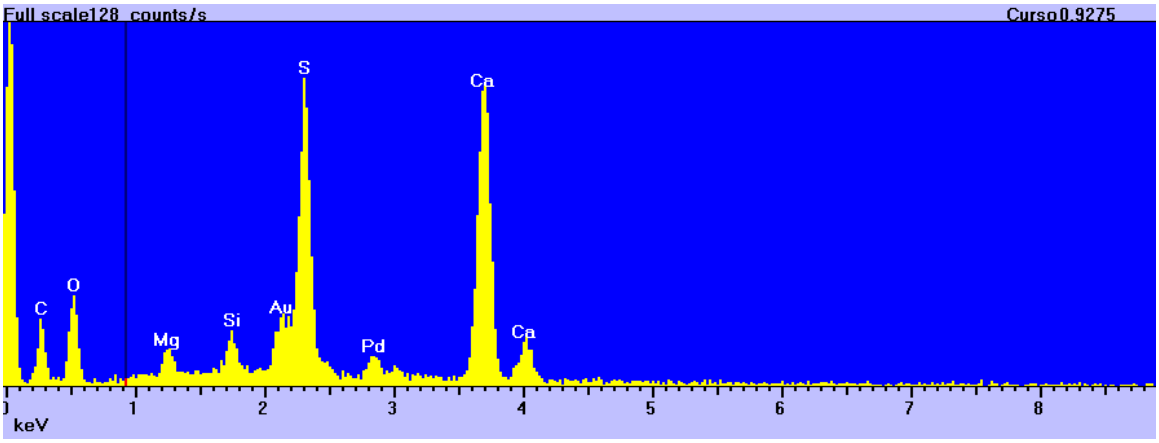

SH21, 3.0m (BL5-5)

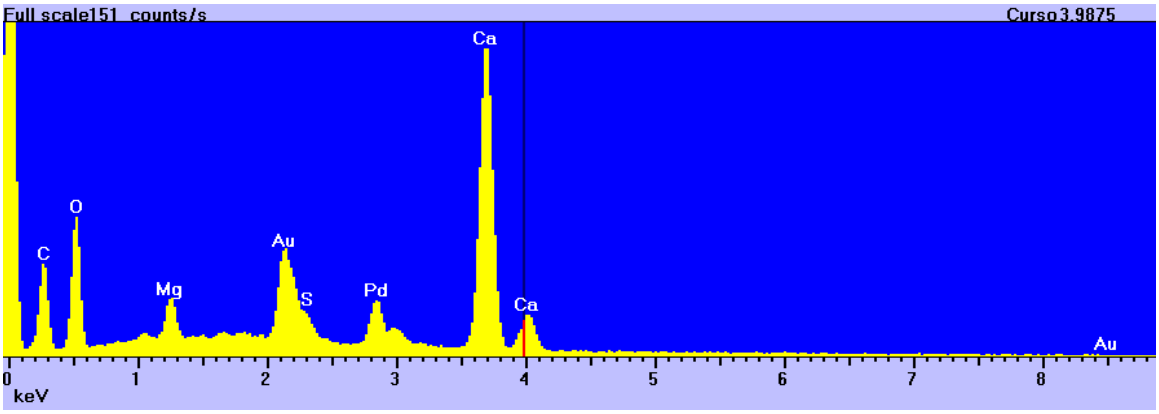

SH17, 0.0m (BL9-3)

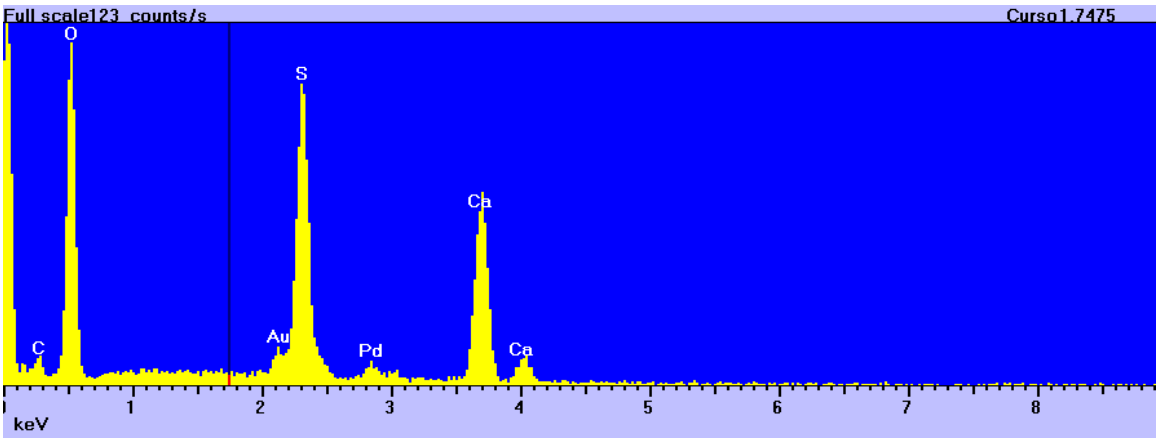

SH17, 2.0m (BL10-2)

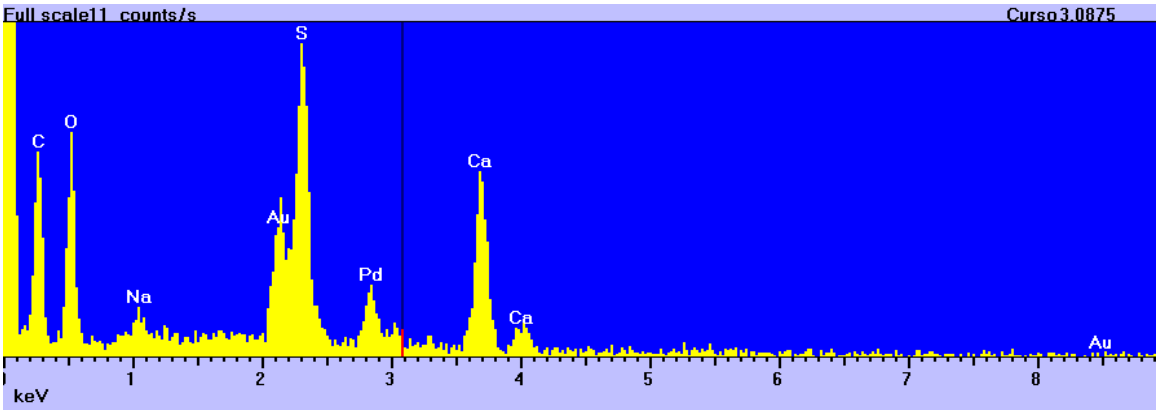

SH37, 13.0m (BL12-4)

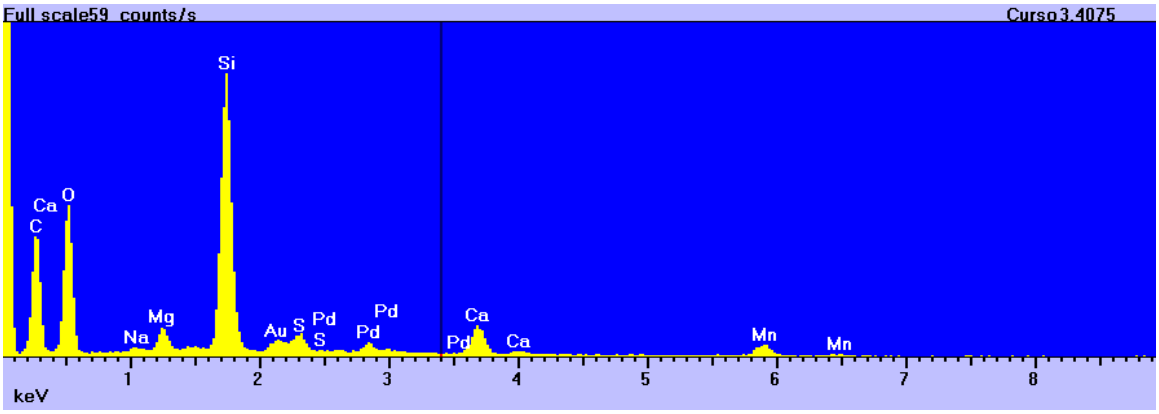

SH11, 2.0m (EDSBL1)

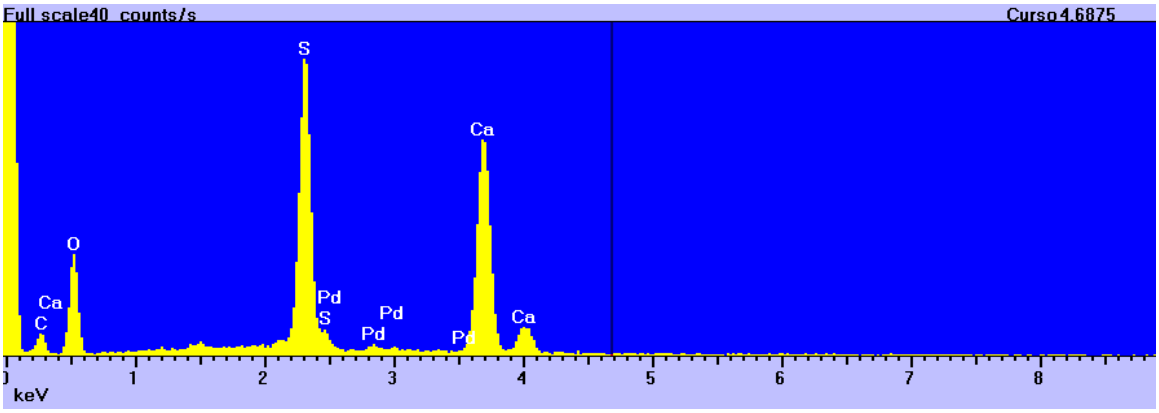

SH17, 1.0m (EDSBL11)

APPENDIX E: WATER COLUMN STRUCTURE

Temperature with Depth - October 2008

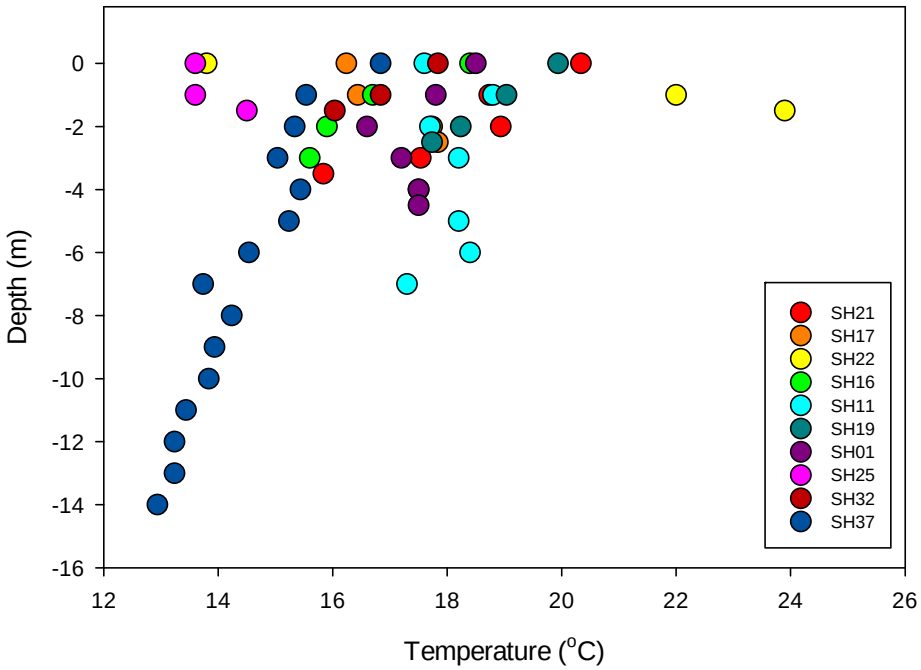

Temperature with Depth - May 2009

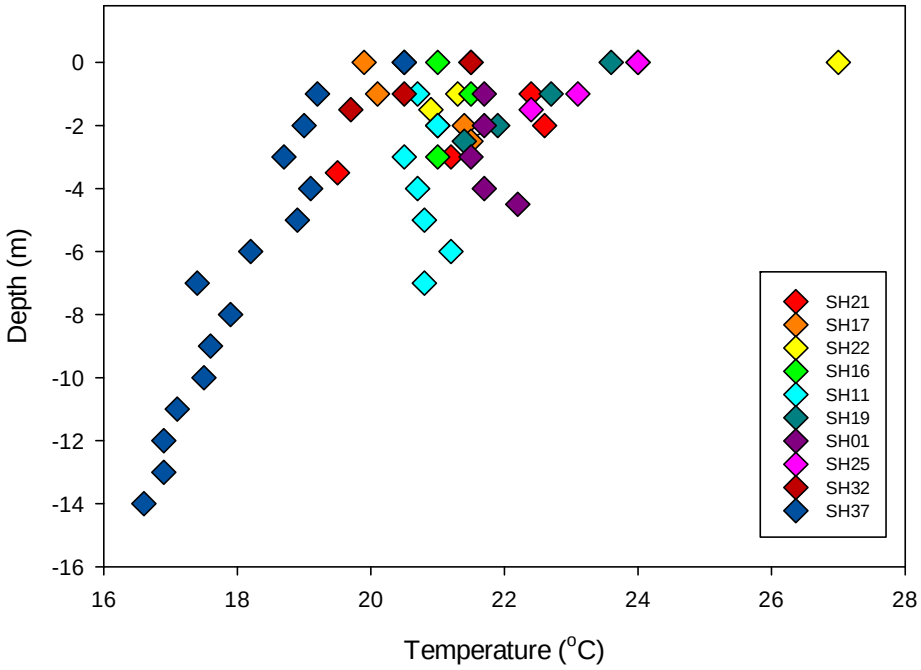

Temperature with Depth

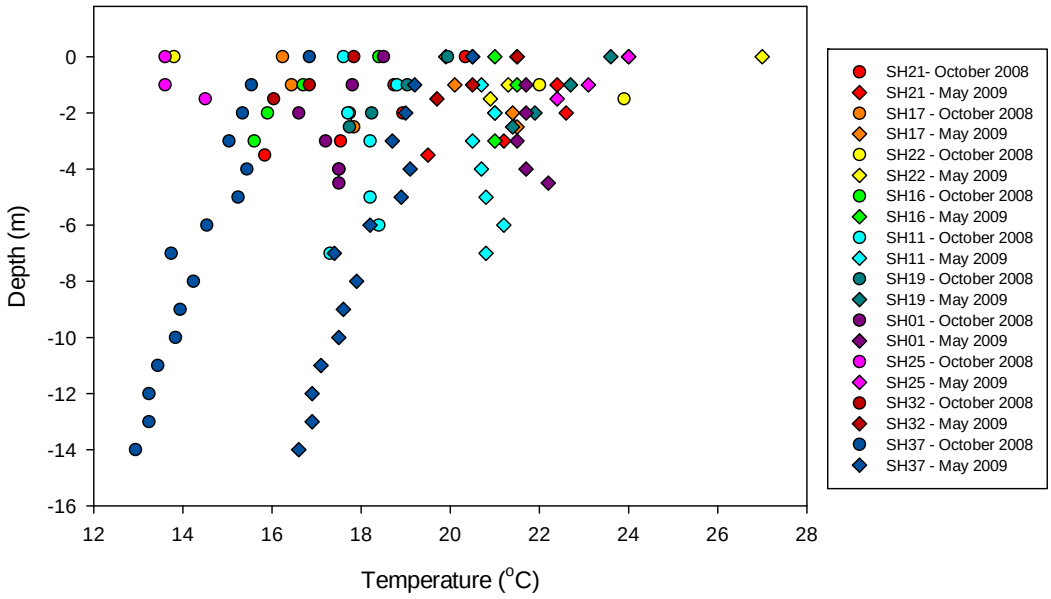

Temperature with Depth - SH17 and SH19

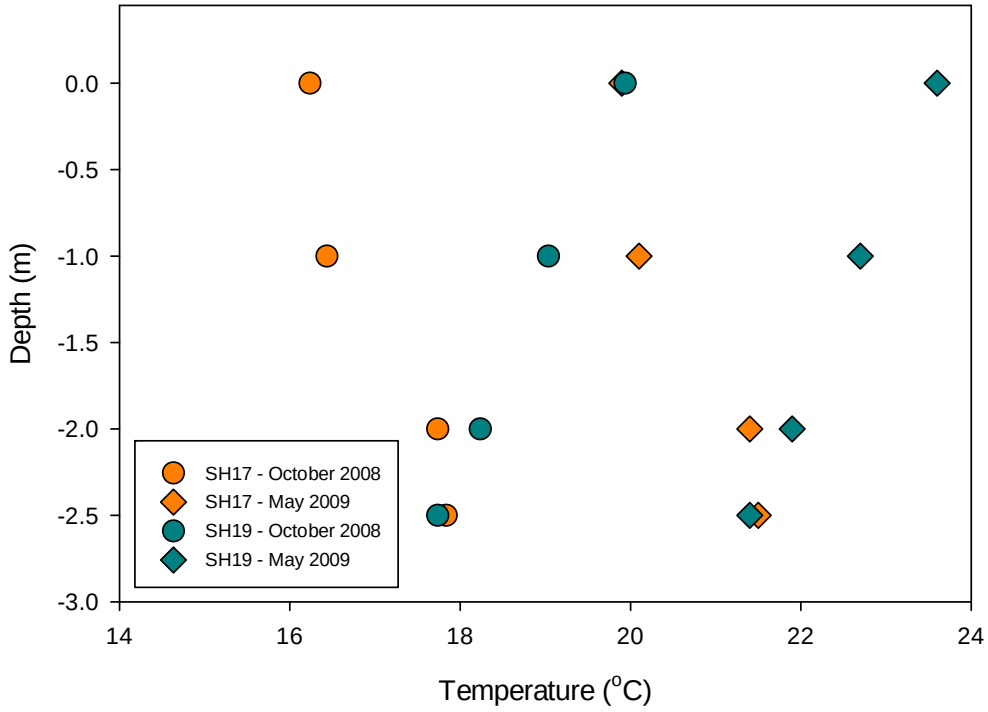

pH with Depth - October 2008

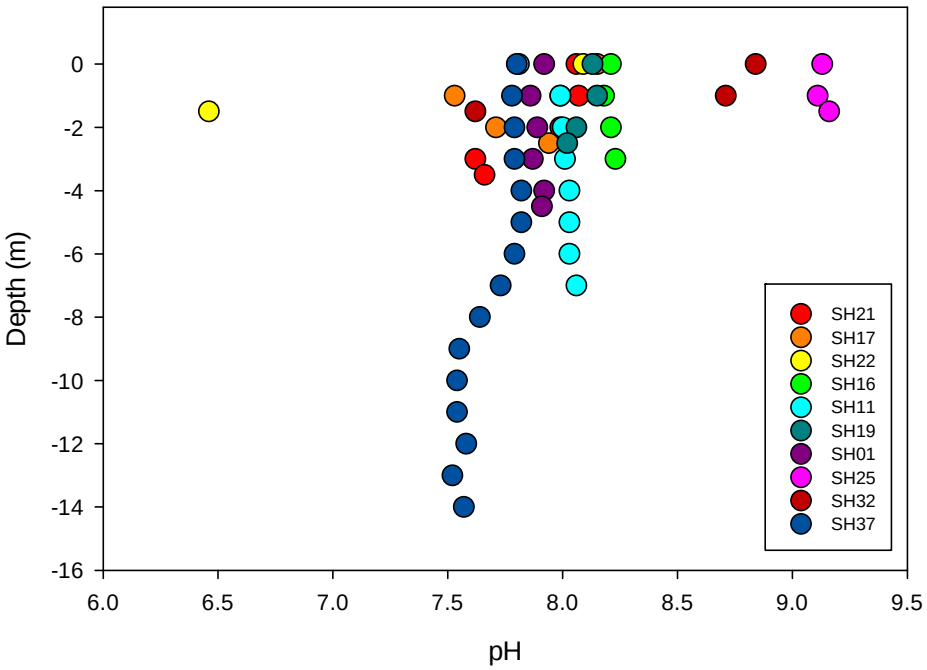

pH with Depth - May 2009

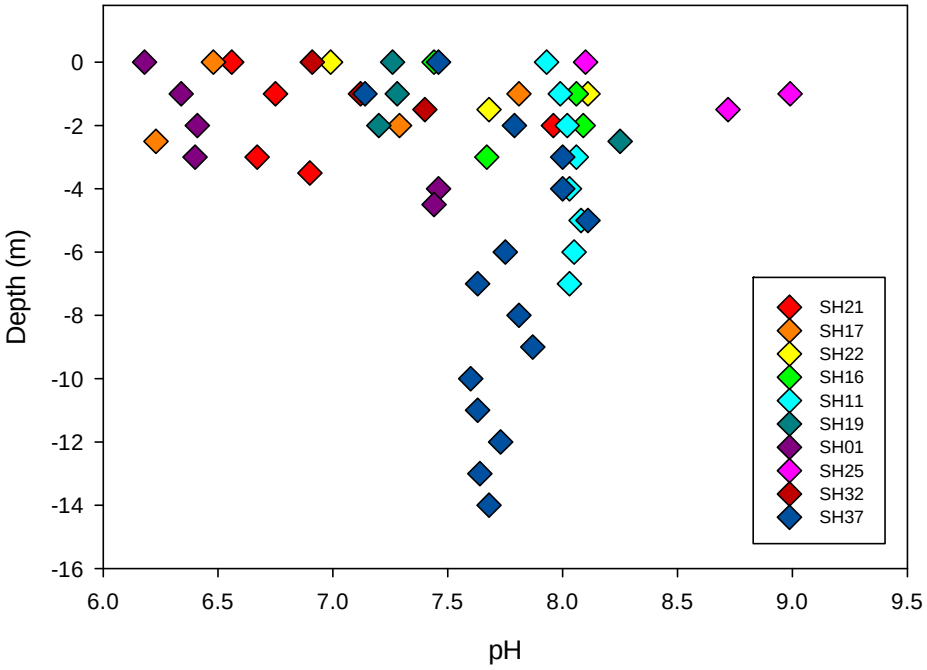

pH with Depth

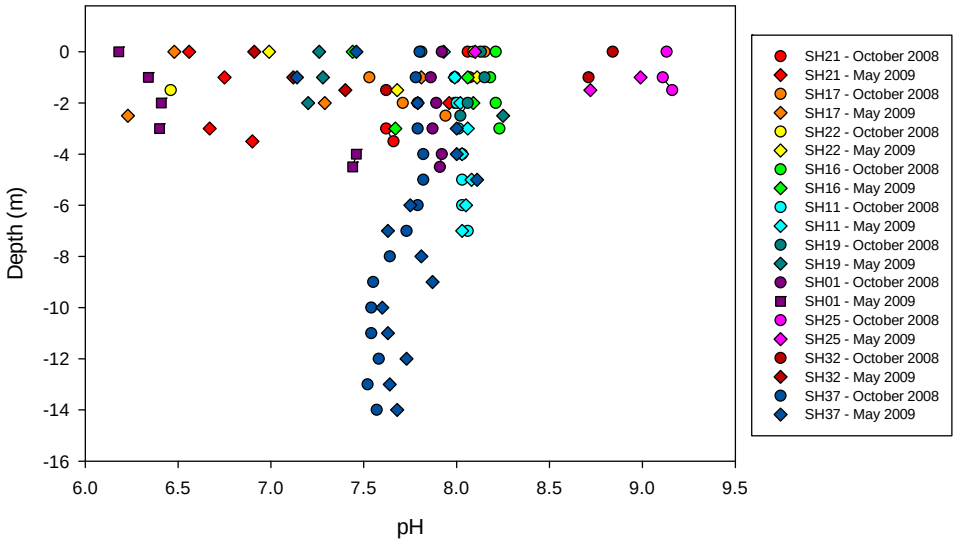

pH with Depth - SH17 and SH19

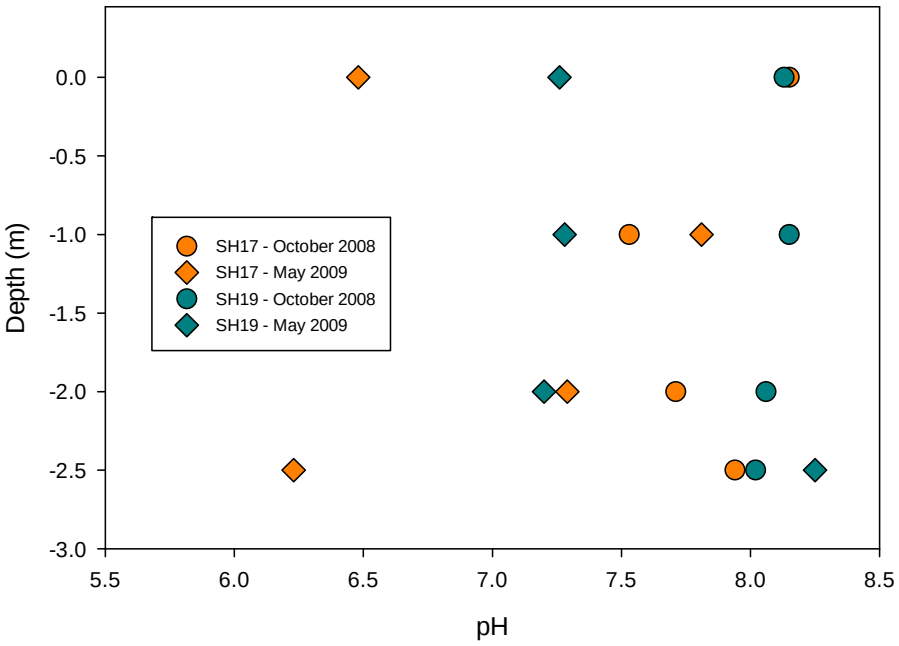

Conductivity with Depth - October 2008

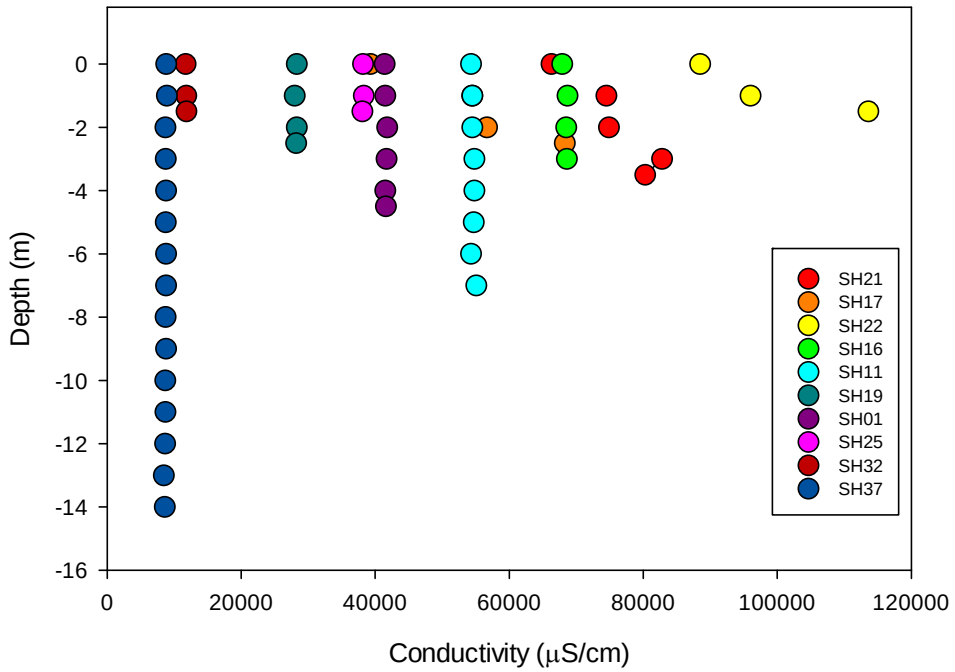

Conductivity with Depth - May 2009

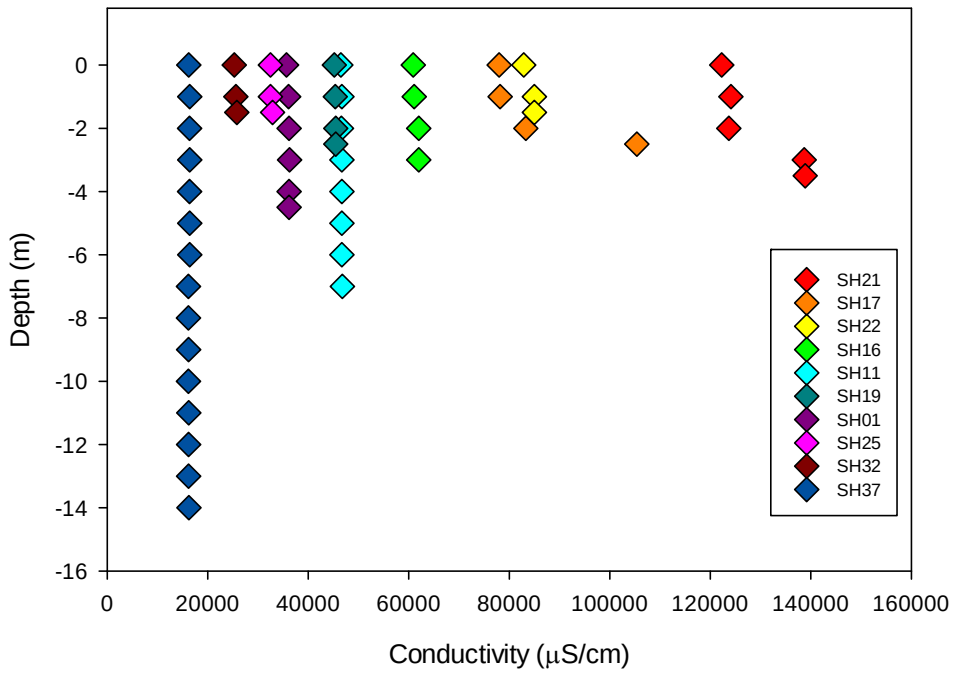

Conductivity with Depth

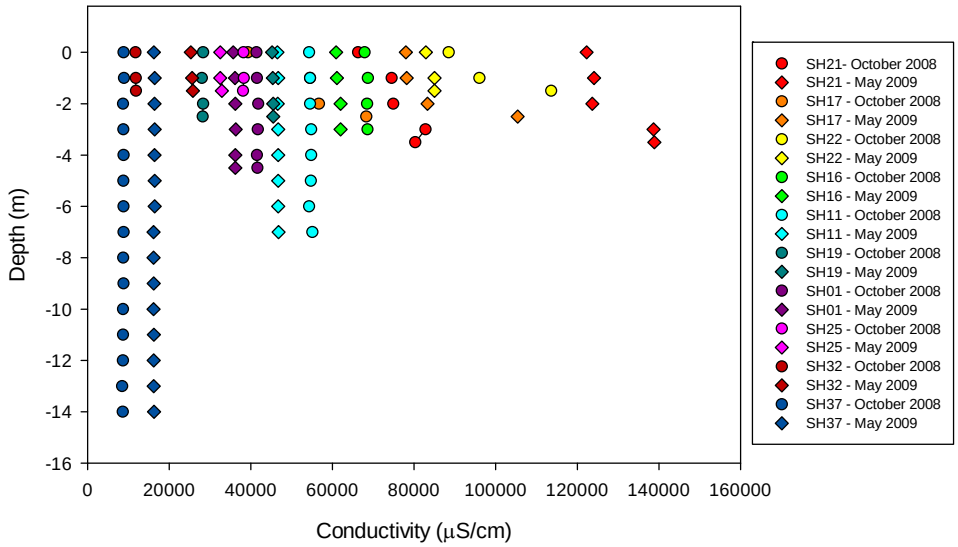

Conductivity with Depth - SH17 and SH19

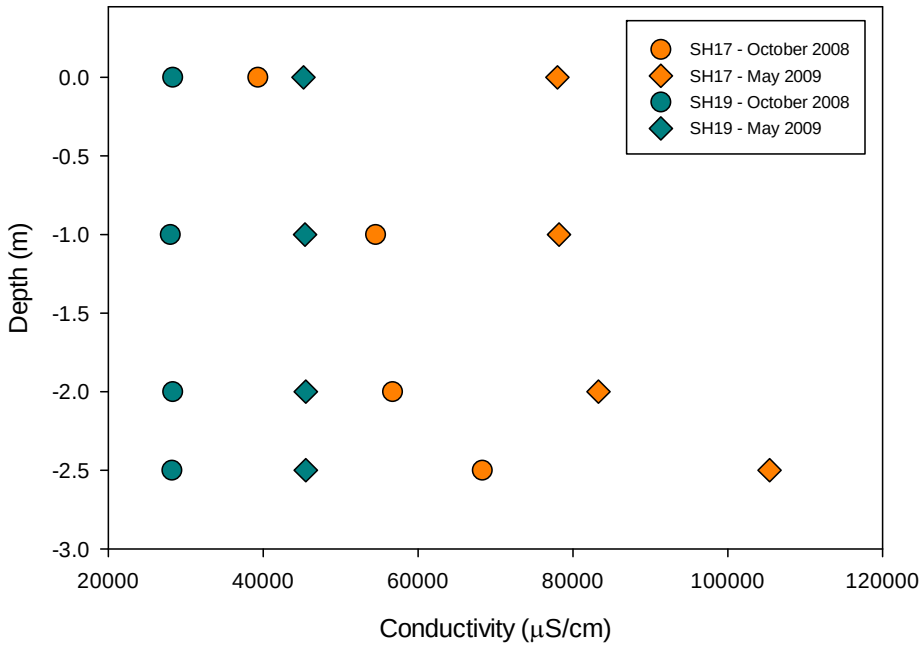

Density with Depth

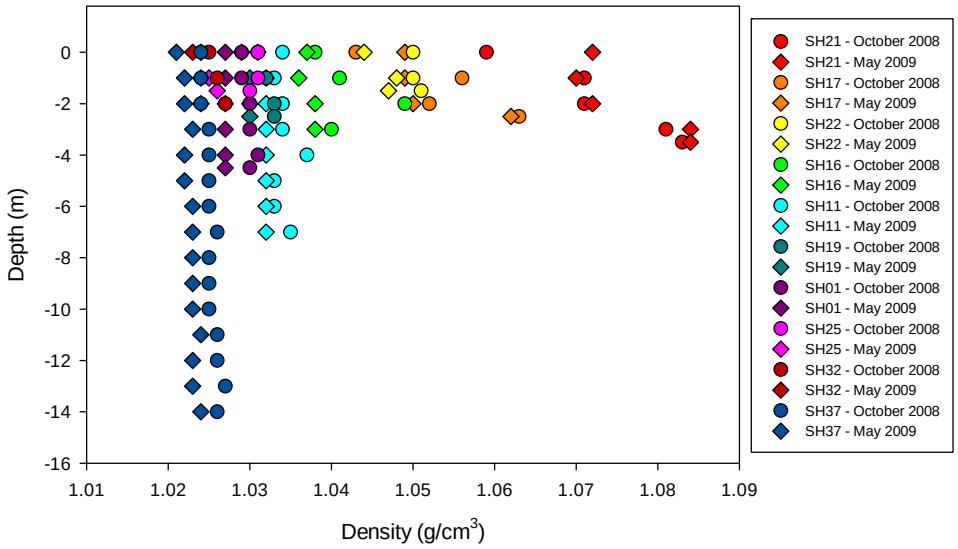

Density with Depth - SH17 and SH19

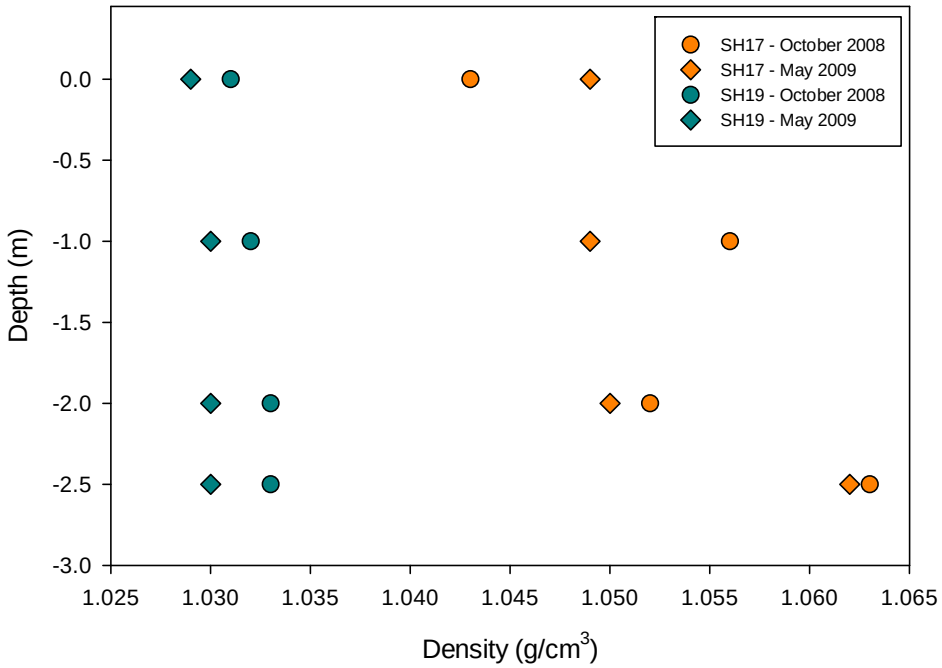

Density with Depth - October 2008

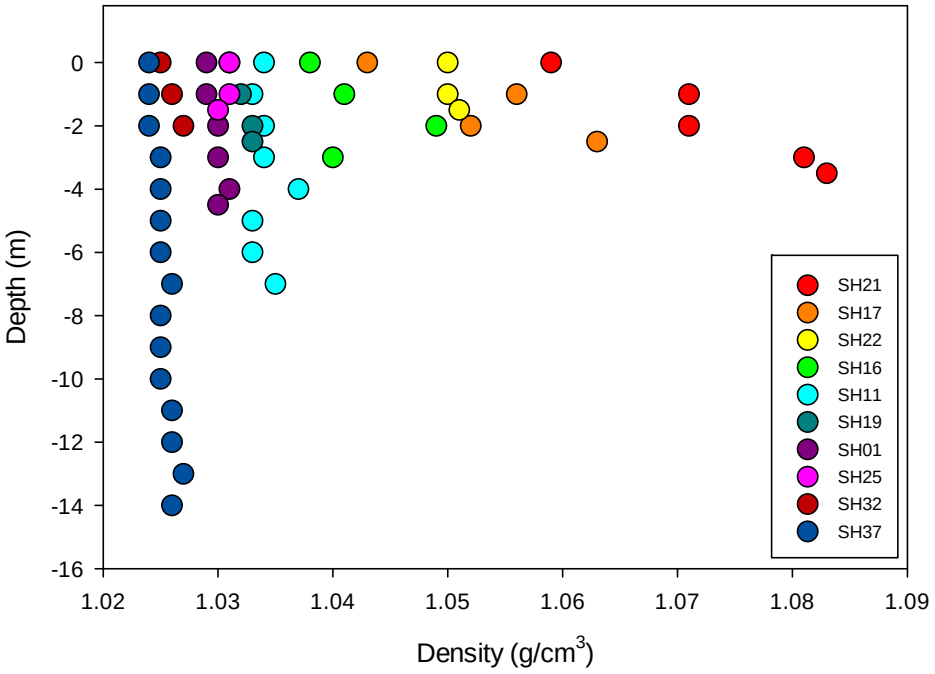

Density with Depth - May 2009

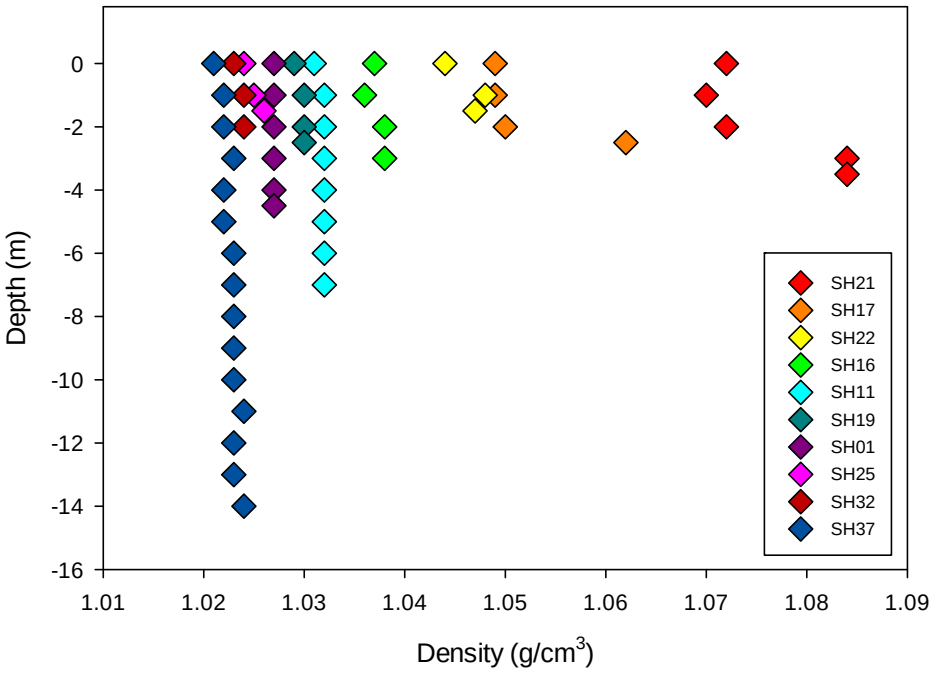

TDS with Depth - May 2009

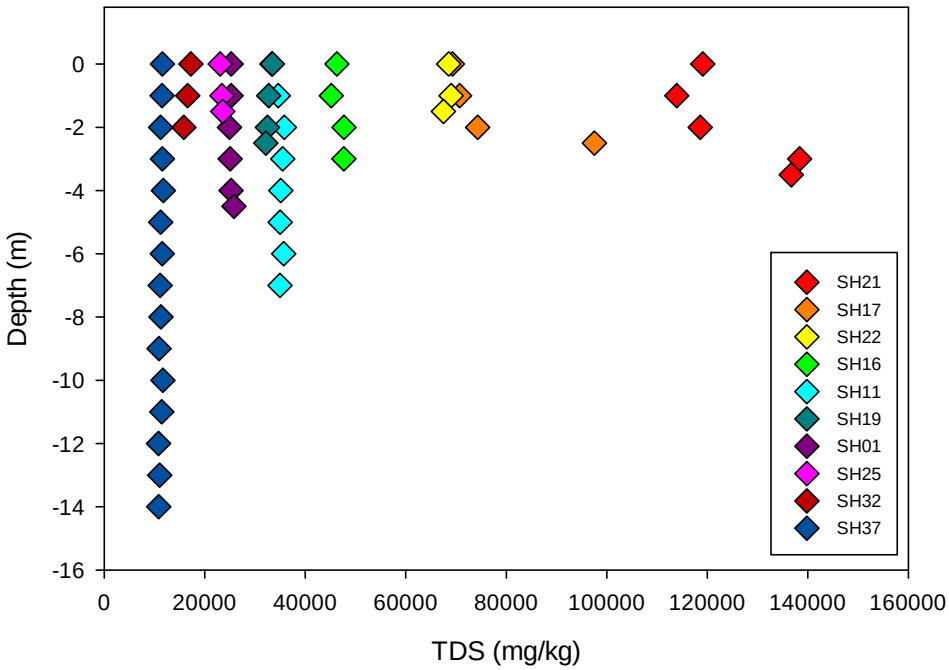

TDS with Depth - October 2008

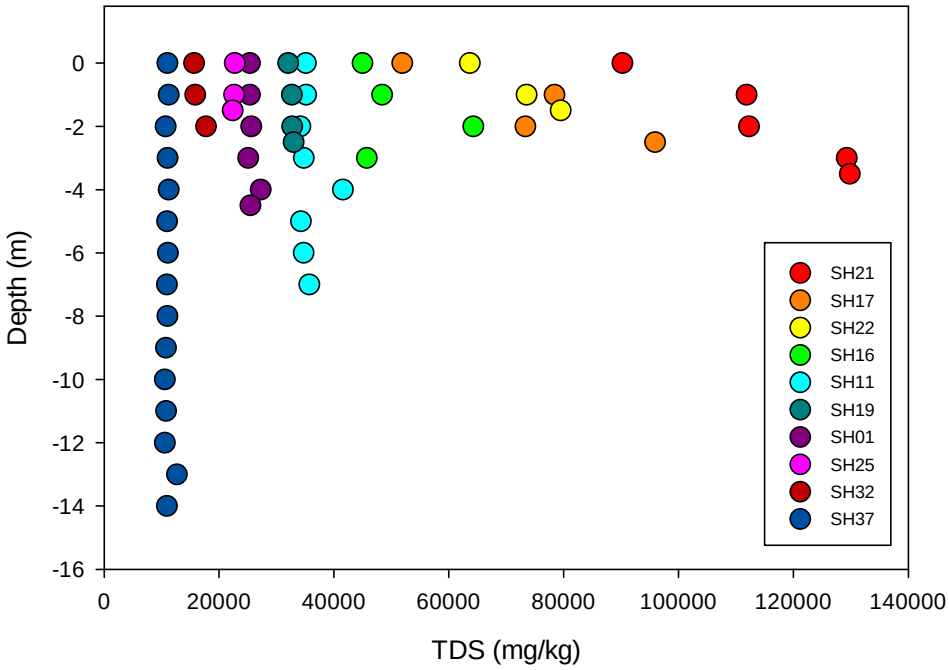

TDS with Depth

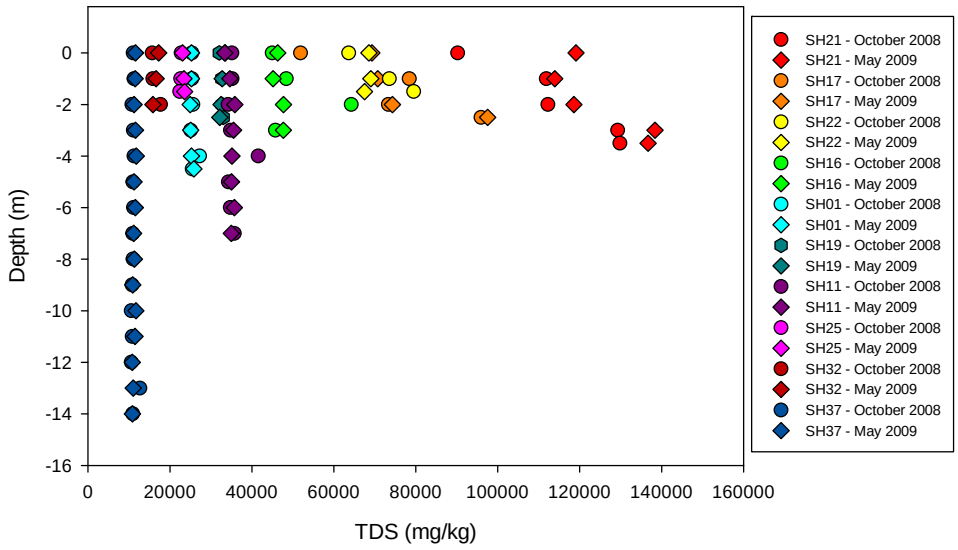

TDS with Depth - SH17 and SH19

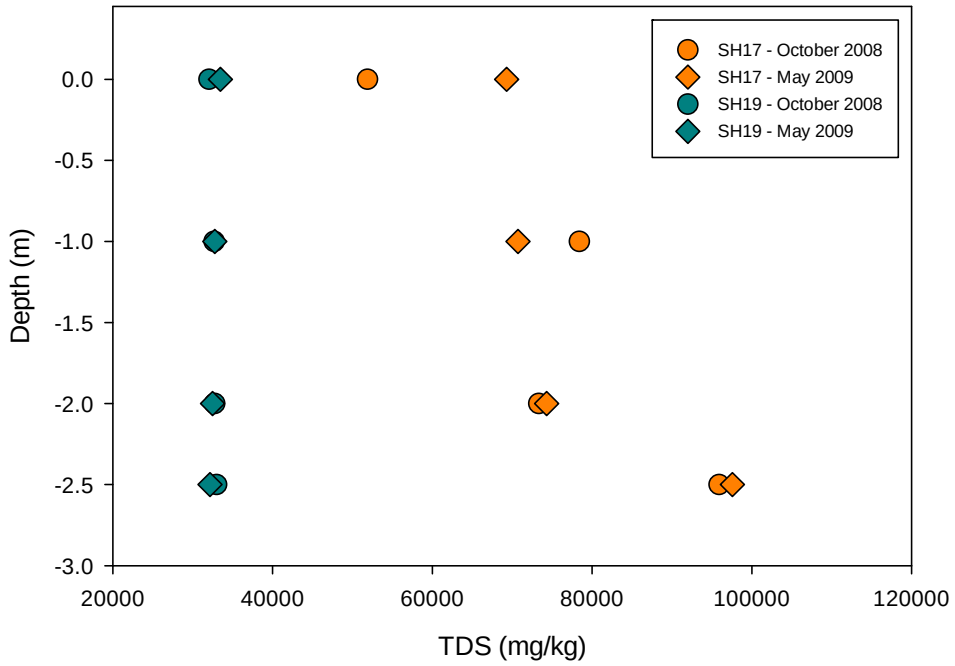

[Cl-] with Depth - October 2008

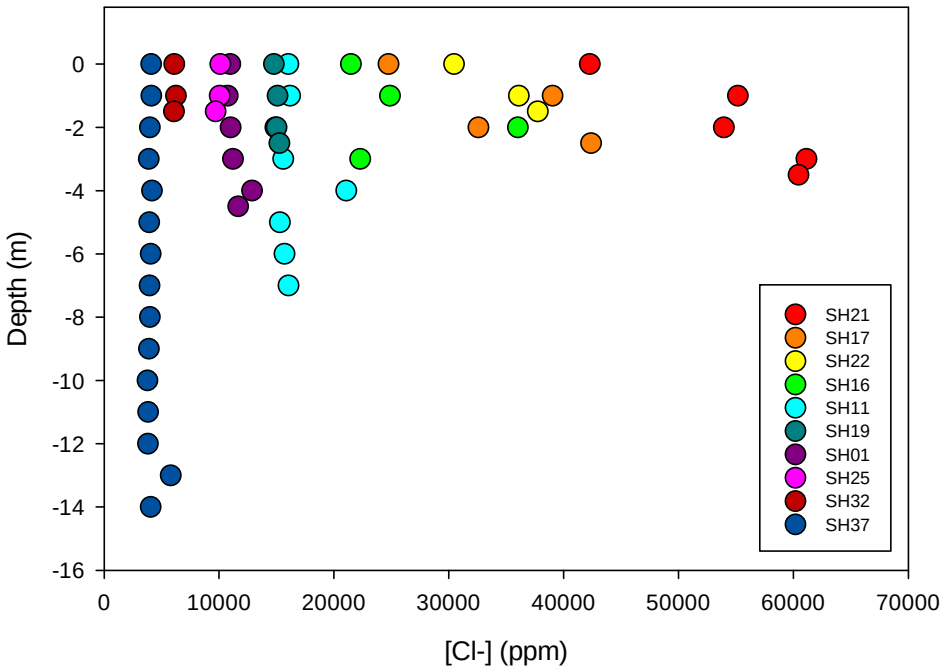

[Cl-] with Depth - May 2009

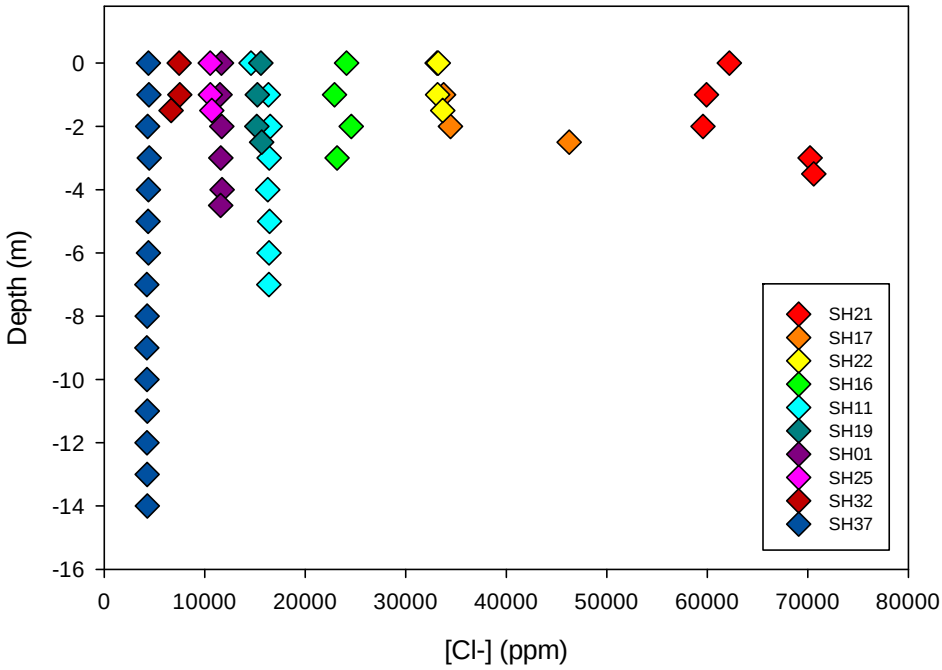

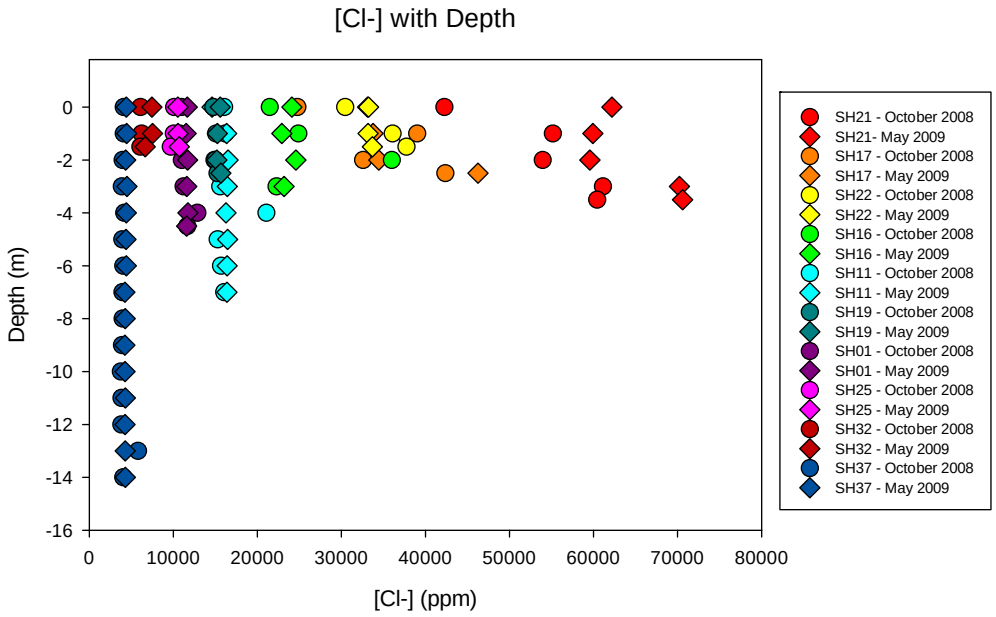
[Cl-] with Depth
Depth (m)
0
-2
-4
-6
-8
-10
-12
-14
-16
0
10000
20000
30000
40000
50000
60000
70000
80000
[Cl-] (ppm)
SH21 - October 2008
SH21- May 2009
SH17 - October 2008
SH17 - May 2009
SH22 - October 2008
SH22 - May 2009
SH16 - October 2008
SH16 - May 2009
SH11 - October 2008
SH11 - May 2009
SH19 - October 2008
SH19 - May 2009
SH01 - October 2008
SH01 - May 2009
SH25 - October 2008
SH25 - May 2009
SH32 - October 2008
SH32 - May 2009
SH37 - October 2008
SH37 - May 2009

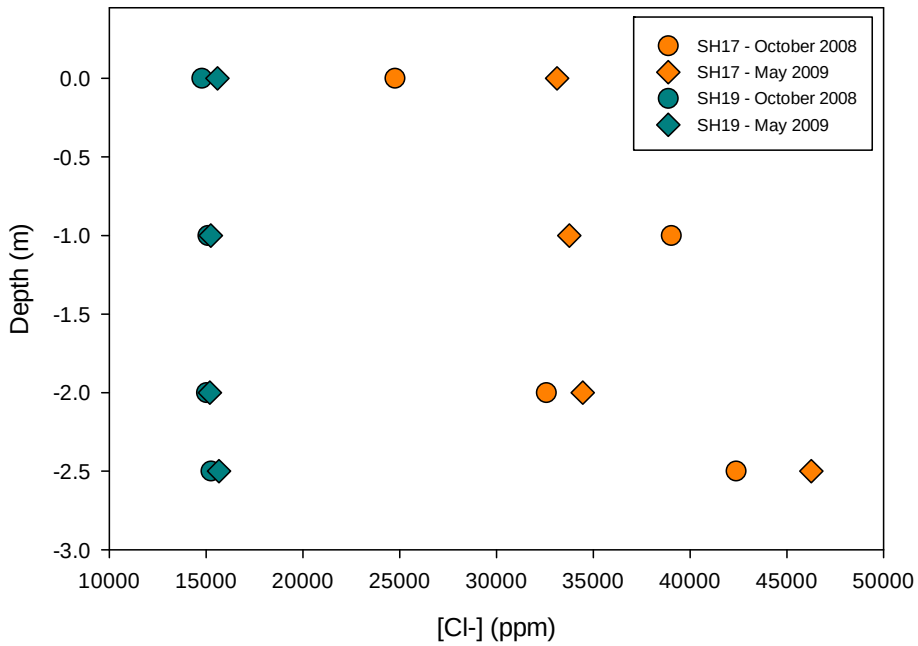
[Cl-] with Depth - SH17 and SH19
Depth (m)
0.0
-0.5
-1.0
-1.5
-2.0
-2.5
-3.0
10000
15000
20000
25000
30000
35000
40000
45000
50000
[Cl-] (ppm)
SH17 - October 2008
SH17 - May 2009
SH19 - October 2008
SH19 - May 2009

SO_4 with Depth - October 2008

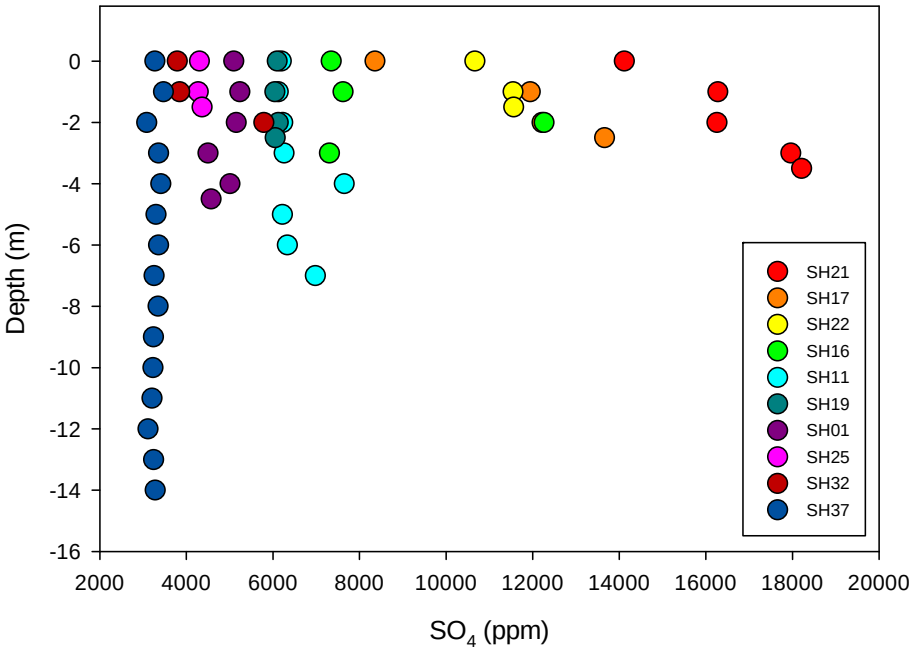

SO_4 with Depth - May 2009

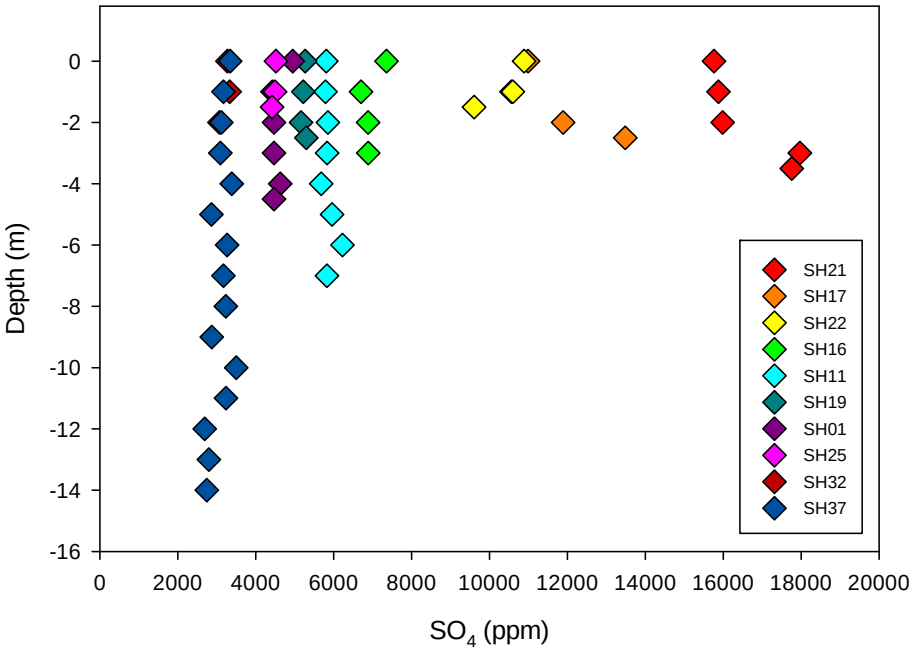

SO_4 with Depth

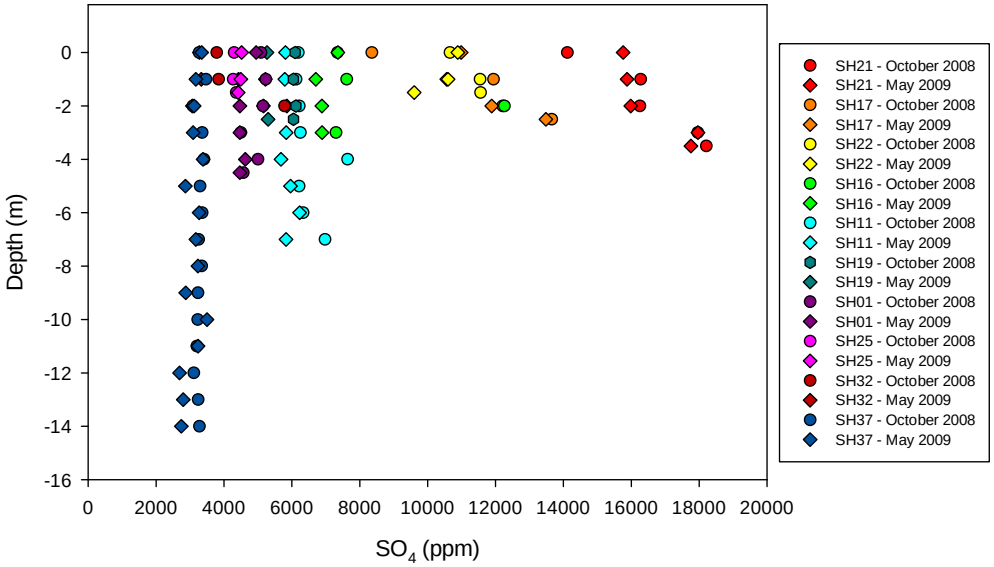

SO_4 with Depth - SH17 and SH19

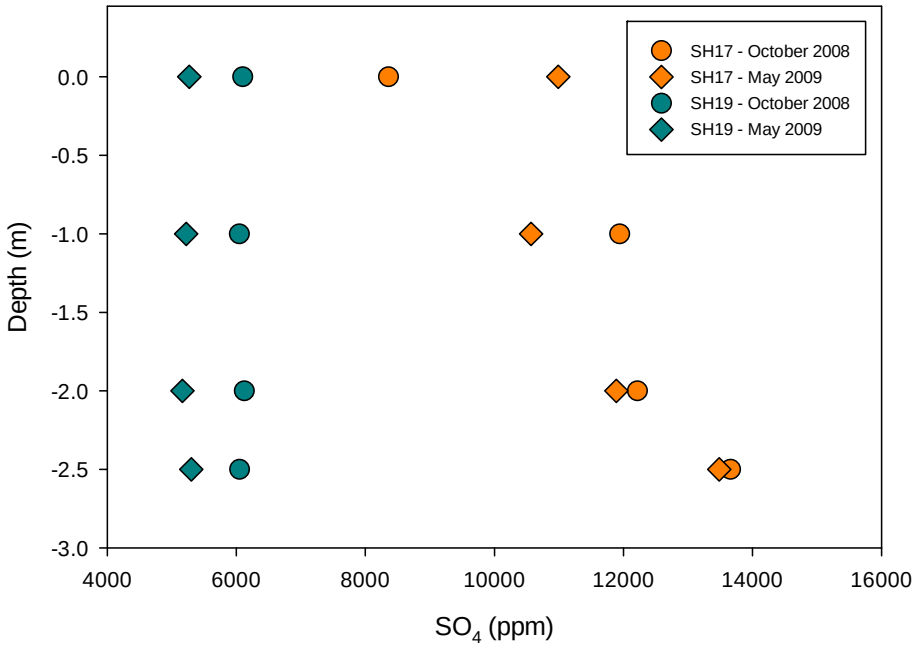

HCO_3 with Depth - October 2008

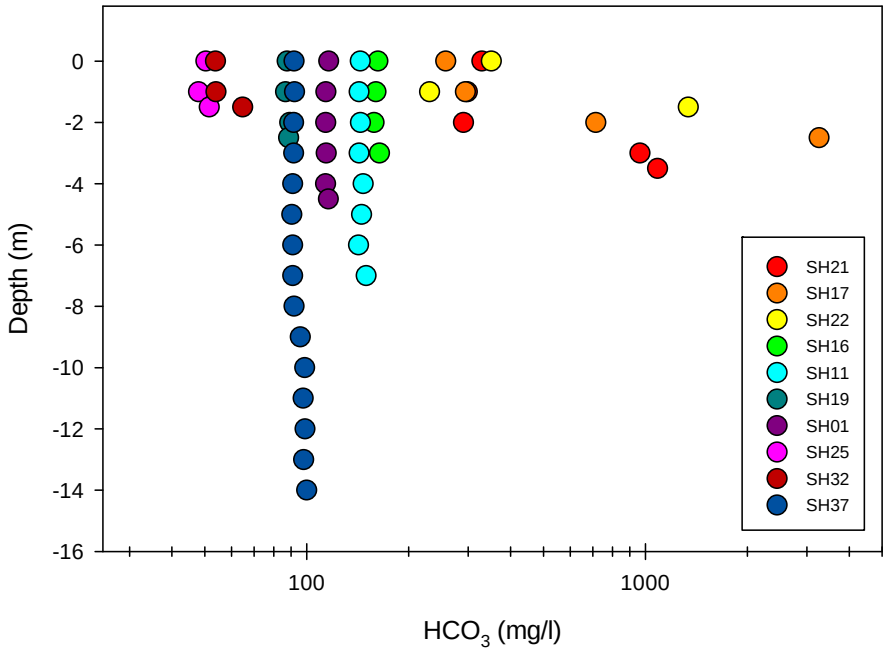

HCO_3 with Depth - May 2009

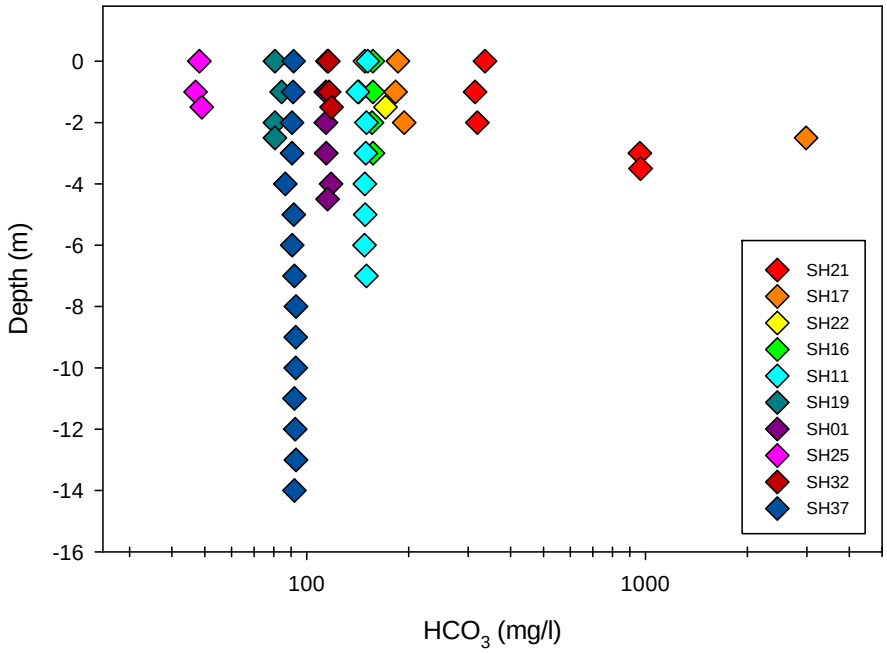

HCO_3 with Depth

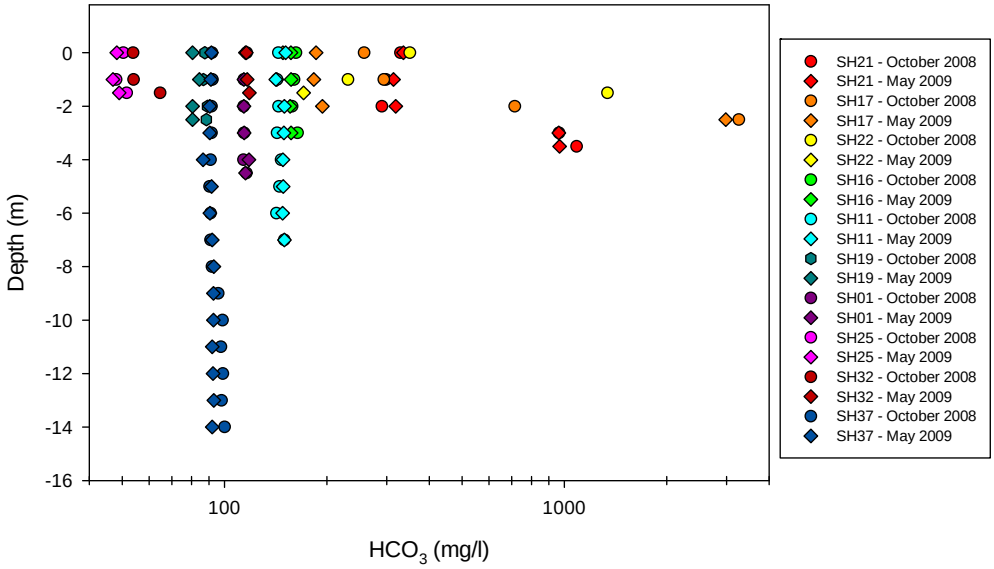

HCO_3 with Depth - SH17 and SH19

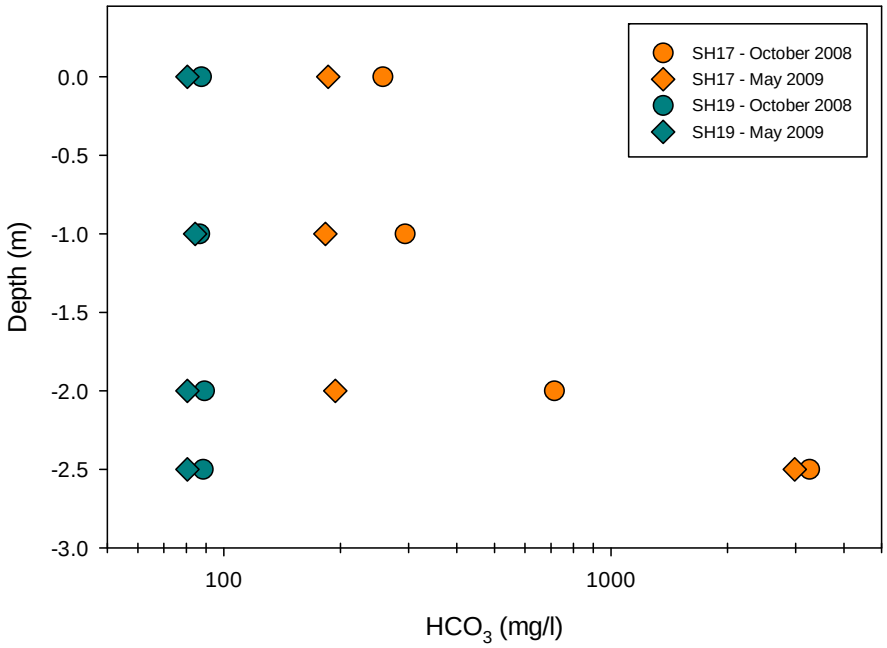

Ca with Depth - October 2008

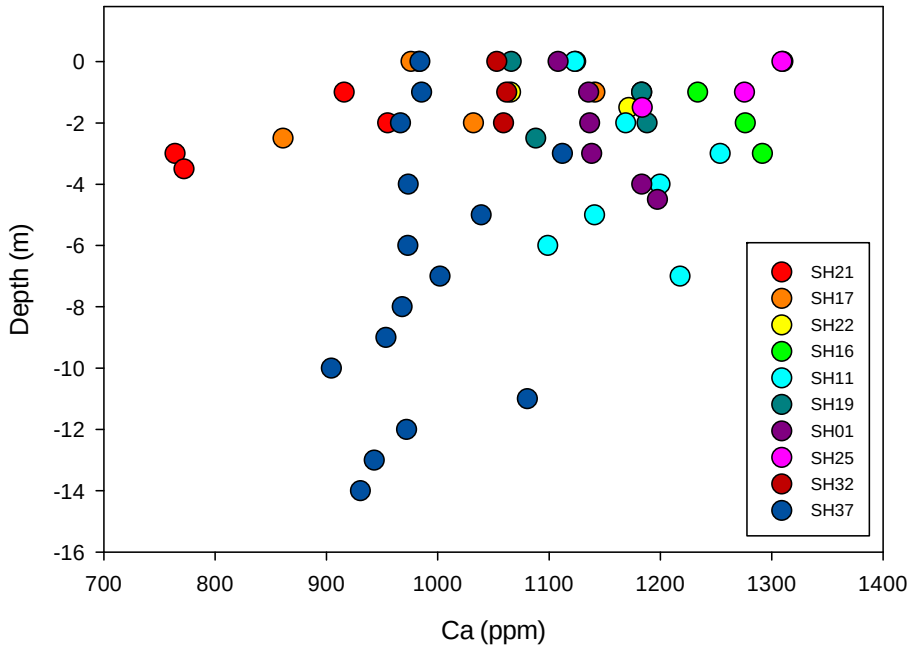

Ca with Depth - May 2009

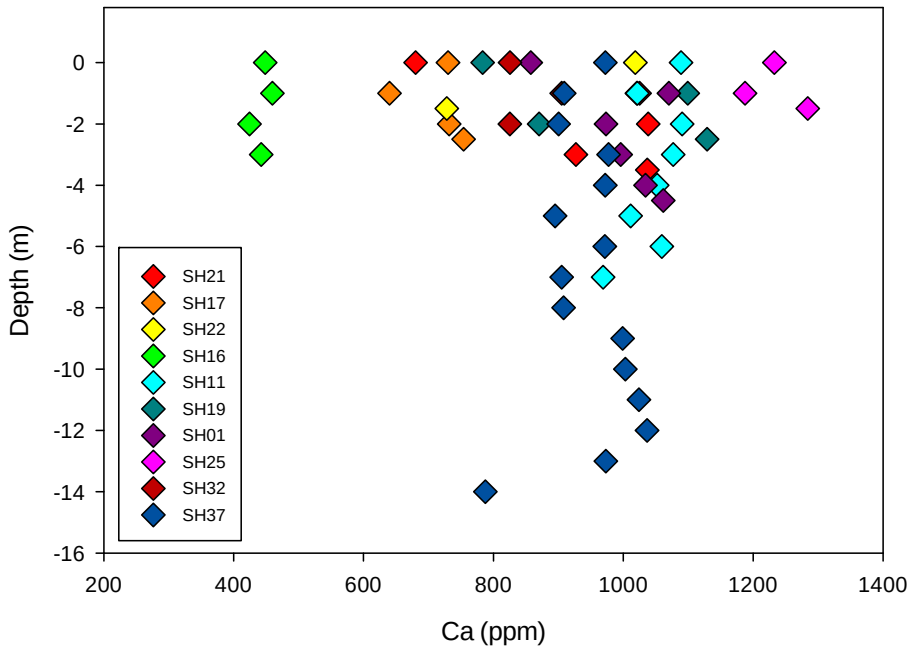

Ca with Depth

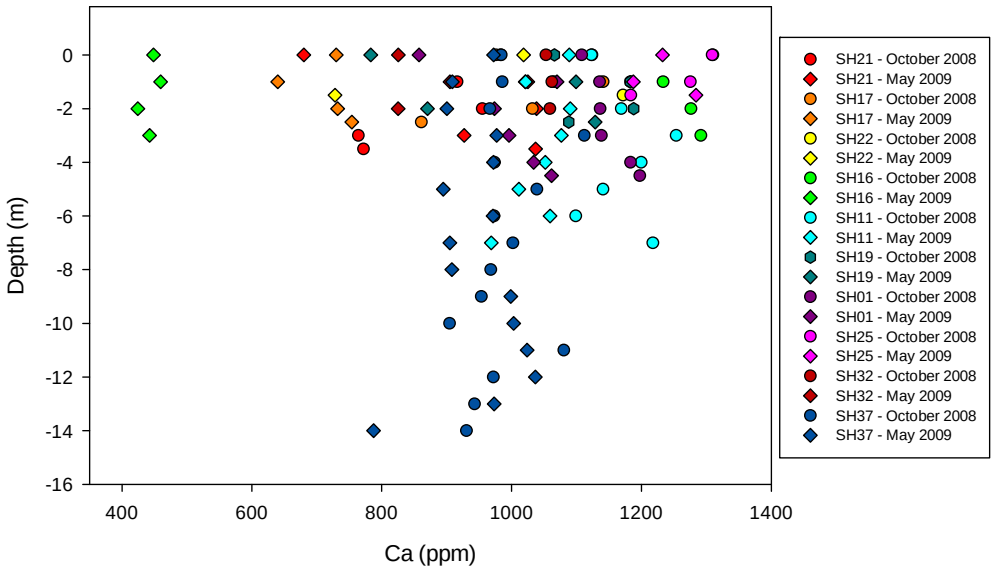

Ca with Depth - SH17 and SH19

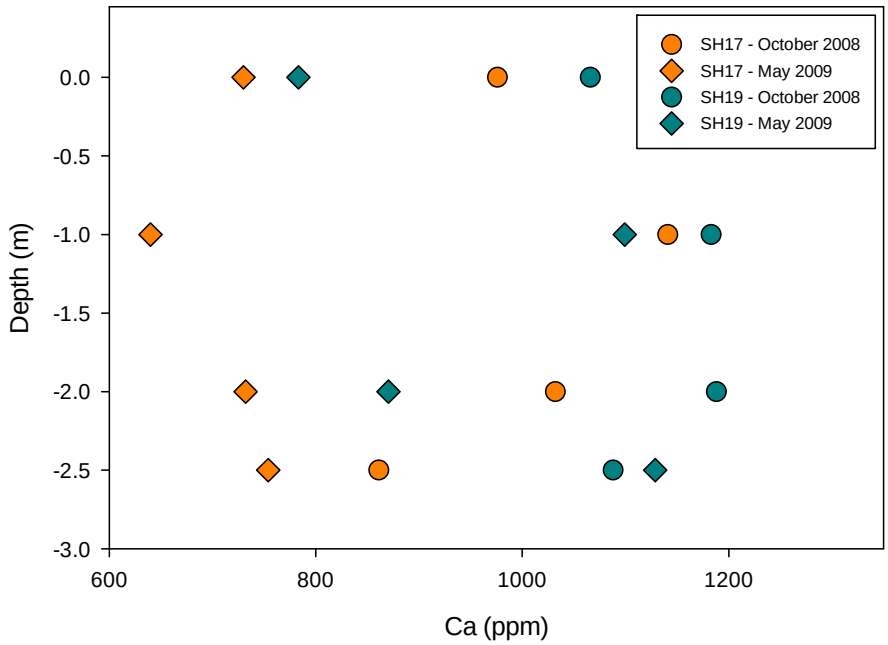

Mg with Depth - October 2008

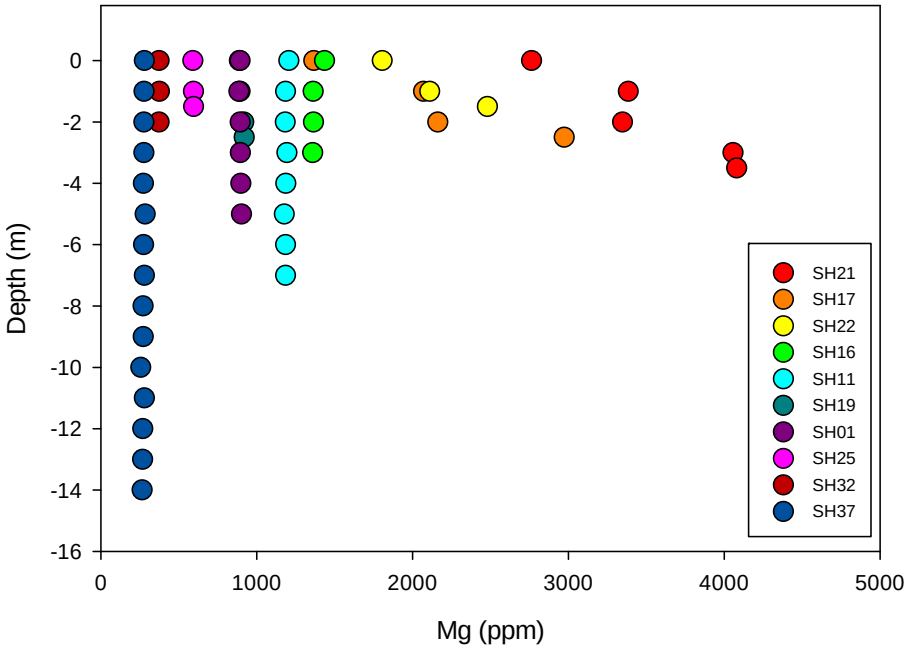

Mg with Depth - May 2009

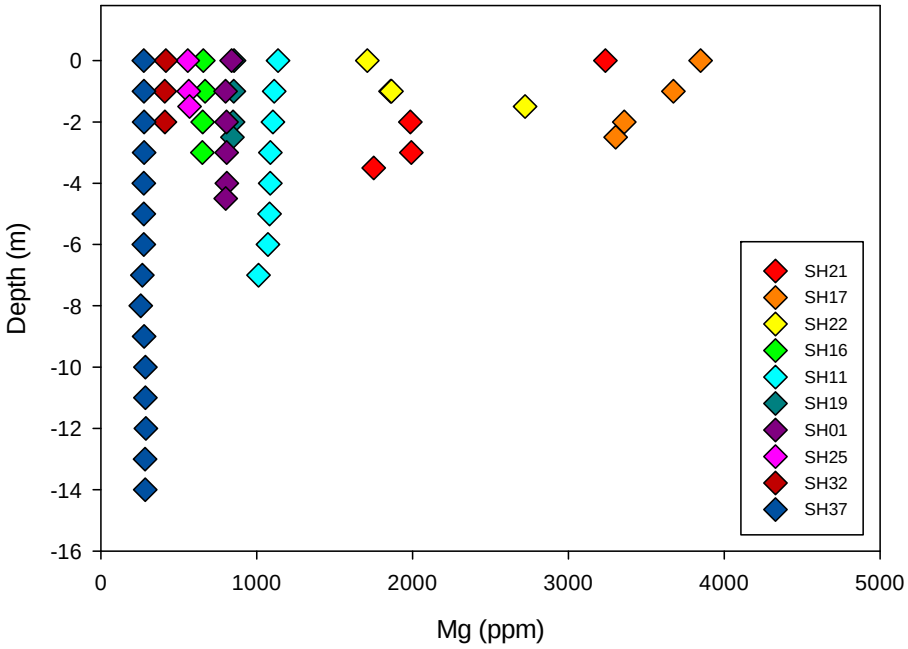

Mg with Depth

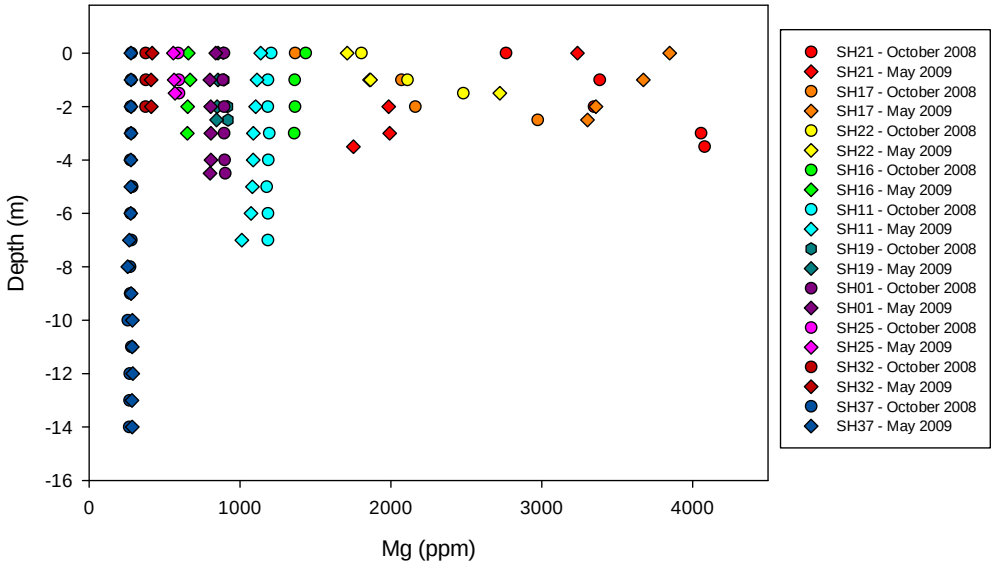

Mg with Depth - SH17 and SH19

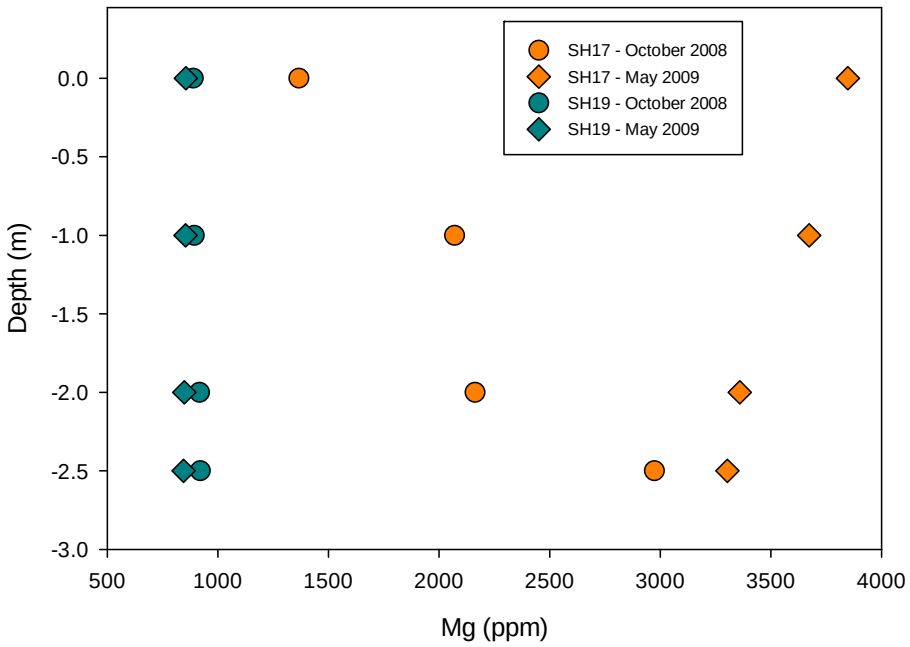

Na with Depth - October 2008

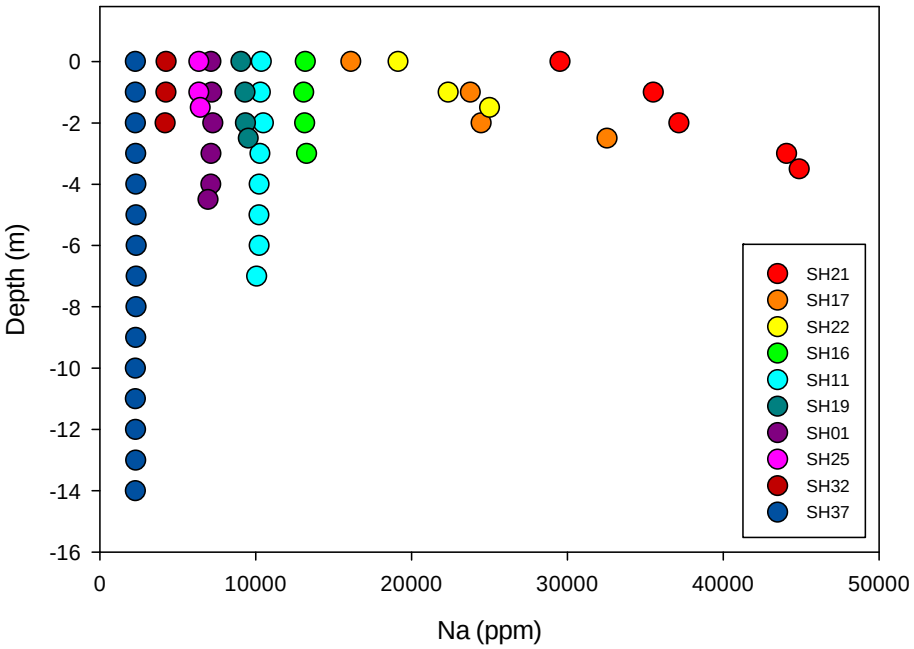

Na with Depth - May 2009

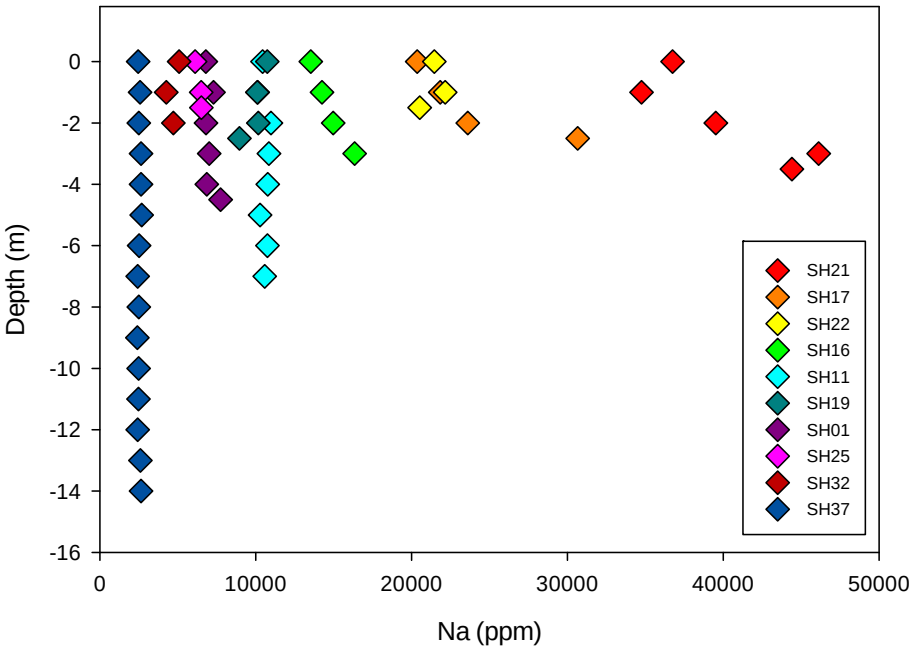

Na with Depth

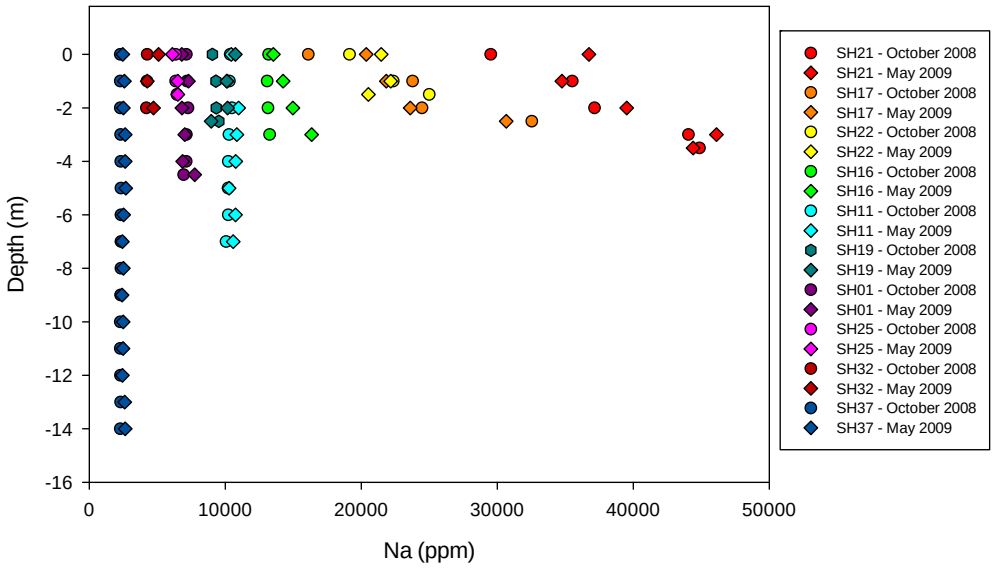

Na with Depth - SH17 and SH19

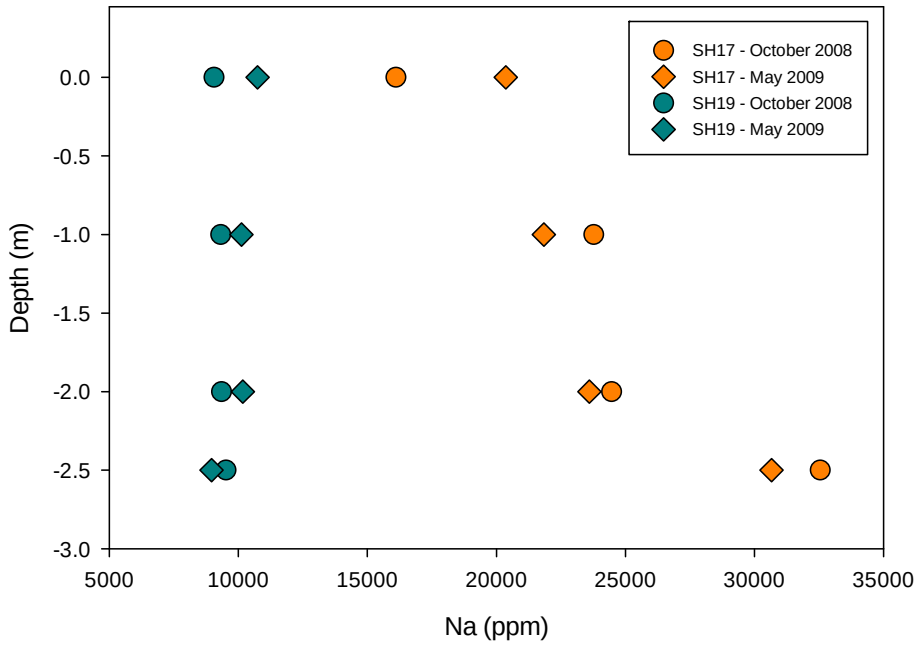

K with Depth - October 2008

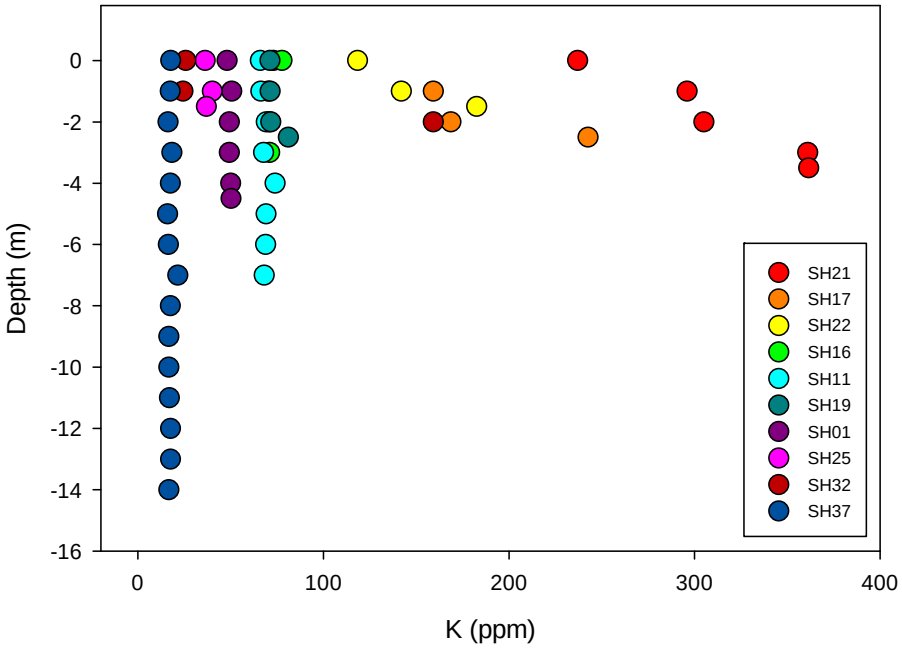

K with Depth - May 2009

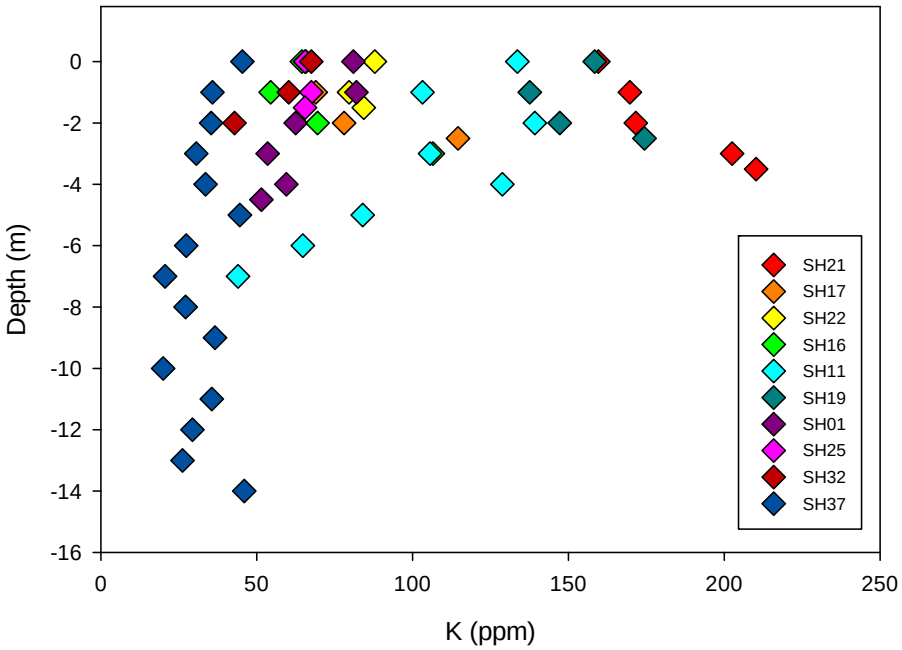

K with Depth

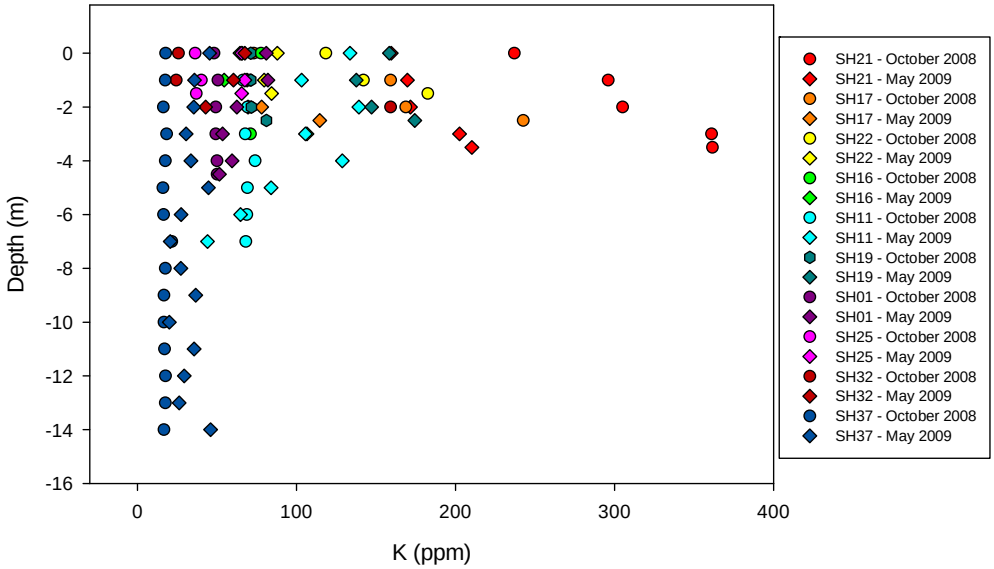

K with Depth - SH17 and SH19

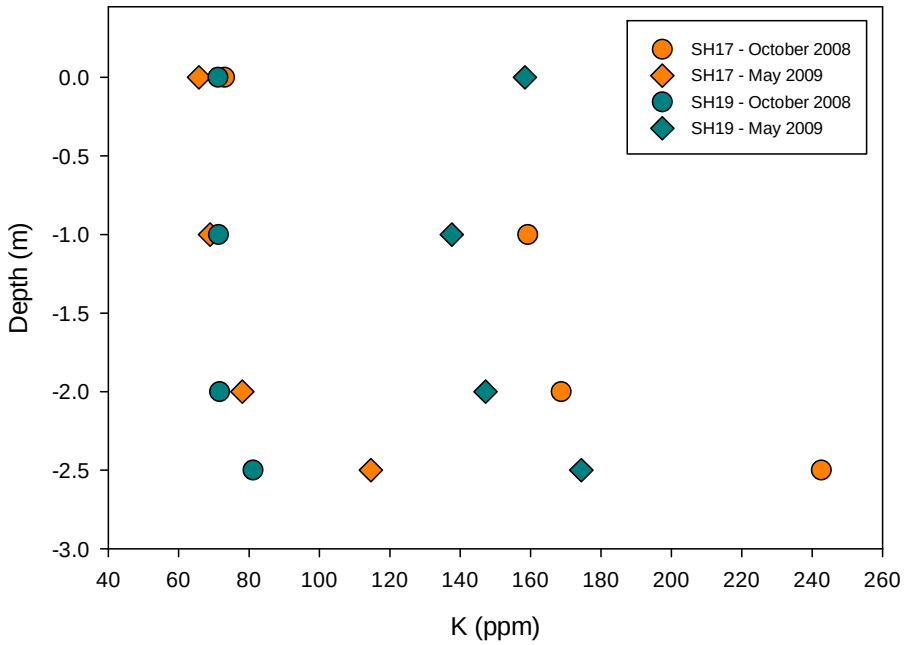

SI Calcite with Depth - October 2008

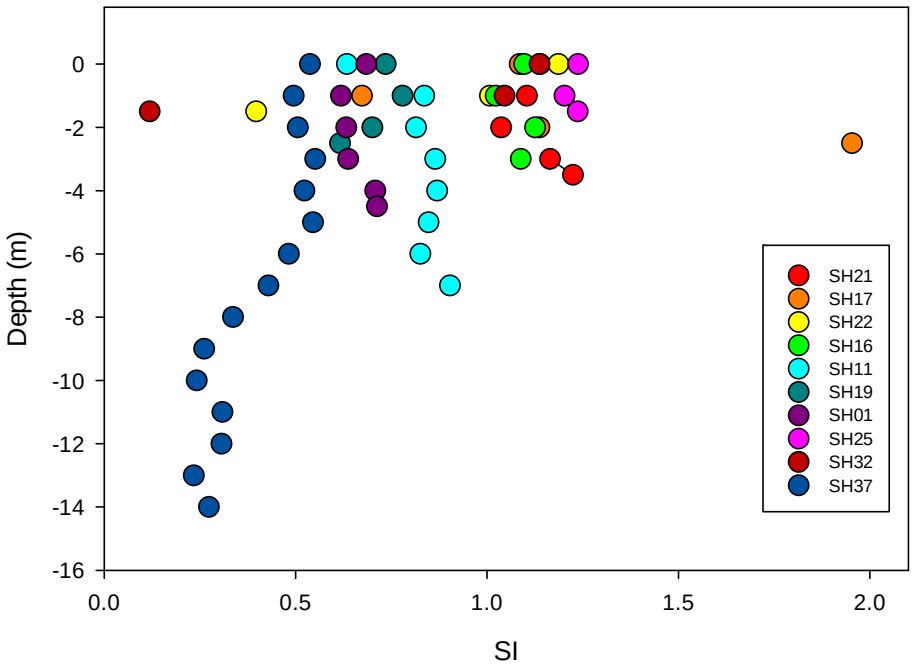

SI Calcite with Depth - May 2009

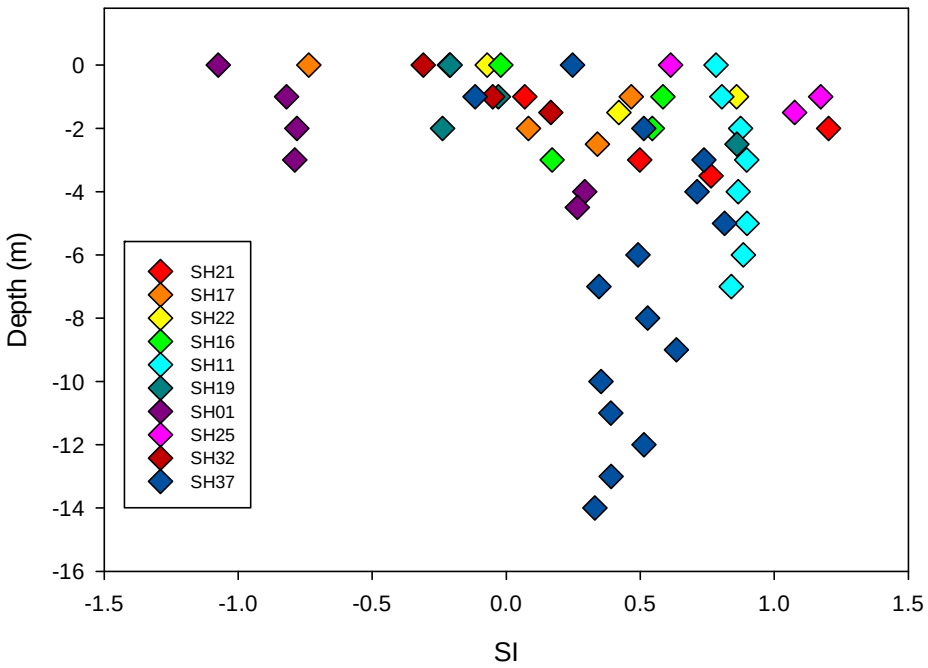

SI Calcite with Depth

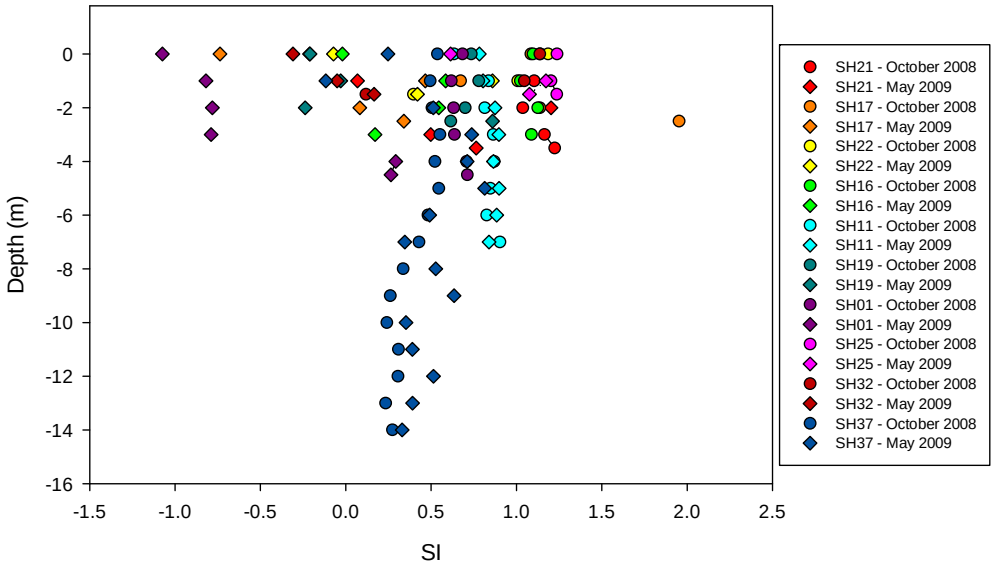

SI Calcite with Depth - SH17 and SH19

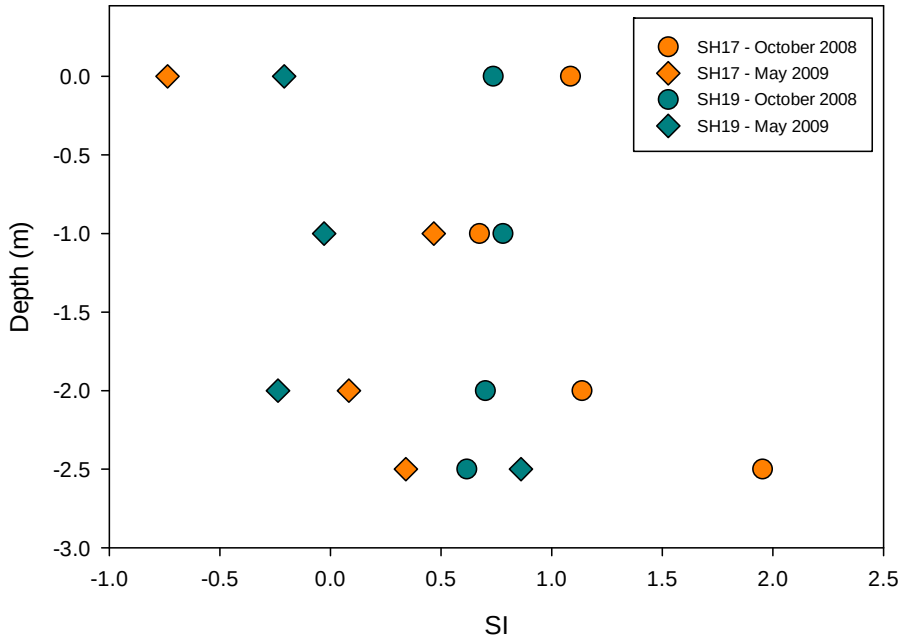

SI Gypsum with Depth - October 2008

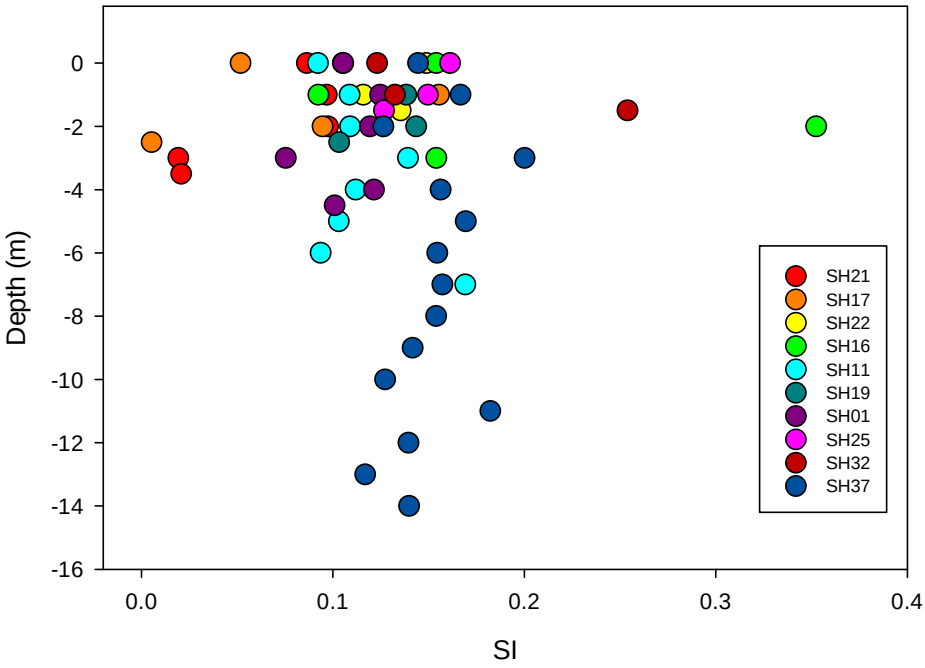

SI Gypsum with Depth - May 2009

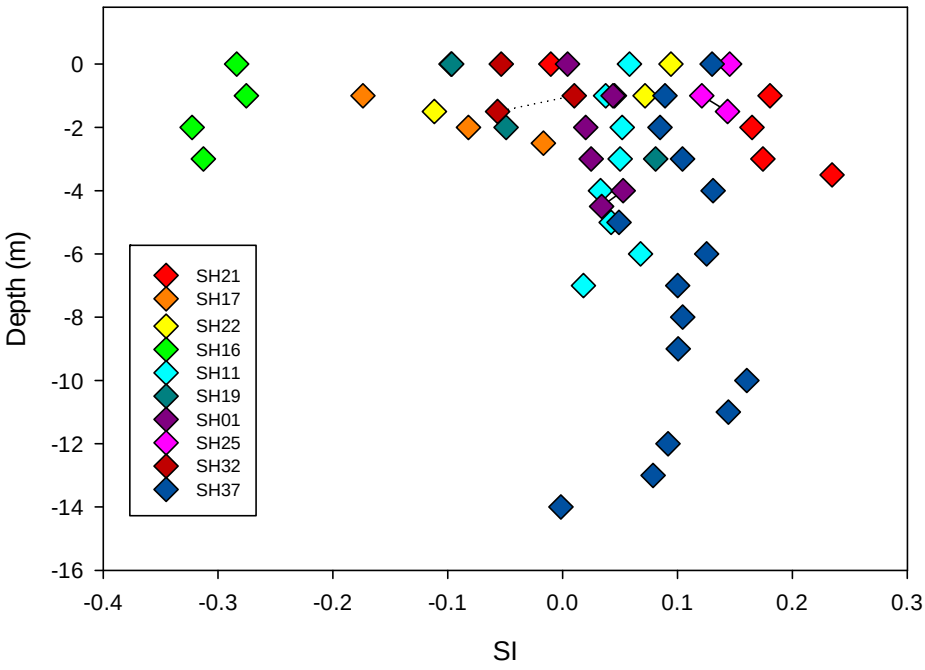

SI Gypsum with Depth

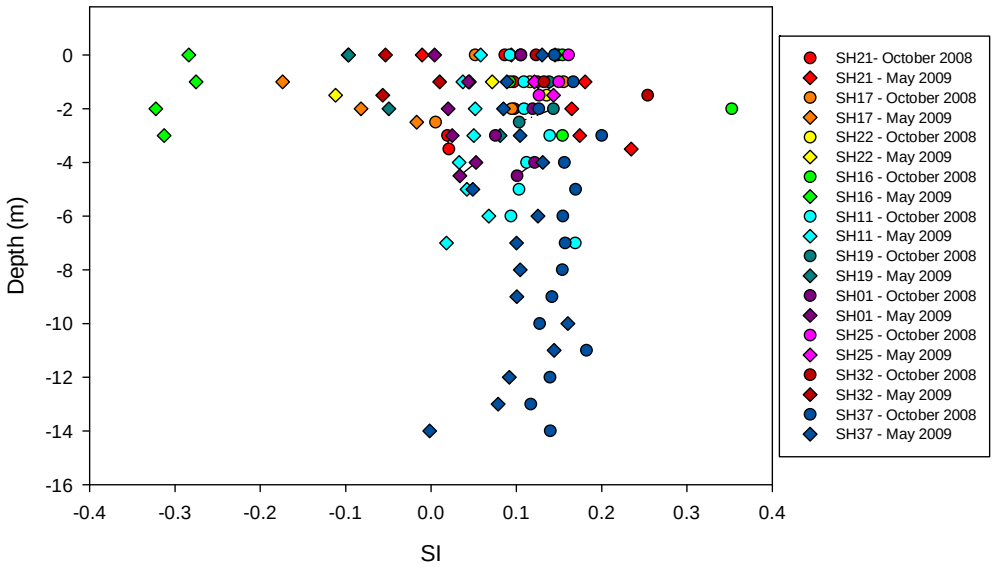

SI Gypsum with Depth 0 SH17 and SH19

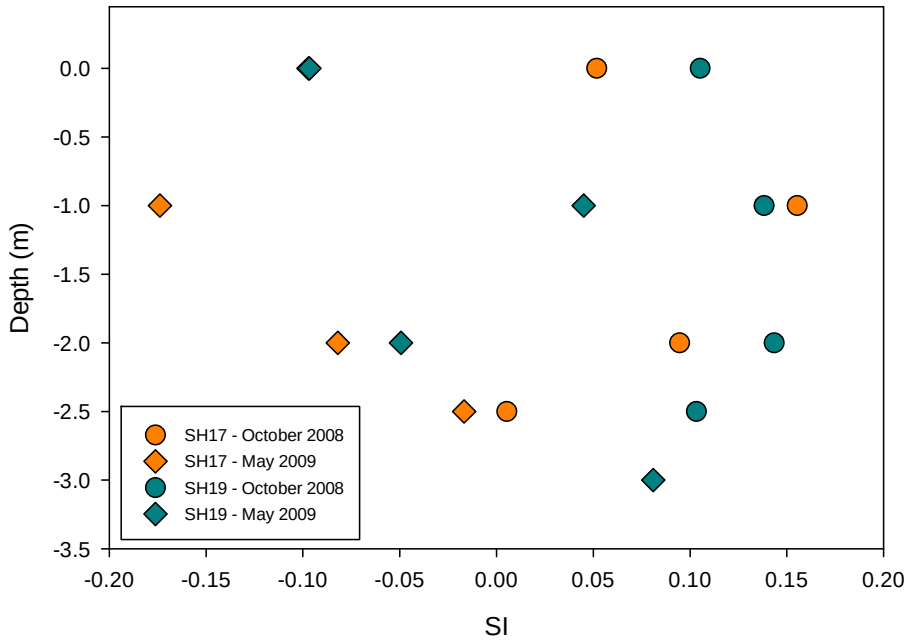

log PCO_2 with Depth - October 2008

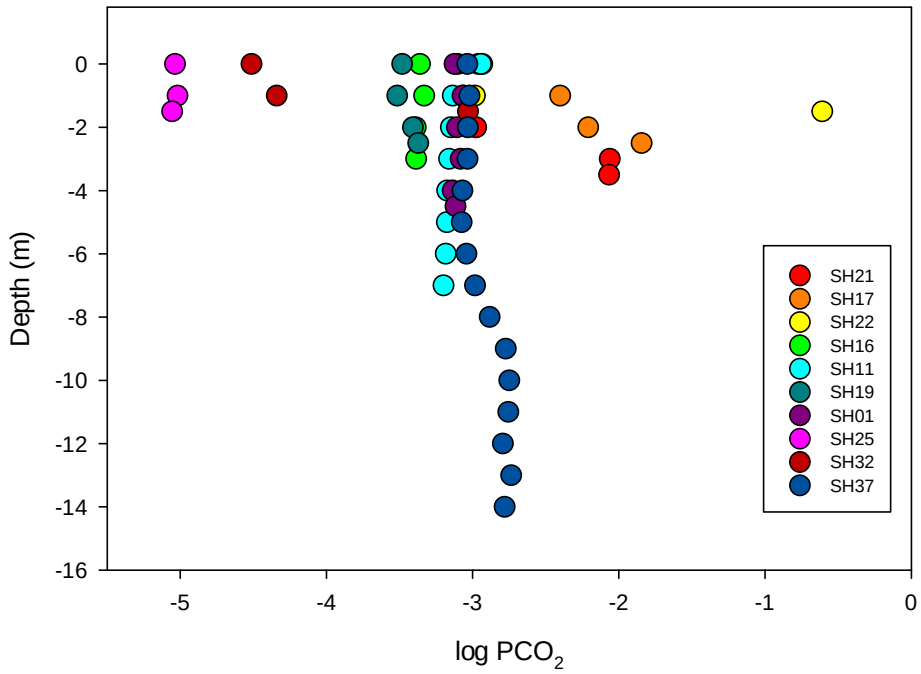

log PCO_2 with Depth - May 2009

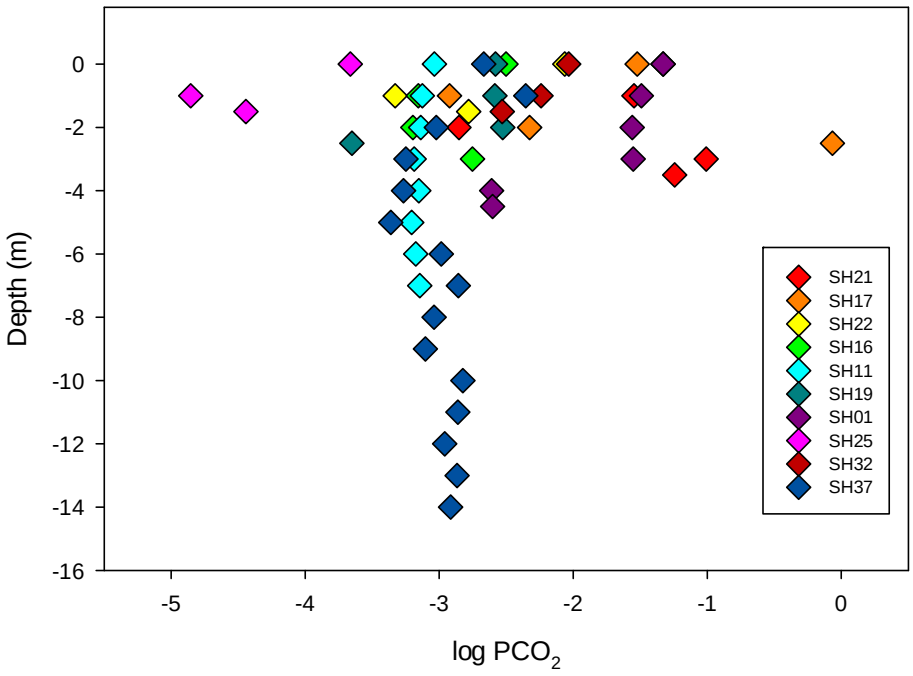

log PCO_2 with Depth

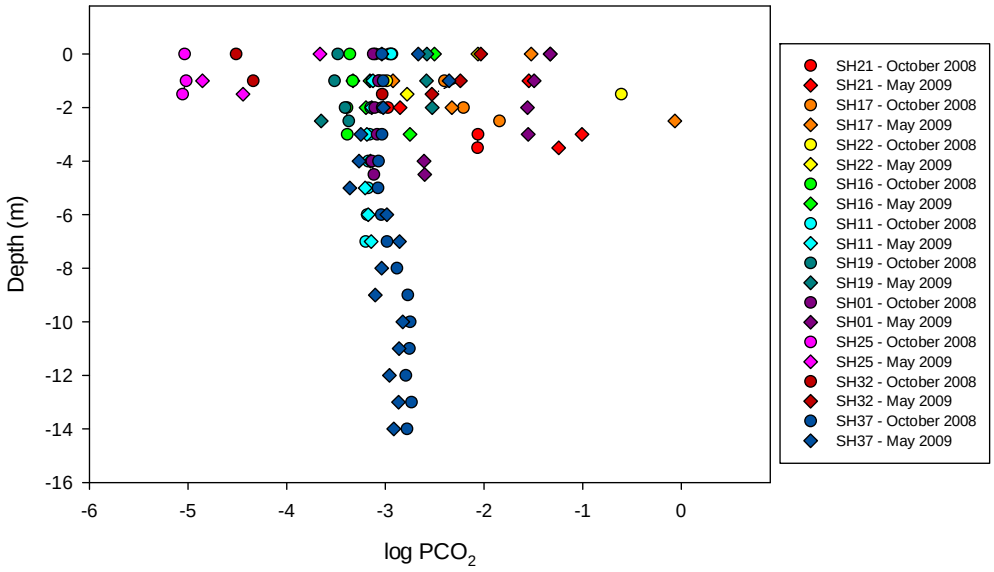

log PCO_2 with Depth - SH17 and SH19

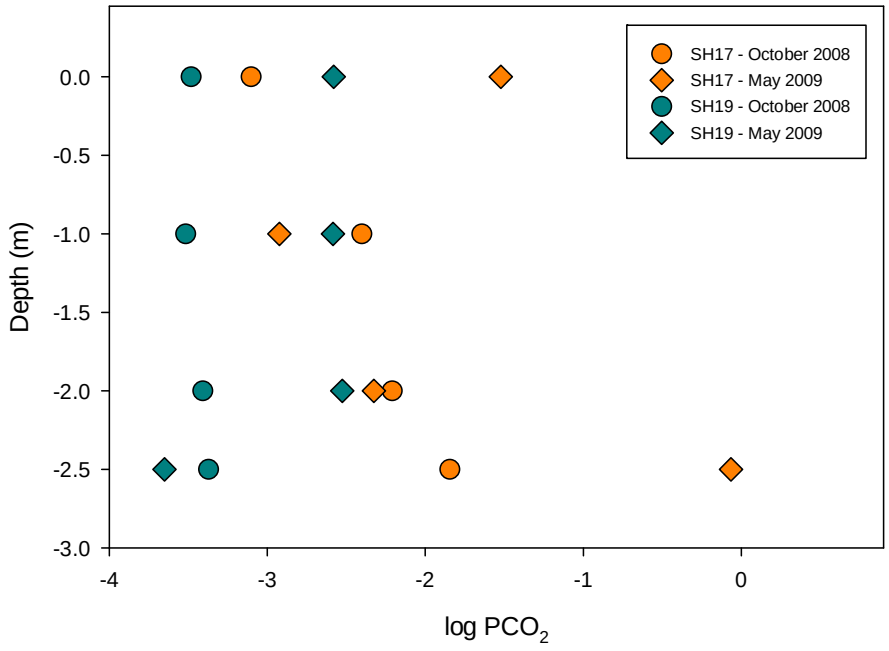

SI Magnesite with Depth - October 2008

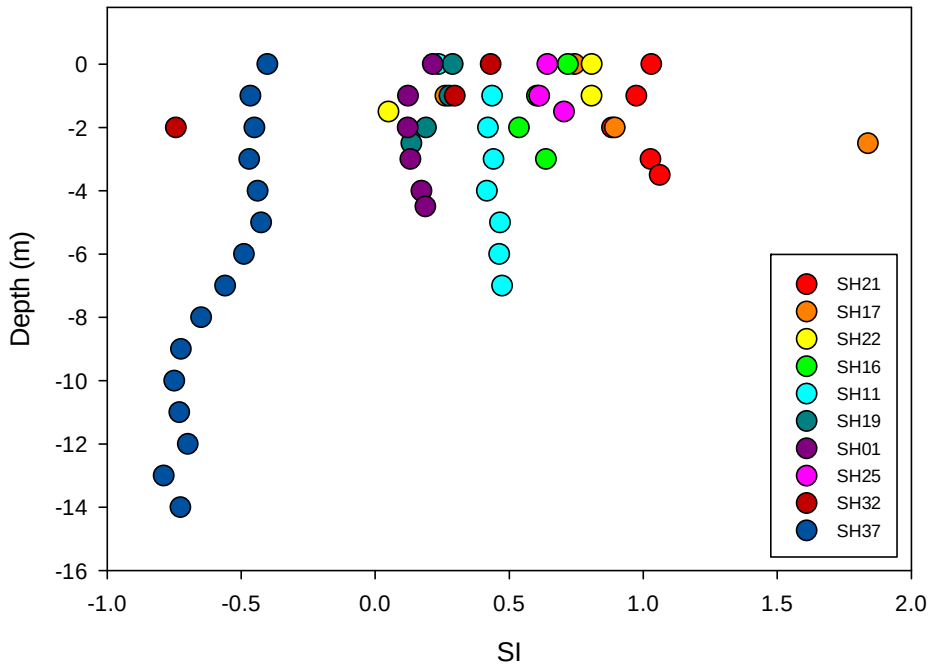

SI Magnesite with Depth - May 2009

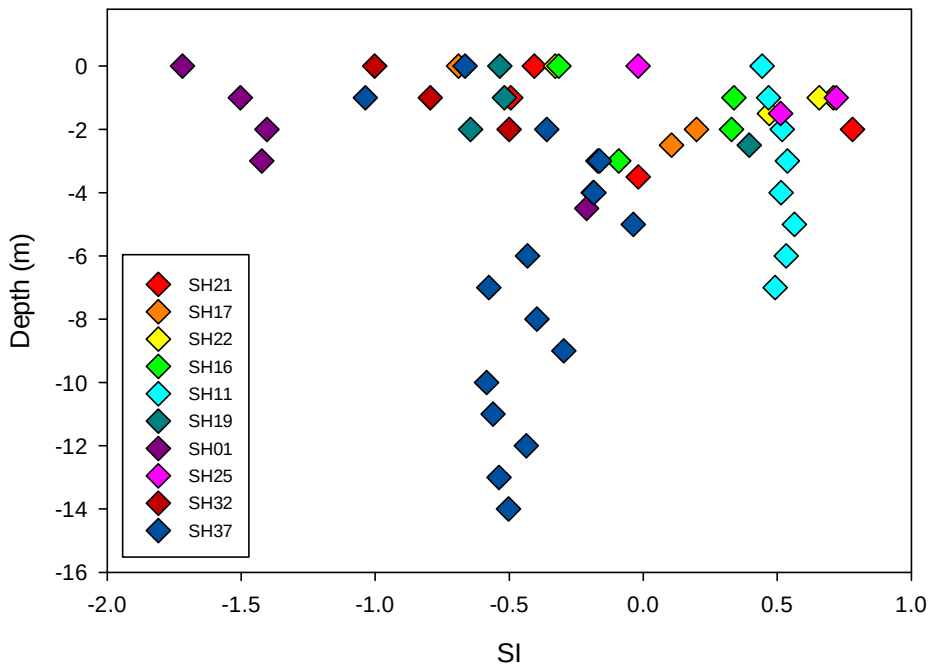

SI Magnesite with Depth

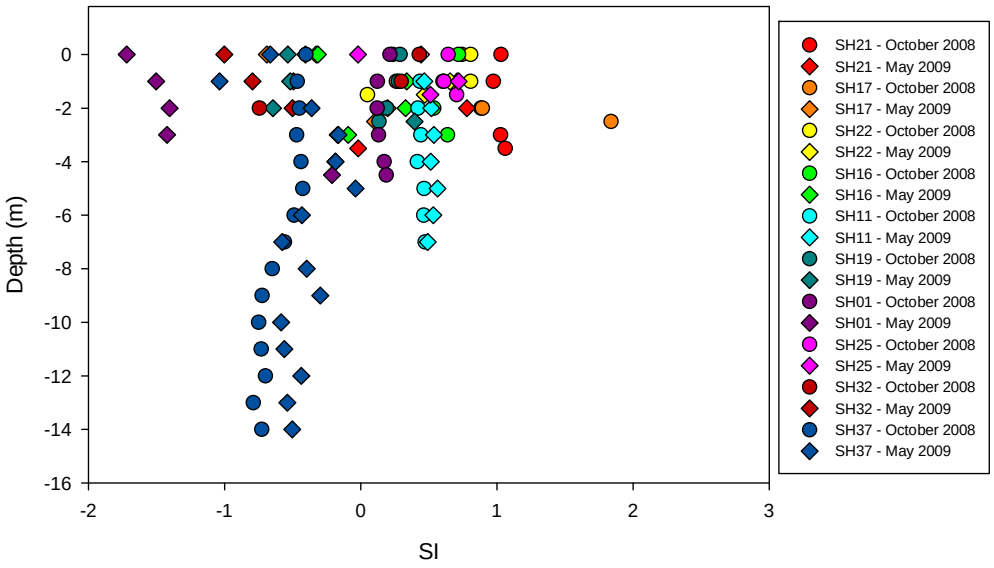

SI Magnesite with Depth - SH17 and SH19

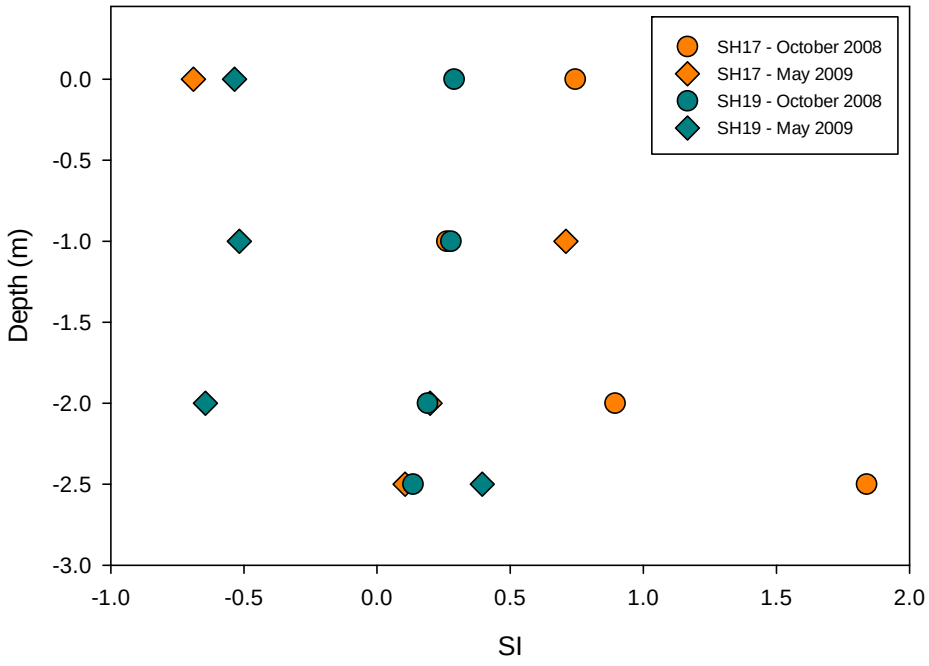

[Cl-] with Depth

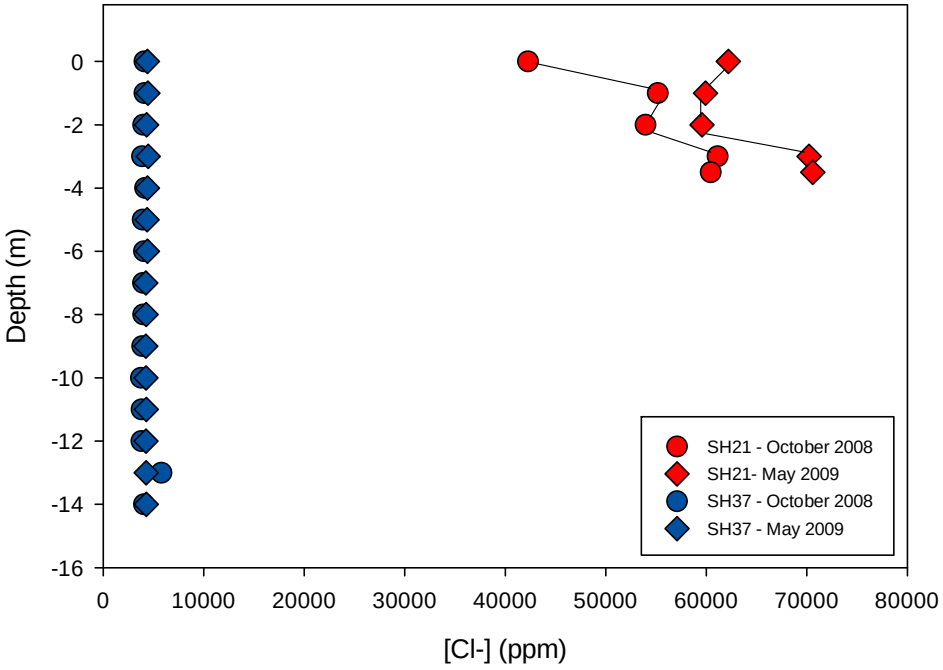

SO_4 with Depth

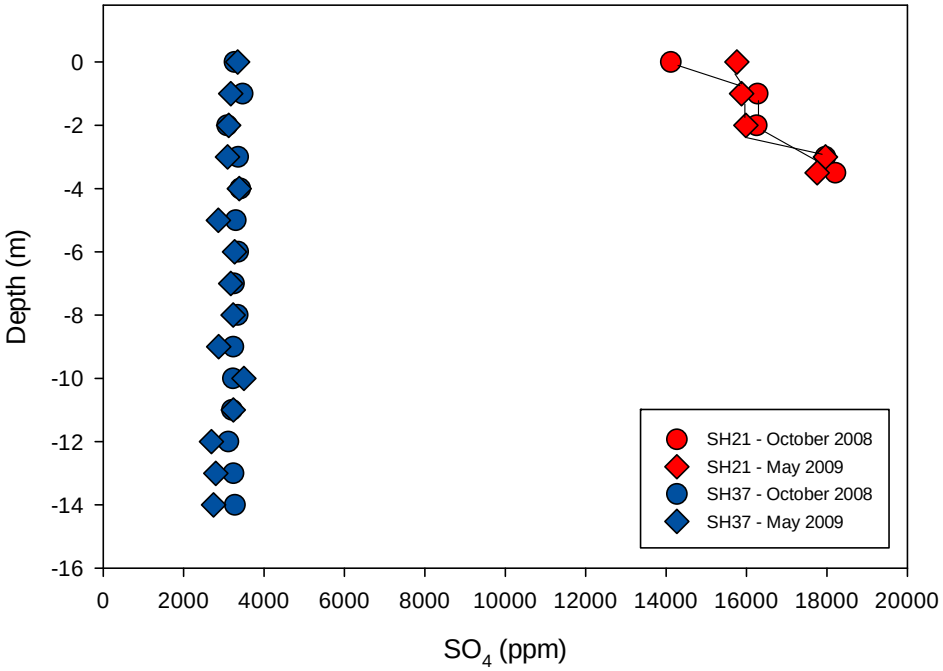

HCO_3 with Depth

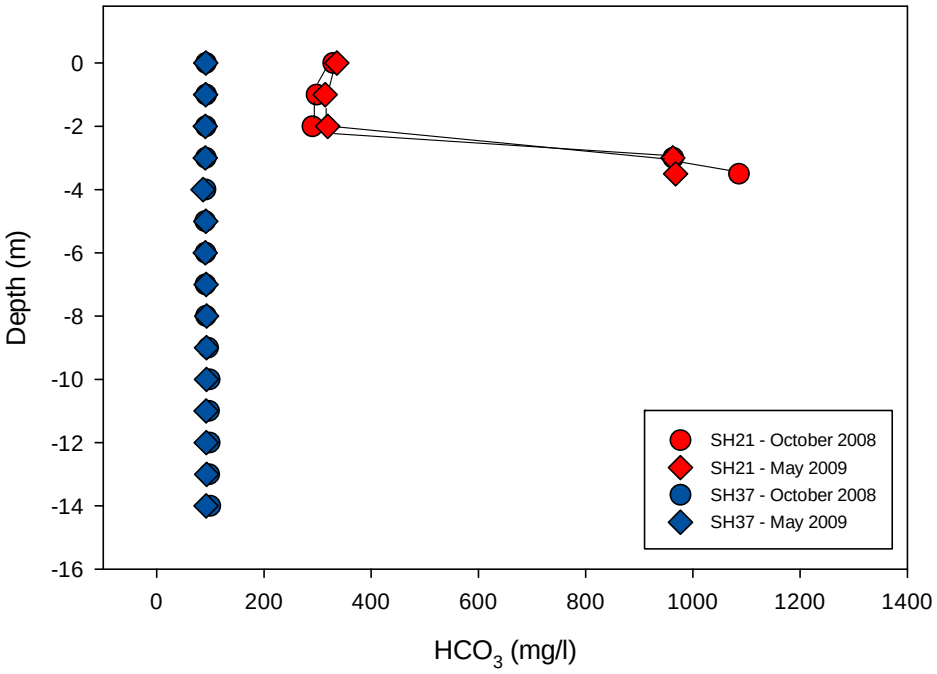

Ca with Depth

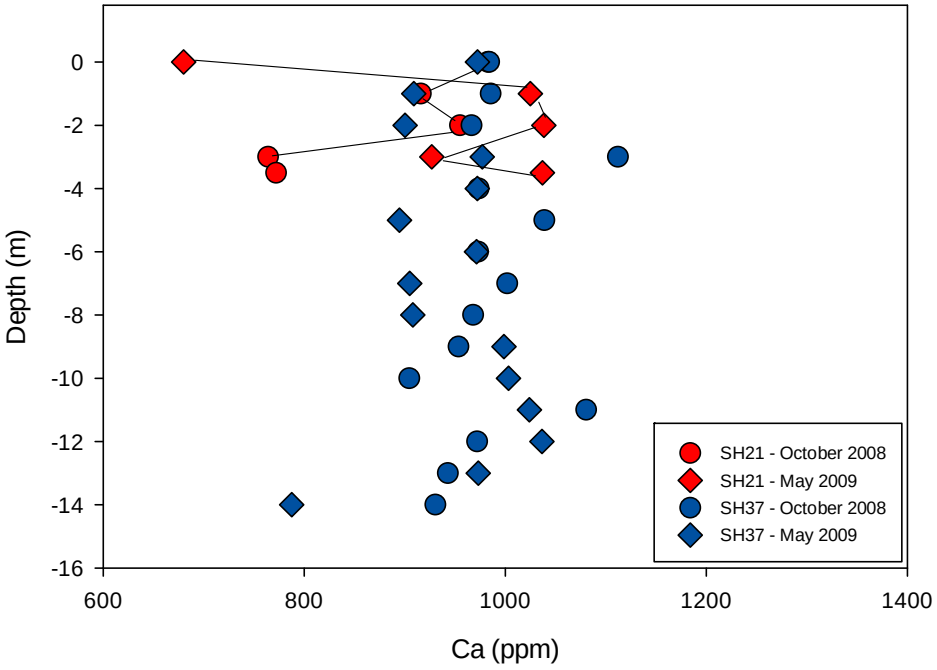

K with Depth

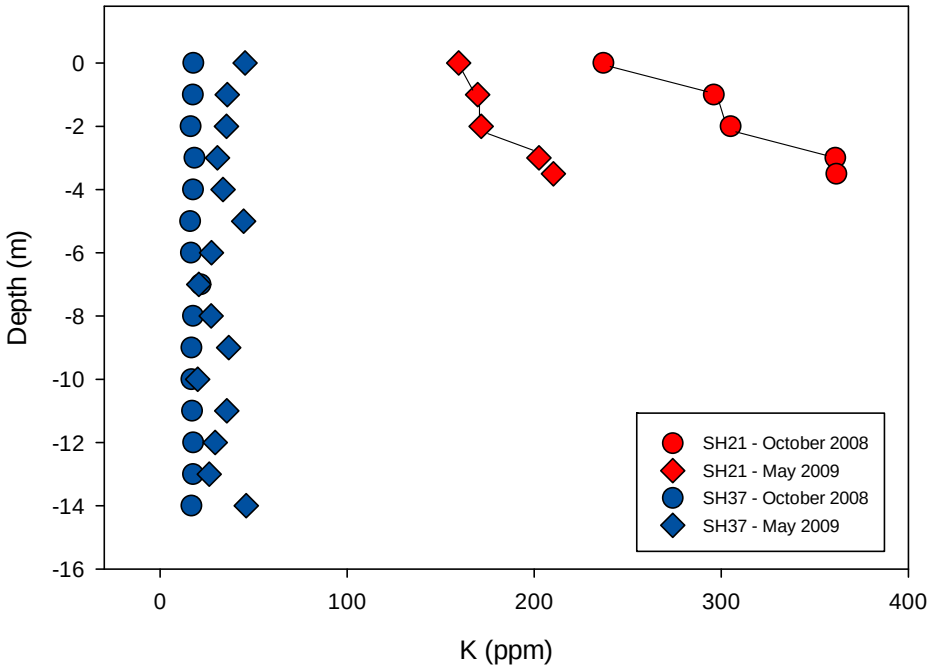

Na with Depth

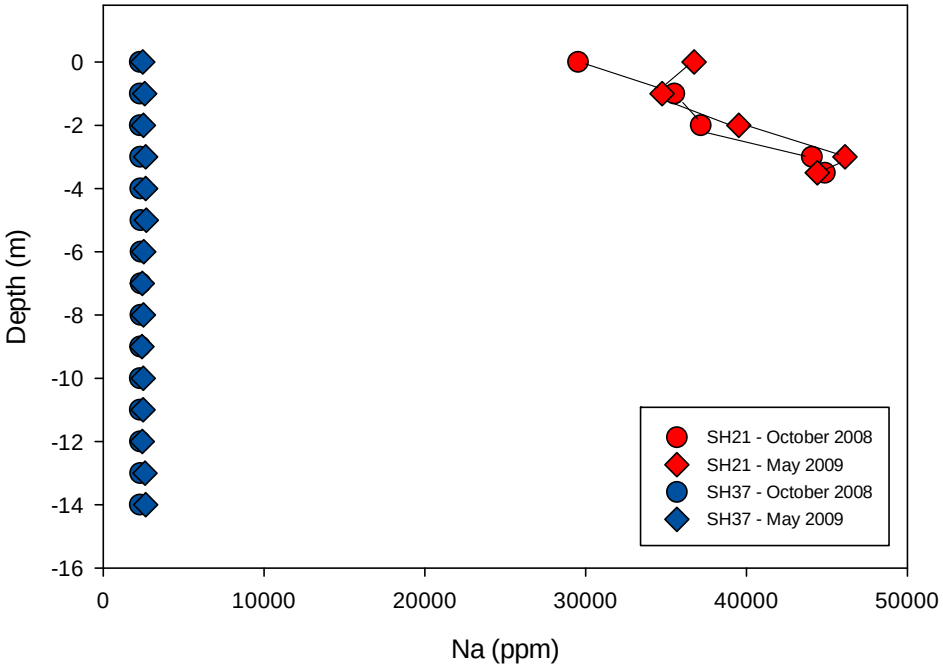

Mg with Depth

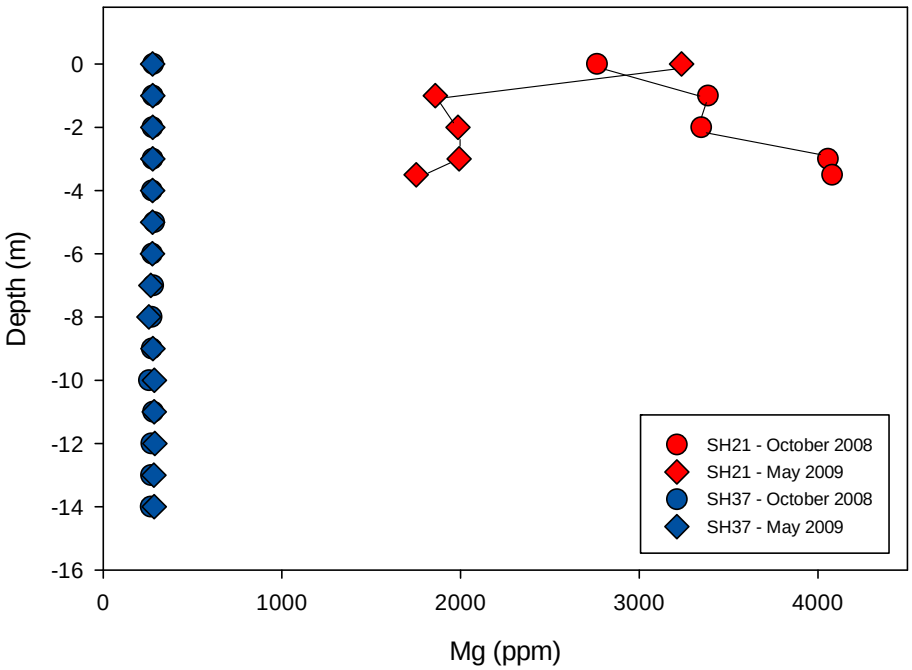

SI Magnesite with Depth

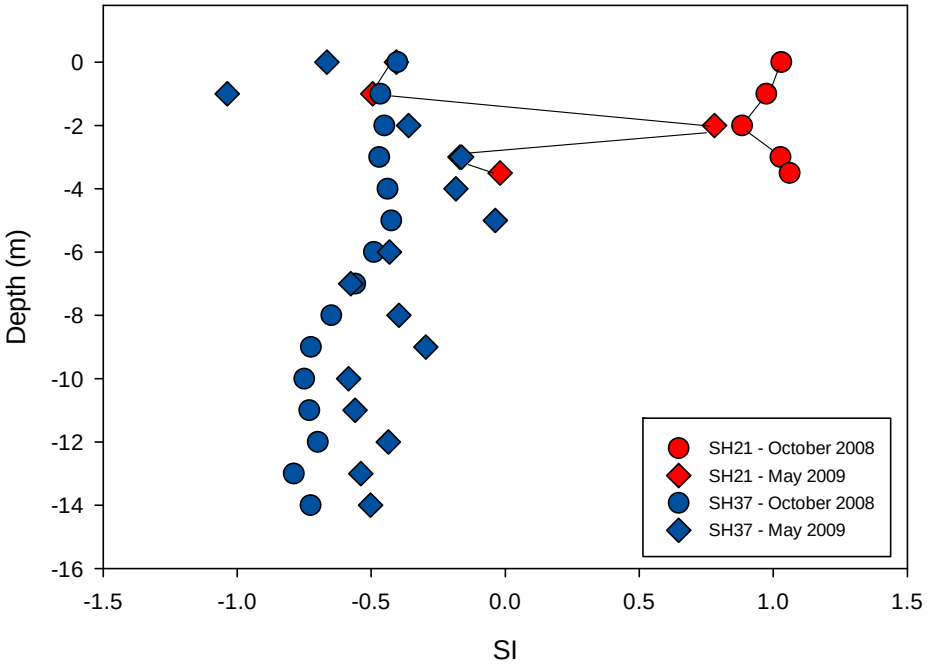

SI Calcite with Depth

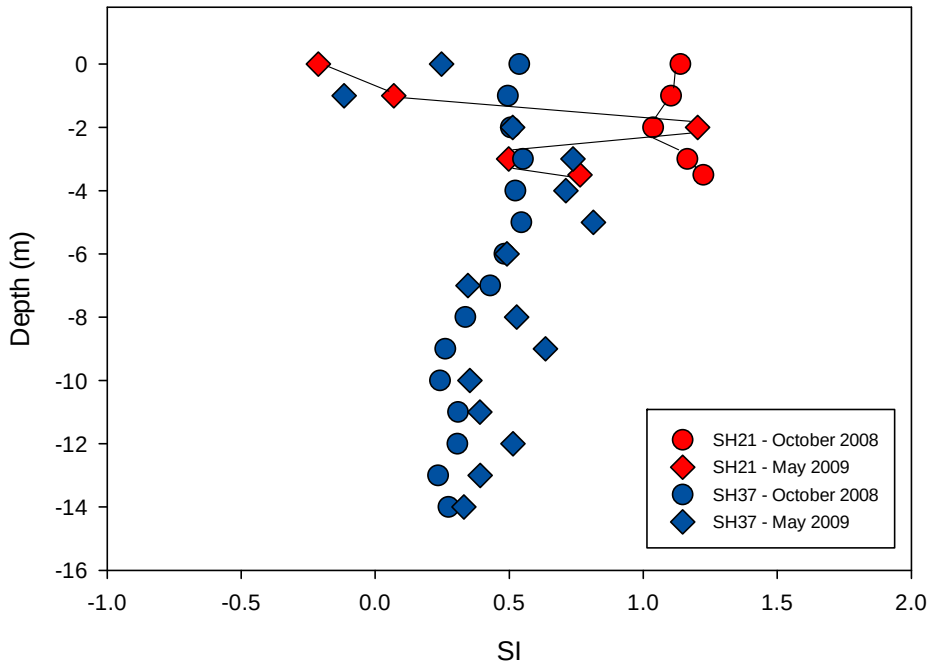

SI Gypsum with Depth

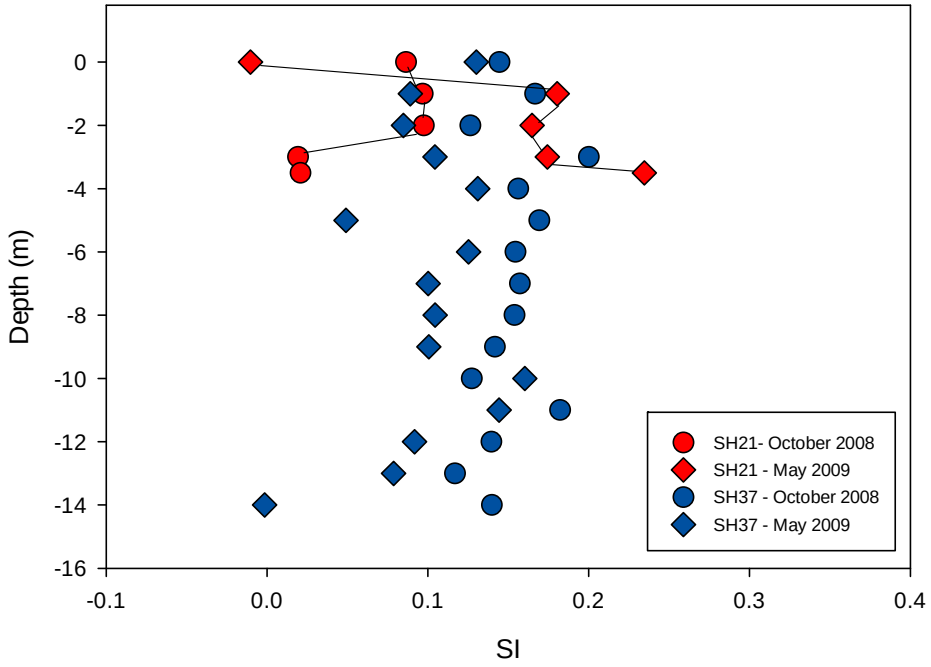

Halite SI with Depth

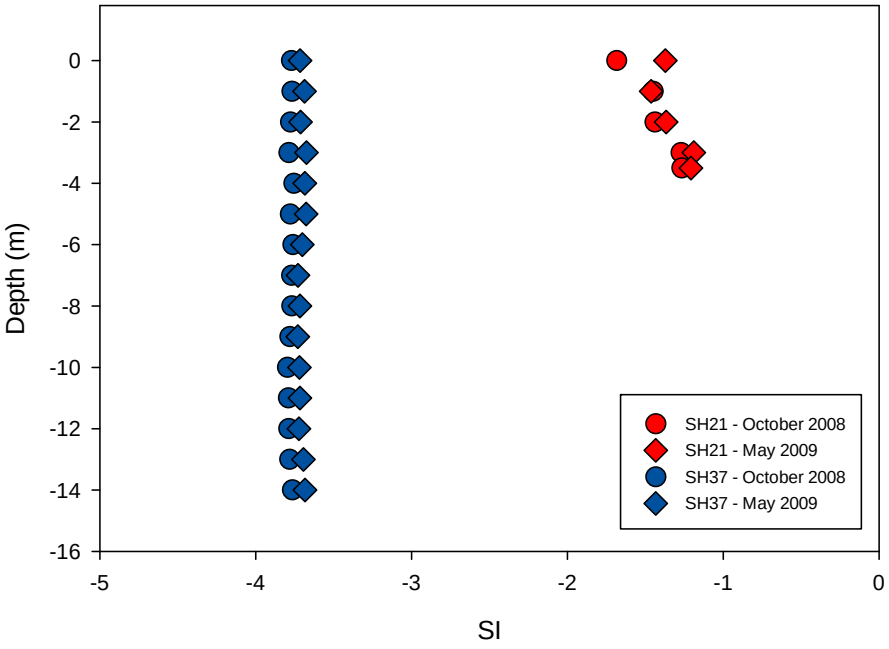

log PCO_2 with Depth

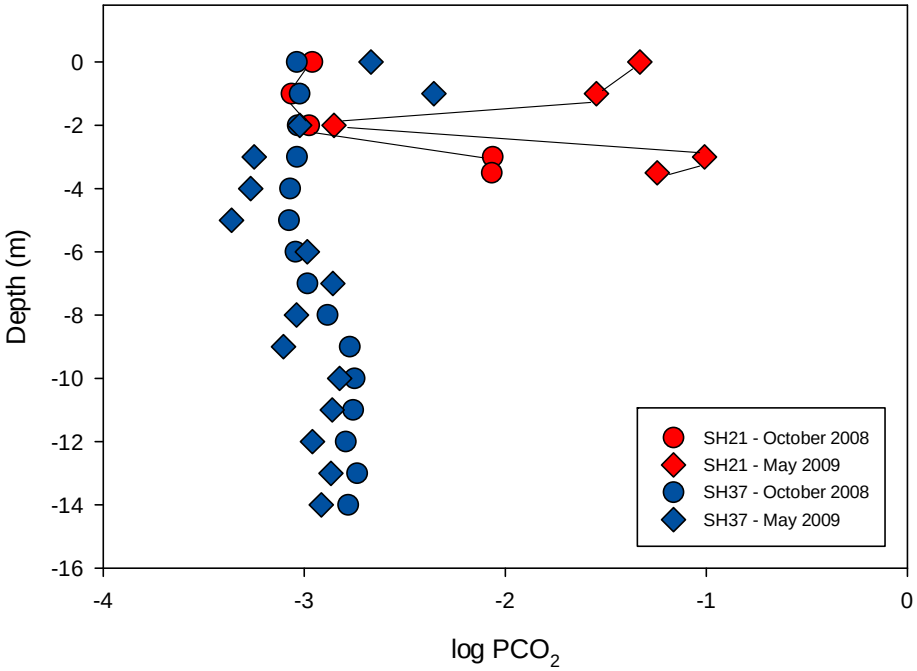

$\delta^{18}O$ with Depth - October 2008

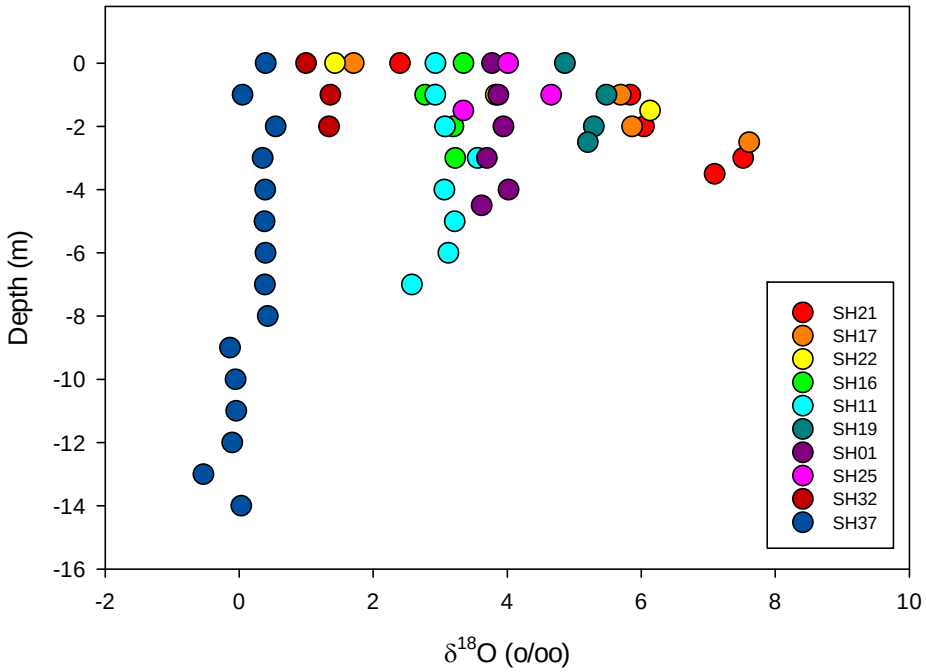

$\delta^{18}O$ with Depth - May 2009

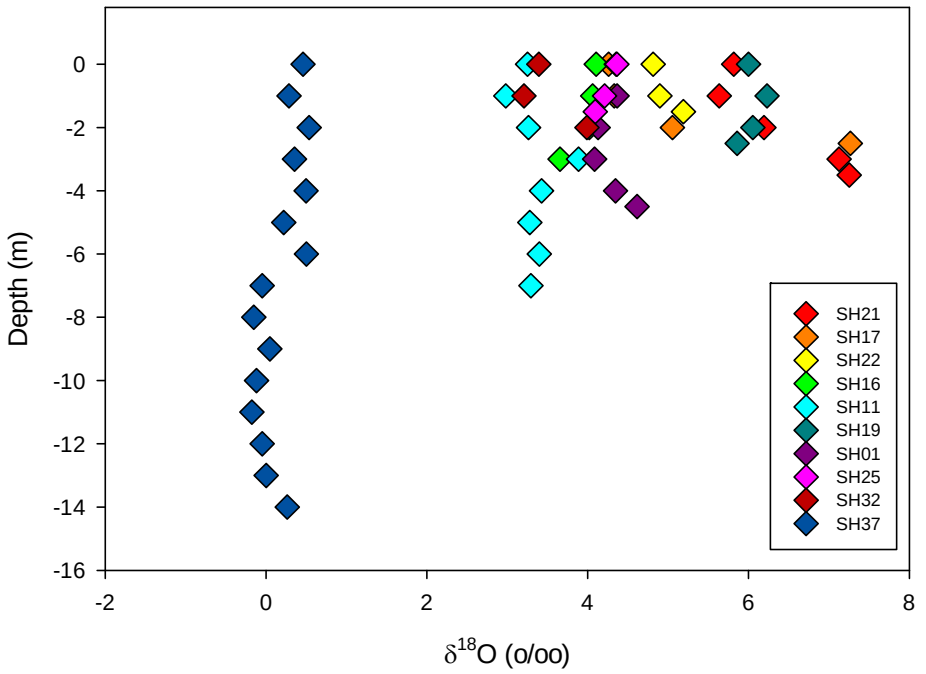

$\delta^{18}O$ with Depth

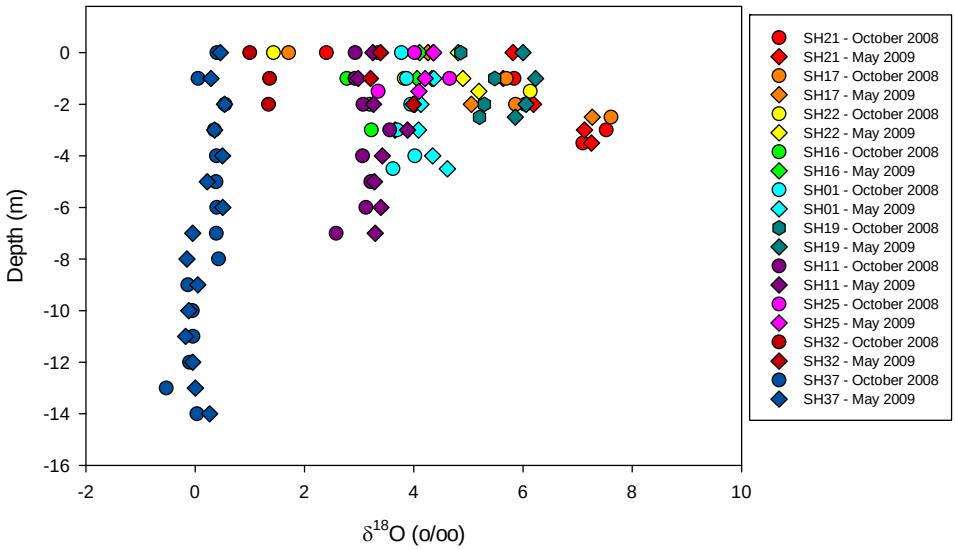

$\delta^{18}O$ with Depth - SH17 and SH19

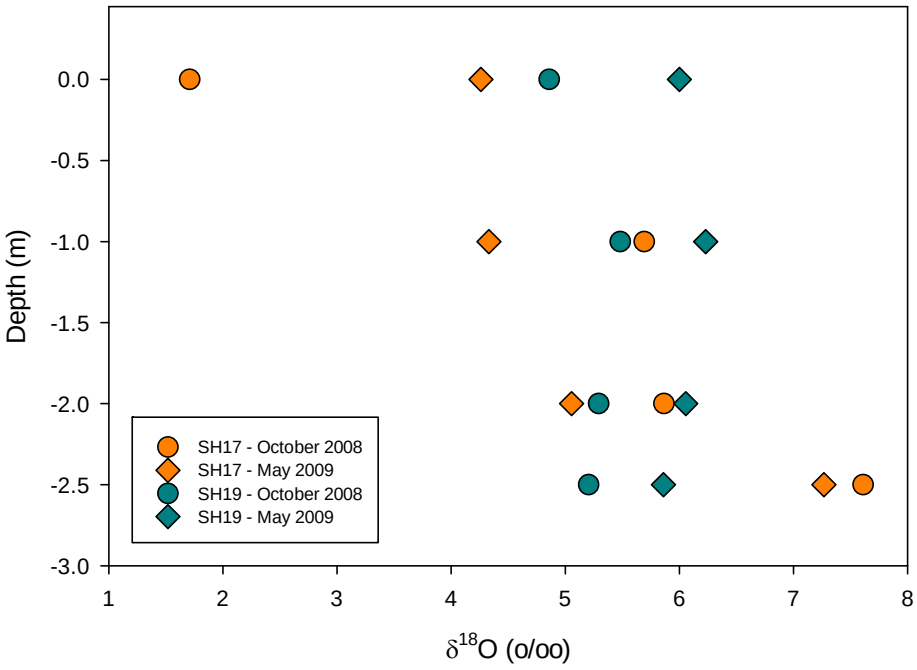

δD with Depth - October 2008

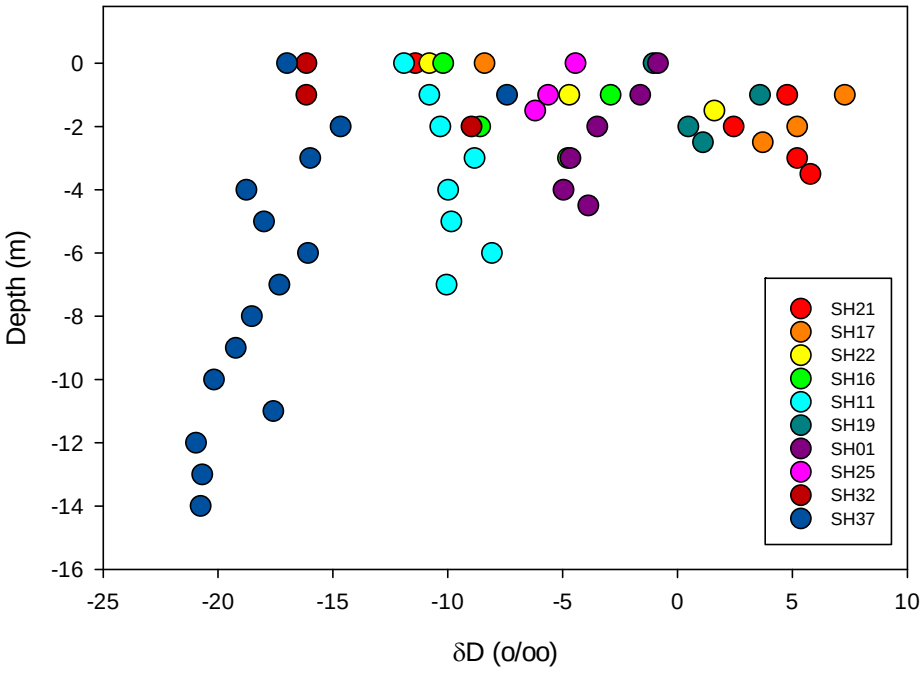

δD with Depth - May 2009

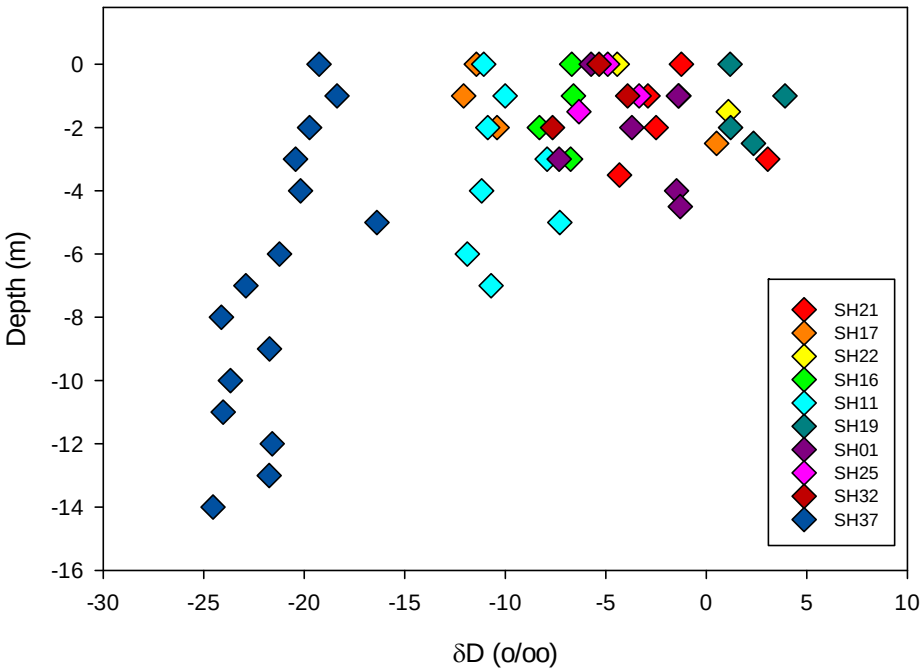

δD with Depth

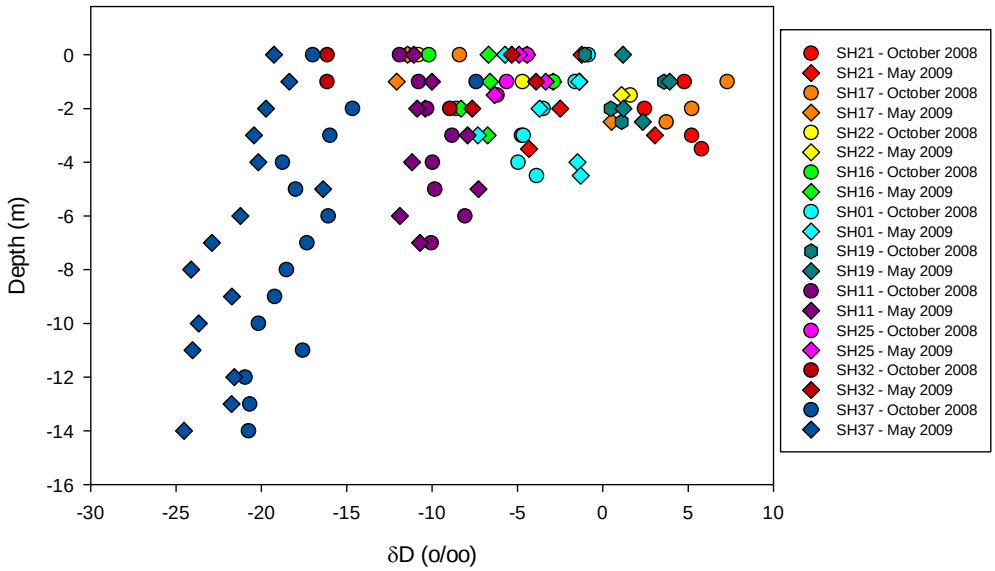

δD with Depth - SH17 and SH19

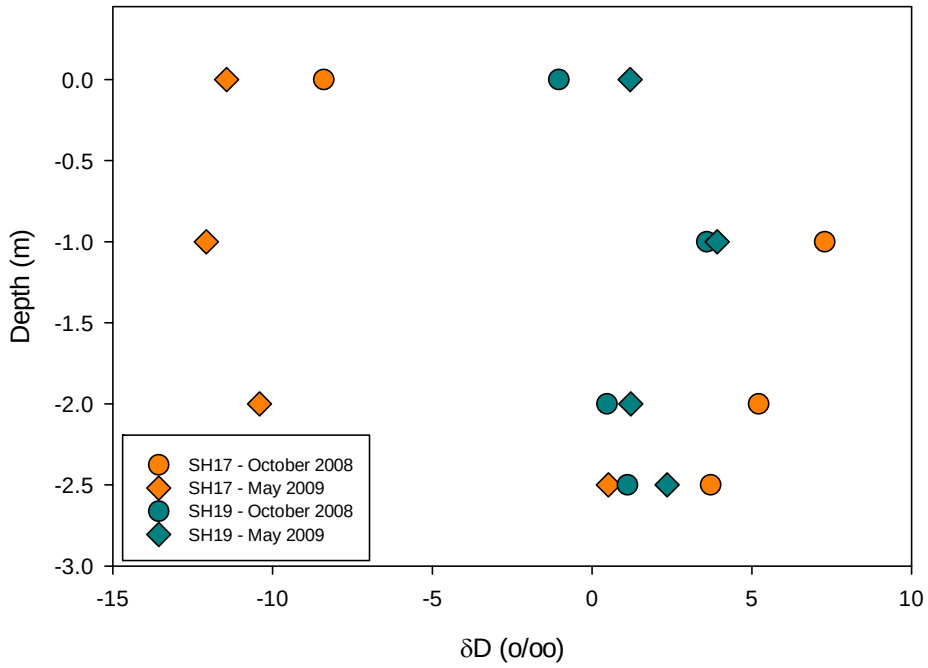

$\delta^{18}O$ with Depth

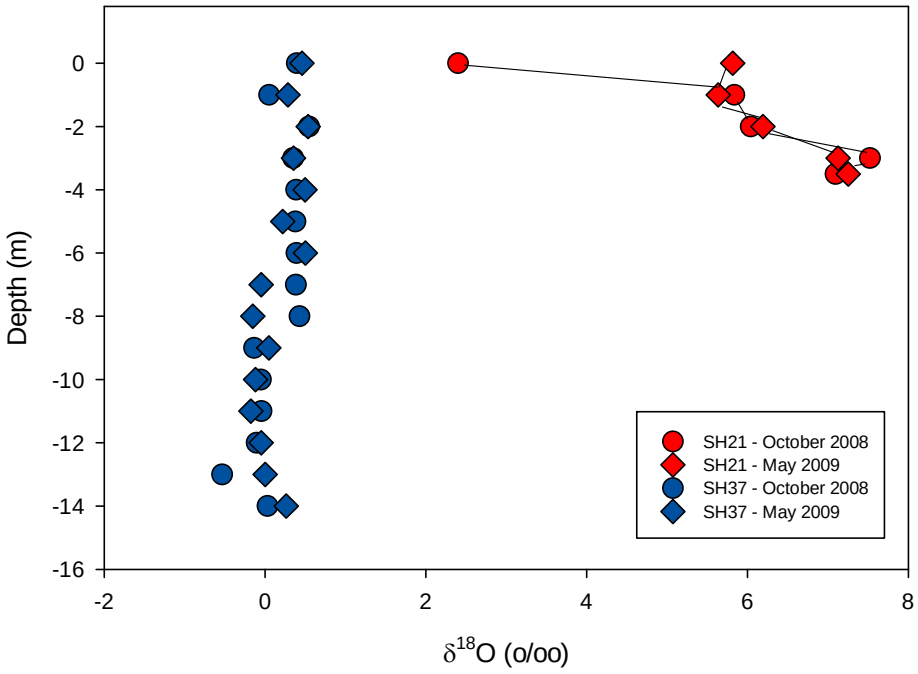

δD with Depth

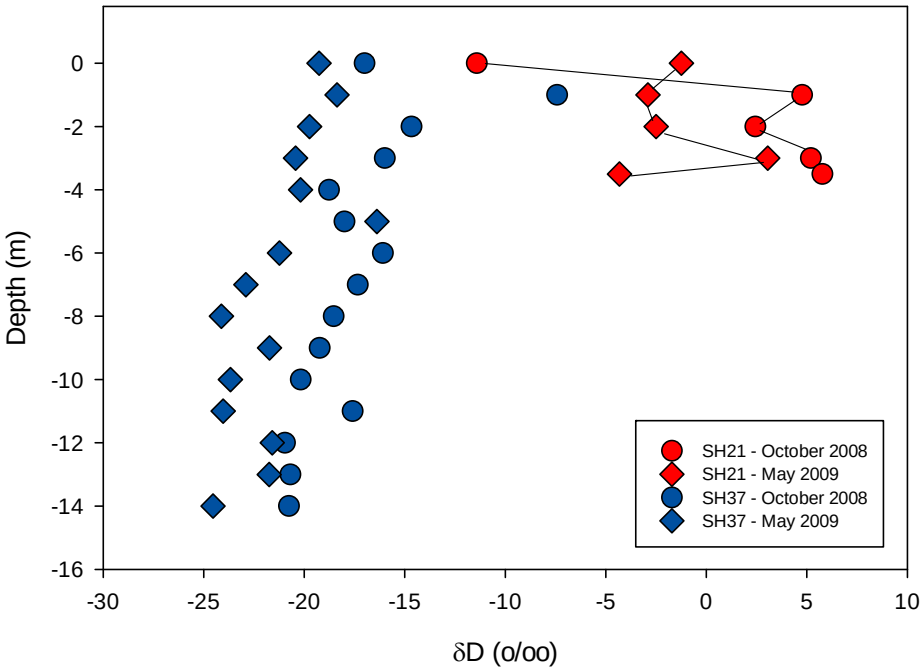

Density with Depth

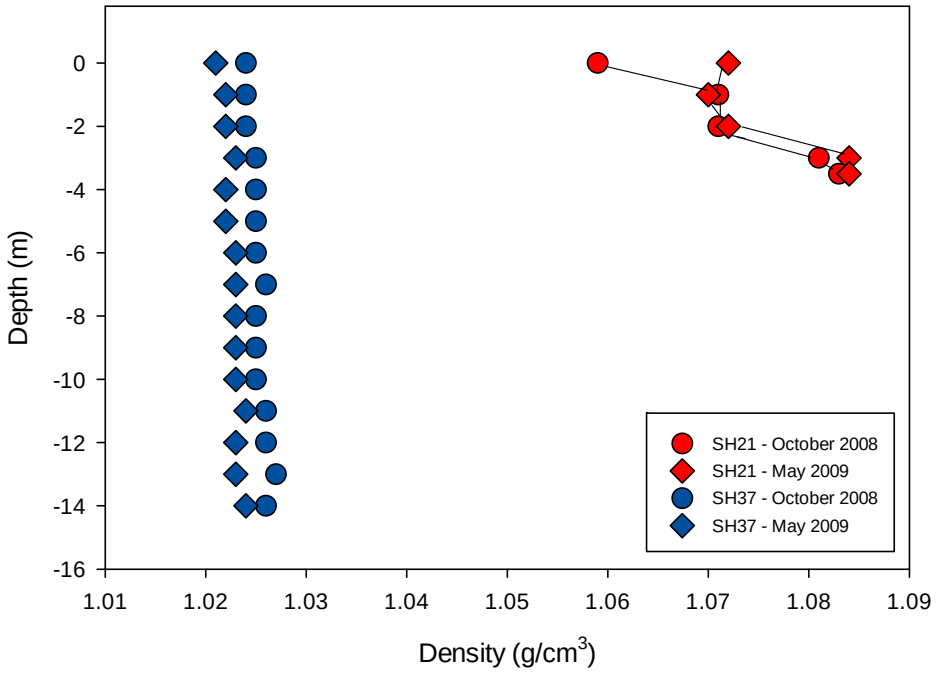

TDS with Depth

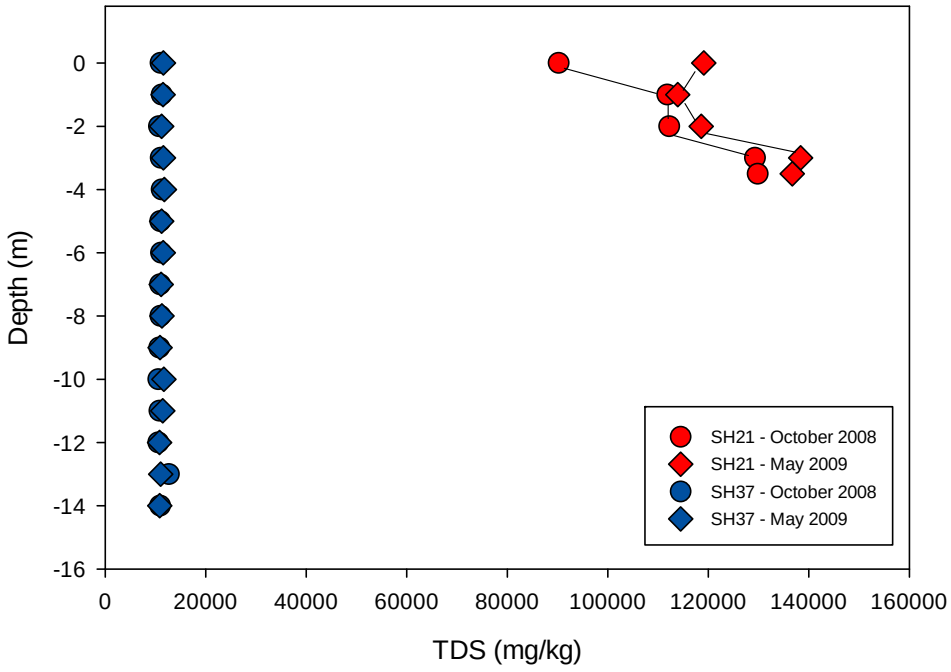

Conductivity with Depth

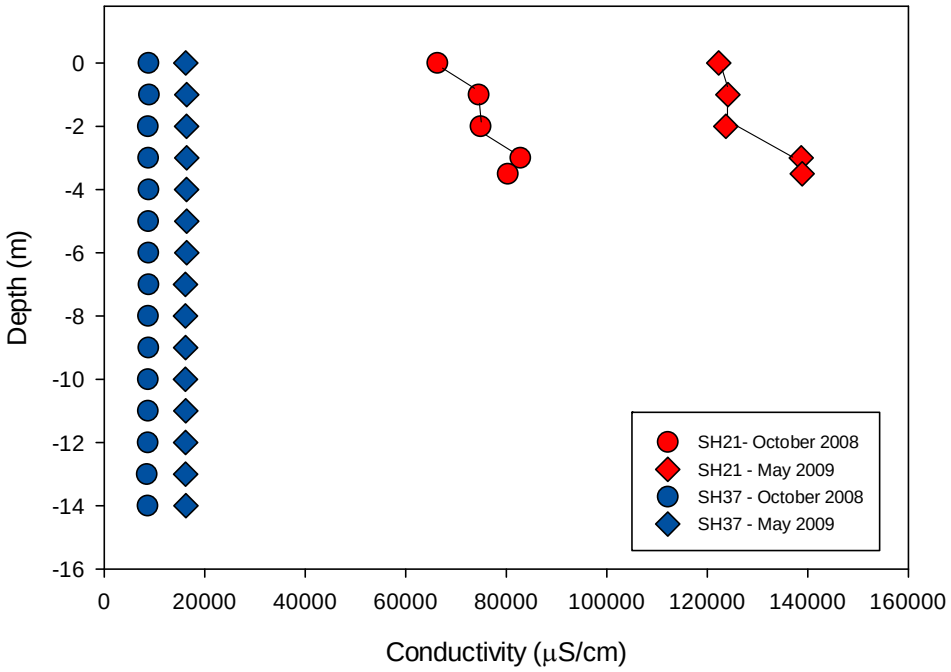

pH with Depth

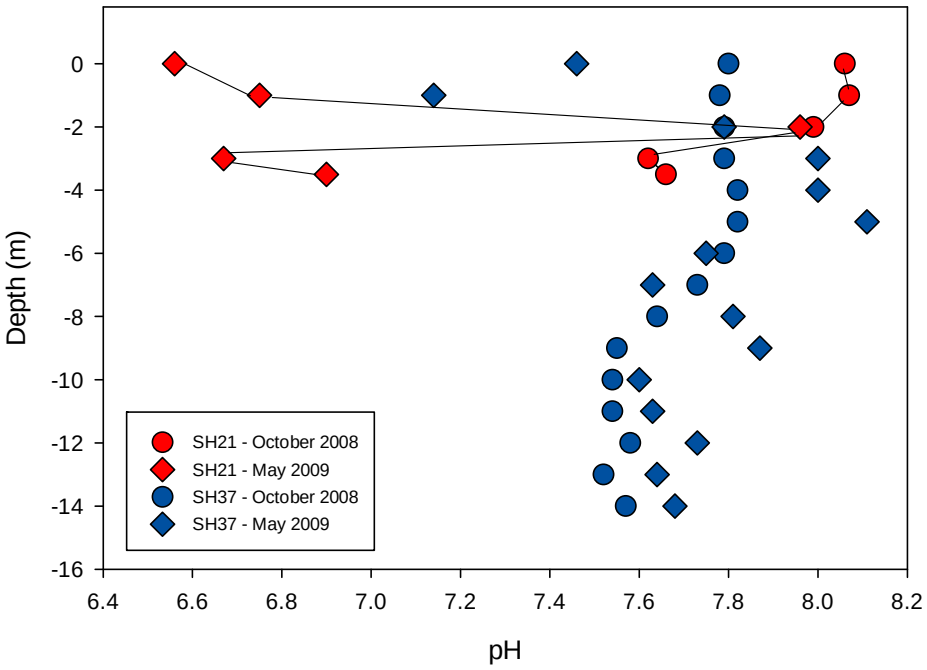

REFERENCES

Adams, J.E., Frenzel, H.N., 1950. Capitan Barrier Reef, Texas and New Mexico. The Journal of Geology. Volume 58, Number 4, Reef Issue (July 1950), pp. 289-312.

Bachman, G.O., 1987. Karst in Evaporites in Southeastern New Mexico. SAND86-7078, Albuquerque, NM, Sandia National Laboratories. 82p.

Barroll, P., Shomaker, J., 2003. Regional Hydrology of the Roswell Artesian Basin and the Capitan Aquifer. Water Resources of the Lower Pecos Region, New Mexico – Science, Policy, and a Look to the Future. Decision-Makers Field Conference 2003. pp. 23-27.

Bauer, P., Johnson, P., and Timmons, S., 2007. Springs of the Rio Grande Gorge, Taos County, New Mexico: Inventory, data report, and preliminary geochemistry. Final Technical Report, New Mexico Bureau of Geology and Mineral Resources Open-File Report 506.

Bednarz, J.C., 1979. Ecology and Status of the Pecos Gambusia, Gambusia nobilis (Poeciliidae), in New Mexico. The Southwestern Naturalist, Volume 24, Number 2. pp. 311-322.

Bethke, C. 2008. Geochmical and Biogeochemical Reaction Modelling, 2nd Edition. Cambridge University Press, Cambridge, U.K. 543 p.

Craig, H., 1961. Isotopic Variations in Meteoric Waters. Science, New Series, Volume 133, Number 3465. pp. 1702-1703.

Crossey, L.J., Fischer, T.P., Patchett, P.J., Karlstrom, K.E., Hilton, D.R., Huntoon, P., and Reynolds, A.C., 2006, Dissected hydrologic system at Grand Canyon: Interaction between upper world and lower world waters in modern springs and travertine: Geology, v. 34, p. 25-28.

Crossey, L.J., Karlstrom, K.E., Springer, A., Newell, D., Hilton, D., and Fischer, T., 2009, Degassing of mantle-derived CO2 and 3He from springs in the southern Colorado Plateau region— neotectonic connections and implications for groundwater systems: Geological Society of America Bulletin, v. 121, p. 1034-1053. DOI 10.1130/B26394.

Dekker N.P., Lammel C.J., Brooks G.F., 1991. Scanning Electron Microscopy of Piliated Neisseria Gonorrhoeae Processed with Hexamethyldisilazane. J Electr Micro Tech 19:461–467.

Drever, J.I., 1997, The geochemistry of natural waters: New Jersey, Prentice Hall, 436 p.
Faure, G., 1986. Principles of Isotope Geology. New York: John Wiley and Sons, Inc.

Fiedler, A.G. and Nye, S.S., 1933. Geology and Ground-Water Resources of the Roswell Artesian Basin, New Mexico. U.S. Geological Survey Water-Supply Paper 639.
Forbes, J., Nance, R., 1997. Stratigraphy, Sedimentology, and Structural Geology of Gypsum Caves in East Central New Mexico. Carbonates and Evaporites. Volume 12, Number 1. pp. 64-72.

Giggenbach W.F. (1992) The composition of gases in geothermal and volcanic systems as a function of tectonic setting. In Proc. 7th Int. Symp. Water-Rock Interaction, Park City, Utah, 873-878

Harrington, E.R., 1957. Sinkholes, Bottomless Lakes, and the Pecos River. The Scientific Monthly. Volume 84, Number 6, pp. 302-308.

Havenor, K.C., 1968. Structure, Stratigraphy, and Hydrogeology of the Northern Roswell Artesian Basin, Chaves County, New Mexico. Circular 93: Socorro, New Mexico, New Mexico Institute of Mining and Technology, 30.

Hirsch, R.J., 1988. Hydrogeologic Study to Investigate a Potential Connection Between Producing Zones of RA-2887 and 2888 and the Intermittent Flows of the Rio Hondo in the Vicinity of the Hondo Reservoir Six Miles West of Roswell, New Mexico. Rio Hondo Stream System Lincoln and Chaves Counties. New Mexico State Engineer Office. 24p.

Huff, G.F., 2004. An Overview of the Hydrogeology of Saline Ground Water in New Mexico. Water Desalination and Reuse Strategies for New Mexico. New Mexico Water Resources Research Institute. September 2004. 14p.

Hoy, N.H. and Gross, G.W., 1982. A Baseline Study of Oxygen 18 and Deuterium in the Roswell, New Mexico Groundwater Basin. New Mexico Water Resources Research Institute. Technical Report 144, 104p.

Inkenbrandt, P.C., Doss, P.K., Pickett, T.J., Brown, R.J., 2005. Barometric and Earth-Tide Induced Water-Level Changes in the Inglefield Sandstone in Southwestern Indiana. Proceedings of the Indiana Academy of Science. Volume 114, Number 1. 8p.

Kelley, V.C., 1971. Geology of the Pecos Country, Southeastern New Mexico. New Mexico Bureau of Mines and Mineral Resources Memoir. Volume 24. 75p.

Kondrat'eva, E.N., 1965. Photosynthetic Bacteria. Oldbourne Press, London. 243 p.

Land, L., 2003. Regional Geology of the Pecos Country, New Mexico. Water Resources of the Lower Pecos Region, New Mexico – Science, Policy, and a Look to the Future. Decision-Makers Field Conference 2003. pp. 10-13.

Land, L., 2005, Evaluation of groundwater residence time in a karstic aquifer using environmental tracers: Roswell Artesian Basin, New Mexico, in Proceedings of the Tenth

Multidisciplinary Conference on Sinkholes and the Engineering and Environmental Impacts of Karst, San Antonio, Texas, 2005: ASCE Geotechnical Special Publication no. 144, p. 432-440.

Land, L. and Huff, G.F., 2010. Multi-tracer Investigation of Groundwater Residence Time in a Karstic Aquifer: Bitter Lakes National Wildlife Refuge, New Mexico, USA. Hydrogeology Journal, 18: 455-472.
Land, L., Newton, B.T., 2007. Seasonal and Long-Term Variations in Hydraulic Head in a Karstic Aquifer: Roswell Artesian Basin, New Mexico. New Mexico Bureau of Geology and Mineral Resources. Open File Report 503, 38p.

Land, L. and Newton, B.T., 2008. Seasonal and Long-Term Variations in Hydraulic Head in a Karstic Aquifer: Roswell Artesian Basin, New Mexico. Journal of the American Water Resources Association, Volume 44, Number 1, pp. 175-191.

Longworth, J., Carron, J., 2003. Water Resources of the Lower Pecos Region, New Mexico – Science, Policy, and a Look to the Future. Decision-Makers Field Conference 2003. pp. 20-22.

Lyford, F.P., 1973. Valley Fill in the Roswell-Artesia Area, New Mexico. Open-File Report - U.S.Geological Survey. pp. 26-26.

MacRae, R.K., Lusk, J.D., Radke, W.R., 2001. Investigation of the Role of Environmental Contaminants upon Ecological Sentinel Species and Their Habitats at Bitter Lake National Wildlife Refuge, New Mexico. U.S. Department of the Interior Fish and Wildlife Service Region 2. Project ID#2N27 9620001.A. 38p.

Marechal, J.C., Sarma, M.P., Ahmed, S., Lachassagne, P., 2002. Establishment of Earth Tide Effect on Water-Level Fluctuations in an Unconfined Hard Rock Aquifer Using Spectral Analysis. Current Science. Volume 83, Number 1. 4p.

McCraw, D.J., Rawling, G., Land, L.A., 2007. Geological Map of the Bitter Lake Quadrangle, Chaves County, New Mexico. New Mexico Bureau of Geology and Mineral Resources. Open File Geologic Map 151.

Merriam, D.F., Mann, C.J., 1957. Sinkholes and Related Geologic Features in Kansas. Transactions of the Kansas Academy of Science (1903-), Volume 60, Number 3 (Autumn, 1957), pp. 207-243.

Minckley, C.O. and Deacon, J.E., 1975. Foods of the Devil's Hole pupfish, Cyprinodon diabolis (Cyprinodonitae): the Southwestern naturalist, 20, pp. 105-111.

Musgrove, M. and Banner, J.L., 1993. Regional Ground-Water Mixing and the Origin of Saline Fluids: Midcontinent, United States. Science, New Series, Volume 259, Number 5103, pp. 1877-1882.

Talon Newton, Stacy Timmons, Geoffrey Rawling, Frederick Partey, Trevor Kludt, LewisLand, Mike Timmons, and Patrick Walsh, Sacramento Mtns Hydrogeology Study, NMB, 2009; OFR 518.

Parkhurst, D.L., 1995, User's guide to PHREEQC—A computer program for speciation, reaction-path, advectivetransport, and inverse geochemical calculations: U.S. Geological Survey Water Resources Investigations Report 95-4227, 143 p.

Partey, F.K., Land, L.A., Frey, B., 2008. Final Report on the Geochemistry of Bitter Lakes National Wildlife Refuge, Roswell, New Mexico. New Mexico Bureau of Geology and Mineral Resources. Open File Report 526, 17p.

Pfennig, N. 1967. Photosynthetic Bacteria. Annual Review of Microbiology. 21: 285-324.

Reiter, M., Jordan, D.L., 1996. Hydrogeothermal Studies Across the Pecos River Valley, Southeastern New Mexico. GSA Bulletin, June 1996. Volume 108, Number 6. pp. 747-756.

Sharp, Z. 2007. Principles of stable isotope geochemistry. Prentice Hall, New Jersey. 344 p.

Stipp, T.F., 1956. Major Structural Features and Geologic History of Southeastern New Mexico. Oil and Gas Fields of Southeastern New Mexico--a Symposium . pp. 16-20.

Summers, W.K., 1972. Geology and Regional Hydrology of the Pecos River Basin, New Mexico. The New Mexico Water Resources Research Institute. Open File Report 37, 393p.

Stafford, K.W., Land, L., Klimchouk, A., 2008. Hypogenic Speleogenesis within Seven Rivers Evaporites: Coffee Cave, Eddy County, New Mexico. Journal of Cave and Karst Studies, Volume 70, Number 1, pp. 47-61.

Stafford, K.W., Land, L., Kimchouk, A.B., Gary, M.O., 2009. The Pecos River Hypogene Speleogenetic Province: A Basin-Scale Karst Paradigm for Eastern New Mexico and West Texas, USA. Advances in Hypogene Karst Studies. NCKRI Symposium 1. 15p.

Masayuki Takahashi, M. and Ichimura, S., 1970. Photosynthetic Properties and Growth of Photosynthetic Sulfur Bacteria in Lakes. *Limnology and Oceanography* Vol. 15, No. 6 (Nov., 1970), pp. 929-944.

Tashjian, P.L., 2003. The Biohydrology of the Middle Pecos Region, New Mexico. Water Resources of the Lower Pecos Region, New Mexico – Science, Policy, and a Look to the Future. Decision-Makers Field Conference 2003. pp. 28-31.

United States Environmental Protection Agency (USEPA), 2002. 40 CRF 143.3: Secondary Maximum Contaminant Levels. Accessed through: http://edocket.access.gpo.gov/cfr_2002/julqtr/pdf/40cfr143.3.pdf

United States Fish and Wildlife Service (USFWS), 2009. Pecos River Restoration: Control of the Invasive Saltcedar (Tamarix spp.) along the Pecos River and the Salt Cedar Wilderness on Bitter Lake National Wildlife Refuge, Chaves County, New Mexico. Environmental Assessment. October 2009. 27p.

Warren, J.K., 1989. Evaporite Sedimentology. Prentice-Hall. 285p.

Welder, G.E., 1983. Geohydrologic Framework of the Roswell Ground-Water Basin, Chaves and Eddy Counties, New Mexico. New Mexico State Engineer. Technical Report 42, 62p.

Yuan, F., Miyamoto, S., 2008. Characteristics of Oxygen-18 and Deuterium Composition in Waters from the Pecos River in American Southwest. Chemical Geology 255 (2008), pp. 220-230.